Exploration in Extra-Dimension in the Era of LHC and Beyond

A thesis submitted for the degree of
Doctor of Philosophy(Science)

in Physics

by

Tapoja Jha

Department of Physics
University of Calcutta

2017

Exploration in Extra-Dimension in the Era of LHC and Beyond

Abstract of the PhD thesis

In this thesis, we have considered a particular incarnation of BSM scenario, the Universal Extra Dimensional model (UED) in its basic as well as in its non-minimal version (nmUED). Non-minimality in Universal Extra Dimensional (UED) framework is realized by adding kinetic and Yukawa terms and also the mass and quartic coupling terms of various fields with arbitrary coefficients to the action at boundary points of the extra space like dimension. This thesis mainly deals with the different processes and their corresponding results of constraining the parameter space of this model from a generic study of unitarity (in scalar sector) and also from the difference between the branching ratio of $Z \to b\bar{b}$ decay obtained from LEP collaboration and its SM estimate. After that we study some flavor changing rare top decays. We examine the unitarity constraints in gauge and scalar sectors. We have shown that some of the tree-level two-body scattering amplitudes in gauge and scalar sectors do not respect partial wave unitarity. Unitarity of scalar sector of this model leads to an upper bound on gauge or scalar boundary-localized (BLT) parameter which depends on the maximum number of Kaluza-Klein (KK) mode considered in the analysis. We have also shown that the variation of the upper bound of the gauge or scalar BLT parameter decreases with the increasing KK-modes. The results are, in effect, independent of the inverse of compactifiaction radius. The upper bound on boundary-localized parameter results in a lower bound on gauge and scalar KK-masses. Besides, a recent estimation of the Standard Model (SM) contribution to $Zb\bar{b}$ coupling at two loop level, points to a 1.2σ discrepancy between the experimental data and the SM result. We compare our calculation with the difference between the SM prediction and the experimental estimation of the above coupling and constrain the parameter space of nmUED. We also review the limit on compactification radius of UED in view of the new theoretical estimation of SM contribution to $Zb\bar{b}$ coupling. For suitable choice of coefficients of boundary-localized terms (which is permissible from unitarity analysis), 95% C.L. lower limit on R^{-1} comes out to be in the range of 1 TeV in the framework of nmUED; while in UED, the lower limit on R^{-1} is 350 GeV which is a marginal improvement over an earlier estimate. The flavor changing decays of the top quark are severely suppressed in the Standard Model by virtue of the Glashow-Iliopoulos-Maiani mechanism. We perform a complete one-loop calculation of the flavor changing top quark decays $t \to c\gamma$ and $t \to ch$ in this model. We find that the decay

Jahnoja Jha

rates in the minimal variant of the model do not change much from their Standard Model values. In the non-minimal version of this model, these decay rates can be higher for specific choices of the boundary localized parameters for a certain range of inverse compactification radius. But these model parameters lead to Kaluza-Klein particle masses that are in tension with various searches at the LHC and at the LEP.

Tapoja Jha

Tapoja Jha

Acknowledgements

I express my sincere acknowledgement to my supervisor Dr. Anindya Datta for his valuable guidance, constant support and above all his patience with me, without his support it would not be possible to complete the journey of my five-year Ph.D. life. I shall also remain grateful to Prof. Anirban Kundu, Prof. Abhijit Bhattacharyya, Dr. Indrajit Mitra and my supervisor for their vital contributions in the classes during my M.Sc. and introducing me to this enlightening world of Quantum Field Theory and Particle Physics. I also thank Prof. Amitava Raychaudhuri for his valuable suggestions and many insightful comments on my research work.

I am really grateful to my collaborator Ujjal (Dey) for all the discussions which help me understand the subject better. Besides I also thank him for carefully reading the draft and making some useful comments. I express my gratitude to Ayon-da (Patra) and Rashidul-da (Islam) for their helpful guidance. I want to thank my friend Ipsita (Saha) for giving me the thesis format and for many useful discussions. I am truly thankful to my friend Susobhan (Paul) and my brother Adrish (Maity) for their immense technical help.

It is my pleasure to thank my colleagues and juniors Nandini Midya, Indrani Chakraborty, Soumita Pramanick, Parna Roy, Swagata Ghosh, Tanay Paul, Nabanita Ganguly, Saumi Dutta, Dipti Chakraborty, Somajit Dey and Triparno Bandyopadhyay who have made my journey comfortable and enjoyable. A special thanks to Tanay Paul and Prithwish Mahapatra (Chemistry Department) for always being so helpful and cooperative in any official matter. Parna, Swagata, Tanay and me, we four were always partners in taking initiative in any kind of departmental celebrations among scholars. I will always cherish those moments and how much fun we have had!!

Furthermore, I shall always remain indebted to my childhood Maths teachers, my grandfather Late (Dr.) Bhabesh Chandra Jha, Shri Haricharan Kundu, and Shri Sumit Mahalanobis for their vital contributions in my life. I also want to thank my father Dr. Biswanath Jha for his guidance and support. I also thank him for carefully reading the draft and pointing out some mistakes. A special thanks to my mother Mrs. Shayamali Jha for her unconditional support. Last but not least, I thank my sisters (Ru, Bubi and Boul) for all the celebrations, *addas* and fights we have altogether.

Tapoja Jha
Kolkata, India

List of Publications

- **T. Jha** and A. Datta,
  "$Z \to bb$ in non-minimal Universal Extra Dimensional Model",
  JHEP **1503** (2015) 012, [arXiv:1410.5098[hep-ph]].

- U. K. Dey and **T. Jha**,
  "Rare top decays in minimal and nonminimal universal extra dimension models",
  Phys. Rev. D **94** (2016) 056011, [arXiv:1602.03286[hep-ph]].

- **T. Jha**,
  "Unitarity Constraints on non-minimal Universal Extra Dimensional Model",
  [arXiv:1604.02481[hep-ph]].

Contents

List of Figures

List of Tables

Abbreviations

SM	**S**tandard **M**odel
BSM	**B**eyond the **S**tandard **M**odel
LHC	**L**arge **H**adron **C**ollider
FCC	**F**uture **C**ircular **C**ollider
UED	**U**niversal **E**xtra **D**imension
mUED	**m**inimal **U**niversal **E**xtra **D**imension
nmUED	**non**-**M**inimal **U**niversal **E**xtra **D**imension
KK	**K**aluza-**K**lein
BLKT	**B**oundary-**L**ocalized **K**inetic **T**erm
BLYT	**B**oundary-**L**ocalized **Y**ukawa **T**erm
BLT	**B**oundary-**L**ocalized **T**erm
LED	**L**arge **E**xtra **D**imension
RS	**R**andall-**S**undrum
DM	**D**ark **M**atter
WIMP	**W**eekly **I**nteracting **M**assive **P**article
GIM	**G**lashow-**I**liopoulos-**M**aiani
CKM	**C**abibbo-**K**obayashi-**M**askawa

To My Grandfather

1

Standard Model

The Standard Model (SM) of particle physics is immensely successful and our best formulation till date in explaining almost all the classification of elementary particles and their interactions observed in high energy colliders like the Tevatron and the LHC. Fundamentally it is a quantum field theory which elucidates the dynamics of our universe through matter and forces. All the matter fields consist of fermions which interact among each other via vector fields. The vector fields in the theory act as force carriers of the electro-weak and strong forces. The theory incorporates a unified picture of three fundamental forces of the universe: the strong, the weak and the electromagnetic forces.

In quantum field theory, so in the SM, the elementary particles are described by fields which are local in spacetime with definite transformation properties under some particular symmetries. Therefore, it is necessary to start with the definitions of the symmetry group, in order to understand the field content of the SM properly.

1.1 Symmetries and Particle Content

Symmetries have always been powerful guiding principles in particle physics. The SM has been formulated respecting the same path; it is a theory based on local symmetry.

Let us start with Noether's theorem which states that any conservation law of physics originally results from the symmetries of a particular theory. One important example is the theory of Quantum Electrodynamics (QED). If we make a local symmetry in the free Lagrangian of the fermion field, the invariance of the action requires new local field which is basically the gauge field with some definite properties. The free Dirac Lagrangian can be written as

$$\mathcal{L}_\psi = \overline{\psi}\left(i\partial\!\!\!/ - m\right)\psi, \tag{1.1}$$

where, ψ is the spin-1/2 Dirac field, $\overline{\psi} \equiv \psi^\dagger\gamma^0$, and γ^μ are the 4×4 Dirac matrices. This Lagrangian is invariant under the global transformation $\psi \rightarrow \exp(-ieQ\theta)\psi$ where, θ is the global parameter being the same at all spacetime, Q is the charge of ψ in the unit of electron charge e. The invariance of action under this global transformation implies a conserved Dirac current j^μ by Noether's theorem:

$$\partial_\mu j^\mu = 0; \qquad j^\mu = eQ\overline{\psi}\gamma^\mu\psi. \tag{1.2}$$

However, the Lagrangian $\mathcal{L}_\psi$ is not invariant under local symmetry, *i.e.* when θ is a function of spacetime. This evidently suggests that the derivative should be redefined as

$$\partial_\mu \rightarrow \mathcal{D}_\mu \equiv \partial_\mu - ieQA_\mu, \tag{1.3}$$

where, A_μ is a vector field. The $\mathcal{L}_\psi$ (given in Eq. 1.1) with the replacement $\partial_\mu \rightarrow \mathcal{D}_\mu$ is now invariant under the following local transformations

$$\psi \rightarrow \psi' = \exp(-ieQ\theta(x))\psi, \tag{1.4}$$

$$A_\mu \rightarrow A'_\mu = A_\mu - \partial_\mu\theta(x), \tag{1.5}$$

and is finally expressed as

$$\mathcal{L}'_\psi = \mathcal{L}_\psi + eQ\overline{\psi}\gamma_\mu A^\mu\psi. \tag{1.6}$$

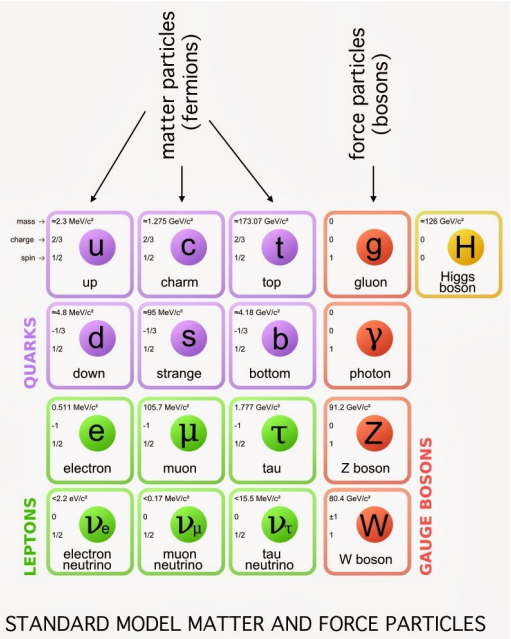

FIGURE 1.1: The particle content of the Standard Model.

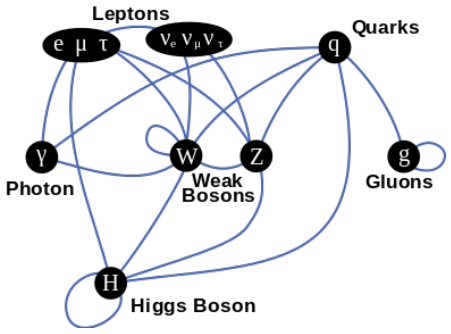

FIGURE 1.2: Standard Model interactions.

Thus all the terms that were invariant under the global phase rotation are now invariant under the local phase rotation provided we make the minimal substitution $\partial_\mu \to \mathcal{D}_\mu$. We obtain the second term in Eq. 1.6 from the imposition of local invariance. It demonstrates that, in principle, a theory having only matter fields evidently mandates the existence of vector fields that govern the interactions amongst fermions. One can thus generalize this principle for all interactions through specific symmetries imposed on the theory. This is basically the fundamental idea for constructing the SM that was initially proposed by Glashow [1] and independently by Salam and Ward [2] which was extended later by Weinberg [3] and Salam [4]. The Standard Model (SM) is a specific form of gauge field theory based on well known gauge symmetry $SU(3)_c \otimes SU(2)_L \otimes U(1)_Y$. The $SU(3)_c$ part of the gauge group characterizes the strong interactions and is independently called *Quantum Chromodynamics* (QCD), whereas the $SU(2)_L \otimes U(1)_Y$ part describes a unified picture of the electromagnetic and the weak interactions and is called the *Electroweak sector* of the theory. The fundamental particles of the SM is summarized in Fig. 1.1.

The gauge symmetry of the electroweak sector is described by $SU(2)_L \otimes U(1)_Y$. The $SU(2)_L$ group is related to the weak force where 'L' signifies that only left-handed fermions transform under this group operation, whereas the $U(1)_Y$ represents the weak hypercharge group (Y denotes the hypercharge). $SU(2)$ has three generators and $U(1)$ has one. In doublet representation of $SU(2)$ the generators can be represented as $T_a = \sigma_a/2$, where σ_a $(a = 1, 2, 3)$ are the Pauli matrices, given by

$$\sigma_1 = \begin{pmatrix} 0 & 1 \\ 1 & 0 \end{pmatrix}, \quad \sigma_2 = \begin{pmatrix} 0 & -i \\ i & 0 \end{pmatrix}, \quad \sigma_3 = \begin{pmatrix} 1 & 0 \\ 0 & -1 \end{pmatrix}. \tag{1.7}$$

However, it is convenient to consider these matrices in the following combinations:

$$\sigma_+ \equiv \frac{1}{\sqrt{2}}(\sigma_1 + i\sigma_2) = \begin{pmatrix} 0 & \sqrt{2} \\ 0 & 0 \end{pmatrix}, \quad \sigma_- \equiv \frac{1}{\sqrt{2}}(\sigma_1 - i\sigma_2) = \begin{pmatrix} 0 & 0 \\ \sqrt{2} & 0 \end{pmatrix}, \quad \sigma_3. \tag{1.8}$$

An important feature of this group is the chiral nature of interactions. Unlike strong interactions[1], the left- and right-chiral parts of the fields act differently under the electroweak gauge transformations. Fermions are the set of spin-1/2 particles. Based on their electric charge and ability to interact with strong nuclear force, they are subdivided into two types: leptons and quarks. The leptonic sector consists of three flavors with a progressive mass hierarchy, which contains integral or zero electric charged particles (defined in the unit of electron charge e). Each charged lepton is also associated with a neutral left-handed particle called neutrino. We represent the left-handed leptons as

$$\mathsf{L}_e = \begin{pmatrix} \nu_e \\ e^- \end{pmatrix}_L, \quad \mathsf{L}_\mu = \begin{pmatrix} \nu_\mu \\ \mu^- \end{pmatrix}_L, \quad \mathsf{L}_\tau = \begin{pmatrix} \nu_\tau \\ \tau^- \end{pmatrix}_L, \tag{1.9}$$

with weak isospin 1/2 and weak hypercharge $Y(\mathsf{L}_\ell) = -1$; where 'ℓ' corresponds to three different lepton flavors with ℓ: e, μ, τ. The right-handed charged leptons are

$$\mathsf{E}_\ell = e_R,\ \mu_R,\ \tau_R, \tag{1.10}$$

with weak hypercharge $Y(\mathsf{E}_\ell) = -2$. The right-handed fields are singlets under $SU(2)$. The observed electric charges are given by $Q = T_3 + \frac{Y}{2}$. Both e_L and e_R have electric charge (-1), while ν_{eL} is uncharged justifying the hypercharge assignments for those fields. There is no right-chiral neutrino in the theory which implies that the neutrinos are massless.

Quarks are distinguished from leptons for their interactions via the strong color force and their fractional electric charge. Due to the requirements of color neutrality and strong force confinement at low energies, free quarks are not accessible in nature. Similar to the leptons, based on the masses, there exists a generational hierarchy of distinct quark flavor doublets. The left-handed quarks are given by

[1] We shall discuss it shortly.

$$q_1 = \begin{pmatrix} u \\ d \end{pmatrix}_L , \quad q_2 = \begin{pmatrix} c \\ s \end{pmatrix}_L , \quad q_3 = \begin{pmatrix} t \\ b \end{pmatrix}_L , \tag{1.11}$$

with weak isospin 1/2 and weak hypercharge $Y(q_i) = 1/3$; and their right-handed counterparts are represented by

$$u_A = u_R, c_R, t_R \text{ and } d_A = d_R, s_R, b_R, \tag{1.12}$$

with weak hypercharges $Y(u_A) = 4/3$ and $Y(d_A) = -2/3$; 'A' corresponds to generation index of quark running from 1 to 3. The different properties of quarks and leptons such as mass, charge, baryon number ($\mathscr{B}$), lepton number ($\mathscr{L}$) are listed in Table. 1.1 and in Table. 1.2 [5].

Lepton	Mass (MeV)	Charge (in unit e)	$\mathscr{L}_e$	$\mathscr{L}_\mu$	$\mathscr{L}_\tau$	$SU(3)_c$ quantum numbers
e^-	0.51	-1	1	0	0	1
μ^-	105.65	-1	0	1	0	1
τ^-	1777.03	-1	0	0	1	1
ν_e	$< 3 \times 10^{-6}$	0	1	0	0	1
ν_μ	< 0.19	0	0	1	0	1
ν_τ	< 18.2	0	0	0	1	1

TABLE 1.1: Properties of Leptons

Quark	Mass	Charge (in unit e)	$\mathscr{B}$	$\mathscr{L}$	$SU(3)_c$ quantum number
u	1.8-3 MeV	2/3	1/3	0	3
d	4.5-5.3 MeV	$-1/3$	1/3	0	3
c	1.25-1.3 GeV	2/3	1/3	0	3
s	90-100 MeV	$-1/3$	1/3	0	3
t	174.98 GeV	2/3	1/3	0	3
b	4.15-4.21 GeV	$-1/3$	1/3	0	3

TABLE 1.2: Properties of Quarks

Since identical quantum numbers can mix with each other there arises coupling terms (*e.g.* Yukawa Coupling) that mix the generations of three different quarks. Alternatively, one can diagonalize the Yukawa coupling by incorporating a new basis for quark fields. The weak eigenstates in Eq. 1.11 are considered to be the linear combinations of the mass eigenstates. Let u'^i_L and d'^i_L denote the mass eigenstates, *i.e.* quarks in the basis that diagonalizes their Higgs couplings. This latter basis is the physical one since it diagonalizes the mass matrix. The two bases are related by unitary transformations:

$$u^i_L = U^{ij}_u u'^j_L, \qquad d^i_L = U^{ij}_d d'^j_L. \tag{1.13}$$

However, this simplification of the Higgs coupling results in a complication in the gauge coupling. The gauge boson current will take the following form

$$J^{\mu+}_{gauge} = \frac{1}{\sqrt{2}}\overline{u}^i_L\gamma^\mu d^i_L = \frac{1}{\sqrt{2}}\overline{u}'^i_L\gamma^\mu V_{ij}d'^j_L. \tag{1.14}$$

Here,

$$V_{ij} = (U^\dagger_u U_d)_{ij}, \tag{1.15}$$

which is a unitary matrix called the Cabibbo-Kobayashi-Maskawa (CKM) matrix. The off-diagonal terms in V_{ij} enable weak-interaction transitions among the three quark generations. As an example, for simplicity considering only two generations we can have

$$V_{1j}d'^j_L = \cos\theta_c d'_L + \sin\theta_c s'_L. \tag{1.16}$$

The term $\sin\theta_c$ allows an s quark to decay weakly to a u quark. However, it is noteworthy that no such mixing occurs in the leptonic sector of the SM. No difference can be made between the flavor and the mass eigenstates, since the neutrinos are massless in the SM[2]. It is evident that, mixing between different generations of quarks leads to flavor violation and experimental observations have set high constraints on this *flavor changing neutral current* (FCNC). Glashow-Iliopoulos-Maiani [6] showed that if we demand $V_{\rm CKM}$ to be a unitary matrix that in turn would result in highly suppressed flavor changing processes mediated by neutral gauge bosons. A simple parameter counting of a $n \times n$ unitary matrix generates $n(n-1)/2$ independent real mixing angles and $(n-1)(n-2)/2$ independent complex phases. Clearly, the Cabibbo [7]-Kobayashi-Maskawa [8] matrix ($V_{\rm CKM}$) contains three real mixing angles and one complex phase factor. The complex phase factor is the only source of complex gauge interactions that violates CP symmetry within the framework of the SM. The unitarity condition implies various relations between its elements. For example, we have

$$V_{ud}V^*_{ub} + V_{cd}V^*_{cb} + V_{td}V^*_{tb} = 0. \tag{1.17}$$

The above relation can be represented as a "unitarity" triangle. The other five unitarity triangles can be constructed corresponding to their orthogonal relations [9, 10]. The areas of all the unitarity triangles are the same and related to the measure of CP violation as [11–13]:

$$\mid J_{\rm CP} \mid = 2 \cdot \Delta, \tag{1.18}$$

where Δ corresponds to the area of the unitarity triangle. Currently, the best-fit values of the various elements of the CKM matrix obtained from experiments are [5]

[2]It is worth mentioning that, discovery of neutrino mass necessitates a mixing matrix in the neutrino sector as well, which is called PMNS (Pontecorvo–Maki–Nakagawa–Sakata) matrix.

$$\begin{pmatrix} |V_{ud}| = 0.974 & |V_{us}| = 0.225 & |V_{ub}| = 0.004 \\ |V_{cd}| = 0.220 & |V_{cs}| = 0.995 & |V_{cb}| = 0.041 \\ |V_{td}| = 0.0082 & |V_{ts}| = 0.04 & |V_{tb}| = 1.009 \end{pmatrix}. \tag{1.19}$$

SM is a chiral theory, completely free of axial vector anomalies among the gauge currents. The cancellation of anomalies requires that leptons and quarks should appear in complete multiplets associated with the structure as $(\mathsf{L}_\ell, \mathsf{E}_\ell, q_A, u_A, d_A)$, which in turn results in equal number of quarks and leptons appearing in Nature. A prerequisite condition of the theory to be renormalizable is that it has to be anomaly-free which eventually ensures that the higher order corrections in any perturbation theory will respect the same gauge symmetry as that of the tree level in that theory [14].

The electroweak gauge group provides two sets of gauge fields: set of weak isovectors $\mathcal{W}^a_\mu$ with coupling constant g and a weak isoscalar $\mathcal{B}_\mu$ with corresponding coupling constant g'. For the requirement of the gauge invariance of the Lagrangian, gauge fields $\mathcal{W}^a_\mu$ must transform in some way to compensate the variation of the fermionic field under an infinitesimal weak-isospin rotation generated by $G = 1 + i\alpha \cdot \mathbf{T}$ which is given as:

$$\psi \to (1 + i\alpha^a T^a)\,\psi, \tag{1.20}$$

where, α^a is a local parameter. This requires the transformation of the gauge fields to be $\mathcal{W}^a_\mu \to \mathcal{W}^a_\mu + (1/g)\partial_\mu\alpha^a + f^{abc}\mathcal{W}^b_\mu\alpha^c$, whereas $\mathcal{B}_\mu$ should transform as $\mathcal{B}_\mu \to \mathcal{B}_\mu - (1/g')\partial_\mu\alpha$ under an infinitesimal hypercharge phase rotation. These transformation laws in consequence imply the covariant derivative of ψ has the same transformation pattern as ψ itself. The corresponding field-strength tensors are defined as

$$\mathcal{F}^a_{\mu\nu} \equiv \partial_\mu\mathcal{W}^a_\nu - \partial_\nu\mathcal{W}^a_\mu + g f^{abc}\mathcal{W}^b_\mu\mathcal{W}^c_\nu \tag{1.21}$$

and

$$\mathcal{B}_{\mu\nu} = \partial_\mu\mathcal{B}_\nu - \partial_\nu\mathcal{B}_\mu. \tag{1.22}$$

In the above, $a = 1, 2, 3$ for the three components of the weak isovector, f^{abc} is the antisymmetric structure constant with $f^{123} = +1$.

We can now briefly sketch the SM electroweak interactions by the following Lagrangian,

$$\mathcal{L}_{electroweak} = \mathcal{L}_{\text{gauge}} + \mathcal{L}_{\text{leptons}} + \mathcal{L}_{\text{quarks}} \tag{1.23}$$

with

$$\mathcal{L}_{\text{gauge}} = -\frac{1}{4}\sum_a \mathcal{F}^a_{\mu\nu}\mathcal{F}^{a\,\mu\nu} - \frac{1}{4}\mathcal{B}_{\mu\nu}\mathcal{B}^{\mu\nu}, \tag{1.24}$$

$$\begin{aligned}\mathcal{L}_{\text{leptons}} &= \sum_{\ell} \overline{L}_{\ell}\, i\gamma^{\mu} \left(\partial_{\mu} - i\frac{g}{2}\sigma \cdot \mathcal{W}_{\mu} - i\frac{g'}{2}\mathcal{B}_{\mu}Y\right) L_{\ell} \\ &\quad + \sum_{\ell} \overline{E}_{\ell}\, i\gamma^{\mu} \left(\partial_{\mu} - i\frac{g'}{2}B_{\mu}Y\right) E_{\ell}, \end{aligned} \tag{1.25}$$

where ℓ is the generational index and runs over e, μ, τ, and

$$\begin{aligned}\mathcal{L}_{\text{quarks}} &= \sum_{A} \overline{q}_{A}\, i\gamma^{\mu} \left(\partial_{\mu} - i\frac{g}{2}\sigma \cdot \mathcal{W}_{\mu} - i\frac{g'}{2}\mathcal{B}_{\mu}Y\right) q_{A} \\ &\quad + \sum_{A} \overline{u}_{A}\, i\gamma^{\mu} \left(\partial_{\mu} - i\frac{g'}{2}\mathcal{B}_{\mu}Y\right) u_{A} \\ &\quad + \sum_{A} \overline{d}_{A}\, i\gamma^{\mu} \left(\partial_{\mu} - i\frac{g'}{2}B_{\mu}Y\right) d_{A}, \end{aligned} \tag{1.26}$$

where A being the generation index of quarks, runs over $1, 2, 3$ (previously mentioned). The objects in parentheses in Eqs. 1.25 and 1.26 are the *covariant derivatives* ($\mathcal{D}_{\mu}$).

The $\mathcal{L}_{\text{gauge}}$ describes four massless electroweak gauge bosons, *viz.* $\mathcal{W}^1_{\mu}$, $\mathcal{W}^2_{\mu}$, $\mathcal{W}^3_{\mu}$, $\mathcal{B}_{\mu}$. Mass terms such as $\frac{1}{2}m^2\mathcal{W}_{\mu}\mathcal{W}^{\mu}$ and $\frac{1}{2}m^2\mathcal{B}_{\mu}\mathcal{B}^{\mu}$ are prohibited by gauge symmetry. On the other hand, massless gauge fields interact in infinite range[3]. In Nature, only electromagnetism matches with this criteria with the respective gauge field called the *photon*. Moreover, the gauge symmetry forbids fermion mass terms of the form $m_f\bar{\psi}\psi = m_f(\bar{\psi}_{\text{R}}\psi_{\text{L}} + \bar{\psi}_{\text{L}}\psi_{\text{R}})$ in Eqs. 1.25 and 1.26, where ψ_{L} is left-handed fermion doublet and ψ_{R} is right-handed fermion singlet. The left-chiral and right-chiral components of the fields transform differently under gauge symmetry, *i.e.*

$$\text{left} - \text{handed doublet}: \;\; \psi_L \rightarrow \psi'_L = e^{i\mathcal{W}^a \cdot T_a \,+\, i\alpha Y}\psi_L,$$

$$\text{right} - \text{handed singlet}: \;\; \psi_R \rightarrow \psi'_R = e^{i\alpha Y}\psi_R.$$

This means the mass terms are not invariant under $SU(2)_L \times U(1)_Y$ *rotations*.

The masses of gauge bosons (except photon) and chiral fermions can be generated in a very unique way. We demand that gauge symmetries are respected everywhere except at vacuum state. The *mechanism* of generation of masses keeping intact the gauge invariance of the theory which is only broken by vacuum state, is called the *spontaneous breaking of the gauge symmetry*. This mechanism will be discussed elaborately in the next Sec. 1.2. This idea of symmetry breaking was first proposed by Nambu in the context of superconductivity, later Nambu and Jona-Lasinio suggested the idea of generation of masses of elementary particles in a similar manner [15, 16]. Goldstone then suggested a theorem of the existence of a massless particle in spontaneous symmetry breaking (SSB) [17], the general proof was shown in relativistic theory [18]

[3]However, massless gluon fields mediate the short range strong force. We will soon discuss on it.

by Goldstone, Salam and Weinberg. In particle physics this is called the *Higgs mechanism* [19–22] which is a relativistic generalization of the Ginzburg-Landau theory [23] of superconductivity.

Now, let us focus on the strong interaction part of the SM. This part, as previously mentioned, is called *Quantum Chromodynamics* or QCD which is governed by the $SU(3)_c$ gauge group. Here 'c' stands for the color charge. Quarks are the only matter fields which interacts strongly. Each flavor of quark has three color states. Leptons do not carry color charge and therefore do not participate in the strong interactions. They are singlets under the $SU(3)$ transformation. The Lagrangian density for $SU(3)$ gauge group can be written as [24–26]

$$\mathcal{L}_{QCD} = -\frac{1}{4}\mathcal{G}^p_{\mu\nu}\mathcal{G}^{p\mu\nu} + \sum_k \bar{q}_{k\alpha}\left(i\,\not{\mathcal{D}}^\alpha_\beta - m_q\right) q^\beta_k, \tag{1.27}$$

with

$$\mathcal{G}^p_{\mu\nu} = \partial_\mu \mathcal{G}^p_\nu - \partial_\nu \mathcal{G}^p_\mu + g_s f'^{\,pqm}\, \mathcal{G}^q_\mu\, \mathcal{G}^m_\nu \tag{1.28}$$

where, $\mathcal{G}^p_{\mu\nu}$ is the field strength tensor for the gluon fields $\mathcal{G}^p_\mu$, $p = 1, \ldots, 8$ and g_s is the QCD gauge coupling constant. There are eight generators λ^p of $SU(3)_c$ group mediate strong interaction among quarks. The structure constants $f'^{\,pqm}$ $(p, q, m = 1, \ldots, 8)$ are defined by

$$[\lambda^p, \lambda^q] = 2i f'^{\,pqm}\lambda^m, \tag{1.29}$$

where the λs are normalized by $\mathrm{Tr}\,(\lambda^p\lambda^q) = 2\delta^{pq}$, and $\mathrm{Tr}\,([\lambda^p, \lambda^q]\lambda^m) = 4i f'^{\,pqm}$.

The first term in the Lagrangian (Eq. 1.27) gives the self-interactions of gluons and $\mathcal{D}^\alpha_\beta$ corresponds to the covariant derivative for quarks; q_k is the 'k'th quark flavor; $\alpha, \beta = 1, 2, 3$ are color indices $(q_{\text{red}}, q_{\text{green}}, q_{\text{blue}})$ and

$$\mathcal{D}^\alpha_{\mu\beta} = (\mathcal{D}_\mu)_{\alpha\beta} = \partial_\mu\delta_{\alpha\beta} - i g_s\, G^k_\mu\, L^k_{\alpha\beta}, \tag{1.30}$$

where $L^k = \lambda^k/2$ in the fundamental representation and λ^ks are the 3×3 traceless Gell-Mann matrices:

$$\lambda^1 = \begin{pmatrix} 0 & 1 & 0 \\ 1 & 0 & 0 \\ 0 & 0 & 0 \end{pmatrix}, \quad \lambda^2 = \begin{pmatrix} 0 & -i & 0 \\ i & 0 & 0 \\ 0 & 0 & 0 \end{pmatrix}, \quad \lambda^3 = \begin{pmatrix} 1 & 0 & 0 \\ 0 & -1 & 0 \\ 0 & 0 & 0 \end{pmatrix}, \quad \lambda^4 = \begin{pmatrix} 0 & 0 & 1 \\ 0 & 0 & 0 \\ 1 & 0 & 0 \end{pmatrix},$$

$$\lambda^5 = \begin{pmatrix} 0 & 0 & -i \\ 0 & 0 & 0 \\ i & 0 & 0 \end{pmatrix}, \quad \lambda^6 = \begin{pmatrix} 0 & 0 & 0 \\ 0 & 0 & 1 \\ 0 & 1 & 0 \end{pmatrix}, \quad \lambda^7 = \begin{pmatrix} 0 & 1 & 0 \\ 1 & 0 & -i \\ 0 & i & 0 \end{pmatrix}, \quad \lambda^8 = \frac{1}{\sqrt{3}}\begin{pmatrix} 1 & 0 & 0 \\ 0 & 1 & 0 \\ 0 & 0 & -2 \end{pmatrix}.$$

The transformations of quarks and gluons under the $SU(3)$ gauge transformation are given by

$$\psi_{\rm q} \to \psi_{\rm q}{}' = e^{i\alpha^a\, L^a}\psi_{\rm q},$$

$$\mathcal{G}^p_\mu \to \mathcal{G}^p_\mu + (1/g)\partial_\mu\alpha^p + f'^{\,pqm}\mathcal{G}^q_\mu\alpha^m.$$

The color interactions are purely vector like and hence parity conserving. These interactions are diagonal in the flavor indices. In addition, there exist ghost fields and respective gauge-fixing terms which help in the quantization of the $SU(3)$ as well as in the electroweak part of the theory. In QCD, at high energies the coupling becomes weak, enabling perturbative study at these energy scales or at short distances and implying the asymptotic freedom [27, 28]; whereas, at low energies or at large distances it becomes strongly coupled [29] which is sometimes termed as *infrared slavery*, leading to the confinement of quarks and gluons. The confinement of quarks and gluons gives rise to a complicated scenario of non-perturbative phenomenon.

The theoretical picture of QCD described above has been rigorously verified by multitude of collider experiments. The scaling of structure functions in the deep inelastic collisions of nucleons furnished the first signatures of hadronic substructure where parton model of hadrons was invoked to explain this phenomenon. The scaling violations, that were discovered later, provided the indirect hint of perturbative QCD. All particle interactions of the SM have been shown in Fig. 1.2.

1.2 Brout-Englert-Higgs Mechanism

Higgs proposed the idea of generating mass in particle physics in a relativistic invariant way [20, 21]. Though that treatment was purely classical. At that time, Brout and Englart demonstrated that the same idea could be incorporated in non-Abelian models as well [19]. Guralnik, Hagen and Kibble showed the different formalism how to evade Goldstone theorem [22]. The idea of generating masses of the gauge bosons was exhibited first time by Weinberg and Salam [3, 4]. Finally, the proof of renormalizability of such a spontaneously broken gauge theory was provided by 't Hooft [30, 31]. In this way, along with the Glashow's idea [1] of extending the gauge group from $SU(2)_L$ to $SU(2)_L \otimes U(1)_Y$ (thus giving a unified picture of the electromagnetic and weak interactions), the work of Weinberg and Salam marked the completion of the Standard Model of the particle physics [3, 4] (also known as *Glashow-Weinberg-Salam model*) where the gauge bosons and the fermions acquire their masses via the *Brout-Englert-Higgs mechanism* (BEH mechanism).

Let us introduce a complex scalar in this context. Since we intend the Lagrangian to retain all its symmetries, we can only add $SU(2)_L \otimes U(1)_Y$ multiplets. So the complex scalar is an

isospin doublet, *i.e.* it is a left-handed doublet with weak isospin 1/2. The electric charges of the upper and the lower component of the doublet are chosen to ensure that the hypercharge or $U(1)$ charge is $Y = +1$. This requirement is very essential and important for reasons that will become more evident later. The scalar doublet is given by

$$\Phi = \begin{pmatrix} \phi^+ \\ \phi^0 \end{pmatrix} = \begin{pmatrix} \frac{1}{\sqrt{2}}(\phi_1 + i\phi_2) \\ \frac{1}{\sqrt{2}}(\phi_3 + i\phi_4) \end{pmatrix}. \tag{1.31}$$

The Lagrangian for the field Φ which is gauge invariant may be written as,

$$\mathcal{L}_\Phi = (\mathcal{D}^\mu \Phi)^\dagger (\mathcal{D}_\mu \Phi) - V(\Phi), \tag{1.32}$$

where $V(\Phi)$ is the scalar potential given by

$$V(\Phi) = \frac{1}{2}\mu_h^2 \left(\sum_{i=1}^{4} \phi_i^2 \right) + \frac{1}{4}\lambda_h \left(\sum_{i=1}^{4} \phi_i^2 \right)^2. \tag{1.33}$$

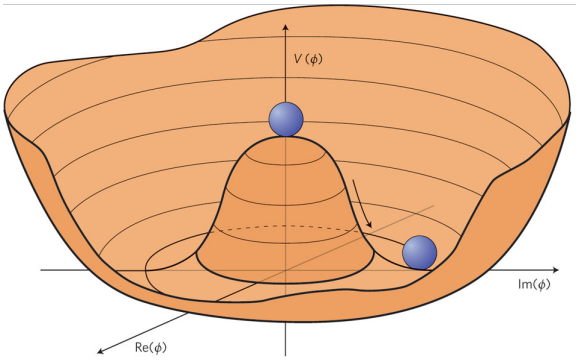

FIGURE 1.3: The Higgs potential in the Standard Model.

The Higgs potential in Eq. 1.33, for $\mu_h^2 < 0$, takes the form depicted in Fig. 1.3. Any choice of the vacuum that breaks a symmetry will generate the masses of the gauge bosons in the SM. We choose $\phi_1 = \phi_2 = \phi_4 = 0$ and $\phi_3 = v$:

$$\text{Vacuum} = \Phi_0 = \frac{1}{\sqrt{2}} \begin{pmatrix} 0 \\ v \end{pmatrix} \tag{1.34}$$

This vacuum defined in such a way is electrically neutral since $T_3 = -\frac{1}{2}$ and with our choice of $Y = +1$ we have $Q = T_3 + \frac{1}{2}Y = 0$. This choice of the vacuum breaks $SU(2)_L \otimes U(1)_Y$, but leaves $U(1)_{\text{EM}}$ invariant, leaving only the photon massless and results in the breaking of the gauge symmetry at the vacuum state.

Let us consider an infinitesimal rotation of Φ as $(1 + i\alpha R)\Phi_0 = \Phi_0$ and invariance implies $R\Phi_0 = 0$, where R is associated with some kind of *rotation*. The status of $SU(2)_L$, $U(1)_Y$ and $U(1)_{\text{EM}}$ generators under symmetry breaking are:

$$SU(2)_L: \qquad \sigma_1 \Phi_0 = \begin{pmatrix} 0 & 1 \\ 1 & 0 \end{pmatrix} \frac{1}{\sqrt{2}} \begin{pmatrix} 0 \\ v \end{pmatrix} = +\frac{1}{\sqrt{2}} \begin{pmatrix} v \\ 0 \end{pmatrix} \neq 0 \rightarrow \text{broken}. \tag{1.35}$$

$$\sigma_2\Phi_0 = \begin{pmatrix} 0 & -i \\ i & 0 \end{pmatrix} \frac{1}{\sqrt{2}} \begin{pmatrix} 0 \\ v \end{pmatrix} = -\frac{i}{\sqrt{2}} \begin{pmatrix} v \\ 0 \end{pmatrix} \neq 0 \rightarrow \text{broken.} \tag{1.36}$$

$$\sigma_3\Phi_0 = \begin{pmatrix} 1 & 0 \\ 0 & -1 \end{pmatrix} \frac{1}{\sqrt{2}} \begin{pmatrix} 0 \\ v \end{pmatrix} = -\frac{1}{\sqrt{2}} \begin{pmatrix} 0 \\ v \end{pmatrix} \neq 0 \rightarrow \text{broken.} \tag{1.37}$$

$$U(1)_Y : \qquad Y\Phi_0 = \begin{pmatrix} 1 & 0 \\ 0 & 1 \end{pmatrix} \frac{1}{\sqrt{2}} \begin{pmatrix} 0 \\ v \end{pmatrix} = +\frac{1}{\sqrt{2}} \begin{pmatrix} 0 \\ v \end{pmatrix} \neq 0 \rightarrow \text{broken.} \tag{1.38}$$

This implies that all the four gauge bosons ($\mathcal{W}^1, \mathcal{W}^2, \mathcal{W}^3$ and $\mathcal{B}$) acquire their masses through the Higgs mechanism, while for the photon to remain massless the $U(1)_{\text{EM}}$ symmetry should leave the vacuum invariant and indeed:

$$U(1)_{\text{EM}} : \qquad Q\Phi_0 = \frac{1}{2}(\sigma_3 + Y)\Phi_0 = \begin{pmatrix} 1 & 0 \\ 0 & 0 \end{pmatrix} \frac{1}{\sqrt{2}} \begin{pmatrix} 0 \\ v \end{pmatrix} = 0 \rightarrow \text{unbroken.} \tag{1.39}$$

So $U(1)_{\text{EM}}$ is conserved as the vacuum is neutral and we have:

$$\Phi_0 \rightarrow e^{i\alpha Q}\Phi_0 = \Phi_0 \tag{1.40}$$

Let us introduce the physical scalar Φ' defined by the relation

$$\Phi = \frac{1}{\sqrt{2}} \begin{pmatrix} 0 \\ v \end{pmatrix} + \Phi', \tag{1.41}$$

where $\langle 0|\Phi'|0\rangle = 0$. The field Φ cannot be treated as quantum field since its VEV is non-zero and so it cannot be expanded as creation and annihilation operators. In that sense Φ' is quantum field. Alternatively, Φ can be written as [32]

$$\Phi = \frac{1}{\sqrt{2}} e^{i\sum \xi^a \frac{1}{2}\sigma^a} \begin{pmatrix} 0 \\ v + h \end{pmatrix}. \tag{1.42}$$

Here h is the physical Higgs scalar. The ξ^a are the massless pseudoscalars Nambu-Goldstone bosons [15–18,33] that are associated with broken symmetry generators. These are the unphysical fields in the theory. The ξ field is the phase of the field Φ. We know any phase, even if, it is a spacetime dependent one, is irrelevant because of local $U(1)$ symmetry. For some specific choice of gauge, we can have

$$\Phi \rightarrow \tilde{\Phi} = e^{-i\sum \xi^a \frac{1}{2}\sigma^a}\Phi = \frac{1}{\sqrt{2}} \begin{pmatrix} 0 \\ v + h \end{pmatrix}, \tag{1.43}$$

which in turn implies the disappearance of the ξ field from the Lagrangian. The Lagrangian then contains only physical fields and the gauge in which these unphysical fields disappear from

the physical spectrum is called *unitary gauge*. The scalar degrees of freedom have been *eaten up* by the gauge bosons and increase the longitudinal degrees of freedom, thus creating the masses of the gauge bosons. The covariant derivative of Φ can be written as

$$\mathcal{D}_\mu \tilde{\Phi} = \left(\partial_\mu - i\frac{g}{2}\sigma \cdot \mathcal{W}_\mu - i\frac{g'}{2}\mathcal{B}_\mu Y\right)\tilde{\Phi}. \tag{1.44}$$

The gauge boson mass terms come from the square of Eq. 1.44, evaluated at the vacuum expectation value of the scalar field:

$$(\mathcal{D}_\mu \tilde{\Phi})^\dagger (\mathcal{D}^\mu \tilde{\Phi}) \Rightarrow \frac{1}{2}(0\ v)\left[\frac{g}{2}\sigma^a \mathcal{W}^a_\mu + \frac{g'}{2}\mathcal{B}_\mu\right]^2 \begin{pmatrix} 0 \\ v \end{pmatrix} + h \text{ terms}, \tag{1.45}$$

where the interactions and mass terms involving the physical h field have been clubbed together as the 'h terms'. If we simplify the above expression explicitly, we find

$$\Delta\mathcal{L} = \frac{1}{2}\frac{v^2}{4}\left[g^2\{(\mathcal{W}^1_\mu)^2 + (\mathcal{W}^2_\mu)^2\} + (-g\mathcal{W}^3_\mu + g'\mathcal{B}_\mu)^2\right]. \tag{1.46}$$

After the spontaneous breaking of the electroweak gauge group, the third component of the $SU(2)_L$ gauge field $\mathcal{W}^3_\mu$ and the $U(1)_Y$ gauge field $\mathcal{B}_\mu$ have identical quantum numbers and they get mixed in the Higgs kinetic term. The three massive vector bosons are given by:

$$W^\pm_\mu = \frac{1}{\sqrt{2}}(\mathcal{W}^1_\mu \mp i\mathcal{W}^2_\mu) \quad \text{with mass} \quad M_W = \frac{gv}{2}; \tag{1.47}$$

$$Z_\mu = \frac{1}{\sqrt{g^2+g'^2}}\left(g\mathcal{W}^3_\mu - g'\mathcal{B}_\mu\right) \quad \text{with mass} \quad M_Z = \frac{\sqrt{g^2+g'^2}}{2}v; \tag{1.48}$$

The fourth vector field, orthogonal to Z_μ is the photon field which remains massless:

$$A_\mu = \frac{1}{\sqrt{g^2+g'^2}}\left(g'\mathcal{W}^3_\mu + g\mathcal{B}_\mu\right) \qquad \text{with mass} \quad M_A = 0. \tag{1.49}$$

The covariant derivative in terms of mass-eigenstates can be written as

$$\begin{aligned}\mathcal{D}_\mu &= \partial_\mu - i\,g(W^+_\mu T^+ + W^-_\mu T^-) - i\frac{1}{\sqrt{g^2+g'^2}}Z_\mu\left(g^2T^3 - g'^2\frac{Y}{2}\right) \\ &\quad -i\frac{g\,g'}{\sqrt{g^2+g'^2}}A_\mu(T^3 + \frac{Y}{2}),\end{aligned} \tag{1.50}$$

with

$$T^\pm = \frac{1}{\sqrt{2}}(T^1 \pm iT^2) = \frac{1}{2}\sigma^\pm. \tag{1.51}$$

It is evident that the last term in Eq. 1.50 shows that the massless photon field A_μ couples to the gauge generator $(T^3 + \frac{Y}{2})$ which is nothing but the electric charge quantum number Q; hence the coefficient of the electromagnetic interaction which is the last term of Eq. 1.50 can be

identified with the electron charge e by

$$e = \frac{gg'}{\sqrt{g^2 + g'^2}}. \tag{1.52}$$

To further simplify the expression of Eq. 1.50, let us define the *weak-mixing angle* θ_W which is the mixing angle of the basis $(\mathcal{W}^3_\mu,\ \mathcal{B}_\mu)$ and related to the $(Z_\mu,\ A_\mu)$ basis as:

$$\begin{pmatrix} Z_\mu \\ A_\mu \end{pmatrix} = \begin{pmatrix} \cos\theta_W & -\sin\theta_W \\ \sin\theta_W & \cos\theta_W \end{pmatrix} \begin{pmatrix} \mathcal{W}^3_\mu \\ \mathcal{B}_\mu \end{pmatrix} \tag{1.53}$$

so that

$$\cos\theta_W = \frac{g}{\sqrt{g^2 + g'^2}}, \qquad \sin\theta_W = \frac{g'}{\sqrt{g^2 + g'^2}}. \tag{1.54}$$

The Z_μ coupling and then $\mathcal{D}_\mu$ can be rewritten as

$$g^2 T^3 - g'^2 \frac{Y}{2} = (g^2 + g'^2)T^3 - g'^2 Q, \tag{1.55}$$

$$\mathcal{D}_\mu = \partial_\mu - ig(W^+_\mu T^+ + W^-_\mu T^-) - i\frac{g}{\cos\theta_W} Z_\mu (T^3 - \sin^2\theta_W Q) - ieA_\mu Q, \tag{1.56}$$

with $g = e/\sin\theta_W$. Clearly, the masses of W and Z bosons are not independent, but are related by $M_W = M_Z \cos\theta_W$. The Fermi constant is related to gauge boson mass by

$$\frac{G_F}{\sqrt{2}} = \frac{g^2}{8M_W^2}, \tag{1.57}$$

where $G_F \simeq 1.16637 \times 10^{-5}\text{GeV}^{-2}$ (determined from the muon lifetime measurements). The weak scale v is given by:

$$v = \frac{2M_W}{g} \simeq (\sqrt{2}G_F)^{-1/2} \simeq 246 \text{ GeV}. \tag{1.58}$$

The fermions can have masses by Higgs mechanism. They can have gauge invariant interactions involving the Higgs bosons. To generalize for all the fermionic fields, we can write the Yukawa-type interactions as:

$$\mathcal{L}_{\text{Yukawa}} = -y^u_{jk} \bar{q}^j_L \Phi^c u^k_R - y^d_{jk} \bar{q}^j_L \Phi d^k_R - y^l_{jk} \bar{L}^j_L \Phi E^k_R + \text{h.c.} \tag{1.59}$$

where, $\Phi^c = i\sigma_2 \Phi^*$; j, k represent the generational index and y^u, y^d, y^l are the respective up-quark, down-quark and charged lepton Yukawa coupling matrices. After spontaneous symmetry breaking the general form of the mass term of leptons can be written as $m_f \overline{\psi}_L \psi_R$ with the mass matrices $(\text{m}_u)_{jk} \propto y^u_{jk} v$, $(\text{m}_d)_{jk} \propto y^d_{jk} v$, $(\text{m}_l)_{jk} \propto y^l_{jk} v$ [4]. These mass matrices are in the

[4]The mass terms of the fermions also break the chiral symmetry of the theory.

flavor basis, and not in the mass basis. Due to absence of right-handed counterpart the neutrino remains massless in the SM.

1.3 Present Experimental Status of the Standard Model

1.3.1 The Higgs

The observations from the collider experiments at center of mass (c.m.) energy $\sqrt{s} \leq 1$ TeV have profoundly consolidated the Standard Model. The last milestone in the high energy frontier has been the discovery of the Higgs boson at the LHC [34, 35] which marks the completion of the Standard Model (SM) of particle physics. The path towards the discovery of the Higgs boson has been gone through many experiments, much more data have been scrutinized, and hence there is hardly any sign of anomaly in the Higgs measurements. Precisely, it has been tested through all its dominant production modes (gluon fusion, fusion of vector boson, W or Z Higgstrahlung, and $t\bar{t}H$ production) and also through the most sensitive decays of Higgs boson at the Large Hadron Collider (LHC): $\gamma\gamma$, WW, $\tau\tau$, 4-leptons and $b\bar{b}$. One of the agreed measurement with the theoretical expectations is the signal strength μ which is defined as the observed cross-section times the branching fraction of a process divided by the SM expectation of that process.

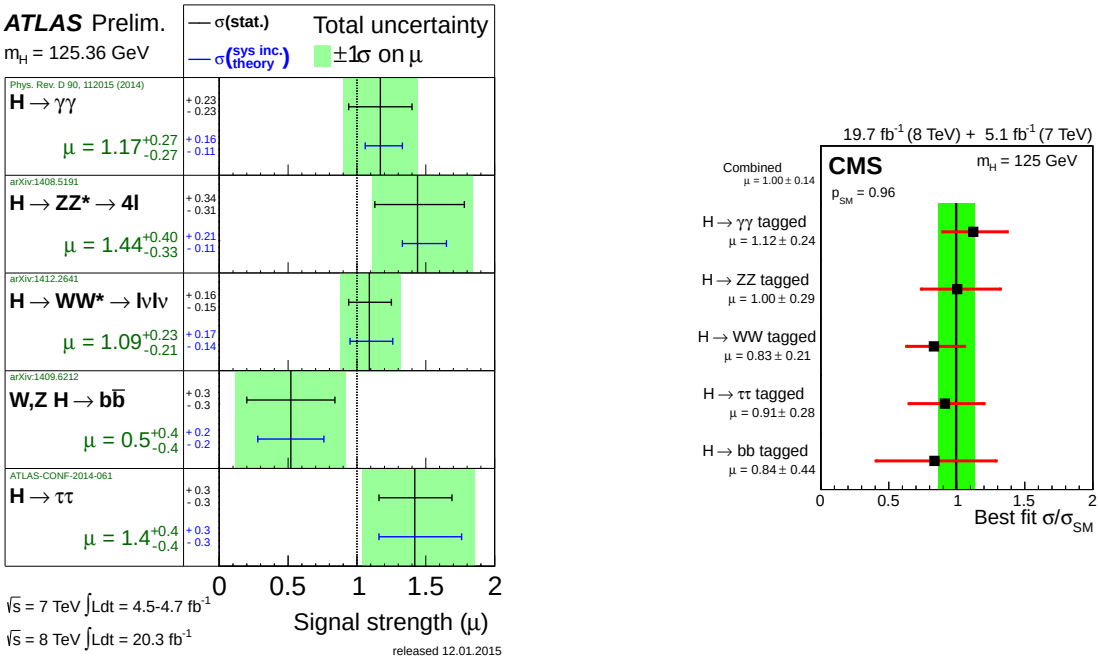

FIGURE 1.4: The measurement of the signal strengths $\mu = \sigma/\sigma_{\rm SM}$ of the various decay channels of Higgs by the experiments ATLAS [36] (left) and CMS [37] (right).

Fig. 1.4 shows the signal strengths of the various decay channels analyzed by both ATLAS and CMS at 25 fb^{-1} integrated luminosity and at c.m. energy $\sqrt{s} = 7 - 8$ TeV corresponding to a production of about 10^6 Higgs boson in the dominant production modes. More concretely, the

results are consistent with the SM within 1σ. By the year 2022, the LHC is expected to produce around 300 fb^{-1} integrated luminosity at c.m. energy of $\sqrt{s} = 13 - 14$ TeV. There remains a fair possibility that the LHC will be upgraded into the high-luminosity LHC (HL-LHC) and expected to deliver about 3000 fb^{-1} of data at c.m. energy $\sqrt{s} = 14$ TeV by the year 2035 [38]. Fig. 1.5 shows the projected precision of signal strength by the ATLAS experiment[5].

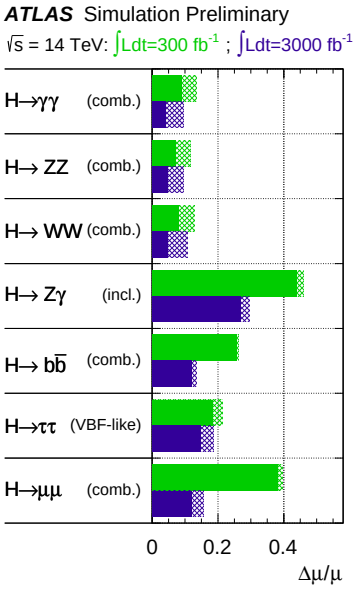

FIGURE 1.5: The ATLAS prospects for the measurements of the signal strengths of the various Higgs decay channels with integrated luminosity 300 fb^{-1} and 3000 fb^{-1} [38] by the year 2035. The hashed areas indicate the theoretical uncertainties.

1.3.2 Other Aspects

Earlier, the electroweak theory was formulated mainly in the context of β decay; to put it in another way, the construction of this theory was based on the experimental evidences of the charged-current weak interactions. The Fermi theory of these weak interactions had been developed and tested experimentally prior to the formulation of the SM[6]. The detailed analysis of unitarity of four-fermion interactions ($\nu_\mu + e^- \to \nu_e + \mu^-$) showed that the momenta of initial state fermions should be less than ~ 300 GeV [39]. This necessitated the effective Lagrangian $\mathcal{L}_{\text{eff}}$ should be modified at high momentum transfer, *i.e.* at small distance. Some agents are needed to transmit the action of a current from one point (say, x) to another point (say, x')

[5] In these Figs. 1.4 and in 1.5, H is basically the SM Higgs h according to the notation used in this thesis.

[6] Before the construction of the SM, the effective Lagrangian was considered to have the form as $\mathcal{L}_{\text{eff}} = \mathcal{L}_{jj} + \mathcal{L}_{\mathcal{J}i} + \mathcal{L}_{\mathcal{J}\mathcal{J}}$ [39]. Here, $\mathcal{L}_{jj}$ corresponds to purely leptonic part such as muon decay, $\mathcal{L}_{\mathcal{J}i}$ stands for all partial leptonic interactions such as β decay and $\mathcal{L}_{\mathcal{J}\mathcal{J}}$ represents all the leptonic weak interactions such as $\Lambda^0 \to p + \pi^-$. In these Lagrangians, all the corresponding currents were taken at the same spacetime point x.

to generate such "effective" nonlocality[7]. This gave the possibility to assume the existence of heavy massive charged gauge bosons. The smallest unitary group which contains an off-diagonal generator (corresponding to the charged gauge boson) is $SU(2)$ with the relevant generators σ_1 and σ_2. To explain the infinite range electromagnetic interaction a massless gauge boson has to be incorporated. Only σ_3 would not serve the purpose since that would lead to a contradiction of charge assignment of particles. More precisely, the next simplest construction was to take $SU(2) \times U(1)$, instead of $SU(2)$.

The weak neutral current (WNC) was discovered in 1973 by the Gargamelle collaboration at CERN [40–42] and by HPW (Harvard-Pennsylvania-Wisconsin) group at Fermilab [43]. The structure of the WNC has been verified in many processes including (purely weak) neutrino scattering such as $\nu e \to \nu e$; weak-electromagnetic interference, atomic parity violation and in polarized Möller scattering. The W and Z bosons were discovered at CERN by the UA1 [44] and UA2 [45] groups in 1983. Even the measurements of their masses have been in excellent agreement with the SM expectations. The LEP II runs profoundly verified the SM gauge group with the non-abelian nature as well as the spontaneous symmetry breaking of the gauge group [46]. The LEP and SLC allowed tests of the SM at a precision of $\sim 10^{-3}$. The four LEP experiments ALEPH, DELPHI, L3, and OPAL at CERN produced some 2×10^7 Z's at the Z-pole in the reactions $e^+e^- \to Z \to l^+l^-/q\bar{q}$ [47, 48]. The SLD experiment at SLAC had a relatively smaller number of production of Z's $\sim 10^5$ but had the significant advantage of the high polarization ($\sim 75\%$) of the e^- beam [47, 48]. One important aspect about the Z factories was the most precise measurements of the number of light neutrino types N_ν which comes from the studies of Z production in e^+e^- collisions. The Z boson decays into quarks and charged leptons. The invisible width is assumed to be due to N_ν light neutrino species each contributing to $\Gamma_{\rm inv}$, which is estimated by subtracting the measured visible partial widths corresponding to Z decays into quarks and charged leptons, from the total Z width as given by the Standard Model. The combined results from four LEP experiments give the stringent constraint on the number of ordinary neutrinos as $N_\nu = 2.9841 \pm 0.0083$ [46], which consequently gave the hint of the existence of the three generation flavor structure of the SM. On the other hand, the study of charged current interactions is now based on the study of Cabibbo-Kobayashi-Maskawa (CKM) matrix which measures the mismatch between the family structure of the left-handed u-type and d-type quarks. The magnitudes of $|V_{ij}|$ for CKM elements has been given in previous section (Eq. 1.19).

The SM has also been verified at high level accuracy beyond the tree level. Experimental measurements on the Z-pole at LEP has tested the radiative corrections to the gauge boson propagators at high precision. There are four two-point functions: $\Pi_{\gamma\gamma}(q^2)$, $\Pi_{\gamma Z}(q^2)$, $\Pi_{ZZ}(q^2)$, $\Pi_{WW}(q^2)$, where the measurements have been made at two energy scales: $q^2 = 0, M_Z^2$. So

[7] The $\mathcal{L}_{\rm eff}$ can be replaced by $\int [j_\lambda(x)]^*_\mu S(x-x')[j_\lambda(x')]_e \, dx' + \ldots$; where $j_\lambda(x)$ being the corresponding current density at that point x and $S(x-x')$ being the scattering wave amplitude [39].

there are eight two-point correlators, corresponding to four types at two different energy scale. Ward identity ensures $\Pi_{\gamma\gamma}(0) = \Pi_{\gamma Z}(0)$. From remaining six, three linear combinations can be absorbed in the redefinition of the parameters: Fine-structure constant, Fermi coupling (extracted from muon decay) and M_Z [49]. The remaining three combinations are called the Peskin-Takeuchi parameters or oblique corrections or S, T and U parameters [50].

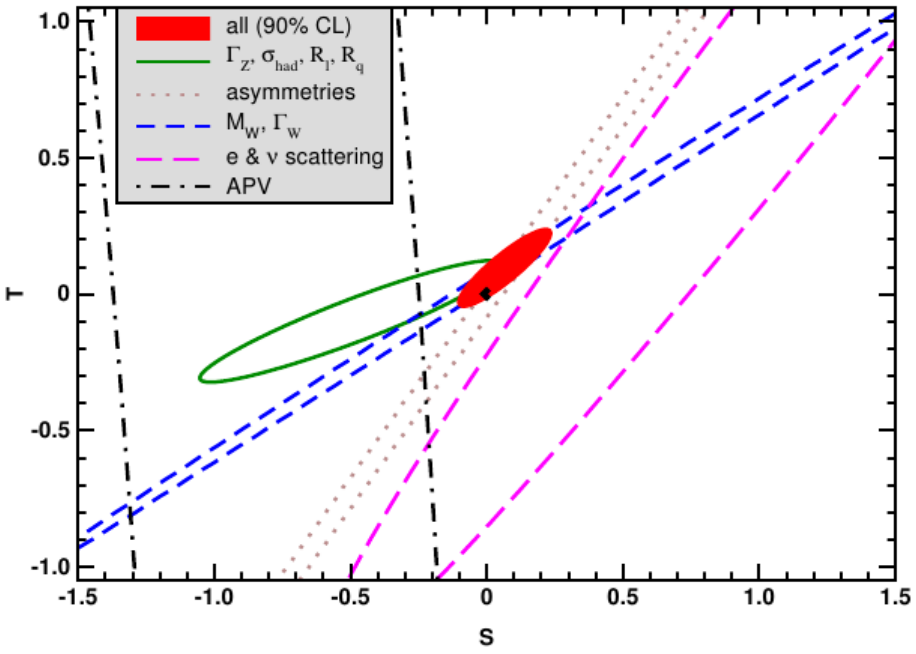

FIGURE 1.6: 1σ constraints (39.35% for the closed contours and 68% for the others) in the TS plane. S and T represent the contributions of new physics only. The black dot indicates the Standard Model values $S = T = 0$ [5].

The T parameter is proportional to the difference between the Z and W self-energies at $q^2 = 0$, while S and $(S + U)$ are associated with the difference between the Z and W self-energy at $q^2 = M^2_{Z/W}$ and $q^2 = 0$ respectively. S, T and U parameters are correlated. The most recent fit to the electroweak precision data gives [5],

$$S = 0.05 \pm 0.11, \qquad T = 0.09 \pm 0.13, \qquad U = 0.01 \pm 0.11. \tag{1.60}$$

Fixing $U = 0$ (same as in Fig. 1.6) moves S and T slightly upwards,

$$S = 0.07 \pm 0.08, \qquad T = 0.10 \pm 0.07, \tag{1.61}$$

with T having a 1.5σ deviation from zero [5]. Fig. 1.6 shows the allowed region in the $T - S$ plane. The SM contributions have been subtracted from the parameter, *i.e.* $S \to S_{\rm exp} - S_{\rm SM}$ and $T \to T_{\rm exp} - T_{\rm SM}$. The SM point on this plane is the origin $(0, 0)$. Evidently, this is in good

agreement with experimental bounds and hence sets strong constraints on any extension of the SM.

1.4 Shadows over the SM

SM has been immensely successful model in explaining many experimental observations regarding particle interactions, but it suffers from a few shortcomings. Some of these issues have been discussed below.

1.4.1 Gauge-Hierarchy Problem

Let us take a simple example of interaction of a single fermion ψ coupled to a massive scalar ϕ. The Lagrangian is given by

$$\mathcal{L} = i\bar{\psi}\gamma_\mu\partial^\mu\psi + \frac{1}{2}\partial^\mu\phi\partial_\mu\phi - \lambda_f\bar{\psi}\psi\phi - \frac{m_s^2}{2}\phi^2 - \frac{\lambda}{4}\phi^4. \tag{1.62}$$

After the spontaneous symmetry has been broken, the fermion gets mass $m_f = \lambda_f v/\sqrt{2}$. The corrections of fermion mass is shown in Fig. 1.7 (a), *i.e.* it is given by one loop correction to the fermionic propagators due to scalar particle. The corrected mass is given by

$$m_f(\text{new}) = m_f + \delta m_f. \tag{1.63}$$

The correction depends on the cutoff Λ of the theory:

$$\delta m_f = -\frac{3\lambda_f^2 m_f}{32\pi^2}\ln\frac{\Lambda}{m_f} + \cdots \tag{1.64}$$

where, $\cdots$ indicates terms independent of Λ. The correction to the mass of the fermion depends explicitly on m_f. In the limit where the fermion masses are very small, the Lagrangian 1.62 is invariant under chiral transformations. The decreasing fermion mass increases the symmetry of the theory and hence it is said that the fermion masses are protected by the *chiral symmetry*.

Similarly, we can compute corrections to the scalar propagator due to the fermion loop and scalar loop as shown in Figs. 1.7 (b-c). Considering, Figs. 1.7 (b) and (c) the scalar obtains a correction as

$$\delta m_s^2 = \frac{\Lambda^2}{16\pi^2}(-2\lambda_f^2 + \lambda). \tag{1.65}$$

Unlike the corrections for fermionic mass, the mass correction for a scalar particle is found to be quadratically divergent. For this reason, nothing can actually protect the mass of the scalar

particle which has very large mass corrections. If we assume the theory to be valid up to the Planck scale ($M_{Pl} \sim 10^{19}$ GeV), *i.e.* scale at which the quantum corrections to gravity become important, corrections to the scalar particles will be of that order of magnitude. If the mass of the particle and its correction are not at most of the same order, the theory is said to have a *naturalness* problem. The same thing happens for the SM Higgs boson.

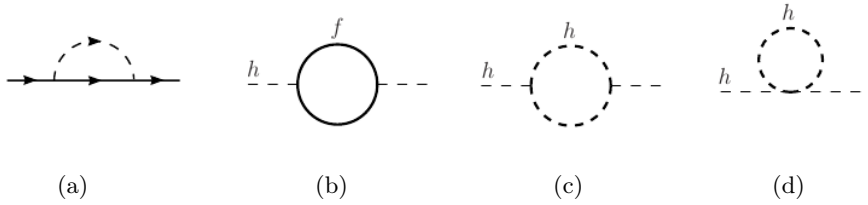

FIGURE 1.7: One-loop quantum corrections to the fermion mass (a) and to the Higgs mass (b, c, d) in the SM.

The radiative corrections to the fermions or the gauge bosons are always proportional to their masses and hence one cannot generate the masses of these fields purely from radiative contributions. This happens because there is a mismatch in the degrees of freedom of a massive and massless gauge boson or fermion. In the case of fundamental scalars, the situation is entirely different; Eq. 1.65 reflects the fact that one can generate their masses radiatively even if they are massless at tree level. So, all in all, there is a lack of symmetry that can protect the Higgs mass. Furthermore, the large hierarchy between the weak scale and the Planck scale makes it difficult to explain the light Higgs mass (~ 125 GeV) within the SM. This is known as the *gauge hierarchy problem* which is, in principle, a naturalness issue with the SM.

1.4.2 Neutrino Mass and Fermion Mass Hierarchy Problem

In the SM, neutrinos have exactly zero mass since there is no right-handed neutrino. With no suitable right-handed partner, it is impossible to explain the existence of masses of neutrinos. Measurements of neutrino oscillations signify that neutrinos spontaneously change flavors which in turn implies that they have non zero masses. However, the measurements of the neutrino oscillation probabilities shed lights on the mass-squared difference of the different flavors of the neutrinos and not on the absolute masses of neutrinos. The best constraint on the absolute mass of the neutrinos has been obtained from the precision measurements of tritium decay which provides an upper limit as 2 eV on the mass on electron-neutrinos (ν_e) [51]. Clearly, neutrinos have masses at least seven orders of magnitude lighter than that of the electron in the SM. Another issue that is not well explained by the SM is related to the hierarchical pattern of the fermion masses.

Experimentally, the CKM matrix is constrained and follows a hierarchy. In principle, the SM gives no prediction for the hierarchy observed in the CKM matrix. This hierarchy is related to the hierarchy obtained from the experimental values for the masses of the fermions. Since the fermion masses are generated from the *spontaneous symmetry breaking mechanism*, it is unnatural to obtain masses with so different order of magnitude. For instance, the ratio $m_{\text{electron}}/m_{\text{top}}$ is of the order of 3×10^{-6}. This issue is usually known as the *fermion mass hierarchy*. These altogether necessitate an extension of the Standard Model and indicates the existence of new physics at the TeV scale.

1.4.3 Strong CP Problem

CP symmetry is the combination of charge conjugation (C) and parity (P). Though both symmetries hold for electromagnetic interactions they are separately violated in weak interactions [52, 53]. To ameliorate the problem of individual C and P violations, CP symmetry had been proposed. Experimentally, the CP violation has been discovered in 1964 by Cronin and Fitch by the experiments with K^0 [54, 55]. Later the violation of CP symmetry in case of B mesons has been observed [56–58]. If we consider the QCD Lagrangian, one can add a CP violating term $\frac{\theta}{32\pi^2} g_s^2 \mathcal{G}_{\mu\nu}\tilde{\mathcal{G}}^{\mu\nu}$ to the Lagrangian, where $\tilde{\mathcal{G}}_{\mu\nu} = \epsilon_{\mu\nu\alpha\beta}\mathcal{G}^{\alpha\beta}$ is the dual field and θ is an arbitrary dimensionless parameter [59]. One cannot make the term zero by simply setting the θ to zero, since weak interaction corrections result in a shift in θ by $\delta\theta|_{\text{weak}} \sim 10^{-3}$ which in turn requires a fine-tuned cancellation among the tree and the weak contributions. This issue is known as *strong CP problem*. The best possible theory has been introduced by Peccei and Quinn [59, 60] to solve this issue which postulates the existence of a new particle names axion, generated from a spontaneous breaking of a new symmetry called *Peccei-Quinn symmetry* (PQ symmetry).

1.4.4 Existence of Dark Matter

From various astrophysical observations it has become evident that our universe consists of 4.9% ordinary matter (constituted out of SM particles), 26.8% dark matter (DM) and 68.3% dark energy [61]. The earliest astrophysical evidence of DM came from the study of rotation curves in spiral galaxies; it was observed that the outer constituents of the Coma cluster [62] were moving far too quickly than what can be explained by the visible cluster mass. Virial theorem can explain this observation only if one postulates that the cluster contains another large component of mass which is invisible, *viz.* dark matter. The relation between the luminosity (L) and the maximum circular velocity (v_{max}) of the constituent members of spiral galaxies $L \propto v_{\text{max}}^{\beta}$ with $\beta = 3 \sim 4$, can be explained using virial theorem only if the existence of DM is taken into account [63]. Other evidences of DM can be obtained from Gravitational lensing [64, 65] and

Bullet cluster [66]. Some of the recent experimental observations [61,67] show that the baryonic density and total matter density are different. This ensures that the DM is necessarily non-baryonic. The many evidences of existence of DM mandates that DM should have the following properties:

- DM is *electrically neutral*. Otherwise it would be able to emit photons which in turn could have modified observations from astrophysical objects, like quasars.
- The DM interacts *feebly* with baryons.
- The DM must be *stable*, *i.e.* DM must have lifetime larger than the age of the universe.
- Large scale structure formation demands the DM to be *non-relativistic*.
- DM can not be comprised of SM particles as most of them are charged. Among the SM constituents neutrinos can be a viable DM candidate. But neutrinos are very light particles, it is of the order of eV [51]. With this small mass it can not contribute significantly to the matter density of the Universe. Moreover, since the neutrinos are so light, they are still relativistic and can constitute what is called hot dark matter. This type of hot DM can not give any explanation for the galaxy formation rate of the universe after the big bang.

Thus it becomes obvious that SM can not accommodate a suitable DM candidate. The most popular examples of DM candidates are axions and WIMPs (or weakly interacting massive particles). Many BSM models like Supersymmetry and Inert Higgs Doublet Model can provide suitable DM candidate. In mininal Universal Extra Dimensional (mUED) model the first KK-level photon $\gamma^{(1)}$ (or to be precise the $\mathcal{B}^{(1)}$) is the LKP (the *lightest Kaluza-Klein particle*). The stability of LKP is mandated by the conservation of KK-parity. Various aspects of LKP as a dark matter has been discussed rigorously in Refs. [68–80]. In the case of non-minimal Universal Extra Dimensional (nmUED) model the identity of LKP is no longer fixed like the case of UED, rather it can change depending on the choice of parameters of the theory. This flexibility shows that either of $\gamma^{(1)}$ (or $\mathcal{B}^{(1)}$), $Z^{(1)}$ (or $\mathcal{W}_3^{(1)}$), $\nu^{(1)}$ and $H^{(1)}$ [81,82] can be the DM candidate in nmUED.

2

The Extra Dimensional Models

2.1 A Historical Journey to the Birth of an Extra Dimension

Of all the properties of spacetime, dimensionality has drawn a considerable attention which has always been a matter of curiosity and discussion among all the scientists and the philosophers of all time. Why is the space three-dimensional? There have been two different perspectives addressing this issue. One obvious answer is to seek for the possibility of existence of one more dimension, a fourth dimension; other approach is completely having historical interest though some of these are still compelling. This is to anyway deduce the only possible value of dimensionality of space as three. One of the important arguments made by Ehrenfest [83] and many others[1] that for $d = 3$ planetary orbits are stable[2]. For $d > 4$, Newton's inverse-square law of gravitation gets modifications. Though the justification for taking $d = 3$ is based on the validity of law of gravitation at all length scale, the modern-day searches for extra dimension look for such discrepancies from inverse-square law at short distances.

[1] For complete lists and arguments see Refs. [84, 85].

[2] The stability argument does not rule out the possibility of $d < 3$, but the values of $d = 4, 5, \ldots$ onwards, are obviously ruled out.

Introduction of extra-dimension became immensely popular in physics with the advent of relativity. Minkowski's geometrical interpretation of the Lorentz transformations in a four-dimensional spacetime had already stepped towards the direction of the era of extra dimensions. Minkowski did not initiate a fourth dimension; rather he reinterpreted time as a dimension.

But in physics, the concept of theorizing a dimension or more dimensions was developed from an effort to unify the different forces of Nature. In 1914, a year before Einstein published General relativity, Gunnar Nordström [86] propounded a five-dimensional vector theory concurrently describing the theory of electromagnetism and a scalar version of gravity. On the other side, Theodore Kaluza, in 1919 worked out a tensor theory [87]. To explain the issue related to the query how the extra dimension is hidden from our physical world, both Nordström and Kaluza assumed that the fields do not depend on the fifth dimension, *i.e.* all the derivatives of the fields with respect to the fifth dimensional coordinate vanish. This condition is recognized as "cylinder" condition. Kaluza actually considered a five-dimensional tensor theory in the absence of any matter. The five-dimensional metric g_{MN} decomposes into a four-dimensional metric $g_{\mu\nu}$, a vector potential A_μ and a scalar ϕ. Kaluza identified $g_{\mu\nu}$ with the usual four-dimensional metric which is related to gravitation, and the vector $g_{\mu 4}$ as the electromagnetic potential. Kaluza ignored the scalar by setting it unity which leads to the unphysical condition $\mathcal{F}_{\mu\nu}\mathcal{F}^{\mu\nu} = 0$ [84,88].

To treat extra dimensions at par with other dimensions, Oskar Klein came up with the idea [89] that the extra dimension could be compactified to very small size. This extra dimension could be assigned a circular topology S^1 with the radius of the circle very tiny. He also gave a convincing proposal on the non-appearance of extra dimension from the physical world by suggesting that the presence of extra dimension would not be observed unless the experiments have a resolution higher than the radius of the compactified circle. Fields on the circle can be expanded as a Fourier series having infinite number (n, say) of modes, which is termed as Kaluza-Klein or KK-modes. Each mode is associated with quantum number $|n|/R$ which is nothing but the discretized momentum p_5 in the extra dimension, R being the radius of compactified circle. The unusual smallness of R results in very large value of momentum for all modes $n > 0$, which eventually makes them beyond the reach of observation. Only the zero mode ($n = 0$) remains observable. Klein thus recreated Kaluza's cylinder conditions by incorporating a tiny compactification radius. Since $U(1)$ is the symmetry group associated with S^1, compactification of extra dimension on a circle essentially introduces a $U(1)$ gauge-invariance in the theory. The $U(1)$ invariance of the five-dimensional theory implies that KK-fields have electric charge quantized in terms of the mode number. So the $n = 1$ mode could be treated as the physical electron whereas the physical charge of electron could be identified as the quantized-charge of Kaluza-Klein theory. But this logic of charge-quantization works only for higher modes (from $n = 1$ and onwards) which on the other hand have masses proportional to a very large scale. This internal contradiction and the

discovery of nuclear forces, *i.e.* the existence of two other fundamental forces in Nature other than electromagnetism and gravitation were the major setback of the Kaluza-Klein theory[3].

Higher dimensional theories resurrected with renewed interests in the late 1970's and 1980's with the advent of supergravity and superstring theories. In the 1960s, the Quantum Chromodynamics was not developed and String theory was suggested as a theory of strong interactions. In 1968, Gabriele Veneziano proposed a form of scattering amplitude which described the picture of strongly interacting particles [91,92]. This model came with the realization that the spectrum of hadronic states could be determined from relativistic string. Initially this string picture was strikingly successful, but the appearance of spin-2 hadron in the spectrum of states of a closed string had no analogue in the hadronic spectrum and made this model abandoned.

Scherk and Schwarz [93] revived the idea of string by proposing it not as a theory for hadrons only, rather they reinterpreted this theory as a theory of all interactions, which eventually includes gravity. The spin-2 massless excitation of closed string was to be interpreted as a graviton. Quantization of this theory leads to some negative-norm states in the string spectrum and also some other unavoidable problems. But these problems disappear if the spacetime dimensionality is taken to be 26. The requirement for consistency in quantum theory of strings leads to the higher dimensionality of spacetime in string theory. So it is evident that higher dimensionality of spacetime in string theories is not an *a priori assumption*. In a sense, the idea of unification of fundamental interactions evolves naturally from string theories; the quantization of the open and closed string follows the similar path except the open string has a spin-1 massless mode whereas the closed string has spin-2 massless mode, indicating a possible way to the unification of Yang-Mills theory and gravity. This quantization is for bosonic string only. To take care of the fermions in the picture one should impose supersymmetry on the action and identify the Majorana fermions as the superpartners to the bosonic coordinates; the spacetime dimensionality will be 10 instead of 26 to maintain the internal consistency of the theory. However, the extra dimensions considered in these theories are extremely small (of the order of Planck length M_{Pl}^{-1}) and were beyond the scope of any possible experimental reach.

In 1990s, people started to think of the possibility of extra dimensions much larger than the Planck length:

- A TeV^{-1}-size extra dimension was first propounded by Antoniadis [94] in the year 1990 related to the phenomenon of supersymmetry (SUSY) breaking.
- In the year 1996, Hořava and Witten [95, 96] proposed an extra dimension in M-theory which can move down the string scale to the grand unification scale $M_{\text{GUT}} \sim 10^{16}$ GeV and thus unifying the gravity with other forces at the same scale.

[3]On this account see Reference [90].

- With the advent of D-theory by Polchinski [97] in 1995, a natural setting for different fields living in different number of extra dimensions came into picture, where the Standard Model (SM) fields which are localized on lower-dimensional D-branes can be represented by open strings whereas the gravitons were identified with the closed strings propagating in all dimensions.

- In the year 1998, the idea of extra dimension mainly came into limelight in phenomenology when Arkani-Hamed, Dimpopoulos and Dvali [98] suggested large extra dimensions (LED) as a solution to the hierarchy problem.

- A model with a small fifth dimension but with a warped five-dimensional geometry was proposed by Randall and Sundrum [99,100] in 1999 gives the solution to hierarchy problem. Also, the ADS/CFT theory by Maldacena [101] in 1998 provides new possibilities to explain and construct models related to the weak scale.

- Another extra dimensional model is Universal Extra Dimensional (UED) model where all particles propagate along some flat compactified extra dimensions. The remarkable feature of UED is that the remnant of translational invariance along the extra dimensions remains preserved making the KK-modes incapable to couple to the zero-modes [102]. This model which is the main part of this thesis, will be described elaborately in the next section of this chapter.

Below the primary features of LED and Randall-Sundrum (RS) model will be briefly mentioned.

2.1.1 Large Extra Dimension

Gauge hierarchy problem as described in the previous chapter is actually the issue related to the large difference between the electroweak scale ($\sim$ 100-1000 GeV) and the Planck scale ($\sim 10^{19}$ GeV). In SM, the electroweak symmetry is broken by the vacuum expectation value of the Higgs field. This electroweak scale eventually becomes unstable under the radiative corrections since the mass-squared of the Higgs field gets quadratic contributions from its interactions. The natural scale to cutoff the quadratic contributions is the Planck scale where the quantum corrections of gravity become significant. To put the problem in another way is raising the question: why is the gravity so weak relative to the other interactions of SM? To address this issue Arkani-Hamed, Dimpopoulos and Dvali [98] proposed a theory of $4 + d$ extra dimensions with Standard Model particles being confined to a 3-brane (which is actually a $3+1$ dimensional surface) whereas only the gravitons propagate in the full d-dimensions. Evidently, the extra dimensions have to be compactified to get the usual $3 + 1$ dimensional effective theory. But compactification can be arranged by considering only d number of extra dimensions with a common scale R which is relatively large leading to the possibility that scale of quantum gravity

is much lower than that of the Planck scale (M_{Pl}). The magnitude of R could vary from a millimeter to a fermi according to the number of large extra dimensions. Newton's law in $4+d$ dimensions is given by,

$$F(r) \sim \frac{G_N^{(4+d)} m_1 m_2}{r^{d+2}} = \frac{1}{M_{Pl(4+d)}^{d+2}} \frac{m_1 m_2}{r^{d+2}}, \tag{2.1}$$

which can be decomposed to two expressions according to the relation between r and R as:

$$F(r) \sim \frac{1}{M_{Pl(4+d)}^{d+2}} \frac{m_1 m_2}{r^{d+2}}, \quad \text{for } r \ll R, \tag{2.2}$$

$$F(r) \sim \frac{1}{M_{Pl(4+d)}^{d+2}} \frac{m_1 m_2}{R^d r^2}, \quad \text{for } r \gg R. \tag{2.3}$$

Comparing the last expression with the four-dimensional Newton's law,

$$F(r) \sim \frac{1}{M_{Pl}^2} \frac{m_1 m_2}{r^2}, \tag{2.4}$$

we have

$$M_{Pl}^2 \sim M_{Pl(4+d)}^{d+2} R^d. \tag{2.5}$$

If we take the fundamental scale $M_{Pl(4+d)} \sim 1$ TeV and demand that R can be chosen to reproduce the four-dimensional Planck scale $M_{Pl} \sim 10^{19}$ GeV, then we have

$$R \sim \left(\frac{M_{Pl}^2}{M_{Pl(4+d)}^{d+2}} \right)^{1/d} \sim 10^{32/d} \text{ TeV}^{-1} \sim 10^{32/d} 10^{-17} \text{ cm}, \tag{2.6}$$

$$\begin{aligned} d &= 1 \Rightarrow R \sim 10^{15} \text{ cm } (> 1 \text{ AU}), \text{which is ruled out,} \\ d &= 2 \Rightarrow R \sim 1 \text{ mm }, \\ d &= 3 \Rightarrow R \sim 10^{-6} \text{ cm }. \end{aligned}$$

So, in this model number of extra dimensions $d \geq 2$ are allowed. But recent experimental observations show that the bound on R is obtained as ≤ 30 μm [5]. On the other hand, no significant bound is obtained for $d > 3$.

2.1.2 Warped Extra Dimension

The above ADD scenario solves the problem of gauge hierarchy, but it introduces another hierarchy between the large extra dimension and the Planck length. To solve this issue, a model with small compact extra dimension was proposed by Randall and Sundrum [99, 100], with a five-dimensional warped geometry. The model has two branes placed at two fixed points of

orbifold at which the fifth dimension is compactified. The novel feature of the model is having warped metric caused by the back-reaction of gravity on the branes. Consideration of the back-reaction has important cosmological implications [103,104]. A four-dimensional theory with only four-dimensional sources necessarily leads to an expanding universe with positive cosmological constant. In warped geometry, one can adjust the bulk cosmological constant to get an effective vanishing four-dimensional cosmological constant.Thus the four-dimensional universe would still appear to be static and flat for an observer on a brane. Now, an incorporation of a bulk cosmological constant is necessary as the five-dimensional background itself is curved. Evidently, there is a transfer of the curvature from the four-dimensional branes, which are made flat, to the bulk which is now significantly curved [105]. This scenario was originally suggested by Rubakov and Shaposhnikov [103, 104]. In the minimal version of the RS model only gravity propagates in the bulk while the SM fields are localized on the brane where the warp factor is small. The corresponding metric in five-dimension can be written as

$$ds^2 = e^{-A(y)}\eta_{\mu\nu}dx^\mu dx^\nu - dy^2. \tag{2.7}$$

The warp factor $e^{-A(y)}$ is a measure of the curvature (warping) along the extra dimension. It is an exponential factor involving the fifth dimension as well as the radius of compactification; and clearly this factor comes as a multiplicative factor with the four-dimensional Minkowski part of the metric. This warp factor is the main ingredient that helps to address the hierarchy issue by "warping down" the Planck scale[4]. For this mechanism to work, the compactification radius should be stabilized against the quantum fluctuations and this can be performed by incorporating a bulk scalar field which generates a potential that allows the stabilization. The associated modulus field radion which describes the fluctuations of the magnitude of the radius obtains a mass of the order of a TeV. Due to the presence of the discrete spectrum of graviton resonances, the collider phenomenology of this model is quite distinct from that of the model of LED. The massive radion offers a very distinct scenario for this model. If warped extra dimension exists in nature, LHC data shows that the size of extra dimensions should be greater than TeV scale [108, 109].

2.2 Universal Extra Dimension

Among many variants of extra dimensional model, this thesis will be devoted to a particular incarnation of extra dimensional theories proposed by Appelquist *et al.* [102]. This is termed as Universal Extra Dimensional (UED) model which is the main focus of this thesis. The *universal* in UED makes it explicit that all the Standard Model (SM) fields can propagate along the extra spatial dimension instead of being confined to a boundary as in the case of ADD and RS model.

[4]For more detailed clarifications see the TASI lectures by Sundrum [106] and Gherghetta [107].

Despite being devoid of the virtue of solving hierarchy issues unlike ADD and RS models, UED has a wide range of phenomenological motivations.

Various phenomena of neutrino mass generation can be fit into flat five-dimensional spacetime scenarios [110]. Such kind of scenarios provide mechanism of supersymmetry breaking [94]. Extra dimensional models solve the puzzle of mass hierarchy in the fermion sector [111–113]. Dynamical electroweak symmetry breaking has been studied in extra dimensional scenarios [114]. The issue related to the gauge coupling unification is also well addressed in the flat extra dimensional theories. Usually these theories predict a unification scale which is considerably below the usual GUT scale [111,115–117]. Proton stability is one of the perplexing issues in particle physics. The six-dimensional operators which result in the violations of baryon and lepton number can cause proton decay and to maintain the constraints of proton lifetime in an SM-only theory leads to an unnatural cutoff. But, by the very construction of the UED model (six-dimensional UED), the operators leading to rapid proton decay can be forbidden [118]. This is the main difference with some other BSM models (*e.g.* SUSY), where ad hoc introduction of some symmetry is required to reduce the problem of rapid proton decay. Moreover and most importantly, UED provides a stable, electrically neutral and colorless state in a natural way[5] which can qualify as a viable dark matter candidate [119].

2.2.1 A Fifth Dimension

In this section, we describe the standard Kaluza-Klein theory which involves an extension of the $1+3$ dimensional Minkowski world $\mathbb{M}_4$ to a $1+4$ dimensional $\mathbb{M}_4 \times \mathbb{S}^1$ world. Here the fourth spatial dimension corresponds to a topology of a circle $\mathbb{S}^1$ with a radius R implying that the extra dimension is *compact*. Einstein described this world as a 'cylindrical world' [120]. The extra dimension is denoted as y. Compactification means the physical identification of the points y and $y + 2\pi R$ along the extra dimension y which means for any field, *viz.* Φ, we have $\Phi(y) \sim \Phi(y + 2\pi R)$. Evidently, there is a periodic boundary condition on any function of spacetime. The coordinate is defined as

$$x^M = \{x^\mu, y\}. \tag{2.8}$$

Here, x^μ ($\mu = 0, 1, 2, 3$) is the four-dimensional non-compact spacetime coordinates; $M = 0, 1, 2, 3, 5$ are five-dimensional Lorentz indices with the metric convention $g_{MN} \equiv \text{diag}(+, -, -, -, -)$.

[5] Though, in the non-minimal version of this UED model, one should add KK-parity conserving boundary-localized terms to get a viable dark matter candidate.

- **Kaluza-Klein Modes**

The existence of the so-called Kaluza-Klein modes in the five-dimensional theory comes as the very first upshot of having an extra dimension in compact form. Let us consider the simplest example of a free real scalar field. The action of a free scalar field in five-dimension is [121]

$$\mathcal{S}_{5D} = \frac{1}{2}\int d^4x \int_0^{2\pi R} dy \left[\partial_M \Phi(x,y)\partial^M \Phi(x,y) - m_0^2 \Phi^2(x,y)\right] \ , \tag{2.9}$$

where the scalar field $\Phi(x,y)$ is the field on this five-dimensional space, or bulk. The periodic boundary condition on y allows us to perform a Fourier series expansion along the y direction as

$$\Phi(x,y) = \frac{1}{\sqrt{2\pi R}} \sum_{n=-\infty}^{\infty} \Phi^{(n)}(x) e^{iny/R}. \tag{2.10}$$

Here, $1/\sqrt{2\pi R}$ is just a normalization factor. In the above, each of the Fourier coefficients $\Phi^{(n)}$ is itself a field over the usual four-dimensional Minkowski space and these fields are the Kaluza-Klein (KK) modes. Plugging the Fourier decomposition of $\Phi(x,y)$ (Eq. 2.10), in Eq. 2.9 and exploiting the orthonormality of y-profiles of the Fourier modes in extra dimension and then integrating over the extra dimension, we finally obtain the effective four-dimensional action:

$$\mathcal{S}_{4D} = \frac{1}{2}\sum_n \int d^4x \left[\partial_\mu \Phi^{(n)}(x)\partial^\mu \Phi^{(n)}(x) - \left(m_0^2 + \frac{n^2}{R^2}\right)(\Phi^{(n)}(x))^2\right] \ . \tag{2.11}$$

This implies that from the four-dimensional point of view the five-dimensional scalar field appears as an infinite tower of KK-modes where the mass of nth KK-mode is given as

$$m_n = \sqrt{m_0^2 + \frac{n^2}{R^2}}. \tag{2.12}$$

The set of KK-modes with monotonously increasing masses with $n = 1, 2, \ldots$ is termed as a Kaluza-Klein tower of states. The zero-mode ($n = 0$) has a bulk mass m_0 and is evidently massless for $m_0 = 0$.

The fifth directional momentum operator in quantum theory can be written as $k_5 = -i\partial_y$ and we can have

$$k_5^{(n)}\Phi(x,y) = \sum_{n=0}^{\infty} \frac{n}{R}\Phi^{(n)}(x)e^{iny/R}, \tag{2.13}$$

i.e. each KK-mode corresponds to a momentum-eigenvalue

$$k_5^{(n)} = n/R. \tag{2.14}$$

The discrete values of momentum are the evident consequence of the periodic boundary conditions. The relativistic energy of the nth KK-mode is

$$E_n = \sqrt{\overrightarrow{k}^2 + [k_5^{(n)}]^2 + m_0^2} = \sqrt{\overrightarrow{k}^2 + m_n^2}. \tag{2.15}$$

The substitution of Eq. 2.14 in the above equation results in Eq. 2.12 which is nothing but the expression for the mass of nth KK-mode. Here comes the natural conclusion that, the KK-masses observed in four dimensions are nothing but the "frozen" components of momentum in the extra dimension [84].

We can similarly perform a Fourier decomposition for the five-dimensional gauge field along the compact dimension [121]:

$$A_M(x^\mu, y) = \frac{1}{\sqrt{2\pi R}} \sum_n A_M^{(n)}(x^\mu) e^{iny/R}. \tag{2.16}$$

The action then becomes

$$\mathcal{S}_{\text{gauge}} = \int d^4x \int_0^{2\pi R} dy \left[-\frac{1}{4} \mathcal{F}_{MN} \mathcal{F}^{MN} \right] = \int d^4x \int_0^{2\pi R} dy \left[-\frac{1}{4} \{ \mathcal{F}_{\mu\nu} \mathcal{F}^{\mu\nu} + 2\mathcal{F}_{\mu 5} \mathcal{F}^{\mu 5} \} \right], \tag{2.17}$$

The derivative along y can be replaced by $\partial_5 \to i(n/R)$ under Fourier series expansion. To remove the mixing terms between $A_5^{(n)}$ and $A_\mu^{(n)}$ we can execute a gauge transformation as

$$A_\mu^{(n)} \to A_\mu^{(n)} - \frac{i}{n/R} \partial_\mu A_5^{(n)}, \tag{2.18}$$

$$A_5^{(n)} \to 0, \quad \text{for} \quad n \neq 0. \tag{2.19}$$

In this gauge we have,

$$\mathcal{S}_{\text{gauge}} = \int d^4x \int_0^{2\pi R} dy \left\{ \left(-\frac{1}{4} \mathcal{F}_{\mu\nu}^{(0)} \mathcal{F}^{(0)\mu\nu} + \frac{1}{2} \partial_\mu A_5^{(0)} \partial^\mu A_5^{(0)} \right) + \sum_{n \geq 1} 2 \left(-\frac{1}{4} \mathcal{F}_{\mu\nu}^{(-n)} F^{(n)\mu\nu} + \frac{1}{2} \frac{n^2}{R^2} A_\mu^{(-n)} A_\mu^{(n)} \right) \right\}. \tag{2.20}$$

So, the end result is that, on a circle, both A_μ and A_5 components have zero modes; the former is a vector whereas the latter is a scalar from the four-dimensional perspective. In case of nonzero modes, $A_5^{(n)}$ is eaten and becomes the longitudinal mode of the corresponding massive vector field $A_\mu^{(n)}$. Naturally, there is no scalar mode left for nonzero KK-modes [121].

- **Fermion on a Circle: Chirality Problem**

One of the unavoidable ramification of one extra dimension is definition of chirality operator in odd dimension is not possible. The possible representation of the $1+4$ dimensional Clifford

algebra for fermions can be given as

$$\{\Gamma^M, \Gamma^N\} = 2g^{MN}, \tag{2.21}$$

with

$$\Gamma_\mu = \gamma_\mu \quad \text{and} \quad \Gamma_5 = i\gamma_5. \tag{2.22}$$

Here, g^{MN} is the Minkowski metric in five-dimension and the representation is provided by the 4×4 Dirac matrices. Thus, we observe that the smallest irreducible representations of five-dimensional fermions has four complex components. The five-dimensional action for fermions is given by

$$\mathcal{S}_{\text{fermion}} = \int d^4x \int_0^{2\pi R} dy\ \bar{\Psi}(x,y)\left(i\partial_\mu \Gamma^M - m_f\right)\Psi(x,y). \tag{2.23}$$

The compactification of extra dimension to a circle results in a similar periodic decomposition of the five-dimensional fermionic field and after integrating over y the effective four-dimensional action for Dirac fermions is given by [106]

$$\mathcal{S}_{\text{fermion}} = \int d^4x \sum_n \bar{\psi}^n(x)\left(i\gamma_\mu\partial^\mu - m_f + i\frac{n}{R}\gamma_5\right)\psi^n(x). \tag{2.24}$$

Again, from the four-dimensional point of view, we obtain a tower of four component Dirac spinors with mass-squared as shown in Eq. 2.12. Considering the case of $m_f = 0$, we obtain *non-chiral* massless modes; $\psi^{(0)}_{\alpha=1-4}$ decomposes as $\sim \left[\psi^{(0)}_L(\alpha = 1,2),\ \psi^{(0)}_R(\alpha = 3,4)\right]$, where L (R) corresponds to left-(right-)chirality under the four-dimensional Lorentz transformation. As γ_5 is being introduced among the five-dimensional Dirac matrices and there is no other matrix with the anti-commuting properties of γ_5, so in a natural way there is no explicit chirality in this theory. Generally, in any dimension whether it be even or odd (say j), we have j number of gamma matrices Γ^l $(l = 1, 2, \ldots, j)$, satisfying $\{\Gamma^l, \Gamma^m\} = 2g^{lm}$. Then the generalized γ_5 can be obtained as

$$\Gamma^{j+1} = \Gamma^1\Gamma^2\ldots\Gamma^j. \tag{2.25}$$

For even number of dimension $(j = 2p)$, Γ^{j+1} will be nilpotent $((\Gamma^{j+1})^2 = 1)$ and anticommute with all Γ^l,

$$\{\Gamma^{j+1}, \Gamma^l\} = 0,\ \forall\ l = 1, 2, \ldots, 2p. \tag{2.26}$$

However, for odd number of dimension, $j = 2p + 1$,

$$[\Gamma^{j+1}, \Gamma^l] = 0,\ \forall\ l = 1, 2, \ldots, 2p + 1, \tag{2.27}$$

and then by Schur's lemma Γ^{j+1} is just a multiple of unit matrix. Evidently, in odd number of dimensions defining chiral fermion is not possible.

2.2.2 Fields on Orbifold

So, all in all, there are two major problems in accommodating SM field in five-dimensional theory:

- For every gauge field $A_\mu(x)$ there exists a degenerate scalar partner $A_5(x)$.
- All the fermions in the theory will essentially be vector-like.

To ameliorate both these problems we need further modification of the space. If compactification is done, not on a circle, but on a line segment imposing suitable boundary conditions to the bulk fields, we can evade these issues. Let us take the example of bulk scalar field $\Phi(x, y)$ with the extra dimension being mapped to a line segment $0 \leq y \leq l$ [84, 122]. Applying the variational principle to the action

$$\delta\mathcal{S}[\Phi] = -\int d^4x \int_0^l dy \left(\partial^M \partial_M \Phi^\dagger + m_0^2 \Phi^\dagger\right) \delta\Phi + \int d^4x \left(\frac{\partial\Phi}{\partial y}\delta\Phi\Big|_{y=l} - \frac{\partial\Phi}{\partial y}\delta\Phi\Big|_{y=0}\right). \quad (2.28)$$

By virtue of variational principle the above expression must vanish for any arbitrary variations $\delta\Phi$. Thus we can immediately have the bulk (Klein-Gordon) equation

$$\partial^M \partial_M \Phi + m_0^2 \Phi = 0, \quad (2.29)$$

and also the boundary condition

$$\int d^4x \left(\frac{\partial\Phi}{\partial y}\delta\Phi\Big|_{y=l} - \frac{\partial\Phi}{\partial y}\delta\Phi\Big|_{y=0}\right) = 0. \quad (2.30)$$

This would be naturally valid on a circle if $y = 0$ and $y = l$ are identified as the same point. On the other hand, this is a line segment and the above equation can only hold if both terms vanish individually. So we can obtain the following boundary conditions:

- At $y = 0$: either N : $\frac{\partial\Phi}{\partial y}\Big|_{y=0}$ or D : $\Phi(x, 0) = 0$
- At $y = l$: either N : $\frac{\partial\Phi}{\partial y}\Big|_{y=l}$ or D : $\Phi(x, l) = 0$

where, D and N correspond to Dirichlet and Neumann types boundary conditions respectively. Evidently, we can have four combinations, *viz.* DD, DN, ND, NN; where first letter stand for $y = 0$ and the second for $y = l$. However, if we want to retain only the DD and NN sets of harmonics, the line segment will have

1. a periodic boundary condition $\Phi(x, y) = \Phi(x, y + 2l)$,

2. a reflection symmetry $\Phi(x, y) = \Phi(x, l - y)$ at the point $y = l$.

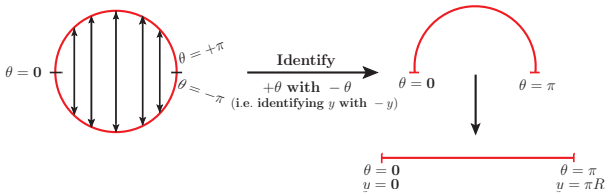

FIGURE 2.1: Pictorial description of the UED compactification: orbifolding.

Physically, these conditions correspond to a $\mathbb{S}^1/\mathbb{Z}_2$ orbifold as depicted in Figure 2.1. We can, therefore, relate l to a compactification radius R by $l = \pi R$. To repeat in another way, if we have a topology of a $\mathbb{S}^1/\mathbb{Z}_2$ orbifold, and if $\Phi(x, y) = \Phi(x)\,\eta(y)$; then the harmonics reconcilable with the boundary conditions will be $\eta_{NN}(y)$ and $\eta_{DD}(y)$ functions.

Orbifold projection eliminates the phenomenologically undesirable degrees of freedom (DoF) at the zero-mode level. The bulk scalar field can be expanded as

$$\Phi(x, y) \xrightarrow{y \to -y} \Phi(x, -y) = \begin{cases} +\Phi_{NN}(x, y), \\ -\Phi_{DD}(x, y). \end{cases} \tag{2.31}$$

Clearly, depending on the choice of boundary conditions, we have two different physical scalars given as

$$\Phi_{NN}(x, y) = \frac{1}{\sqrt{\pi R}}\Phi^{(0)}_{NN}(x) + \sqrt{\frac{2}{\pi R}}\sum_{n=1}^{\infty}\Phi^{(n)}_{NN}(x)\cos\left(\frac{ny}{R}\right), \tag{2.32}$$

$$\Phi_{DD}(x, y) = \sqrt{\frac{2}{\pi R}}\sum_{n=1}^{\infty}\Phi^{(n)}_{DD}(x)\sin\left(\frac{ny}{R}\right). \tag{2.33}$$

So, $\Phi_{NN}(x, y)$ is even under the fifth component of parity $y \to -y$ whereas the other, $\Phi_{DD}(x, y)$ is odd under $y \to -y$. Here, $\Phi^{(0)}_{NN}(x)$ would play the role of the SM field. Thus, to get rid of the SM fields and to have only KK excitations, we should impose DD boundary conditions. On the other hand, to retain the SM field along with their KK excitations NN boundary conditions should be imposed. This is the distinctive feature of the application of $\mathbb{S}^1/\mathbb{Z}_2$ topology that is applied profitably to formulate the theory of Universal Extra Dimension (UED).

- **Defining Chiral Fermion**

Based on the previous discussion of the section 2.2.1, the title seems purely paradoxical and self-contradictory, since there is no chiral projections of a Dirac fermion as there is no analogue

of γ_5 in odd dimensions. And yet, this very concept becomes feasible in four dimensions with orbifold compactification. The Dirac matrices given in Eq. 2.22 can be used to formulate the spinor representation of the bulk Lorentz group $SO(1,4)$, since compactification reduces the symmetry to the usual Lorenz group $SO(1,3)$ of the four non-compact dimensions [84]. Taking this fact into account, we can construct the projection operators

$$P_{\pm} = \frac{1}{2}\left(\mathbb{I} \pm i\Gamma^0\Gamma^1\Gamma^2\Gamma^3\right) \tag{2.34}$$

that act on the bulk spinor $\Psi(x,y)$ to yield projections $\Psi^{\pm}(x,y) = P_{\pm}\Psi(x,y)$ with, $\Psi(x,y) = \Psi^{+}(x,y) + \Psi^{-}(x,y)$. These projection operators are numerically same with the right and left chiral projection operators in four dimensions; but these can not be termed as so called right- or left-projectors as this very idea does not exist in five dimensions. But, by similar manner, applying orbifold compactification we can have the bulk spinor as even spinor

$$\Psi_{NN}(x,y) = \frac{1}{\sqrt{\pi R}}\psi^{(0)}_{NN}(x) + \sqrt{\frac{2}{\pi R}}\sum_{n=1}^{\infty}\psi^{(n)}_{NN}(x)\cos\left(\frac{ny}{R}\right), \tag{2.35}$$

or as an odd spinor

$$\Psi_{DD}(x,y) = \sqrt{\frac{2}{\pi R}}\sum_{n=1}^{\infty}\psi^{(n)}_{DD}(x)\sin\left(\frac{ny}{R}\right). \tag{2.36}$$

Applying $P_{\pm}$ operators to both sides of Eq. 2.35, we obtain

$$\Psi^{+}_{NN}(x,y) = P_{+}\Psi_{NN}(x,y) = \frac{1}{\sqrt{\pi R}}[\psi^{(0)}_{NN}]_R(x) + \sqrt{\frac{2}{\pi R}}\sum_{n=1}^{\infty}[\psi^{(n)}_{NN}]_R(x)\cos\left(\frac{ny}{R}\right), \tag{2.37}$$

$$\Psi^{-}_{NN}(x,y) = P_{-}\Psi_{NN}(x,y) = \frac{1}{\sqrt{\pi R}}[\psi^{(0)}_{NN}]_L(x) + \sqrt{\frac{2}{\pi R}}\sum_{n=1}^{\infty}[\psi^{(n)}_{NN}]_L(x)\cos\left(\frac{ny}{R}\right). \tag{2.38}$$

Since, $P_{\pm}$ operate on a four-dimensional spinor, we get $P_{\pm} = P_{R/L}$ respectively, since chirality is a valid concept for the four-dimensional spinors $\psi^{(0)}_{NN}$ and $\psi^{(n)}_{NN}$. Similarly, we can get a similar set of odd fermions

$$\Psi^{+}_{DD}(x,y) = P_{+}\Psi_{DD}(x,y) = \sqrt{\frac{2}{\pi R}}\sum_{n=1}^{\infty}[\psi^{(n)}_{DD}]_R(x)\sin\left(\frac{ny}{R}\right), \tag{2.39}$$

$$\Psi^{-}_{DD}(x,y) = P_{-}\Psi_{DD}(x,y) = \sqrt{\frac{2}{\pi R}}\sum_{n=1}^{\infty}[\psi^{(n)}_{DD}]_L(x)\sin\left(\frac{ny}{R}\right). \tag{2.40}$$

However, since there can exist either N or D boundary conditions at the orbifold fixed points, we can have any one of Eqs. 2.37 or 2.38, and again, any one of Eqs. 2.39 or 2.40. As the zero-mode is identified with the SM fields, it clearly follows that SM fermions will be chiral. Similar mechanism can be applicable to the five-dimensional vector field $A^M(x,y)$. The fifth component, $A_5(x,y)$ is nothing but the polarization of the gauge field along the extra dimension and from four-dimensional point of view, after compactification, this just behaves as a (infinite)

tower of spinless KK-modes. Clearly, this A_5 will have no zero mode and will be an odd field. The corresponding KK decomposition for the gauge field will be

$$A^{\mu}_{NN}(x,y) = \frac{1}{\sqrt{\pi R}} A^{\mu(0)}_{NN}(x) + \sqrt{\frac{2}{\pi R}} \sum_{n=1}^{\infty} A^{\mu(n)}_{NN}(x) \cos\frac{ny}{R}, \tag{2.41}$$

$$A^{5}_{DD}(x,y) = \sqrt{\frac{2}{\pi R}} \sum_{n=1}^{\infty} A^{5(n)}(x) \sin\frac{ny}{R}. \tag{2.42}$$

Thus, introducing the trick of orbifolding we can get rid of the gauge scalars in the SM, such type of scalars will only be present among the KK excitations, and, can in principle, be detected.

2.2.3 KK-Parity

Once, orbifolding is done, the translational invariance is broken and hence the fifth dimensional momentum p_5 is no more a conserved quantity, unlike the four-dimensional momentum. Therefore, KK-number is evidently violated[6]. However, there remains an additional symmetry, an accidental discrete symmetry, called KK-parity. "KK-parity" conservation is being manifested as the translational symmetry $y \to y - \pi R$. Thus for the nth level particle KK-parity is $(-1)^n$. Evidently, all SM fields are of even KK-parity. It is worth mentioning that KK-parity is not the $\mathbb{Z}_2$ symmetry of $S^1/\mathbb{Z}_2$ [122]. Conservation of KK-parity implies [123]

- the stability of the lightest level-one KK-mode (LKP),
- odd level KK-modes can only be produced in pairs,
- all direct couplings of SM particles to even number KK states are loop suppressed and can occur through brane-localized interactions.

Generally, in the minimal version of UED, KK-parity remains a good symmetry and remains unbroken so long as no explicit KK-parity violating interactions are introduced at the orbifold fixed points.

2.2.4 SM in Five Dimensions

After a detailed analysis of the fundamental essence of extra dimensional theories, we are now all set to discuss the SM embedded in five-dimensional theory, where all SM fields can propagate in the bulk (the five-dimensional whole space). The five-dimensional action consists of the same

[6]KK-number is still a good quantum number in (m)UED, which remains preserved in all interactions and decays, if we ignore the orbifolding fixed points.

fields of SM and would respect the same $SU(3)_c \otimes SU(2)_L \otimes U(1)_Y$ gauge symmetry as that of SM. The five-dimensional action will be given by,

$$\mathcal{S} = \int d^4x \int_0^{\pi R} dy \, (\mathcal{L}_g + \mathcal{L}_\Phi + \mathcal{L}_l + \mathcal{L}_q + \mathcal{L}_Y) \tag{2.43}$$

where,

$$\mathcal{L}_g = -\frac{1}{4}\mathcal{F}^{MNa}\mathcal{F}^a_{MN} - \frac{1}{4}\mathcal{B}^{MN}\mathcal{B}_{MN} - \frac{1}{4}\mathcal{G}^p_{MN}\mathcal{G}^{pMN}, \tag{2.44a}$$

$$\mathcal{L}_\Phi = (\mathcal{D}_M\Phi)^\dagger(\mathcal{D}^M\Phi) + \mu^2_{(5)h}\Phi^\dagger\Phi - \lambda_{(5)h}(\Phi^\dagger\Phi)^2, \tag{2.44b}$$

$$\mathcal{L}_l = \sum_{j=\text{generation}} \left[\bar{L}_j \left(i\Gamma^M\mathcal{D}_M\right) L_j + \bar{E}_j \left(i\Gamma^M\mathcal{D}_M\right) E_j\right], \tag{2.44c}$$

$$\mathcal{L}_q = \sum_{j=\text{generation}} \left[\bar{Q}_j \left(i\Gamma^M\mathcal{D}_M\right) Q_j + \bar{U}_j \left(i\Gamma^M\mathcal{D}_M\right) U_j + \bar{D}_j \left(i\Gamma^M\mathcal{D}_M\right) D_j\right], \tag{2.44d}$$

$$\mathcal{L}_Y = \sum_{i,\ j=\text{generation}} \left[-\tilde{y}^u_{ij}\bar{Q}_i\Phi^c U_j - \tilde{y}^d_{ij}\bar{Q}_i\Phi D_j - \tilde{y}^l_{ij}\bar{L}_i\Phi\, E_j + \text{h.c.}\right]. \tag{2.44e}$$

In the above, the $\mathcal{L}_g$, $\mathcal{L}_\Phi$, $\mathcal{L}_l$, $\mathcal{L}_q$ correspond to the five-dimensional Lagrangian for gauge field, scalar field, lepton and quark field respectively whereas $\mathcal{L}_Y$ denotes the five-dimensional Yukawa Lagrangian. The symbols $\mu_{(5)h}$ and $\lambda_{(5)h}$ respectively represent the five-dimensional bulk Higgs mass parameter and scalar self-coupling. Here, $\mathcal{G}^p_M$, $\mathcal{W}^a_M$ and $\mathcal{B}_M$ are the gauge fields of the respective gauge groups $SU(3)_c$, $SU(2)_L$ and $U(1)_Y$; the suffices p and a represent the $SU(3)$ and $SU(2)_L$ gauge indices respectively where the sum over the repeated gauge indices are implied. In the above formulae, $M, N = 0, 1, 2, 3, 5$ are the five-dimensional Lorentz indices. We will be using the *mostly minus* metric convention, *i.e.,* $g_{MN} \equiv \text{diag}(+1, -1, -1, -1, -1)$. The five-dimensional gamma matrices are $\Gamma^M = (\gamma^\mu, -i\gamma_5)$ (Sec. 2.2.1). The field strength tensor for the gauge fields, $\mathcal{B}_M$, $\mathcal{W}^a_M$ and $\mathcal{G}^p_M$ are given by

$$\mathcal{B}_{MN} = \partial_M\mathcal{B}_N - \partial_N\mathcal{B}_M, \tag{2.45}$$

$$\mathcal{F}^a_{MN} = \partial_M\mathcal{W}^a_N - \partial_N\mathcal{W}^a_M + \widetilde{g}f^{abc}\mathcal{W}^b_M\mathcal{W}^c_N, \tag{2.46}$$

$$\mathcal{G}^p_{MN} = \partial_M\mathcal{G}^p_N - \partial_N\mathcal{G}^p_M + \widetilde{g}_s f'^{\,pqm}\mathcal{G}^q_M\mathcal{G}^m_N. \tag{2.47}$$

The covariant derivative, in general, is given as

$$\mathcal{D}_M \equiv \partial_M - i\widetilde{g}\mathcal{W}^a_M T^a - i\widetilde{g}'\mathcal{B}_M Y, \tag{2.48}$$

where $\widetilde{g}$ and $\widetilde{g}'$ are the five-dimensional gauge coupling constants of $SU(2)_L$ and $U(1)_Y$ respectively, and T^a and Y are the corresponding generators. The scalar field Φ and $\Phi^c = i\tau^2\Phi^*$ denote the standard Higgs doublet and its charge conjugated field, and $\widetilde{y}^u_{ij}$, $\widetilde{y}^d_{ij}$ are the Yukawa matrices in the five-dimensional theory; they mix different generations. The fermionic fields Q,

D and U are the four-component Dirac spinors and carry the same quantum numbers as the corresponding SM fields. As covariant derivative, in a sense, determines the interaction between the fermion and the gauge boson, the explicit form of $\mathcal{D}_M$ will be given by the interaction properties of the corresponding fermionic field. For example, the covariant derivative for the quarks are given by

$$\mathcal{D}_M \equiv \partial_M - i\widetilde{g}\mathcal{W}_M^a T^a - i\widetilde{g}'\mathcal{B}_M Y - i\widetilde{g}_s \frac{\lambda^p}{2}\mathcal{G}_M^p, \tag{2.49}$$

where λ^p $(p = 1, 2, 3, \ldots, 8)$ are Gell-Mann matrices which are related to the generators of $SU(3)_c$ gauge group and $\widetilde{g}_s$ corresponds to the five-dimensional gauge coupling of this gauge group. The five-dimensional gauge couplings are dimensionful parameters, and there exist scaling relations between the five-dimensional and its four-dimensional counterpart, which in the context of UED is given as

$$g_i = \frac{\widetilde{g}_i}{\sqrt{\pi R}}, \tag{2.50}$$

where, g_i is the usual four-dimensional coupling. The Fourier expansion of the fields are given by,

$$\begin{aligned}
Q(x,y) &= \frac{1}{\sqrt{\pi R}}Q_L^{(0)}(x) + \sqrt{\frac{2}{\pi R}}\sum_{n=1}\left[Q_L^{(n)}(x)\cos\left(\frac{ny}{R}\right)\right. \\
&\quad \left. + Q_R^{(n)}(x)\sin\left(\frac{ny}{R}\right)\right], \qquad (2.51)\\
U(x,y) &= \frac{1}{\sqrt{\pi R}}U_R^{(0)}(x) + \sqrt{\frac{2}{\pi R}}\sum_{n=1}\left[U_R^{(n)}(x)\cos\left(\frac{ny}{R}\right)\right. \\
&\quad \left. + U_L^{(n)}(x)\sin\left(\frac{ny}{R}\right)\right], \qquad (2.52)\\
A_\mu(x,y) &= \frac{1}{\sqrt{\pi R}}A_\mu^{(0)}(x) + \sqrt{\frac{2}{\pi R}}\sum_{n=1}A_\mu^{(n)}(x)\cos\left(\frac{ny}{R}\right), \qquad (2.53)\\
A_5(x,y) &= \sqrt{\frac{2}{\pi R}}\sum_{n=1}A_5^{(n)}(x)\sin\left(\frac{ny}{R}\right). \qquad (2.54)
\end{aligned}$$

We thus obtain the desired zero modes $Q_L^{(0)}$, $U_R^{(0)}$ and $A_\mu^{(0)}$ corresponding to the SM fields[7]. The expansion for U is valid also for D. The expansion for lepton doublet will be similar to that of the quark doublet $Q(x,y)$ whereas the lepton singlet can have the expansion similar to that of U or D. The expansion of the scalar Higgs field will have the same form as that of A_μ. We must also expand the zero-mode Higgs doublet around its vacuum expectation value, and express the KK Higgs doublets in terms of their component fields:

$$\Phi^{(0)} = \begin{pmatrix} \phi^{(0)+} \\ \frac{1}{\sqrt{2}}\left(v + h^{(0)} + i\,\chi^{(0)}\right) \end{pmatrix}, \quad \Phi^{(n)} = \begin{pmatrix} \phi^{(n)+} \\ \frac{1}{\sqrt{2}}\left(h^{(n)} + i\,\chi^{(n)}\right) \end{pmatrix}. \tag{2.55}$$

[7]This part will be described elaborately in the last part of this chapter.

Here v is the usual four-dimensional Higgs VEV, $h^{(0)}$ is the physical zero-mode Higgs, and $\chi^{(0)}$, $\phi^{(0)\pm}$ are the zero-mode Goldstone bosons. The $h^{(n)}$ are the KK excitations of CP-even Higgs and the $\chi^{(n)}$ are KK excitations of CP-odd scalars. The four-dimensional effective Lagrangian would also contain bilinear terms involving the KK excitations (starting from KK-level $n = 1$ and above) of the 5th components of $W^{\pm}$ (Z) bosons and the KK excitations of $\phi^{(0)\pm}$ ($\chi^{(0)}$) of the Higgs doublet field [124]. There exists also the mixing terms between $A_{\mu}^{(n)}$ and $A_5^{(n)}$. To remove all these mixings, gauge-fixing Lagrangian should be added. The gauge-fixing action is given by

$$\begin{aligned}\mathcal{S}_{\rm GF} &= \int d^4x \int_0^{\pi R} dy \left[-\frac{1}{2\xi}(\partial_\mu \mathcal{G}^\mu + \xi\partial_5 \mathcal{G}^5)^2 - \frac{1}{2\xi}(\partial_\mu A^\mu + \xi\partial_5 A^5)^2 \right. \\ &\quad -\frac{1}{2\xi}\{\partial_\mu Z^\mu + \xi_y(\partial_5 Z^5 - iM_Z\chi)\}^2 \\ &\quad \left. -\frac{1}{\xi}\left(\partial_\mu W^{\mu+} + \xi(\partial_5 W^{5+} - iM_W\phi^+)\right)\left(\partial_\mu W^{\mu-} + \xi(\partial_5 W^{5-} + iM_W\phi^-)\right)\right]. \quad (2.56)\end{aligned}$$

The mass matrices upon diagonalization would lead to a tower of charged Goldstone bosons (with mass-squared $\xi(m_n^2 + M_W^2)$) and a physical charged Higgs pair (with mass-squared $m_n^2 + M_W^2$); and a tower of neutral Goldstone bosons (with mass-squared $\xi(m_n^2 + M_Z^2)$) along with a tower of physical CP-odd Higgs (with mass-squared $m_n^2 + M_Z^2$). The new spectrum also consists of a tower of KK-modes with masses m_n^2 for both $A_{\mu}^{(n)}$ and $A_5^{(n)}$ and a massless zero-mode photon.

There exist bilinear terms involving the doublet and singlet states of the fermions and the strength (off-diagonal terms) of the mixing is proportional to fermionic mass, so that the mixing is only important for top quark (we will denote top quark mass by m_t in the following). The detailed analysis will be elucidated in the latter part of this chapter (Sec. 2.5) while describing the model description on non-minimal Universal Extra Dimensional model (nmUED) and as we proceed we will point out how to revert to UED.

2.2.4.1 Particle Interactions and Couplings

The above discussions show that from the four-dimensional point of view the five-dimensional fields appear as infinite towers of KK-modes. The KK excitations, whether follow NN or DD boundary conditions have masses given in Eq. 2.12. The zero-mode SM particle has the mass m_0 which is the same as the bulk mass. An evident feature of this model is, in the limit of large R^{-1}, all the KK excitations having a particular order n will have a common mass $m_n \simeq n/R$. Later we will see that this degeneracy can be broken by radiative corrections of masses.

Now we put our attention to the interactions among the particles of UED model. Calculating the interactions is straightforward but a bit tedious. The steps of extracting the coupling of UED are the following:

- Write the SM in five-dimensions.
- Replace every bulk field (scalar, fermion or vector) by its corresponding KK expansion, keeping general mode numbers.
- Lastly, integrate over the fifth co-ordinate y to obtain the effective four-dimensional coupling in compactification limit.

While calculating all these interactions, we should keep in mind that the coupling in zero-mode sector will be exactly the same as that of SM coupling. Let us take the example of the interactions among fermions and gauge bosons. Now, these couplings arise from the fermion kinetic term, $i\bar{f}(x,y)\Gamma^M\mathcal{D}_M f(x,y)$, where $f(x,y)$ is any arbitrary five-dimensional fermionic field. Then,

$$i\bar{f}(x,y)\Gamma^M\mathcal{D}_M f(x,y) = i\bar{f}(x,y)\gamma^\mu\mathcal{D}_\mu f(x,y) + i\bar{f}(x,y)(-i\gamma_5)\mathcal{D}_5 f(x,y). \tag{2.57}$$

For the time being, we focus on the first term only and write, illustratively, $\mathcal{D}_\mu = \partial_\mu - i\widetilde{g}A_\mu$. Thus, the interaction between gauge field A_μ and fermion f will be $\widetilde{g}\bar{f}(x,y)\not{A}(x,y)f(x,y)$. By plugging the KK expansion of each field in this term we have,

$$\begin{aligned}\widetilde{g}\int d^4x\int_0^{\pi R}dy\sum_{p,q,r}\Bigg[&\left(\frac{1}{\sqrt{\pi R}}\bar{f}^{(0)}(x)+\frac{\sqrt{2}}{\sqrt{\pi R}}\sum_p\left\{\bar{f}^{(p)}_{NN}(x)\cos\left(\frac{py}{R}\right)+\bar{f}^{(p)}_{DD}(x)\sin\left(\frac{py}{R}\right)\right\}\right)\\&\times\gamma_\mu\left(\frac{1}{\sqrt{\pi R}}A^{\mu(0)}(x)+\frac{\sqrt{2}}{\sqrt{\pi R}}\sum_q A^{\mu(q)}_{NN}(x)\cos\frac{qy}{R}\right)\\&\times\left(\frac{1}{\sqrt{\pi R}}f^{(0)}(x)+\frac{\sqrt{2}}{\sqrt{\pi R}}\sum_r\left\{f^{(r)}_{NN}(x)\cos\left(\frac{ry}{R}\right)+f^{(r)}_{DD}(x)\sin\left(\frac{ry}{R}\right)\right\}\right)\Bigg].\end{aligned} \tag{2.58}$$

From this equation, we can obtain the coupling between f and A_μ for any arbitrary KK-level. We can have the zero-mode coupling for $p=q=r=0$, which is given as

$$\begin{aligned}\frac{\widetilde{g}}{(\pi R)^{3/2}}\int d^4x\int_0^{\pi R}dy\bar{f}^{(0)}(x)\gamma_\mu A^{\mu(0)}(x)f^{(0)}(x)&\\=\frac{\widetilde{g}}{\sqrt{\pi R}}\int d^4x\bar{f}^{(0)}(x)\gamma_\mu A^{\mu(0)}(x)f^{(0)}(x)&\\=g\int d^4x\bar{f}^{(0)}(x)\gamma_\mu A^{\mu(0)}(x)f^{(0)}(x).&\end{aligned} \tag{2.59}$$

Clearly, we will get the exact zero-mode coupling as that of SM if $g=\widetilde{g}/\sqrt{\pi R}$, which is the correct scaling between the four- and five-dimensional coupling, as we mentioned in Eq. 2.50. We can generalize a trilinear coupling for different KK-level, *e.g.* the coefficient of $\bar{f}^{(p)}A^{(q)}f^{(r)}$. This can be written as

$$\int d^4x\left(\bar{f}^{(p)}(x)\gamma_\mu A^{\mu(q)}(x)f^{(r)}(x)\right)\int_0^{\pi R}dy\frac{\widetilde{g}}{(\pi R)^{3/2}}\left\{\cos\left(\frac{py}{R}\right)\cos\left(\frac{qy}{R}\right)\cos\left(\frac{ry}{R}\right)\right.$$

$$+\cos\left(\frac{py}{R}\right)\cos\left(\frac{qy}{R}\right)\sin\left(\frac{ry}{R}\right)+\sin\left(\frac{py}{R}\right)\cos\left(\frac{qy}{R}\right)\cos\left(\frac{ry}{R}\right)+\sin\left(\frac{py}{R}\right)\cos\left(\frac{qy}{R}\right)\sin\left(\frac{ry}{R}\right)\Big\}$$
$$=\int d^4x\left(\bar{f}^{(p)}(x)\gamma_\mu A^{\mu(q)}(x)f^{(r)}(x)\right)\times g\{\Delta(n_p,n_q,n_r)\}, \tag{2.60}$$

where, $\Delta(n_p, n_q, n_r)$ are the admixtures of Krönecker delta symbols alongwith some normalization factors. It can be shown that the KK-number violating couplings are vanishing. Thus a second level particle can not interact with two zeroth level particles at tree level. This type of coupling, however, can be possible at loop level. Also we will see later, that such type of (2)-(0)-(0) coupling is present, even at tree level, in the non-minimal version of UED. Similar procedure of calculation of interactions among different fields will be used in the case of non-minimal version of UED also. Hence, we have altogether the following features of UED model at tree level:

- The SM fields correspond to the zero modes of the bulk fields and always follow the NN boundary conditions. For zero mode, the number of bulk fields is exactly the same as the number of fields in the SM.
- The KK excitations, in general, have both NN and DD boundary conditions.
- The interaction at tree-level preserves the KK-number, *e.g.* in the above example $n_{(p)} + n_{(q)} + n_{(r)} = 0$, where we actually assign the opposite signs to the KK-number for the initial and final states. This is evidently mandated from the fact that the translational invariance is locally retained in the bulk, and hence the momentum along the fifth dimension $p_y = n/R$ remains conserved.

2.3 minimal Universal Extra Dimension

In the previous section, we have discussed UED model and have seen that this model contains a number of almost degenerate states at each KK-level. As the extra dimensional momentum is conserved (ignoring the fixed points of orbifold) the phenomenology of such nearly degenerate states crucially depends on the mass splitting between the KK-modes. We know that radiative corrections play an important role for precision measurements, but it is not expected this correction radically change the nature of processes, like the production and decay of new particles in collider experiments. But this projection can be completely wrong in presence of extra dimensions as KK-masses are quantized at tree level and all the momentum preserving decays are exactly at threshold. Hence radiative corrections [122] become the most important determining factor and the dominant effect in deciding which decay channels are open. Under radiative corrections the mass of nth KK-mode (Eq. 2.12) will be modified as $\sqrt{m_0^2 + (n/R)^2 + \delta m_n^2}$, where δm_n is the correction in mass due to the radiative corrections. The mass correction arises from

the higher order contributions to the two-point correlation functions. There are two types of contributions to these mass corrections;

- corrections coming from compactification, which is called *bulk correction*,
- *boundary correction* which arises due to orbifolding.

The *first* type of correction comes from the S^1 compactification which eventually breaks the five-dimensional Lorentz invariance globally. This type of non-local effect results in internal loops in Feynman diagrams, which wind around the circle of the compactified dimension (see Fig. 2.2). The contributions generating from this type of loops are well defined and finite. The *second*

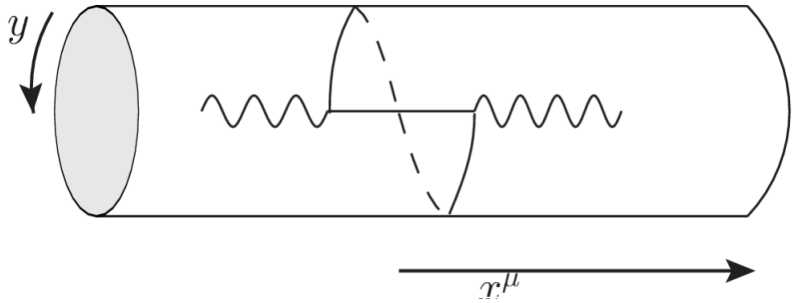

FIGURE 2.2: An example of Lorentz violating loop winding around the extra dimension [122].

type of correction is the immediate upshot of the orbifold compactification $S^1/\mathbb{Z}_2$. Orbifolding introduces fixed points ($y = 0$ and $y = \pi R$ in our case) in the manifold and they results in the additional breaking of five-dimensional Lorentz invariance. This is obviously a local effect. A detailed calculation on radiative corrections of a field theory in $S^1/\mathbb{Z}_2$ orbifold has been shown in Ref. [125]. Unlike bulk contribution, the mass shift resulting from this orbifold correction no longer remains finite, but is logarithmically divergent. To remove these divergent terms one has to perform renormalization which in turn requires the incorporation of counterterms which are localized at the orbifold fixed points. At this point, one can simplify this computation by assuming that the boundary terms at the cutoff Λ are small. This means with no large boundary terms, the logarithmic divergences can be absorbed into the cutoff Λ, where Λ is not too large. Large boundary terms result in the mixing between different KK-levels and hence each mode receives, in addition to the bulk correction, a shift in its mass that is logarithmically dependent on the cutoff Λ. In that case, we have to consider both effects while calculating the radiative corrections.

The scenario with the assumption of vanishing boundary terms at the cutoff Λ is known as *minimal UED (mUED)*. Considering the effect of two types of corrections, the total mass shift

δm_n for various particles are given by [119],

$$\delta m_{Q^{(n)}} = \frac{n}{16\pi^2 R}\left(6g_s^2 + \frac{27}{8}g^2 + \frac{1}{8}g'^2\right)\ln(\Lambda R), \tag{2.61a}$$

$$\delta m_{U^{(n)}} = \frac{n}{16\pi^2 R}\left(6g_s^2 + 2g'^2\right)\ln(\Lambda R), \tag{2.61b}$$

$$\delta m_{D^{(n)}} = \frac{n}{16\pi^2 R}\left(6g_s^2 + \frac{1}{2}g'^2\right)\ln(\Lambda R), \tag{2.61c}$$

$$\delta m_{L^{(n)}} = \frac{n}{16\pi^2 R}\left(\frac{27}{8}g^2 + \frac{9}{8}g'^2\right)\ln(\Lambda R), \tag{2.61d}$$

$$\delta m_{E^{(n)}} = \frac{n}{16\pi^2 R}\frac{9}{2}g'^2\ln(\Lambda R), \tag{2.61e}$$

$$\delta m^2_{\mathcal{B}^{(n)}} = \frac{g'^2}{16\pi^2 R^2}\left(-\frac{39}{2}\frac{\zeta(3)}{\pi^2} - \frac{n^2}{3}\ln(\Lambda R)\right), \tag{2.61f}$$

$$\delta m^2_{\mathcal{W}^{(n)}} = \frac{g^2}{16\pi^2 R^2}\left(-\frac{5}{2}\frac{\zeta(3)}{\pi^2} + 15n^2\ln(\Lambda R)\right), \tag{2.61g}$$

$$\delta m^2_{\mathcal{G}^{(n)}} = \frac{g_s^2}{16\pi^2 R^2}\left(-\frac{3}{2}\frac{\zeta(3)}{\pi^2} + 23n^2\ln(\Lambda R)\right), \tag{2.61h}$$

$$\delta m^2_{h^{(n)}} = \frac{n^2}{16\pi^2 R^2}\left(3g^2 + \frac{3}{2}g'^2 - 2\lambda_h\right)\ln(\Lambda R), \tag{2.61i}$$

where g', g and g_s are the gauge couplings for the $U(1)_Y$, $SU(2)_L$ and $SU(3)_c$ groups respectively (previously mentioned) and λ_h is the Higgs quartic coupling. The above expressions show that there are no bulk corrections to the Higgs scalar mass or the fermion masses. The factor $\zeta(3) = \sum_{n=1}^{\infty} n^{-3} \approx 1.202$, is the third Riemann zeta function. The factor $\ln(\Lambda R)$ in the Eqs. 2.61 corresponds to the orbifold corrections and the Λ independent contributions are from bulk corrections. Actually, the factor is $\ln\left(\frac{\Lambda}{\mu'}\right)$, where μ' is the renormalization scale. The factor ΛR counts the number of KK-levels below the cutoff Λ. If the contributions coming from Yukawa coupling is taken into account (which is important for top quark), then $SU(2)$ doublet quark Q and singlet U get corrections as

$$\delta_{\text{Yuk}} m_{Q^{(n)}} = \frac{n}{16\pi^2 R}\left(-\frac{3}{2}(y^u)^2\right)\ln(\Lambda R), \tag{2.62a}$$

$$\delta_{\text{Yuk}} m_{U^{(n)}} = \frac{n}{16\pi^2 R}\left(-3y^u\right)\ln(\Lambda R). \tag{2.62b}$$

Thus to obtain the radiatively corrected mass for nth mode top quark, we should add the above results with appropriate corrections presented in Eqs. 2.61. As we know the nonzero KK-level fermions are vector-like, so the appropriate eigenstates and mass eigenvalues of the KK fermions can be obtained by diagonalizing the mass matrix of the form

$$\begin{pmatrix} \frac{n}{R} + \delta' m(F^{(n)}) & m_f \\ m_f & -\frac{n}{R} - \delta' m(f^{(n)}) \end{pmatrix}, \tag{2.63}$$

where m_f is the zero-mode mass obtained from electroweak symmetry breaking (EWSB), $F^{(n)}$ and $f^{(n)}$ correspond to $SU(2)$ doublet and singlet fermions respectively. The δ' indicates the total corrections obtained from both bulk as well as boundary corrections.

There are other mixings that occur among the KK excitations. There exists mixing between the $\mathcal{W}^{3(n)}$ and $\mathcal{B}^{(n)}$ gauge bosons. The mass-squared matrix in the $\mathcal{B}^{(n)}$ and $\mathcal{W}^{3(n)}$ basis is

$$\begin{pmatrix} \frac{1}{4}g'^2v^2 + \hat{\delta}m^2_{\mathcal{B}^{(n)}} + \frac{n^2}{R^2} & -\frac{1}{4}g'gv^2 \\ -\frac{1}{4}g'gv^2 & \frac{1}{4}g^2v^2 + \hat{\delta}m^2_{\mathcal{W}^{3(n)}} + \frac{n^2}{R^2} \end{pmatrix} \tag{2.64}$$

The mass eigenstates and eigenvalues of the KK photons and Z bosons for each KK-mode can be derived from the above mass matrix. The terms corresponding to $\hat{\delta}$ represent the corrections due to both bulk and boundary conditions. It is evident that, for the zeroth level the diagonal entries will have only the v^2 dependent terms and the eigenvalues of this matrix will be $\{0, (g^2 + g'^2)v^2/4\}$, where zero corresponds to the mass eigenvalue of the SM photon and $(g^2 + g'^2)v^2/4$ is the mass-squared eigenvalue of the SM Z boson. For $n > 0$ the full matrix in Eq. 2.64 is to be used. Clearly, for the KK excitations, the Weinberg mixing angle θ_n will also be different from that of zero-mode particles (SM) and is given by

$$\theta_n = \frac{1}{2}\tan^{-1}\left(\frac{g'gv^2}{2\left[\hat{\delta}m^2_{\mathcal{B}^{(n)}} - \hat{\delta}m^2_{\mathcal{W}^{3(n)}} + \frac{v^2}{4}(g'^2 - g^2)\right]}\right). \tag{2.65}$$

However, the value of θ_n is small which eventually makes the KK photon more $\mathcal{B}^{(n)}$-like and the KK Z boson more $\mathcal{W}^{3(n)}$-like [122]. They are often applied exchangeably.

Unlike four-dimensional SM, in mUED the KK W and Z boson acquire their masses by absorbing the linear combination of the fifth component of the corresponding gauge fields and their respective KK Goldstone bosons. After this, there remains four scalar states for each KK-level: two charged scalars $H^{(n)\pm}$, CP-even neutral scalar $h^{(n)}$ and CP-odd neutral scalar $A^{(n)}$. The zero modes $H^{(0)\pm}$ and $A^{(0)}$ are the usual Goldstone bosons ($\phi^\pm$ and χ) of the SM. The one loop corrected masses of these extra scalar states are

$$m^2_{H^{(n)\pm}} = M^2_{W^{(0)}} + \frac{n^2}{R^2} + \delta m^2_{h^{(n)}}, \tag{2.66}$$

$$m^2_{A^{(n)}} = M^2_{Z^{(0)}} + \frac{n^2}{R^2} + \delta m^2_{h^{(n)}}, \tag{2.67}$$

where, $\delta m^2_{h^{(n)}}$ is given by Eq. 2.61i.

2.3.1 Mass Spectrum

After a detailed discussion on radiative corrections of the masses for different particles, we shall now describe the particle spectrum of the full one loop corrected mUED. It is clear from the previous section that, the shift in the mass is different for different types of particles (see Eqs. 2.61 and 2.62). Naturally for nonzero KK-level, mass spectrum will no longer be degenerate. As a consequence, the phenomenology of the model will be considerably different from what would have been the case for the tree level degenerate spectrum. As an illustration, the mass spectrum for $n = 1$ corresponding a definite choice of mUED parameters (m_h, $1/R$ and Λ)[8] has been shown in Fig. 2.3 [122][9].

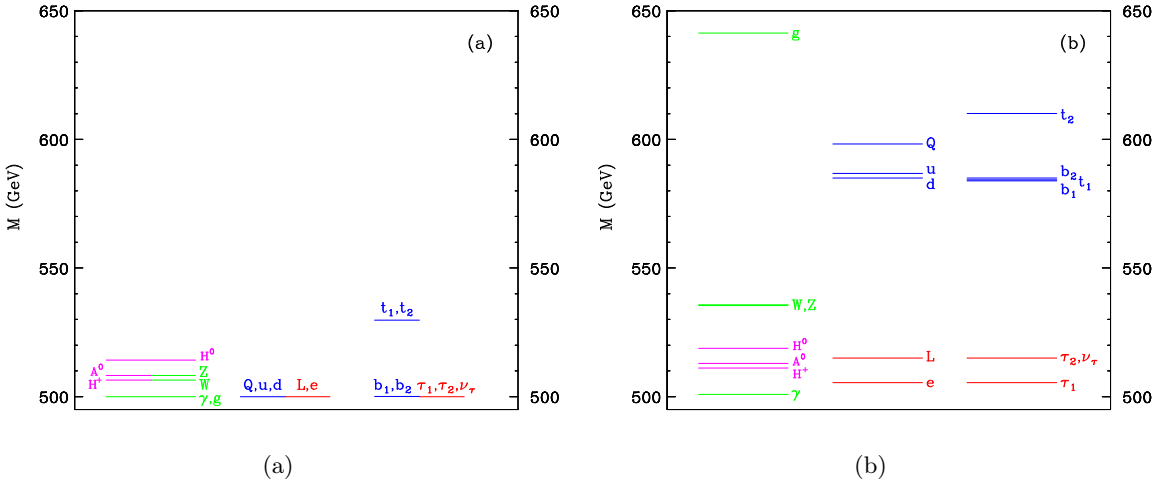

(a) (b)

FIGURE 2.3: Particle spectrum for the first level KK particles at tree level (left) and after the inclusion of one loop correction (right) with Higgs mass $m_h = 120$ GeV, $1/R = 500$ GeV and $\Lambda R = 20$. Plot courtesy [122].

A significant consequence is that at any specific level the mass of KK photon ($\gamma^{(n)}$) receives negligible contribution from the radiative corrections. The immediate conclusion which can be drawn from this observation is that the first level photon, *i.e.* $\gamma^{(1)}$ (or $\mathcal{B}^{(1)}$, so to say) is the lightest KK particle (LKP); $\mathcal{B}^{(1)}$ is a particle with odd KK-parity. The decay of this particle to any other KK-level particle is kinematically impermissible and to SM particles is forbidden as the very upshot of the conservation of KK-parity. Thus $\mathcal{B}^{(1)}$ is a stable particle having all the properties which can be counted as a viable dark matter candidate [128, 129].

[8] Here m_h is the mass of SM Higgs boson. After the discovery of Higgs boson [34, 126] and following the subsequent analysis in Ref. [127], $m_h = 125.9 \pm 0.4$ GeV.

[9] In this figure, H^0 is basically the SM Higgs $h^{(0)}$ according to the notation used in this thesis.

2.4 Constraints on (m)UED Scenario

The (m)UED model, as we have described, is fundamentally a one-parameter extension of the SM. Several experimental and theoretical observations put constraints on the parameter space of (m)UED. Agashe *et al.* [130] first pointed out the fact that charged Higgs bosons at first KK-level could contribute to the radiative B decays through the quark transition $b \to s\gamma$. Many other processes like K and B decays and the measurement $(g-2)_\mu$ considerably restrict the mUED model [131]. The radiative B decays set constraint on the lower bound on R^{-1} as, $R^{-1} > 250$ GeV. A recent study on this same decay [132] including next-to-next-to leading order QCD corrections contributes a stricter bound as $R^{-1} > 323$ GeV. Electroweak precision tests at the LEP-1 and LEP-2 colliders provide slightly more stringent bounds. The mUED contributions to the S and T parameters (represented as $\hat{S}$ and $\hat{T}$ respectively) are given [133] as

$$\begin{aligned} \hat{S} &= \frac{g^2\zeta(2)}{4(4\pi)^2R^{-2}}\left\{\frac{2}{3}m_t^2 + \frac{1}{6}m_h^2\right\}, \\ \hat{T} &= \frac{g^2\zeta(2)}{(4\pi)^2R^{-2}}\left\{\frac{m_t^4}{M_W^2} - \frac{5}{12}\frac{\sin^2\theta_W}{\cos^2\theta_W}m_h^2\right\}. \end{aligned}$$

The above equations show that the contribution to $\hat{T}$ is much greater than to that of the $\hat{S}$ due to the effect of large quark mass. The KK excitations of top quarks as well as of KK Higgs states in one loop contribute to these variables at significant level, whereas the electroweak gauge boson propagators give the merest contributions. In the wake of the discovery of Higgs boson a detailed study has been performed on the new physics contributions to these variables [134] which provides a constraint on the parameter space as $R^{-1} > 680$ GeV.

Another studies on $(g-2)_\mu$ [135], FCNC processes [136, 137], ρ-parameter [138] and studies on some electroweak processes [139–141] results in the lower bound on $R^{-1} \geq 300$ GeV.

The results from the LHC and the Tevatron also set limits on (m)UED parameters. The constraints have been obtained from LHC analysis and also from many other experiments in searching of dark matter [142–144]. Some other projected bounds from the LHC is in the range of TeV [145–147]. The contributions coming from the KK excitations in loop modify the Higgs production and decay rate [148]. The constraints mainly arise from $gg \to h \to \gamma\gamma, WW^*, ZZ^*$. However, the data from the ATLAS [149] and the CMS [150] experiments show that among all these channels, $h \to WW^*$ gives the most stringent constraint on R^{-1}. The ATLAS Higgs data with the combined center-of-mass energies 7 TeV and 8 TeV at 25 fb^{-1} luminosity gives a constraint as $R^{-1} > 460$ GeV, whereas CMS provides a much stricter bound of $R^{-1} > 1300$ GeV [151]. Such kind of large deviation occur mainly due to the large difference in signal strengths (μ value) registered by the two experiments. In all the processes described till now, the constraints on UED parameter space comes from their loop induced contributions to those processes. Apart from such kind of indirect constraints, some direct searches for mUED signal

also set limits on this scenario. Level-1 KK particles are produced in pair at the LHC and thereafter they cascade into SM particles and the LKP. A search for $\gamma\gamma$ events with large missing transverse momentum for $\sqrt{s} = 7$ TeV at luminosity 4.8 fb^{-1} by the ATLAS experiment absolutely rules out R^{-1} up to 1.41 TeV [152]. We know that level-2 KK gauge bosons in mUED do not interact to any SM particle (level-0) at tree level as that would result KK-number violation. However, an effective coupling among these particles may occur at one loop level that respect KK-parity. This has a remarkable importance since it permits the resonance production of level-2 gauge bosons at the LHC. Many new physics models with higher symmetry group claim the existence of additional gauge bosons (Z' or W'). The level-2 electroweak gauge bosons in mUED ($\gamma^{(2)}, Z^{(2)}$ or $W^{(2)\pm}$) can be considered as such additional gauge boson candidates. Clearly, the absence of such signals, can lead to bounds on level-2 KK gauge bosons. CMS search for such resonant Z' in the dilepton channel results in a constraint of $R^{-1} > 715$ GeV for mUED [153].

In previous chapter, it has been already mentioned that LKP can be a viable WIMP dark matter candidate. The level-1 KK photon ($\gamma^{(1)}$) can be treated as LKP and hence the prospective dark matter candidate. The relic density is defined as the measure of dark matter present in today's Universe. The current value of the relic density from Planck data [61] is $\Omega_{\rm DM}h^2 \sim 0.1198 \pm 0.0026$. In an mUED scenario corresponding to a cutoff scale $\Lambda = 20R^{-1}$, the value of R^{-1} which gives the correct relic density is around 1300 GeV [75, 154]. The actual constraint may vary depending on the nature of the dark matter and the mass splitting with other particles. However, one can avoid the bounds in many possible ways and make the constraint more flexible. For example, constraints are less restrictive for a $Z^{(1)}$ WIMP or for a multi-component dark matter scenario. Clearly, the constraints depend on various assumptions and in actual situation may be less stringent. It is evident that one should keep the above information in mind while studying the mUED scenario.

So, presently the strongest bound on R^{-1} comes from the consideration of Higgs boson production and decay [151] or from the consideration of relic density [75]. In the last two cases, the derived limits are comparable and yield $R^{-1} \geq 1.3$ TeV.

2.4.1 Finding the Cutoff

In the framework of mUED, the KK-modes of SM particles, would nontrivially affect the running of gauge couplings and as well as the Higgs self coupling λ_h, which in turn affects the Higgs mass [155, 156]. The value of λ_h at the Higgs mass scale is rather small $\lambda_h(m_h) \simeq 6.5 \times 10^{-2}$. With this starting value, the running of $\lambda(Q)$ falls to zero as the energy scale Q rises to around $4R^{-1}$ and becomes negative around $Q \sim (5-6)R^{-1}$. In a sense, the electroweak vacuum would destabilize at that point and hence there must be some cutoff for the mUED theory; the UED framework ceases to work beyond this scale and it serves as a natural cutoff of this framework.

Clearly, R^{-1} being the fundamental mass gap between two consecutive KK-levels, one arrives at this energy scale after crossing the 5-6 KK-levels.

2.5 non-minimal Universal Extra Dimensional Model

We have seen in the previous section that the mass spectrum of the mUED model can be drastically changed by radiative corrections. The mass spectrum has been calculated under the assumption that boundary terms do not contribute to the kinetic terms. This kind of assumption is unnatural and has been pointed out in the Ref. [157] as there exist many boundary-localized kinetic terms which obey all the symmetries, even KK-parity. We have also observed that the orbifold corrections are logarithmically divergent. These can be removed by introducing boundary-localized kinetic terms. A general form of these boundary-localized kinetic terms can be

$$r\{\delta(y) + \delta(y - \pi R)\} \times (\text{appropriate field combinations}) \tag{2.68}$$

The symbol r is the free parameter of the theory. Now we can tune the parameter r in such a way that the boundary-localized terms (BLTs) can be zero at some scale (say, at 1 TeV), but they will be induced again radiatively at some other scale. This unknown coefficient is called boundary-localized parameter which has to be fixed from phenomenological considerations. Every bulk term in the model has their corresponding BLT parameter. In the following, a particular non-minimal scenario will be considered in which the kinetic and Yukawa terms of the respective fields as well as the mass and potential terms of the scalar fields are added to their corresponding five-dimensional actions at the boundary points. Coefficients of the boundary-localized terms (BLTs) are the free parameters of this model.

2.5.1 A Brief Review of the Model

In this section, we will briefly review the model (mainly in electroweak sector) to set the notations and conventions. For completeness first we will describe the general set-up of nmUED with BLTs and as we proceed we will point out how we can go back to UED. For a more detailed discussion of the model see Refs. [81, 128, 157–174].

2.5.1.1 Lagrangian and Interactions

To begin with, consider the five-dimensional action for quarks[10]. The resulting action in five dimensions is given by

$$\begin{aligned}\mathcal{S}_{\text{quark}} \;=\; & \int d^4x \int_0^{\pi R} dy \Big[\overline{Q} i\Gamma^M \mathcal{D}_M Q + r_f\{\delta(y)+\delta(y-\pi R)\}\overline{Q} i\gamma^\mu \mathcal{D}_\mu P_L Q \\ & + \overline{U} i\Gamma^M \mathcal{D}_M U + r_f\{\delta(y)+\delta(y-\pi R)\}\overline{U} i\gamma^\mu \mathcal{D}_\mu P_R U \\ & + \overline{D} i\Gamma^M \mathcal{D}_M D + r_f\{\delta(y)+\delta(y-\pi R)\}\overline{D} i\gamma^\mu \mathcal{D}_\mu P_R D\Big], \end{aligned} \tag{2.69}$$

where the four component five-dimensional fields are comprised of chiral spinors and their Kaluza-Klein excitations and they can be written as

$$Q_{t,b}(x,y) = N_{Q0}\, Q^{(0)}_{t,bL} + \sum_{n=1}^{\infty}\left\{Q^{(n)}_{t,bL}(x) f^{(n)}_L(y) + Q^{(n)}_{t,bR}(x) g^{(n)}_L(y)\right\}, \tag{2.70a}$$

$$U(x,y) = N_{Q0}\, U^{(0)}_R + \sum_{n=1}^{\infty}\left\{U^{(n)}_L(x) f^{(n)}_R(y) + U^{(n)}_R(x) g^{(n)}_R(y)\right\}, \tag{2.70b}$$

$$D(x,y) = N_{Q0}\, D^{(0)}_R + \sum_{n=1}^{\infty}\left\{D^{(n)}_L(x) f^{(n)}_R(y) + D^{(n)}_R(x) g^{(n)}_R(y)\right\}. \tag{2.70c}$$

In the effective four-dimensional theory the zero-modes of Q will give rise to the $SU(2)_L$ doublet quarks whereas the zero-mode of U (D) will be identified with the up (down) type singlet quark, *i.e.* after compactification and orbifolding the zero-modes of Q will be the left-handed doublet comprising of SM t_L and b_L, whereas t_R and b_R would emerge from the U and D respectively. The compact form of quark doublet is $Q \equiv (Q_i, Q_j)^T$, where i and j correspond to up type and down type quark respectively. N_{Q0} is the normalization constant of the fermionic wave functions for zero-mode. In Eq. 2.69 the terms containing the parameter r_f are the BLKTs. Clearly in the UED, r_f is assumed to be vanishing. It is worth mentioning that by setting BLKT parameters to zero one can translate from nmUED to UED.

Now, from the variation of action and considering appropriate boundary conditions, one can obtain the y-dependent mode functions f and g:

$$f_L(y) = g_R(y) = N_{Qn}\begin{cases} \dfrac{\cos[M_{Q_n}\left(y-\frac{\pi R}{2}\right)]}{C_{Q_n}} & \text{for } n \text{ even}, \\ \dfrac{-\sin[M_{Q_n}\left(y-\frac{\pi R}{2}\right)]}{S_{Q_n}} & \text{for } n \text{ odd}, \end{cases} \tag{2.71}$$

[10] Leptonic fields will follow similar procedure.

and

$$g_L(y) = f_R(y) = N_{Qn} \begin{cases} \dfrac{\sin[M_{Q_n}\left(y - \frac{\pi R}{2}\right)]}{C_{Q_n}} & \text{for } n \text{ even}, \\ \dfrac{\cos[M_{Q_n}\left(y - \frac{\pi R}{2}\right)]}{S_{Q_n}} & \text{for } n \text{ odd}, \end{cases} \tag{2.72}$$

with

$$C_{Q_n} = \cos\left(\frac{M_{Q_n}\pi R}{2}\right), \quad S_{Q_n} = \sin\left(\frac{M_{Q_n}\pi R}{2}\right). \tag{2.73}$$

The orthonormality conditions satisfied by fs and gs are given by

$$\int dy \left[1 + r_f\{\delta(y) + \delta(y - \pi R)\}\right]\ k^{(m)}(y)\ k^{(n)}(y) = \delta^{mn} = \int dy\ l^{(m)}(y)\ l^{(n)}(y) \tag{2.74}$$

where, k can be f_L or g_R and l corresponds to g_L or f_R. From the above condition one can obtain the normalization factors as

$$N_{Qn} = \sqrt{\frac{2}{\pi R}} \left[\frac{1}{\sqrt{1 + \frac{r_f^2 M_{Qn}^2}{4} + \frac{r_f}{\pi R}}}\right]. \tag{2.75}$$

For zero-mode, the normalization constant is given by

$$N_{Q0} = \frac{1}{\sqrt{r_f + \pi R}}. \tag{2.76}$$

In passing, we note that $r_f = 0$ implies the usual UED normalization $\sqrt{2/(\pi R)}$ for nth mode, whereas for zero-mode it will be $\sqrt{1/(\pi R)}$. The quantity M_{Qn} in the previous equations represents the KK-mass and is given by the following transcendental equations as,

$$r_f M_{Qn} = \begin{cases} -2\tan\left(\frac{M_{Qn}\pi R}{2}\right) & \text{for } n \text{ even}, \\ 2\cot\left(\frac{M_{Qn}\pi R}{2}\right) & \text{for } n \text{ odd}. \end{cases} \tag{2.77}$$

Clearly for $r_f = 0$ we get back the UED KK-mass n/R. In Fig. 2.4 we show the dependence of KK-mass on the BLKT parameter; here we have taken $1/R$ to be 1 TeV.

After discussing the fermions we now describe the actions for gauge and scalar fields and the Yukawa interactions. The respective actions are given by,

$$\mathcal{S}_{\text{gauge}} = -\frac{1}{4}\int d^4x \int_0^{\pi R} dy \Big[\sum_a \left(\mathcal{F}^{MNa}\mathcal{F}^a_{MN} + r_g\{\delta(y) + \delta(y - \pi R)\}\mathcal{F}^{\mu\nu a}\mathcal{F}^a_{\mu\nu}\right) + \mathcal{B}^{MN}\mathcal{B}_{MN} + r_g\{\delta(y) + \delta(y - \pi R)\}\mathcal{B}^{\mu\nu}\mathcal{B}_{\mu\nu}\Big], \tag{2.78}$$

$$\mathcal{S}_{\text{scalar}} = \int d^4x \int_0^{\pi R} dy \Big[\left(\mathcal{D}^M\Phi\right)^\dagger\left(\mathcal{D}_M\Phi\right) + \mu^2_{(5)h}\Phi^\dagger\Phi - \lambda_{(5)h}(\Phi^\dagger\Phi)^2$$

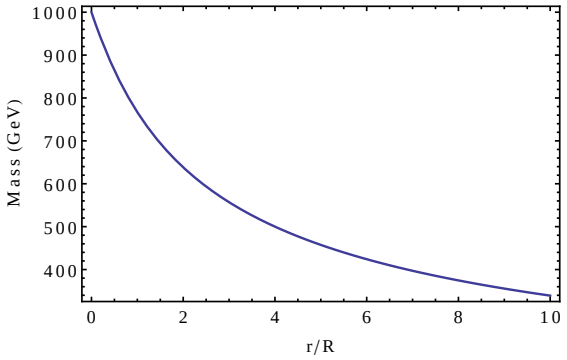

FIGURE 2.4: Dependence of first KK-level mass on the BLKT parameter for $1/R = 1$ TeV.

$$+ \{\delta(y) + \delta(y - \pi R)\}\{r_\phi \left(\mathcal{D}^\mu \Phi\right)^\dagger \left(\mathcal{D}_\mu \Phi\right) + \mu_B^2 \Phi^\dagger \Phi - \lambda_B (\Phi^\dagger \Phi)^2\}\Big], \tag{2.79}$$

$$\mathcal{S}_{\text{yuk}} = -\int d^4x \int_0^{\pi R} dy \Big[\tilde{y}^u \bar{Q} \Phi^c U + \tilde{y}^d \bar{Q} \Phi D + r_y \{\delta(y) + \delta(y - \pi R)\} \times \left(\tilde{y}^u \bar{Q}_L \tilde{\Phi} U_R + \tilde{y}^d \bar{Q}_L \Phi D_R\right) + \text{h.c.}\Big]. \tag{2.80}$$

All the conventions of field-strength tensors, Higgs doublet, gamma matrices and five-dimensional metric are same as given in Sec. 2.2.4. The BLKT parameters for gauge and scalar fields are r_g and r_ϕ respectively, whereas r_y denotes the boundary-localized Yukawa parameter. The symbols $\mu_{(5)h}$ and $\lambda_{(5)h}$ respectively represent the five-dimensional bulk Higgs mass parameter and scalar self-coupling (Sec. 2.2.4); μ_B and λ_B are the boundary-localized Higgs mass parameters and the scalar quartic coupling respectively. In the limit, $r_\phi = r_g$ the scalar and gauge fields will have the same y-dependent profile given in Eqs. 2.81 and 2.82. If the two BLT parameters are taken to be different, the breakdown of electroweak symmetry results in a term proportional to r_ϕ in the differential equations governing the dynamics of the gauge profile in y direction [175]. Consequently, the y-profile solutions of the gauge field will be different from what is given below (Eqs. 2.81 and 2.82). Throughout the analysis, these two BLKT parameters r_ϕ and r_g, will be taken as equal to avoid the nontrivial scenario. Thus the y-dependent wave functions for scalar or gauge fields for nth KK-mode with appropriate boundary conditions are given by

$$f_\phi^{(n)} = N_{\Phi n} \begin{cases} \dfrac{\cos(M_{\Phi_n}\left(y - \frac{\pi R}{2}\right))}{C_{\Phi_n}} & \text{for } n \text{ even}, \\ \dfrac{-\sin(M_{\Phi_n}\left(y - \frac{\pi R}{2}\right))}{S_{\Phi_n}} & \text{for } n \text{ odd}. \end{cases} \tag{2.81}$$

Since the fifth component of gauge field are projected out by $\mathbb{Z}_2$ odd condition, no zero mode appears for $W_5^{\pm}$, and the y-profile for nth KK-mode is given by [165, 169, 171, 172, 176]

$$g_\phi^{(n)} = N_{\Phi n} \begin{cases} \dfrac{\sin(M_{\Phi_n}\left(y-\frac{\pi R}{2}\right))}{C_{\Phi_n}} & \text{for } n \text{ even}, \\ \dfrac{\cos(M_{\Phi_n}\left(y-\frac{\pi R}{2}\right))}{S_{\Phi_n}} & \text{for } n \text{ odd}, \end{cases} \tag{2.82}$$

with

$$C_{\Phi_n} = \cos\left(\frac{M_{\Phi_n}\pi R}{2}\right), \quad S_{\Phi_n} = \sin\left(\frac{M_{\Phi_n}\pi R}{2}\right). \tag{2.83}$$

These wave functions $f_\phi^{(n)}$ and $g_\phi^{(n)}$ satisfy the orthonormality conditions

$$\int dy\,[1 + r_f\{\delta(y) + \delta(y-\pi R)\}]\;\; f_\phi^{(n)}(y)\; f_\phi^{(m)}(y) = \delta^{nm} = \int dy\; g_\phi^{(n)}(y)\; g_\phi^{(m)}(y), \tag{2.84}$$

which give the normalization constant as

$$N_{\Phi n} = \sqrt{\frac{2}{\pi R}}\left[\frac{1}{\sqrt{1 + \frac{r_\phi^2 M_{\Phi n}^2}{4} + \frac{r_\phi}{\pi R}}}\right]. \tag{2.85}$$

The mass $M_{\Phi n}$ of the nth KK-mode now satisfies the following transcendental equations

$$r_\phi M_{\Phi n} = \begin{cases} -2\tan\left(\frac{M_{\Phi n}\pi R}{2}\right) & \text{for } n \text{ even}, \\ 2\cot\left(\frac{M_{\Phi n}\pi R}{2}\right) & \text{for } n \text{ odd}. \end{cases} \tag{2.86}$$

In case of nmUED, the five-dimensional gauge couplings $\tilde{g}$ and $\tilde{g}'$, are related to their four-dimensional counterparts g and g' by

$$g\;(g') = N_{\Phi 0}\;\tilde{g}\;(\tilde{g}') = \frac{\tilde{g}\;(\tilde{g}')}{\sqrt{r_g + \pi R}}. \tag{2.87}$$

For the zeroth mode of Higgs to be flat [165, 177] the following conditions must hold [11].

$$\mu_B^2 = r_\phi \mu_{(5)h}^2 \;\text{ and }\; \lambda_B = r_\phi \lambda_{(5)h}. \tag{2.88}$$

We will use 't Hooft–Feynman gauge in our calculation and its important to spell out the gauge fixing action in this scenario. These actions, following Refs. [169, 176], are given by,

$$\mathcal{S}_{\rm GF}^A \;=\; -\frac{1}{2\xi_y}\int d^4x \int_0^{\pi R} dy\Big(\partial_\mu A^\mu + \xi_y \partial_5 A^5\Big)^2, \tag{2.89}$$

[11] If the boundary parameters are unequal in Eq. 2.79, the mass term would involve KK-mode mixing and diagonalization of KK-mass matrix would modify the wave functions implying a y-dependent zero mode [177].

$$\mathcal{S}^{Z}_{\rm GF} = -\frac{1}{2\xi_y}\int d^4x \int_0^{\pi R} dy\Big\{\partial_\mu Z^\mu + \xi_y(\partial_5 Z^5 - iM_Z\chi\{1+r_\phi\left(\delta(y)+\delta(y-\pi R)\right)\}\Big\}^2, \tag{2.90}$$

$$\mathcal{S}^{W}_{\rm GF} = -\frac{1}{\xi_y}\int d^4x \int_0^{\pi R} dy\Big|\partial_\mu W^{\mu+} + \xi_y(\partial_5 W^{5+} - iM_W\phi^+\{1+r_\phi\left(\delta(y)+\delta(y-\pi R)\right)\}\Big|^2. \tag{2.91}$$

In the above, M_Z and M_W are the respective masses of the Z and W boson; $\mathcal{S}^{A}_{\rm GF}$, $\mathcal{S}^{Z}_{\rm GF}$ and $\mathcal{S}^{W}_{\rm GF}$ are the gauge fixing actions for photon, Z boson and W boson respectively. The gauge fixing parameter ξ_y is related to *physical* gauge fixing parameter ξ (equals to 1 in Feynman gauge, and 0 in Landau gauge) by [169, 171, 172, 176]

$$\frac{1}{\xi_y} = \frac{1}{\xi}\{1+r_\phi\left(\delta(y)+\delta(y-\pi R)\right)\}. \tag{2.92}$$

The standard procedure to calculate the effective four-dimensional couplings is to write the original five-dimensional interaction terms and then replacing each field by their corresponding KK expansions and then integrate out the extra coordinate y. In (m)UED this type of couplings are equivalent to their SM counterparts. But in case of nmUED, the couplings get modification from the overlap integrals of the form,

$$I^{ijk} = \int_0^{\pi R} dy\ f^{(i)}_\alpha(y)\ f^{(j)}_\beta(y)\ f^{(k)}_\gamma(y), \tag{2.93}$$

where the Greek indices (subscripts) denotes the type of field and the Latin indices (superscripts) refer to the KK-level of the respective fields. This type of modification in coupling is characteristic to the nmUED scenario. The root of this modification lies in the fact that unlike (m)UED, the KK-mode function in nmUED has BLT parameter dependence, explicitly in normalization factors and implicitly in KK-masses. Also note that if $(i+j+k)$ is an odd integer then these overlap integrals vanish due to the conservation of KK-parity.

2.5.1.2 Physical Eigenstates

In the effective four-dimensional theory, the presence of higher KK-modes of various fields will mix to give rise to physical fields. This type of mixing will be present in fermionic as well as in scalar/gauge sector.

In the quark sector the strength of mixing is proportional to the quark mass. Thus it is significant for top sector. This mixing matrix can be diagonalized by separate unitary matrices for left-

and right-handed quarks:

$$\mathscr{U}_L^{(n)} = \begin{pmatrix} -\cos\alpha_n & \sin\alpha_n \\ \sin\alpha_n & \cos\alpha_n \end{pmatrix}, \quad \mathscr{U}_R^{(n)} = \begin{pmatrix} \cos\alpha_n & -\sin\alpha_n \\ \sin\alpha_n & \cos\alpha_n \end{pmatrix}, \tag{2.94}$$

where $\alpha_n = \frac{1}{2}\tan^{-1}\left(\frac{m_t}{M_{Qn}}\right)$ with m_t denoting the SM top quark mass. In *nth* KK-level, mass term can be written as,

$$\begin{pmatrix} \bar{Q}_{i_L}^{(m)} & \bar{U}_L^{(m)} \end{pmatrix} \begin{pmatrix} -M_{Qn}\delta^{mn} & m_i\alpha_1\mathcal{I}^{mn} \\ m_i\alpha_1 & M_{Qn}\delta^{mn} \end{pmatrix} \begin{pmatrix} Q_{i_R}^{(n)} \\ U_R^{(n)} \end{pmatrix} + \text{h.c.}, \tag{2.95}$$

where M_{Qn} are the solutions of transcendental equations given in Eq. 2.77. $\mathcal{I}^{mn}$ is an overlap integral of the form

$$\int_0^{\pi R} [1 + r_y\{\delta(y) + \delta(y - \pi R)\}]\, f_L^{(m)}(y) g_R^{(n)}(y)\, dy,$$

and

$$\alpha_1 = \frac{\pi R + r_f}{\pi R + r_Y}.$$

In general $\mathcal{I}^{mn}$ is nonzero whether $n = m$ or $n \neq m$. However, the $n \neq m$ case would lead to the KK-mode mixing among the quarks of a particular flavor. An interesting point to note is that for the choice $r_f = r_y$, $\mathcal{I}^{mn} = \delta_{mn}$ and obviously $\alpha_1 = 1$. Thus to get a simpler form of fermion mixing matrix and avoid the mode mixing we will stick to the choice of equal r_y and r_f. Taking into account of these matrices one can now relate the gauge eigenstates $Q_i^{(n)}$ $(U^{(n)})$ and mass eigenstates $Q_i^{\prime(n)}$ $(U^{\prime(n)})$ as (in this notation i refers to the up quark flavor),

$$Q_{i_{L/R}}^{(n)} = \mp\cos\alpha_n Q_{i_{L/R}}^{\prime(n)} + \sin\alpha_n U_{L/R}^{\prime(n)}, \tag{2.96a}$$

$$U_{L/R}^{(n)} = \pm\sin\alpha_n Q_{i_{L/R}}^{\prime(n)} + \cos\alpha_n U_{L/R}^{\prime(n)}. \tag{2.96b}$$

The mass eigenstates, in this case, share the same mass eigenvalue,

$$m_{Q_t^{\prime(n)}} = m_{U^{\prime(n)}} = \sqrt{m_t^2 + M_{Qn}^2} \equiv M_{\text{top}}. \tag{2.97}$$

Similar procedure follows for the down sector also. While dealing with the four-dimensional effective Lagrangian there also exist bilinear terms involving the KK excitations (from first and higher KK-levels) of the 5th components of Z bosons and the KK excitations of $\chi^{(0)}$ of the Higgs doublet field; and similarly there are mixing terms between the 5th component of $W^{\pm}$ and the KK excitations of $\phi^{(0)\pm}$ of the Higgs doublet field [124]. Mixing between $A_\mu^{(n)}$ and $A_5^{(n)}$ cancels by adding $\mathcal{S}_{\text{GF}}^A$, and the new spectrum consists of a massless zero-mode photon, a tower of KK-modes with masses $M_{\Phi n}^2$ for both $A_\mu^{(n)}$ and $A_5^{(n)}$. Using the gauge fixing actions and

appropriate mode functions of gauge and scalar fields (Eqs. 2.81, 2.82) and finally integrating over y, the mass matrices for the mixing between KK-modes of $Z^{5(n)}$ and $\chi^{(n)}$ and that for the mixing between the KK-modes of $W_5^{\pm(n)}$ and $\phi^{\pm(n)}$ are respectively given by

$$\begin{pmatrix} Z^{5(n)} & \chi^{(n)} \end{pmatrix} \begin{pmatrix} M_Z^2 + \xi M_{\Phi n}^2 & (1-\xi) M_Z M_{\Phi n} \\ (1-\xi) M_Z M_{\Phi n} & M_{\Phi n}^2 + \xi M_Z^2 \end{pmatrix} \begin{pmatrix} Z^{5(n)} \\ \chi^{(n)} \end{pmatrix}, \tag{2.98}$$

and

$$\begin{pmatrix} W_5^{(n)-} & \phi^{(n)-} \end{pmatrix} \begin{pmatrix} M_W^2 + \xi M_{\Phi n}^2 & -i(1-\xi) M_W M_{\Phi n} \\ i(1-\xi) M_W M_{\Phi n} & M_{\Phi n}^2 + \xi M_W^2 \end{pmatrix} \begin{pmatrix} W_5^{(n)+} \\ \phi^{(n)+} \end{pmatrix} + \text{h.c.}. \tag{2.99}$$

Diagonalization of the mass matrix present in Eq. 2.98 would lead to a tower of Goldstone modes of Z ($G_Z^{(n)}$ with mass-squared $\xi(M_{\Phi n}^2 + M_Z^2)$) and a physical CP-odd scalars ($A^{(n)}$ with mass-squared $M_{\Phi n}^2 + M_Z^2$) respectively given as

$$G_Z^{(n)} = \frac{1}{M_{Z_n}} \left(-M_{\Phi n} Z^{5(n)} + M_Z \chi^{(n)} \right), \tag{2.100a}$$

$$A^{(n)} = \frac{1}{M_{Z_n}} \left(M_{\Phi n} \chi^{(n)} + M_Z Z^{5(n)} \right). \tag{2.100b}$$

A similar diagonalization in Eq. 2.99 would also generate KK-tower of charged Goldstone bosons (with mass-squared $\xi(M_{\Phi n}^2 + M_W^2)$) and a physical charged Higgs pair (with mass-squared $M_{\Phi n}^2 + M_W^2$) given by

$$G^{\pm(n)} = \frac{1}{M_{W_n}} \left(M_{\Phi n} W^{\pm 5(n)} \mp i M_W \phi^{\pm(n)} \right), \tag{2.101a}$$

$$H^{\pm(n)} = \frac{1}{M_{W_n}} \left(M_{\Phi n} \phi^{\pm(n)} \mp i M_W W^{\pm 5(n)} \right). \tag{2.101b}$$

The fields $Z^{\mu(n)}$, $G_Z^{(n)}$ and $A^{(n)}$ all possess the common mass eigenvalue as $M_{Zn} \equiv \sqrt{M_{\Phi n}^2 + M_Z^2}$. Similarly $W^{\mu(n)\pm}$, $G^{(n)\pm}$ and $H^{(n)\pm}$ share the same mass eigenvalue $M_{Wn} \equiv \sqrt{M_{\Phi n}^2 + M_W^2}$ in 't-Hooft Feynman gauge ($\xi = 1$). The above combinations of charged Higgs and charged Goldstone ensure the vanishing coupling of $A^{\mu(0)} H^{(n)\pm} W_\nu^{(n)\mp}$[12].

[12]However, another important point to obtain these combinations is to remain careful about the sign used before the non-abelian part of the field strength tensor $\mathcal{F}_{MN}^a$; the couplings required for the above combination comes from $(\mathcal{D}^\mu \Phi)^\dagger (\mathcal{D}_\mu \Phi)$ and $\mathcal{F}_{\mu 5}^a \mathcal{F}^{\mu 5 a}$. The expressions of the charged Higgs and charged Goldstone modes do not depend on the sign used in $(\mathcal{D}^\mu \Phi)^\dagger (\mathcal{D}_\mu \Phi)$, but depends on whether $\mathcal{F}_{MN}^a$ is $\left(\partial_M \mathcal{W}_N^a - \partial_N \mathcal{W}_M^a + \tilde{g} f^{abc} \mathcal{W}_M^b \mathcal{W}_N^c\right)$ or $\left(\partial_M \mathcal{W}_N^a - \partial_N \mathcal{W}_M^a - \tilde{g} f^{abc} \mathcal{W}_M^b \mathcal{W}_N^c\right)$. For $\mathcal{F}_{MN}^a \equiv \left(\partial_M \mathcal{W}_N^a - \partial_N \mathcal{W}_M^a - \tilde{g} f^{abc} \mathcal{W}_M^b \mathcal{W}_N^c\right)$, the combinations which give the vanishing coupling of $A^{\mu(0)} H^{(n)\pm} W_\nu^{(n)\mp}$ are

$$G^{\pm(n)} = \frac{1}{M_{W_n}} \left(M_{\Phi n} W_5^{\pm(n)} \mp i M_W \phi^{\pm(n)} \right),$$

$$H^{\pm(n)} = \frac{1}{M_{W_n}} \left(M_{\Phi n} \phi^{\pm(n)} \mp i M_W W_5^{\pm(n)} \right).$$

2.5.1.3 Asymmetric BLTs

In passing it is worth mentioning that we have used symmetric BLTs which respects KK-parity. If the BLT parameter r is taken to be different at two boundary points, then we have asymmetric BLTs which eventually violate KK-parity. The example of this is given below:

$$\underbrace{r\{\delta(y)+\delta(y-\pi R)\}}_{\text{Symmetric BLT}} \quad \text{and} \quad \underbrace{\{r_1\delta(y)+r_2\delta(y-\pi R)\}}_{\text{Asymmetric BLT}}.$$

The asymmetric BLTs do not obey KK-parity [159]. It has been mentioned that KK-parity is nothing but a remaining translational invariance under the transformation, $y \to y - \pi R$. For symmetric BLTs, we have

$$\begin{aligned} r\{\delta(y)+\delta(y-\pi R)\} &\to r\{\delta(y-\pi R)+\delta(y-2\pi R)\} \\ &= r\{\delta(y-\pi R)+\delta(y)\}, \end{aligned} \tag{2.102}$$

whereas the asymmetric BLTs result in

$$\begin{aligned} \{r_1\delta(y)+r_2\delta(y-\pi R)\} &\to \{r_1\delta(y-\pi R)+r_2\delta(y-2\pi R)\} \\ &= \{r_1\delta(y-\pi R)+r_2\delta(y)\}, \end{aligned} \tag{2.103}$$

Clearly, Eqs. 2.102 and 2.103 show that under $y \to y - \pi R$ the symmetric BLT case remains invariant, which preserves KK-parity, but asymmetric BLTs do not respect KK-parity. Although violation of KK-parity would lead to unstable LKP which in turn results in the lack of good motivation of the Universal Extra Dimensional scenario regarding dark matter, but it has some interesting phenomenology in the context of collider physics [166, 167, 170]. In the literatures (*e.g.* in Refs. [164,165,177]) sometimes, the orbifold fixed points are taken at $y = +\pi R/2$ and at $y = -\pi R/2$. In that case, the respective BLT is written as $r\{\delta(y-L)+\delta(y+L)\}$. By introducing a simple mapping $y \to y + \frac{\pi R}{2}$ the results from here to that of Refs. [164, 165, 168–173] can be obtained, provided the other conventions are taken care of properly. Thus we see that nmUED differs from UED scenario in two ways. The presence of BLTs firstly modify the mass spectrum and secondly the coupling from that of UED values. It is noteworthy that mUED scenario corresponds to an intermediate state between UED and nmUED. In the mUED scenario, the mass corrections are only taken into account but the couplings are left unaltered as that of the UED case.

3

nmUED Confronts Unitarity

In the Standard Model (SM), the presence of Higgs boson ensures the complete restoration of unitarity in the longitudinal scattering of vector bosons (V_L, where $V = W, Z$) at tree level. In a seminal paper by Lee, Quigg and Thacker (LQT) [178], it has been shown that the $V_L V_L \to V_L V_L$ scattering amplitudes grow with center of mass energy (E) if Higgs boson is not included. The immediate ramification of the absence of Higgs boson in the theory is *unitarity violation* which in turn implies the breakdown of quantum mechanical sense of conservation of probability in these scattering amplitudes. Ref. [178] shows that the Higgs mass m_h should be less than 1 TeV to respect unitarity. The discovery of Higgs boson in LHC [34, 35] having mass 125 GeV (which is obviously much lower than the bound mentioned in Ref. [178]) reflects the fact that any process involving the longitudinal vector bosons as well as any other SM particles in external state would remain well-behaved at any arbitrary high energies.

However, in five-dimensional Universal Extra Dimensional model with the missing Kaluza-Klein (KK) Higgs sector, the longitudinal scattering of gauge bosons do not respect partial wave unitarity if other KK-modes are involved. With the inclusion of higher modes of Higgs boson the unitarity is completely preserved [142]. But this is the case of the five-dimensional Universal Extra Dimensional model, where there is no boundary-localized terms (BLT) and the theory is effectively one parameter theory. In this case the only parameter R^{-1} does not play any role in unitarity violation. Things appear to be certainly different in non-minimal Universal Extra Dimensional (nmUED) scenario where the BLTs are present. These terms are associated with

corresponding parameters which are called boundary-localized parameters and it is still a matter of analysis whether BLTs play any role in unitarity violation.

In nmUED, many studies have been done to find the lower limit of the inverse of compactification radius R^{-1} as well as to constrain the allowed range of BLT parameters [164, 169, 172] till date. But no robust studies have been performed yet to set the upper limit on these parameters. The Refs. [122, 125] have shown that the boundary terms are generated by radiative corrections and in a sense, are loop suppressed. Still it is not apparent and not even very clear what would be the actual range of the BLT parameters, the new parameters of the theory. Though the BLT parameters are the coefficients of boundary-localized terms originated from radiative corrections, no drastic conclusion, such as they should be small, can be drawn about their range like since the other parts of the Lagrangian are dependent on these parameters too. Boundary-localized parameters might have some higher values and still can altogether result in BLTs which are in effect loop suppressed. These boundary terms can be considered as some effective operators with some unknown coefficients. All in all, a study of unitarity is therefore essential for determining the upper bound in four-dimensional effective theory. This chapter includes a detailed study on unitarity in gauge and scalar sectors that would set an upper limit on the respective BLT parameters.

We begin by reviewing the basic idea of implementation of unitarity constraint and a short description of the Lagrangian and interactions required in this analysis. Then we refer the processes needed in the analysis. After that we compute the bounds on the parameters. This chapter follows largely from Ref. [173].

3.1 Unitarity Constraints

Any $2 \to 2$ scattering amplitudes, $\mathcal{M}(\theta)$ can be expressed in terms of scattering angle θ. That in turn can be expanded in terms of an infinite sum of partial waves as

$$\mathcal{M}(\theta) = 16\pi \sum_{J=0}^{\infty} a_J \, (2J+1) \, P_J(\cos\theta). \tag{3.1}$$

Here, a_J represents the scattering amplitude of Jth partial wave and $P_J(\cos\theta)$ is Jth order Legendre polynomial. Refs. [178,179] show that the unitarity constraints of scattering amplitudes can be manifested as constraints on partial-wave coefficients, in particular on the zeroth partial wave amplitudes a_0 as

$$|\text{Re } (a_0)| \leq \frac{1}{2}. \tag{3.2}$$

By exploiting the equivalence theorem [178] in the high energy limit the unphysical scalars of the theory can be used instead of the original longitudinal components of the gauge bosons. The

relevant $2 \to 2$ scatterings should get contributions from the quartic couplings only. The contributions coming from the trilinear couplings can be safely ignored as the diagrams originating from those couplings will have an E^2-suppression due to intermediate propagators. Following Ref. [178] a t-matrix (which is t^0 for $J = 0$) can be constructed from different two-particle states represented as rows and columns. Evidently each matrix element corresponds to the scattering amplitudes between the respective 2-particle state in the row and in the column. Consequently, the unitarity constraint can be manifested as the bounds on the eigenvalues of the matrix (t^0) given by

$$|\mathcal{M}| \leq 8\pi. \tag{3.3}$$

However, the procedure of finding the constraint as the bounds on the eigenvalues of matrix can be extremely complicated and leads to an unpalatable scenario in the case of nmUED. In many cases, the trilinear couplings are proportional to the KK-masses. Consequently the contributions coming from these trilinear terms can not be ignored as the matrix elements in those cases are the functions of s, where $\sqrt{s}$ denotes the center of mass energy of the respective scattering processes. So one can end up with an intractable determinant [180]. But this conclusion comes with a caveat that single channel scattering is not enough to analyze the bad high energy behaviour in any five-dimensional compactified theory, whereas the coupled channel analysis is preferable for the study of unitarity violation [179]. Coupled channel analysis is performed by constructing a t^0 matrix for all suitable scattering channels and obtaining the eigenvalues as functions of the model parameters, and hence demanding that no eigenvalues should exceed 8π. Thus, in the present scenario, we would first like to obtain the expressions of a_0 for every possible $2 \to 2$ process in the entire scalar sector of nmUED model. In those cases, the quartic couplings are not suppressed by KK-masses and the BLT parameters can be constrained from Eq. 3.2. Following this we can perform the coupled channel analysis with some selective channels which do not eventually fall with $\sqrt{s}$ and can further constrain the bounds on parameters using Eq. 3.3.

3.2 Lagrangian and Interactions

Now we briefly discuss the Lagrangian and interactions required in the analysis of finding the bound on BLT parameters from unitarity. In this case, all we need are five-dimensional action for gauge fields given in Eq. 2.78 and for the scalar fields given by Eq. 2.79. Here, the kinetic terms for gauge and scalar fields as well as the mass and interaction terms of scalar fields are added to their respective five-dimensional actions at the boundary points. Substituting the Eq. 2.88 in Eq. 2.79, we can have the form of five-dimensional Lagrangian of scalar field $\mathcal{L}_\Phi$ as

$$\mathcal{L}_\Phi = \int_0^{\pi R} dy \Big[\{1 + r_\phi \left(\delta(y) + \delta(y - \pi R)\right)\} \left(\mathcal{D}^\mu \Phi\right)^\dagger \left(\mathcal{D}_\mu \Phi\right)$$

$$+\{1+r_\phi\left(\delta(y)+\delta(y-\pi R)\right)\}(\mu^2_{(5)h}\Phi^\dagger\Phi-\lambda_{(5)h}(\Phi^\dagger\Phi)^2)-(\mathcal{D}_5\Phi)^\dagger(\mathcal{D}_5\Phi)\Big]. \quad (3.4)$$

The terms $\int_0^{\pi R}dy\{1+r_\phi\left(\delta(y)+\delta(y-\pi R)\right)\}(\mu^2_{(5)h}\Phi^\dagger\Phi-\lambda_{(5)h}(\Phi^\dagger\Phi)^2)$ and $\int_0^{\pi R}dy\{-(\mathcal{D}_5\Phi)^\dagger(\mathcal{D}_5\Phi)\}$ in the above equation contribute to the required scalar interactions. Since by virtue of the equivalence theorem in the high energy limit, we can replace all the longitudinal modes of gauge bosons by their respective unphysical scalars or Goldstone modes [178], only scalar interactions are required in this analysis. The Higgs doublet Φ can be expanded [181, 182] in terms of zero-mode and its KK-tower as

$$\Phi=\frac{1}{\sqrt{r_\phi+\pi R}}\Phi^{(0)}+\Phi^{(n)}f^{(n)}_\phi,$$

and consequently $D_5\Phi$ can be written as

$$\mathcal{D}_5\Phi=-M_{\Phi n}\Phi^{(n)}g^{(n)}_\phi-i\widetilde{\mathcal{X}}^{(n)}g^{(n)}_\phi\frac{\Phi^0}{\sqrt{r_\phi+\pi R}}-i\widetilde{\mathcal{X}}^{(p)}g^{(p)}_\phi\Phi^{(n)}f^{(n)}_\phi,$$

with

$$\widetilde{\mathcal{X}}^{(n)}=\frac{1}{2}\begin{pmatrix}\tilde{g}\mathcal{W}^{(n)3}_5+\tilde{g}'\mathcal{B}^{(n)}_5 & \sqrt{2}\tilde{g}W^{(n)+}_5\\ \sqrt{2}\tilde{g}W^{(n)-}_5 & -\tilde{g}\mathcal{W}^{(n)3}_5+\tilde{g}'\mathcal{B}^{(n)}_5\end{pmatrix} \quad (3.5)$$

Substituting all the required y-profiles in the above and integrating over the extra dimension y, the final form of the last two parts of Eq. 3.4 (denoted as $\mathcal{L}_1$ and $\mathcal{L}_2$) can be represented as

$$\begin{aligned}\mathcal{L}_1 &= \mu_h^2(\Phi^{(0)\dagger}\Phi^{(0)})-\lambda_h(\Phi^{(0)\dagger}\Phi^{(0)})^2+\mu_h^2(\Phi^{(n)\dagger}\Phi^{(n)})-2\lambda_h(\Phi^{(0)\dagger}\Phi^{(0)})(\Phi^{(n)\dagger}\Phi^{(n)})\\ &\quad -\lambda_h(\Phi^{(0)\dagger}\Phi^{(n)}+\Phi^{(n)\dagger}\Phi^{(0)})(\Phi^{(0)\dagger}\Phi^{(n)}+\Phi^{(n)\dagger}\Phi^{(0)})\\ &\quad -2\lambda_h\,\mathcal{I}^{npq}(\Phi^{(0)\dagger}\Phi^{(n)}+\Phi^{(n)\dagger}\Phi^{(0)})(\Phi^{(p)\dagger}\Phi^{(q)})-\lambda_h\,\mathcal{I}^{npqr}(\Phi^{(n)\dagger}\Phi^{(p)})(\Phi^{(q)\dagger}\Phi^{(r)}), \quad (3.6)\\ \mathcal{L}_2 &= -M^2_{\Phi n}\Phi^{(n)\dagger}\Phi^{(n)}-iM_{\Phi n}\Phi^{(n)\dagger}\mathcal{X}^{(n)}\Phi^{(0)}+iM_{\Phi n}\Phi^{(0)\dagger}\mathcal{X}^{\dagger(n)}\Phi^{(n)}-\Phi^{(0)\dagger}\mathcal{X}^{\dagger(n)}\mathcal{X}^{(n)}\Phi^{(0)}\\ &\quad -iM_{\Phi n}\,\mathcal{I}_1{}^{npq}\Phi^{(n)\dagger}\mathcal{X}^{(p)}\Phi^{(q)}+iM_{\Phi q}\,\mathcal{I}_1{}^{pqn}\Phi^{(n)\dagger}\mathcal{X}^{(p)\dagger}\Phi^{(q)}-\mathcal{I}_1{}^{npq}\Phi^{(0)\dagger}\mathcal{X}^{(n)\dagger}\mathcal{X}^{(p)}\Phi^{(q)}\\ &\quad -\mathcal{I}_1{}^{pqn}\Phi^{(n)\dagger}\mathcal{X}^{(p)\dagger}\mathcal{X}^{(q)}\Phi^{(0)}-\mathcal{I}_1{}^{pqn}\Phi^{(n)\dagger}\mathcal{X}^{(p)\dagger}\mathcal{X}^{(q)}\Phi^{(0)}\\ &\quad -\mathcal{I}_1{}^{prnq}\Phi^{(n)\dagger}\mathcal{X}^{(p)\dagger}\mathcal{X}^{(r)}\Phi^{(q)}, \quad (3.7)\end{aligned}$$

where the sum over all possible KK-indices are implied. In the above, λ_h is the four-dimensional counterpart of $\lambda_{(5)h}$ given as

$$\lambda_h=\frac{\lambda_{(5)h}}{r_\phi+\pi R},$$

and μ_h is related to its five-dimensional counterpart as

$$\mu_h=\mu_{(5)h}.$$

Here $\mathcal{X}$s are the matrices given as

$$\mathcal{X}^{(n)} = \frac{1}{2}\begin{pmatrix} g\mathcal{W}_5^{(n)3} + g'\mathcal{B}_5^{(n)} & \sqrt{2}gW_5^{(n)+} \\ \sqrt{2}gW_5^{(n)-} & -g\mathcal{W}_5^{(n)3} + g'\mathcal{B}_5^{(n)} \end{pmatrix} \tag{3.8}$$

and are related to its five-dimensional counterpart $\widetilde{\mathcal{X}}$ as

$$\mathcal{X}^{(n)} = \frac{\widetilde{\mathcal{X}}^{(n)}}{\sqrt{r_g + \pi R}}. \tag{3.9}$$

The overlap integrals[1] arising from the integrations of y-profiles are given as

$$\mathcal{I}^{npq} = \sqrt{r_\phi + \pi R}\int_0^{\pi R} dy\ [1 + r_\phi\{\delta(y) + \delta(y - \pi R)\}] f_\phi^{(n)} f_\phi^{(p)} f_\phi^{(q)}, \tag{3.10}$$

$$\mathcal{I}^{npqr} = (r_\phi + \pi R)\int_0^{\pi R} dy\ [1 + r_\phi\{\delta(y) + \delta(y - \pi R)\}] f_\phi^{(n)} f_\phi^{(p)} f_\phi^{(q)} f_\phi^{(r)}, \tag{3.11}$$

$$\mathcal{I}_1{}^{npq} = \sqrt{r_\phi + \pi R}\int_0^{\pi R} dy\ g_\phi^{(n)} g_\phi^{(p)} f_\phi^{(q)}, \tag{3.12}$$

$$\mathcal{I}_1{}^{pqn} = \sqrt{r_\phi + \pi R}\int_0^{\pi R} dy\ g_\phi^{(p)} g_\phi^{(q)} f_\phi^{(n)}, \tag{3.13}$$

$$\mathcal{I}_1{}^{prnq} = (r_\phi + \pi R)\int_0^{\pi R} dy\ g_\phi^{(p)} g_\phi^{(r)} f_\phi^{(n)} f_\phi^{(q)}. \tag{3.14}$$

From Eqs. 3.6 and 3.7, we obtain the mass of nth mode Higgs as $m_{hn} \equiv \sqrt{M_{\Phi n}^2 + m_h^2}$, m_h being the mass of zero-mode Higgs. The overlap integrals are nonzero when the sum of all indices $(n+p+q+r)$ are even and their values will be zero when the sum is odd due to the conservation of KK-parity. Substituting all the expressions (Eqs. 2.100 and 2.101) in terms of $A^{(n)}$, $G_Z^{(n)}$, $H^{(n)\pm}$ and $G^{(n)\pm}$ in Eqs. 3.6 and 3.7 all the couplings and interactions can be obtained. We list all the necessary Feynman rules in Appendices A, B and E.

3.3 Relevant Scattering Processes

Now we are all set to discuss on the relevant processes to find the upper bound on gauge and scalar BLT parameters from unitarity analysis using Eq. 3.2. Initially we will restrict our calculations to (n), $(n) \to (n)$, (n) processes. In these processes, the KK-numbers of the initial and the final states are same and respective quartic couplings are not suppressed by KK-masses. In scalar sector we have altogether 13 processes satisfying these conditions. Considering $2 \to 2$ processes, we have neutral two-particle states and charged two-particle states.

[1] Overlap integrals are actually absent in UED as the wave functions are of simple form like $\sin(\frac{ny}{R})$ or $\cos(\frac{ny}{R})$.

The bases of neutral two-particle states are

$$\left\{\frac{h^{(n)}h^{(n)}}{\sqrt{2}}, \frac{A^{(n)}A^{(n)}}{\sqrt{2}}, \frac{G_Z^{(n)}G_Z^{(n)}}{\sqrt{2}}, G_Z^{(n)}A^{(n)}, H^{(n)+}H^{(n)-}, H^{(n)\pm}G^{(n)\mp}\right\} \text{ and } \left\{h^{(n)}A^{(n)}, h^{(n)}G_Z^{(n)}\right\}, \quad (3.15)$$

and the bases of charged two-particle states are given by

$$\left\{H^{(n)\pm}h^{(n)}, G^{(n)\pm}h^{(n)}, H^{(n)\pm}G_Z^{(n)}\right\} \text{ and } \left\{H^{(n)\pm}A^{(n)}, G^{(n)\pm}A^{(n)}\right\}. \quad (3.16)$$

Eqs. 3.15 and 3.16 show that there exist two types of neutral two-particle states and two kinds of charged two-particle states respectively. Since we are working in CP-conserving scenario, with $h^{(n)}$ being CP-even and $A^{(n)}, G_Z^{(n)}$ being CP-odd it is evident that there will be no mutual interactions among these two different kind of states. The diagrams for all necessary processes are shown in Figs. 3.1-3.6, and their corresponding expressions of a_0 are given in Appendices C and D. In this entire analysis, we have not considered the radiative corrections of Weinberg angle (θ_W) [122] which arises due to the presence of KK-modes.

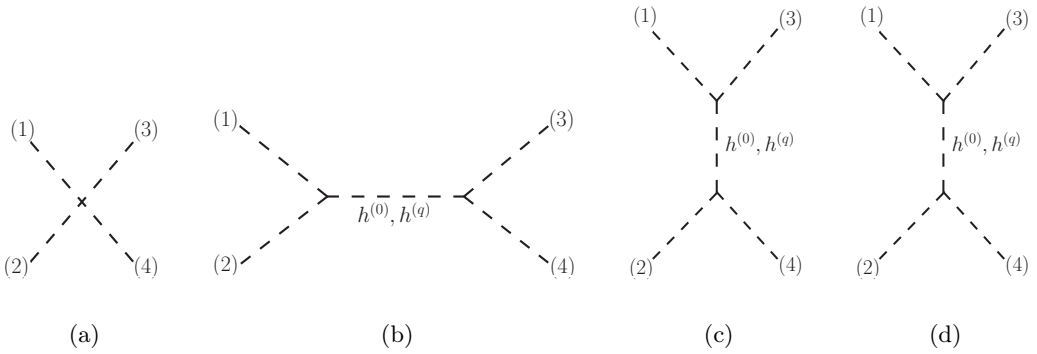

FIGURE 3.1: Diagrams for the processes $h^{(n)}(1)h^{(n)}(2) \to h^{(n)}(3)h^{(n)}(4)$, $A^{(n)}(1)A^{(n)}(2) \to A^{(n)}(3)A^{(n)}(4)$, $G_Z^{(n)}(1)A^{(n)}(2) \to G_Z^{(n)}(3)A^{(n)}(4)$.

The quartic couplings showed in Fig. 3.3 (a) can also generate the processes $h^{(n)}h^{(n)} \to G_Z^{(n)}G_Z^{(n)}$, $h^{(n)}h^{(n)} \to A^{(n)}A^{(n)}$. But the amplitudes in the latter cases will be suppressed by a factor of 1/2 as compared to the amplitudes of the processes given in Fig. 3.3. This suppression occurs due to the normalization factor $1/\sqrt{2}$ arising from the presence of the same bosonic states both in the initial and final states. Same argument will hold for the process $A^{(n)}A^{(n)} \to G_Z^{(n)}G_Z^{(n)}$ resulting from the quartic interaction given in Fig. 3.1 (a). This amplitude will be also suppressed by a factor of 1/2 as compared to the process $A^{(n)}G_Z^{(n)} \to A^{(n)}G_Z^{(n)}$ mentioned in Fig. 3.1 for same reason. The quartic couplings in Fig. 3.5 (a) can also give rise to the processes $h^{(n)}h^{(n)} \to H^{(n)+}H^{(n)-}$, $h^{(n)}h^{(n)} \to G^{(n)+}G^{(n)-}$, $A^{(n)}A^{(n)} \to H^{(n)+}H^{(n)-}$, $A^{(n)}A^{(n)} \to G^{(n)+}G^{(n)-}$, $G_Z^{(n)}G_Z^{(n)} \to H^{(n)+}H^{(n)-}$, which will eventually be suppressed by a factor of $1/\sqrt{2}$

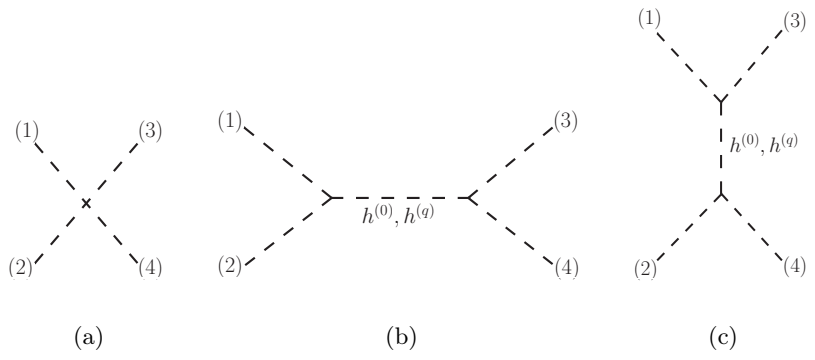

FIGURE 3.2: Diagrams for the process involving $H^{(n)+}(1)H^{(n)-}(2) \to H^{(n)+}(3)H^{(n)-}(4)$.

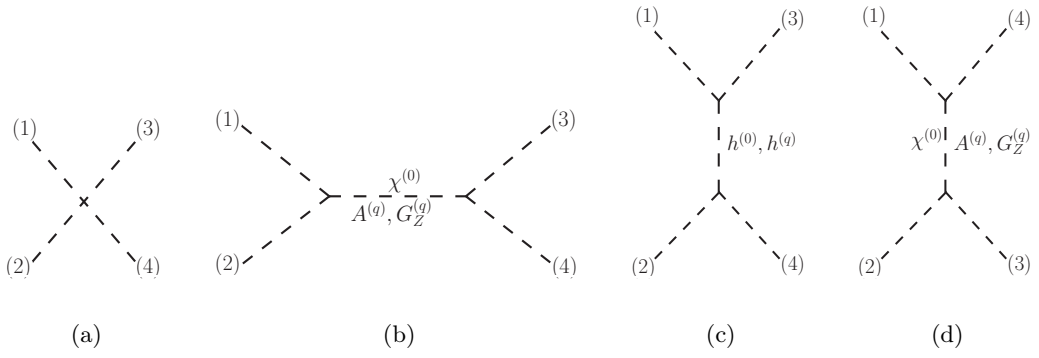

FIGURE 3.3: Diagrams for the processes $h^{(n)}(1)A^{(n)}(2) \to h^{(n)}(3)A^{(n)}(4)$, $h^{(n)}(1)G_Z^{(n)}(2) \to h^{(n)}(3)G_Z^{(n)}(4)$.

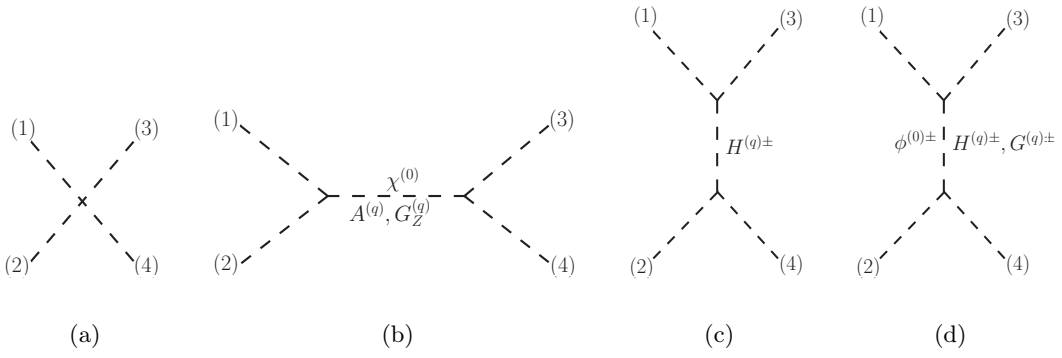

FIGURE 3.4: Diagrams for the process $h^{(n)}(1)G_Z^{(n)}(2) \to H^{(n)\pm}(3)G^{(n)\mp}(4)$.

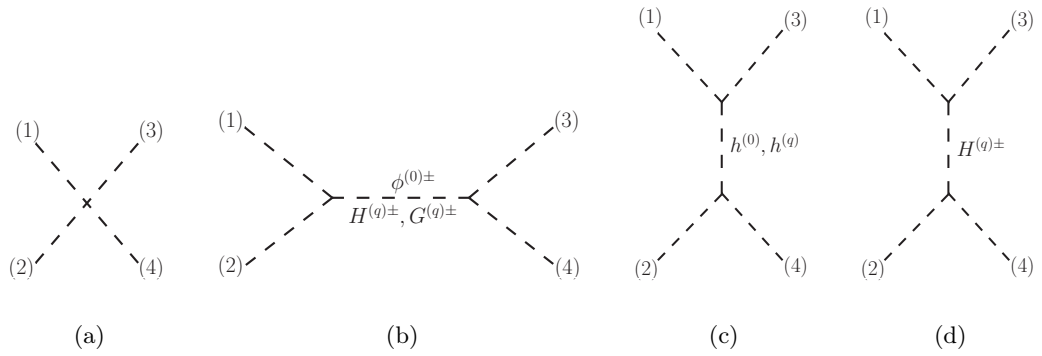

FIGURE 3.5: Diagrams for the processes $H^{(n)\pm}(1)h^{(n)}(2) \to H^{(n)\pm}(3)h^{(n)}(4)$, $G^{(n)\pm}(1)h^{(n)}(2) \to G^{(n)\pm}(3)h^{(n)}(4)$, $H^{(n)\pm}(1)A^{(n)}(2) \to H^{(n)\pm}(3)A^{(n)}(4)$, $G^{(n)\pm}(1)A^{(n)}(2) \to G^{(n)\pm}(3)A^{(n)}(4)$, $H^{(n)\pm}(1)G_Z^{(n)}(2) \to H^{(n)\pm}(3)G_Z^{(n)}(4)$.

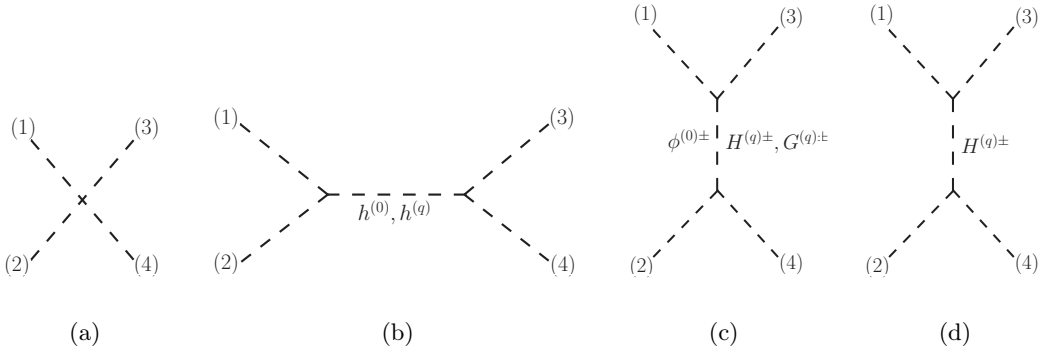

FIGURE 3.6: Diagrams for the process $A^{(n)}(1)G_Z^{(n)}(2) \to G^{(n)\mp}(3)H^{(n)\pm}(4)$.

as compared to the processes mentioned in Fig. 3.5, due to the presence of identical bosonic state in the initial (or in final) state. We are not considering those processes as the a_0 in that case will result in a unitarity violation at larger value of r_ϕ which in turn result in a less stringent bound as compared to the processes mentioned in Figs. 3.1, 3.3 and in Fig. 3.5.

The zeroth mode partial wave amplitude a_0 for each process can be studied as the function of s ($\sqrt{s}$ being the center of mass energy for respective processes) for different values of r_ϕ and one can set an upper limit on BLT parameter by Eq. 3.2. This a_0 can also be studied as function of the BLT parameter r_ϕ for a fixed s. The value of r_ϕ for which $|\text{Re } a_0|$ will be greater than half even at large limit of s, would give us the required upper bound on the BLT parameter for a particular KK-number n.

After analyzing all the relevant (n), $(n) \to (n)$, (n) channels in detail we can perform the coupled channel analysis (mentioned in Section 3.1) for suitable set of channels to obtain further constriant on the upper bound on BLT parameters [179]. However, it is not possible to obtain the channels for this purpose before acquiring the results of single channel scattering analysis.

The computation of t^0 matrix with appropriate basis and the bounds obtained from this will be analyzed elaborately in the next section after getting the results of (n), $(n) \to (n)$, (n) scattering.

3.4 Obtaining the Bounds on BLT Parameters

3.4.1 (n), $(n) \to (n)$, (n) Processes

We start this section by a discussion about the variations of a_0 for different processes as function of s for a fixed value of BLT parameter r_ϕ and vice versa. Since we are dealing only with the (n), $(n) \to (n)$, (n) processes, the variation of a_0 will be analyzed for specific KK-modes. In this single channel scattering analysis, we restrict ourselves to the KK-number up to 4. It would be clear in the latter part of this section that to obtain suitable channels for the coupled channel analysis it is sufficient to study the single channel analysis with KK-mode up to 4.

The Fig. 3.7 shows the variation of a_0 for these six processes $h^{(n)}h^{(n)} \to h^{(n)}h^{(n)}$, $A^{(n)}A^{(n)} \to A^{(n)}A^{(n)}$, $H^{(n)+}H^{(n)-} \to H^{(n)+}H^{(n)-}$, $h^{(n)}A^{(n)} \to h^{(n)}A^{(n)}$, $H^{(n)\pm}A^{(n)} \to H^{(n)\pm}A^{(n)}$, $H^{(n)\pm}h^{(n)} \to H^{(n)\pm}h^{(n)}$. The BLKT parameter r_ϕ is a dimensionful parameter. For convenience, we will use scaled BLKT parameter $R_\phi \equiv r_\phi/R$ while presenting our results. Each plot has two horizontal axes, the lower one corresponds to sR^2 and the other corresponds to R_ϕ. The vertical axis represents the values of a_0 for different values of s and R_ϕ. Here the value of R^{-1} is taken as 1500 GeV. These figures reflect that for $n = 1$, the $|\text{Re } a_0|$ is much less than half with the variation of s even at very large value of R_ϕ. We can see from these figures that $|\text{Re } a_0|$ is almost independent of s for $n = 1$ and there is no unitarity violation for $n = 1$.

The entire scenario has been changed for KK-number $n = 2$. From the Fig. 3.7, it is very clear that the variation of a_0 is quite different for $n = 2$ from the variation of a_0 for $n = 1$. In this case, $|\text{Re } a_0|$ can be greater than half for some specific value of R_ϕ for a given value of R^{-1}. As example, at $R^{-1} = 1500$ GeV, $|\text{Re } a_0|$ for the processes $h^{(n)}h^{(n)} \to h^{(n)}h^{(n)}$, $A^{(n)}A^{(n)} \to A^{(n)}A^{(n)}$, $H^{(n)+}H^{(n)-} \to H^{(n)+}H^{(n)-}$, $h^{(n)}A^{(n)} \to h^{(n)}A^{(n)}$, $H^{(n)\pm}A^{(n)} \to H^{(n)\pm}A^{(n)}$, $H^{(n)\pm}h^{(n)} \to H^{(n)\pm}h^{(n)}$ becomes greater than half when the respective values of R_ϕ are 138, 138, 103, 206, 207 and 206. This will remain same even at large value of sR^2. Clearly among all the processes mentioned in Fig. 3.7, the process $H^{(n)+}H^{(n)-} \to H^{(n)+}H^{(n)-}$ gives the most stringent upper limit on the value of R_ϕ (Fig. 3.7 (c)) for $n = 2$. One can see at $R_\phi = 103$, the value of $|\text{Re } a_0|$ becomes greater than half signaling the breakdown of unitarity.

The discontinuity along the curves in Fig. 3.7 corresponds to different values of pole masses of the propagators. KK-parity conservation ensures that whether $n = 1$ or $n = 2$, only even KK-modes can contribute along the propagators (the KK index along the propagator is denoted by q). These plots also reflect that if a_0 is considered as a function of R_ϕ for a particular sR^2 for

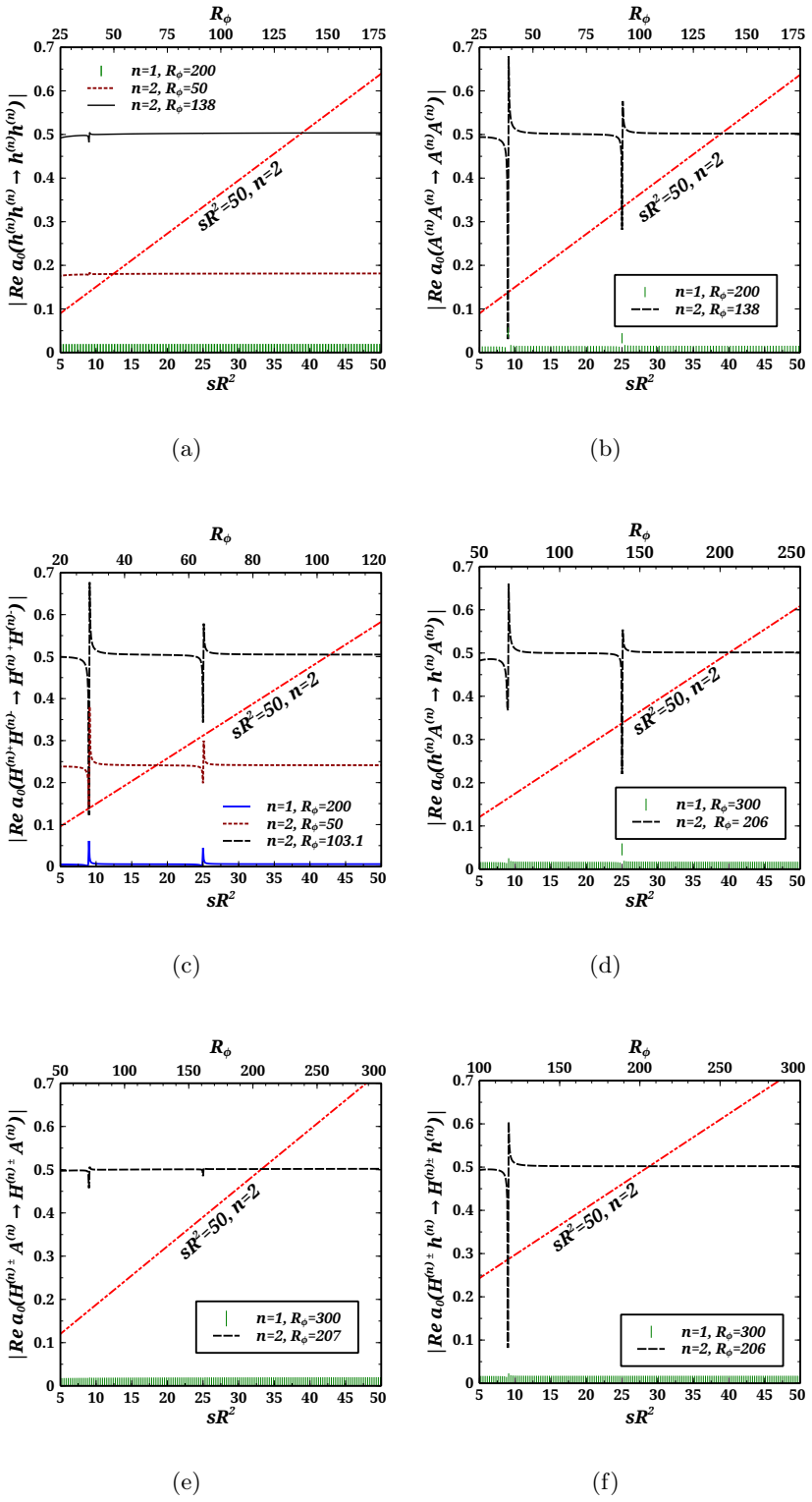

FIGURE 3.7: Variation of a_0 as a function of sR^2 for different KK-mode with different values of R_ϕ, and also as a function of R_ϕ for second KK-mode with $sR^2 = 50$. Each plot has two horizontal axes. The lowest one corresponds to sR^2 for different values of R_ϕ and the upper one shows the variation of a_0 as a function of R_ϕ for a fixed value of sR^2. Both dependences have been shown for specific KK-modes. Variations of a_0 for the processes $h^{(n)}h^{(n)} \to h^{(n)}h^{(n)}$, $A^{(n)}A^{(n)} \to A^{(n)}A^{(n)}$, $H^{(n)+}H^{(n)-} \to H^{(n)+}H^{(n)-}$, $h^{(n)}A^{(n)} \to h^{(n)}A^{(n)}$, $H^{(n)\pm}A^{(n)} \to H^{(n)\pm}A^{(n)}$, $H^{(n)\pm}h^{(n)} \to H^{(n)\pm}h^{(n)}$ are presented with R^{-1} =1500 GeV.

specific KK-mode (in Fig. 3.7, $sR^2 = 50$ and $n = 2$), variation of |Re a_0| is a straight line and will be greater than half at the same value of R_ϕ at which the unitarity violation occurs with the variation of sR^2 even at large s limit.

For $n = 3$ and $n = 4$, with $R^{-1} = 1500$ GeV, the values of R_ϕ at which |Re a_0| $> 1/2$ are shown in Table 3.1. For higher values of KK-modes unitarity breaks down at relatively lower values of R_ϕ reducing the allowed upper bound of BLT parameters. The data in the table exhibits that the process $H^{(n)+}H^{(n)-} \to H^{(n)+}H^{(n)-}$ gives the tightest upper bound on R_ϕ; for $n = 3$ and $n = 4$ the bounds are slightly different, R_ϕ should be less than 99.9 for $n = 3$ and 99.4 for $n = 4$.

Processes	Value of R_ϕ ($n = 3$)	Value of R_ϕ ($n = 4$)
$h^{(n)}h^{(n)} \to h^{(n)}h^{(n)}$	134.2	133.9
$A^{(n)}A^{(n)} \to A^{(n)}A^{(n)}$	134.2	133.7
$H^{(n)+}H^{(n)-} \to H^{(n)+}H^{(n)-}$	99.9	99.4
$h^{(n)}A^{(n)} \to h^{(n)}A^{(n)}$	202.1	202
$H^{(n)\pm}A^{(n)} \to H^{(n)\pm}A^{(n)}$	202.9	202.2
$H^{(n)\pm}h^{(n)} \to H^{(n)\pm}h^{(n)}$	202	201.3

TABLE 3.1: Values of R_ϕ for the KK-modes $n = 3$ and $n = 4$ for the processes $h^{(n)}h^{(n)} \to h^{(n)}h^{(n)}$, $A^{(n)}A^{(n)} \to A^{(n)}A^{(n)}$, $H^{(n)+}H^{(n)-} \to H^{(n)+}H^{(n)-}$, $h^{(n)}A^{(n)} \to h^{(n)}A^{(n)}$, $H^{(n)\pm}A^{(n)} \to H^{(n)\pm}A^{(n)}$, $H^{(n)\pm}h^{(n)} \to H^{(n)\pm}h^{(n)}$, at which unitarity violation occurs, *i.e.* |Re a_0| $> 1/2$. Here, $R^{-1} = 1500$ GeV.

Now, it is important to check the variation of a_0 as function of R^{-1}. The Table 3.2 shows the different values of |Re a_0| of the process $H^{(n)+}H^{(n)-} \to H^{(n)+}H^{(n)-}$ corresponding to different R^{-1} for KK-mode $n = 2, 3$ and 4. In this table, a_0 is separately analyzed considering the contributions arising due to quartic coupling and the contributions coming from quartic coupling along with trilinear contributions. We observe that R^{-1} has a nominal effect on the upper limits of R_ϕ and slightly shifts the bounds to a lower value for all KK-modes when R^{-1} is increased. For $R^{-1} = 1.5$ TeV and $n = 2$, the upper bound on R_ϕ arising from the contributions only from quartic interactions differs from the contributions coming from total amplitude by 0.1 only; considering the quartic interaction the upper bound would be $R_\phi < 103$. This small discrepancy vanishes with higher values of R^{-1} (say, 10 TeV) which results in a nominal shift in bound as $R_\phi < 102.6$ for same KK-mode. The discrepancy vanishes absolutely for R^{-1} from 5 TeV onwards for all KK-modes. For $n = 3$ and $n = 4$, R_ϕ should be less than 99.8 and 99.3 respectively at $R^{-1} = 10$ TeV. Clearly for sufficient large values of R^{-1}, trilinear contributions are fully suppressed by E^2 and a_0 solely depends on R_ϕ and not on R^{-1}; the contributions are effectively governed by quartic couplings. Evidently the sum over KK-modes in the propagators which has been taken up to 4th KK-level does not affect the result considerably. The quartic couplings in the processes mentioned in Fig. 3.7 are not suppressed by KK-masses and also the

overlap integrals are independent of R^{-1}; consequently the results have nominal dependence on R^{-1}.

The Value of R^{-1} in GeV	The value of R_ϕ for $\|\text{Re } a_0\| > \frac{1}{2}$ for different KK-modes					
	$n = 2$		$n = 3$		$n = 4$	
	From quartic coupling	From total amplitude	From quartic coupling	From total amplitude	From quartic coupling	From total amplitude
1500	103	103.1	99.9	99.9	99.3	99.4
2500	102.8	102.8	99.9	99.9	99.3	99.3
5000	102.6	102.6	99.8	99.8	99.3	99.3
7500	102.6	102.6	99.8	99.8	99.3	99.3
10000	102.6	102.6	99.8	99.8	99.3	99.3

TABLE 3.2: Value of R_ϕ signaling the breakdown of unitarity for the process $H^{(n)+}H^{(n)-} \to H^{(n)+}H^{(n)-}$ for different KK-modes and for different values of R^{-1} (GeV). Here contributions to a_0 from quartic coupling and that from the total amplitude have been presented separately.

The Fig. 3.8 shows the variation of a_0 for the processes $G^{(n)\pm}A^{(n)} \to G^{(n)\pm}A^{(n)}$, $G^{(n)\pm}h^{(n)} \to G^{(n)\pm}h^{(n)}$, $G_Z^{(n)}A^{(n)} \to G_Z^{(n)}A^{(n)}$, $h^{(n)}G_Z^{(n)} \to h^{(n)}G_Z^{(n)}$ as a function of sR^2. For KK-mode $n = 1$ there is no unitarity violation. For $n = 2$, the specific nature of a_0 due the contributions of quartic coupling and that from the total amplitude have been separately presented for a particular value of R_ϕ. As an example, for the process $G^{(n)\pm}A^{(n)} \to G^{(n)\pm}A^{(n)}$, $|\text{Re } a_0|$ will become 1/2 for $R_\phi = 741$, whereas the contributions coming from total amplitude are much less than half. The trilinear coupling in this case is effectively proportional to KK-masses and consequently the numerator in the terms generated from trilinear couplings is effectively proportional to the square of KK-masses. Thus, a_0 coming from the contributions of trilinear interactions falls from much higher value than 1/2, resulting in a falling nature of a_0 with variation of s initially. In Fig. 3.8, R^{-1} is taken as 1500 GeV. Evidently higher value of R^{-1} will result in a higher rate of falling of a_0 with sR^2. Besides, Fig. 3.8 shows that the E^2-suppression increases with increasing value of s. The uniratity violation will occur either at very large value of R_ϕ or at very large value of s. It is very clear that the contributions coming from trilinear couplings can not be ignored when the couplings are effectively proportional to KK-masses. Higher KK-modes follow the similar explanations. In this case also, the sum over KK-modes in the propagators has been taken up to 4th KK-level. Further increase in q does not change the result considerably as the contributions from higher modes will decouple from the theory.

The other processes like $A^{(n)}G_Z^{(n)} \to H^{(n)\pm}G^{(n)\mp}$, $h^{(n)}G_Z^{(n)} \to H^{(n)\pm}G^{(n)\mp}$, $H^{(n)\pm}G_Z^{(n)} \to H^{(n)\pm}G_Z^{(n)}$ give unitarity violation at very large values of R_ϕ and therefore are irrelevant to our discussions. For some specific value of R_ϕ, unitarity violation occurs as a result of the large contributions to the scattering amplitudes from the overlap integral I^n (for $n = p = q = r$, I^{npqr} would be I^n) coming from respective quartic interactions. In the Table 3.3, the overlap integral I^n is presented as a function of R_ϕ for different KK-modes ($n = 1 - 4$). This table shows that

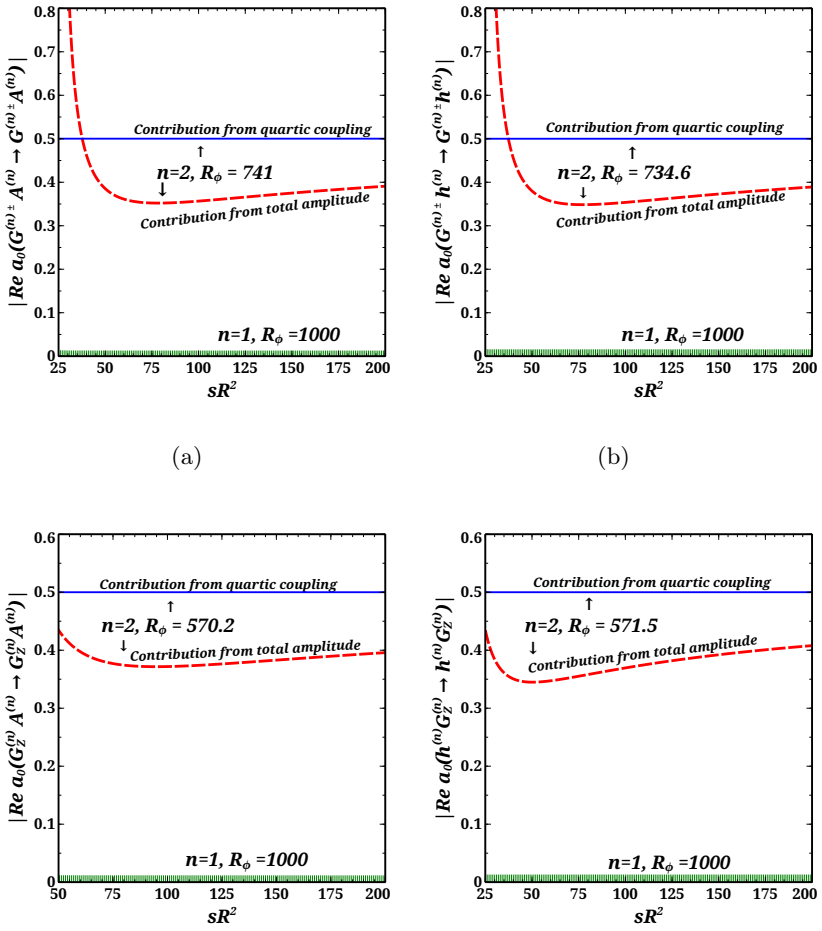

FIGURE 3.8: Variation of a_0 for processes $G^{(n)\pm}A^{(n)} \to G^{(n)\pm}A^{(n)}$, $G^{(n)\pm}h^{(n)} \to G^{(n)\pm}h^{(n)}$, $G_Z^{(n)}A^{(n)} \to G_Z^{(n)}A^{(n)}$, $h^{(n)}G_Z^{(n)} \to h^{(n)}G_Z^{(n)}$ as a function of sR^2 with different KK-modes for different values of R_ϕ. Here R^{-1} is taken as 1500 GeV.

I^n is very small for $n = 1$ even at very large value of R_ϕ, rather it decreases with increasing R_ϕ. This eventually reflects the fact why there is no unitarity violation at $n = 1$.

3.4.2 Coupled Channel Analysis

In the previous section 3.4.1, we have shown a detailed analysis of unitarity violation from a set of suitable (n), $(n) \to (n)$, (n) channels. Coupled channel analysis should be taken into account to get further constraint on the BLT parameter R_ϕ. The coupled channel analysis includes the construction of t^0 matrix generated by different two-body channels as rows and columns; restoration of unitarity demands that each of the eigenvalues of this t^0 matrix should lie below 8π (Eq. 3.3). Clearly we can proceed our analysis with the processes shown in Fig. 3.7, as for these channels unitarity violation takes place at much lower value of R_ϕ. In addition, there is

Value of R_ϕ	Value of I^n $(n=1)$	Value of I^n $(n=2)$	Value of I^n $(n=3)$	Value of I^n $(n=4)$
50	1.03	23.60	24.90	25.16
100	1.02	47.45	48.78	49.04
150	1.01	71.31	72.66	72.91
200	1.01	95.18	96.53	96.79
250	1.01	119.05	120.41	120.66
300	1.01	142.92	144.28	144.53
350	1.00	166.80	168.15	168.41
400	1.00	190.67	192.03	192.28
450	1.00	214.54	215.90	216.15
500	1.00	238.41	239.77	240.03
550	1.00	262.29	263.65	263.90
600	1.00	286.16	287.52	287.77
650	1.00	310.03	311.39	311.65
700	1.00	333.91	335.27	335.52
750	1.00	357.78	359.14	359.40
800	1.00	381.65	383.01	383.27
850	1.00	405.52	406.89	407.14
900	1.00	429.40	430.76	431.02
950	1.00	453.27	454.63	454.89
1000	1.00	477.14	478.51	478.76

TABLE 3.3: The overlap integral I^n as a function of R_ϕ for different KK-modes.

another advantage for taking these channels for t^0 construction; they are s independent and thus the contributions coming from trilinear couplings can safely be ignored. In this case too, we initially start our computation with KK-modes up to 4 only.

From Fig. 3.7, we can see that there can be neutral two-particle states and charged two-particle states in case of t^0 matrix construction. In neutral scenario this t^0 will be a 70×70 matrix and the states are given as

$$\Big\{\frac{h^{(0)}h^{(0)}}{\sqrt{2}}, \frac{h^{(1)}h^{(1)}}{\sqrt{2}}, \frac{h^{(2)}h^{(2)}}{\sqrt{2}}, \frac{h^{(3)}h^{(3)}}{\sqrt{2}}, \frac{h^{(4)}h^{(4)}}{\sqrt{2}}, h^{(0)}h^{(1)}, h^{(0)}h^{(2)}, h^{(0)}h^{(3)}, h^{(0)}h^{(4)}, h^{(1)}h^{(2)}, h^{(1)}h^{(3)},$$
$$h^{(1)}h^{(4)}, h^{(2)}h^{(3)}, h^{(2)}h^{(4)}, h^{(3)}h^{(4)}, \frac{A^{(1)}A^{(1)}}{\sqrt{2}}, \frac{A^{(2)}A^{(2)}}{\sqrt{2}}, \frac{A^{(3)}A^{(3)}}{\sqrt{2}}, \frac{A^{(4)}A^{(4)}}{\sqrt{2}}, A^{(1)}A^{(2)}, A^{(1)}A^{(3)},$$
$$A^{(1)}A^{(4)}, A^{(2)}A^{(3)}, A^{(2)}A^{(4)}, A^{(3)}A^{(4)}, \phi^{(0)+}\phi^{(0)-}, H^{(1)+}H^{(1)-}, H^{(2)+}H^{(2)-}, H^{(3)+}H^{(3)-}, H^{(4)+}H^{(4)-},$$
$$\phi^{(0)+}H^{(1)-}, \phi^{(0)-}H^{(1)+}, \phi^{(0)+}H^{(2)-}, \phi^{(0)-}H^{(2)+}, \phi^{(0)+}H^{(3)-}, \phi^{(0)-}H^{(3)+}, \phi^{(0)+}H^{(4)-}, \phi^{(0)-}H^{(4)+},$$
$$H^{(1)+}H^{(2)-}, H^{(2)+}H^{(1)-}, H^{(1)+}H^{(3)-}, H^{(3)+}H^{(1)-}, H^{(1)+}H^{(4)-}, H^{(4)+}H^{(1)-}, H^{(2)+}H^{(3)-},$$
$$H^{(3)+}H^{(2)-}, H^{(2)+}H^{(4)-}, H^{(4)+}H^{(2)-}, H^{(3)+}H^{(4)-}, H^{(4)+}H^{(3)-}\Big\}, \tag{3.17}$$

and

$$\Big\{h^{(0)}A^{(1)}, h^{(0)}A^{(2)}, h^{(0)}A^{(3)}, h^{(0)}A^{(4)}, h^{(1)}A^{(1)}, h^{(1)}A^{(2)}, h^{(1)}A^{(3)}, h^{(1)}A^{(4)}, h^{(2)}A^{(1)}, h^{(2)}A^{(2)},$$

$$h^{(2)}A^{(3)}, h^{(2)}A^{(4)}, h^{(3)}A^{(1)}, h^{(3)}A^{(2)}, h^{(3)}A^{(3)}, h^{(3)}A^{(4)}, h^{(4)}A^{(1)}, h^{(4)}A^{(2)}, h^{(4)}A^{(3)}, h^{(4)}A^{(4)}\Big\}. \tag{3.18}$$

As a consequence of CP conservation, 70×70 matrix will have 50×50 and 20×20 block diagonal forms and the eigenvalues of these matrices can be separately analyzed as a function of BLT parameter R_ϕ. The 50×50 charge neutral matrix can be written as

$$\mathcal{M}^{(1)}_{NC,50\times50} = \begin{pmatrix} \mathcal{A}_{15\times15} & \mathcal{B}_{15\times10} & \mathcal{C}_{15\times25} \\ \mathcal{B}^T_{10\times15} & \mathcal{D}_{10\times10} & \mathcal{E}_{10\times25} \\ \mathcal{C}^T_{25\times15} & \mathcal{E}^T_{25\times10} & \mathcal{F}_{25\times25} \end{pmatrix}, \tag{3.19}$$

where, the $\mathcal{M}^{(1)}_{NC,50\times50}$ matrix has eigenvalues $\lambda1_{la}$ $(la = 1,\ldots,50)$. Other charge neutral matrix $\mathcal{M}^{(2)}_{NC,20\times20}$ can have eigenvalues $\lambda2_{lb}$ $(lb = 1,\ldots,20)$. General form of matrix elements are given in Appendix E.

Similarly, charged two-particle states can have 45×45 matrix which comprises of 20×20 and 25×25 block diagonal forms as

$$\mathcal{M}_{CC,45\times45} = \begin{pmatrix} \mathcal{G}_{20\times20} & \mathbf{0}_{20\times25} \\ \mathbf{0}_{25\times20} & \mathcal{H}_{25\times25} \end{pmatrix}. \tag{3.20}$$

Here, the matrices $\mathcal{G}_{20\times20}$ and $\mathcal{H}_{25\times25}$ have eigenvalues denoted by $\lambda3_{lb}$ $(lb = 1,\ldots,20)$ and $\lambda4_{lc}$ $(lc = 1,\ldots,25)$ respectively. The set of two charge two-particle states are given by

$$\Big\{\phi^{(0)+}A^{(1)}, \phi^{(0)+}A^{(2)}, \phi^{(0)+}A^{(3)}, \phi^{(0)+}A^{(4)}, H^{(1)+}A^{(1)}, H^{(1)+}A^{(2)}, H^{(1)+}A^{(3)}, H^{(1)+}A^{(4)}, H^{(2)+}A^{(1)},$$
$$H^{(2)+}A^{(2)}, H^{(2)+}A^{(3)}, H^{(2)+}A^{(4)}, H^{(3)+}A^{(1)}, H^{(3)+}A^{(2)}, H^{(3)+}A^{(3)}, H^{(3)+}A^{(4)}, H^{(4)+}A^{(1)}, H^{(4)+}A^{(2)},$$
$$H^{(4)+}A^{(3)}, H^{(4)+}A^{(4)}\Big\}, \tag{3.21}$$

and

$$\Big\{\phi^{(0)+}h^{(0)}, \phi^{(0)+}h^{(1)}, \phi^{(0)+}h^{(2)}, \phi^{(0)+}h^{(3)}, \phi^{(0)+}h^{(4)}, H^{(1)+}h^{(0)}, H^{(1)+}h^{(1)}, H^{(1)+}h^{(2)}, H^{(1)+}h^{(3)},$$
$$H^{(1)+}h^{(4)}, H^{(2)+}h^{(0)}, H^{(2)+}h^{(1)}, H^{(2)+}h^{(2)}, H^{(2)+}h^{(3)}, H^{(2)+}h^{(4)}, H^{(3)+}h^{(0)}, H^{(3)+}h^{(1)}, H^{(3)+}h^{(2)},$$
$$H^{(3)+}h^{(3)}, H^{(3)+}h^{(4)}, H^{(4)+}h^{(0)}, H^{(4)+}h^{(1)}, H^{(4)+}h^{(2)}, H^{(4)+}h^{(3)}, H^{(4)+}h^{(4)}\Big\}. \tag{3.22}$$

Fig. 3.9 shows the variation of the largest eigenvalue corresponding to different R_ϕ. To find the eigenvalues in this case, we have neglected all the masses m_h, M_Z, M_W with respect to KK-masses. Further the quartic interactions in non-abelian Lagrangian part being suppressed by KK-masses or higher power of KK-masses, the channels have negligible contributions from that part and we have neglected that part also. Evidently, the result is R^{-1} independent (Appendix E). The Table 3.2 also reflects the fact that R^{-1} does not play crucial role in unitarity violation.

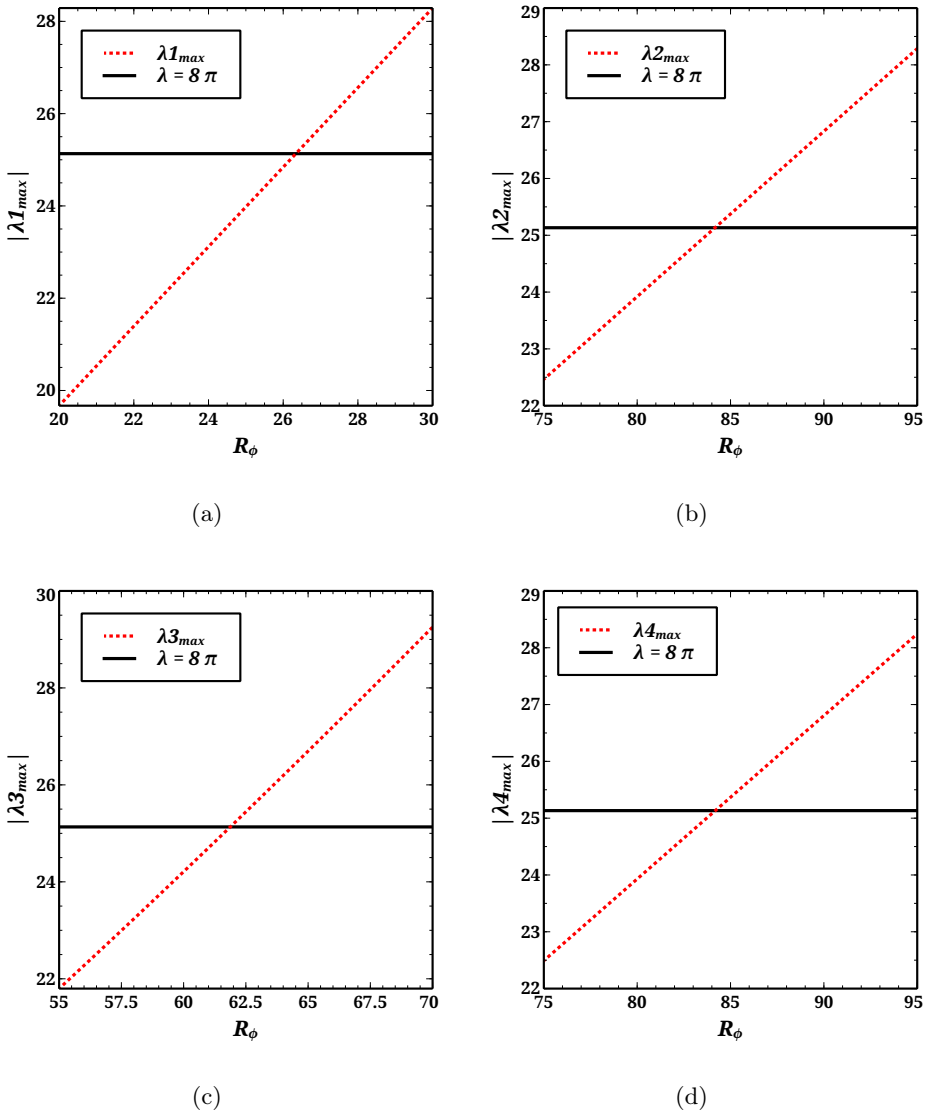

FIGURE 3.9: The variation of the largest eigenvalue (λ_{max}) as function of R_ϕ.

Clearly these simplifications would not affect the actual result. Now, to respect unitarity every eigenvalue of matrix should lie below 8π (Eq. 3.3). As consequence, the analysis of largest eigenvalue (λ_{max}) as function of R_ϕ from each set of 50, 20 or 25 number of eigenvalues would give us the desired result. Fig. 3.9 (a) exhibits that the matrix $\mathcal{M}^{(1)}_{NC,50\times50}$ gives the most stringent upper bound on R_ϕ; at $R_\phi = 26.4$ maximum value of $\lambda 1$ exceeds 8π. Now, the upper bound on R_ϕ implies a lower bound on KK-masses. In Refs. [164, 172], the dependence of KK-masses as a function of scaled BLT parameter has been explicitly shown. The KK-mass decreases with increasing value of R_ϕ so the upper bound on R_ϕ implies a lower bound on KK-masses. Here, the maximum attainable value of R_ϕ should not exceed 26 implies a lower bound on KK-masses which for scalars and gauge field is given by 0.22 R^{-1}, 1.05 R^{-1}, 2.02 R^{-1} and 3.02 R^{-1} for $n = 1 - 4$ respectively. Since the upper bound on R_ϕ is, in effect, independent of R^{-1}, the

results on the lower limits on KK-masses are true for any R^{-1}.

In the above analysis, we have considered KK-modes up to 4. The higher modes will definitely lead to higher dimensional matrices. These higher dimensional matrices would result in the breakdown of unitarity at relatively lower value of R_ϕ. The above analysis shows that Eq. 3.19 gives the most stringent upper bound on R_ϕ and therefore we will extend our analysis with higher KK-modes with this basis only (Eq. 3.17). In the Fig. 3.10, we can see that the upper bound on R_ϕ decreases with increasing KK-modes. If n_{max} be the maximum KK-number taken in the coupled channel analysis the dimension of the respective matrices would be $\{2(n_{max}+1)^2 \times 2(n_{max}+1)^2\}$. Fig. 3.10 reflects that for $n_{max} = 25$ the upper bound on R_ϕ falls down to nearly one. It also exhibits the fact that KK-number from 18 onwards the values of R_ϕ resulting in the unitarity violation are more closely spaced. So, the inclusion of more higher modes, *i.e.* KK-number from 26 onwards, will not change the upper bound on R_ϕ considerably.

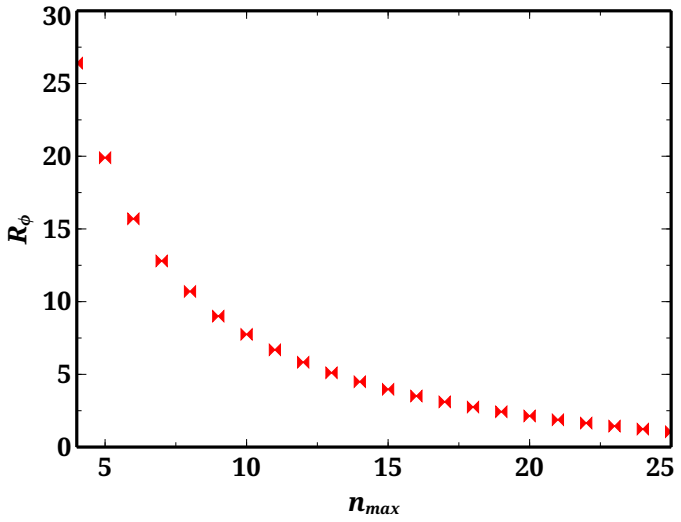

FIGURE 3.10: The variation of R_ϕ (signaling the breakdown of unitarity) as function of maximum KK-number n_{max} considered in the analysis.

However, in Refs. [169, 172] it has been shown explicitly that in case of loop induced decay processes (Sec. 4) higher modes from 5 or 6 onwards, will not change the physical amplitudes significantly. In those cases, the upper bound on R_ϕ can be taken as high as 19, because for $n_{max} = 5$ the violation would occur at $R_\phi \sim 20$. Another noteworthy issue in this case is that the determination of the upper bound on n from unitarity analysis is not possible which can be straightforwardly done in some other five-dimensional theories. The Ref. [179] shows that for a fixed value of R^{-1} one can find a lower bound on the KK-number n as

$$\frac{n}{R} \leq \frac{8\pi^2}{N}\frac{1}{\tilde{g}^2}, \tag{3.23}$$

for a five-dimensional $SU(N)$ Yang-Mills theory. In our case, *i.e.* in nmUED, the scenario is somewhat more nontrivial with the existence of the BLKT parameters which were absent

in the simple Universal Extra Dimensional theories. In this scenario with BLT parameters, the normalized four-dimensional gauge-singlet s-wave amplitude $a_0[(n),(n)\to(m),(m)]$ of Ref. [179] will be modified by some overlap integrals as

$$a_0[(n),(n)\to(m),(m)] = I^{nnmm}\frac{n}{R}\frac{N\tilde{g}^2}{16\pi^2}, \tag{3.24}$$

where, I^{nnmm} is the overlap integral of Eq. 3.11. Consequently, Eq. 3.23 will be modified as

$$\frac{n}{R} \leq \frac{1}{I^{nnmm}}\frac{8\pi^2}{N\tilde{g}^2}. \tag{3.25}$$

The expression of overlap integral I^{nnmm} is given by

$$\begin{aligned} I^{nnmm} \;=\; & \frac{1}{\left(1+\frac{(R_\phi m_{\Phi n})^2}{4}+\frac{R_\phi}{\pi}\right)\left(1+\frac{(R_\phi m_{\Phi m})^2}{4}+\frac{R_\phi}{\pi}\right)}\left\{1+\frac{2R_\phi}{\pi}+\frac{R_\phi^2}{\pi^2}+\frac{1}{4}(R_\phi m_{\Phi n})^2\right. \\ & +\frac{1}{4}(R_\phi m_{\Phi m})^2+\frac{1}{16}(R_\phi^2 m_{\Phi n}m_{\Phi m})^2-\frac{R_\phi^2}{4\pi^2}(R_\phi m_{\Phi n})^2-\frac{R_\phi^2}{4\pi^2}(R_\phi m_{\Phi m})^2 \\ & \left.+\frac{R_\phi}{16\pi}(R_\phi^2 m_{\Phi n}m_{\Phi m})^2\right\}. \end{aligned} \tag{3.26}$$

If we consider $a_0[(n),(n)\to(n),(n)]$ instead of $a_0[(n),(n)\to(m),(m)]$ in Eq. 3.24, the overlap integral I^{nnmm} will be replaced by I^n and that is given as

$$\begin{aligned} I^{n} \;=\; & \frac{3}{\left(1+\frac{(R_\phi m_{\Phi n})^2}{4}+\frac{R_\phi}{\pi}\right)^2}\left\{\frac{1}{2}+\frac{R_\phi}{\pi}+\frac{R_\phi^2}{2\pi^2}+\frac{1}{4}(R_\phi m_{\Phi n})^2+\frac{R_\phi}{8\pi}(R_\phi m_{\Phi n})^2\right. \\ & \left.-\frac{1}{8\pi^2}(R_\phi^2 m_{\Phi n})^2+\frac{1}{32}(R_\phi m_{\Phi n})^4+\frac{R_\phi}{32\pi}(R_\phi m_{\Phi n})^4\right\}. \end{aligned} \tag{3.27}$$

Clearly, the overlap integrals are not directly proportional to the BLT parameter R_ϕ. Moreover, these overlap integrals are explicit functions of R_ϕ as well as of $m_{\Phi n}\equiv M_{\Phi n}R$. On the other hand, $m_{\Phi n}$ has an implicit dependence on the KK-number n. Overall, there would exist one possibility to find out the bound on n through unitarity analysis that at some n_{max} unitarity violation would occur at every possible value of R_ϕ. As from Eq. 2.87 it is very clear that R_ϕ should be greater than $(-\pi)$, so if an n_{max} is to be considered as the upper bound in the nmUED scenario, violation would occur at least for $R_\phi=(-2.99)$ or $R_\phi=(-3.0)$. Though the Fig. 3.10 reflects that the inclusion of higher KK-modes would result in unitarity violation at much lower value of R_ϕ, it also exhibits that from KK-number 18 onwards the values of R_ϕ at which the unitarity violation occurs are more closely spaced. Even the difference between the values of R_ϕ which violate the unitarity at KK-number 24 and 25 is less than 0.2. Therefore, after KK-number 25 there will not be any considerable change in the result, or to be specific the violation would never occur at $R_\phi=(-2.99)$ or at (-3.0) for any n_{max}.

3.5 Conclusions

In this chapter, we have done simple partial wave unitarity analysis as well as coupled channel analysis in gauge and scalar sectors in non-minimal Universal Extra Dimensional (nmUED) model where kinetic terms involving fields as well as mass and potential terms of the scalar fields are added to their respective five-dimensional actions at the fixed boundary points. By exploiting the equivalence theorem, we have used all the Goldstone modes or unphysical scalars instead of the longitudinal modes of vector bosons. First, all the necessary two-body (n), $(n) \to (n)$, (n) tree level scattering amplitudes have been calculated to study the upper bound on scalar BLT parameter by the simple method of partial wave analysis. After that coupled channel analysis (t^0-matrix construction) has been performed for some selective channels to get further constraint.

Any $2 \to 2$ scattering amplitudes can be expressed in terms of an infinite sum of partial waves. For a process to respect unitarity the zeroth partial wave amplitude a_0 should obey the condition $|\text{Re } a_0| \leq 1/2$. Initially the analysis of unitarity with t-matrix construction has not been taken into account as in many cases, contributions coming from trilinear couplings can not be ignored where the interactions are effectively proportional to KK-masses and consequently the contributions are not E^2-suppressed. Therefore, it is evident that some entries of the matrix elements are not simple numbers but are also the functions of center of mass energy $\sqrt{s}$ of respective processes. So to obtain the suitable channels for t^0 construction we should first consider the single channel analysis for (n), $(n) \to (n)$, (n) processes.

While dealing with the single channel scattering processes we have restricted our calculations to two-body scattering processes for specific KK-modes with the condition that KK-numbers for all initial and final particles in the respective processes are same. We have taken only those processes whose quartic interactions are not suppressed by KK-masses. Following these conditions we have altogether thirteen quartic interactions in the entire scalar sectors in nmUED scenario. Besides, the quartic interactions having two same neutral particles in initial states and another same two neutral particles in final states, can generate two kinds of processes. Also the processes that involve two same or different charged particles in initial states and same two neutral particles in final states can give rise to two different kinds of processes. So, only those processes have been preferred where the amplitudes are not suppressed by the factor of $1/2$ or by $1/\sqrt{2}$ arising from normalization factors for the presence of identical bosonic states, as that suppression would result in breakdown of unitarity at some larger value of R_ϕ and thus giving a relative less stringent bound. Here, R_ϕ is the scaled scalar boundary-localized parameter determined as $\equiv r_\phi/R$.

Among all thirteen processes, $H^{(n)+}H^{(n)-} \to H^{(n)+}H^{(n)-}$ gives the most stringent constraint on the upper limit on R_ϕ. A detailed analysis on (n), $(n) \to (n)$, (n) reflects that the channels involving the processes $h^{(n)}h^{(n)} \to h^{(n)}h^{(n)}$, $A^{(n)}A^{(n)} \to A^{(n)}A^{(n)}$, $H^{(n)+}H^{(n)-} \to H^{(n)+}H^{(n)-}$,

$h^{(n)}A^{(n)} \to h^{(n)}A^{(n)}$, $H^{(n)\pm}A^{(n)} \to H^{(n)\pm}A^{(n)}$, $H^{(n)\pm}h^{(n)} \to H^{(n)\pm}h^{(n)}$ are preferable for coupled channel analysis, which is actually the construction of t^0 matrix generated by two-body states as rows and columns. Consequently each matrix element corresponds to the amplitude of respective processes and each eigenvalue of the matrices should lie below 8π to respect the unitarity. Coupled channel analysis leads to an upper bound on R_ϕ corresponding to maximum KK-number (n_{max}) taken in the analysis. If n_{max} is taken to be 4, the BLT parameter R_ϕ should be less than 26.4. The results, in effect, are independent of R^{-1}. As the KK-masses decrease with increasing value of R_ϕ, the upper limit on BLT parameter in turn implies a lower bound on KK-masses for gauge or scalar fields. For $n_{max} = 4$, the upper limit on $R_\phi \sim 26$ leads to lower bounds on KK-masses $\sim 0.22\ R^{-1}$, $1.05\ R^{-1}$, $2.02\ R^{-1}$ and $3.02\ R^{-1}$ for $n = 1 - 4$ respectively. As we know that R^{-1} does not play any role in determining the upper limit on R_ϕ, the results on the lower bounds on KK-masses are true for any R^{-1}. Besides, the value of R_ϕ corresponding to the violation of unitarity decreases if n_{max} in the analysis is being increased. If we take $n_{max} = 25$, the upper bound on R_ϕ falls down to nearly one. From KK-mode 18 onwards, the constraints on the upper limit on scalar BLT parameter change very slowly and will not change significantly for KK-modes higher than 25. Therefore, in this theory, there will be no upper bound on the KK-number n from unitarity analysis.

4

One Loop Effect of Universal Extra Dimensional Models

In this chapter we study the effects of higher KK-modes (with one extra special dimension) in some loop-induced decay processes. The four LEP experiments ALEPH, DELPHI, L3 and OPAL had made high-statistics studies on the precision measurements at the Z boson resonance in the years 1989-95. Precision electroweak variables like R_b (Z boson decay width to a pair of b quarks normalized to total hadronic decay width), A_{FB}^b (forward-backward asymmetry of b quarks at Z pole), ρ(T)-parameter measured by LEP and SLC always play the role of a guiding light in search of the new physics. Incidentally, these electroweak precision variables are very sensitive to radiative corrections and these quantum corrections get significant contributions from large top quark mass. Furthermore, a recent estimation of the Standard Model (SM) contribution to R_b at two loop level points to a 1.2σ discrepancy between the experimental data and the SM estimate [183, 184].

Now let us shift our attention to the flavor changing neutral current (FCNC) interactions in the SM. An important aspect of SM is the absence of the FCNC interactions at the tree-level. However, FCNC is possible in the loop-level, but that too is strongly suppressed by the Glashow-Iliopoulos-Maiani (GIM) mechanism. Generally these types of loop-driven processes involve two different generations of fermions in the initial and in the final states where all possible generation of fermions run in the loop. These FCNC processes are strongly suppressed in the SM; evidently

the discovery of any such process would be a clear hint of some BSM physics. So in the case of any BSM scenario for these types of processes no BSM particle has to be produced on-shell but their effects in the loop would be enough to look into the picture at hand. This is specially important in a time when there is a lack of any direct evidence of new physics at the LHC. In this same vein many BSM scenarios have been studied through these type of FCNC processes. One important place to look for such FCNC processes is the rare decays of top quark in the context of some new physics model. Many studies have been performed to consider the rare decays of the top quark in the SM [185–197] as well as in various BSM scenarios, *e.g.* in supersymmetry [198–205], two Higgs doublet model (2HDM) [206–210], warped extra dimension [211], UED [212] etc. A study on the FCNC top decays based on a model independent effective field theory can be found in Refs. [213, 214].

In this chapter we will see the one-loop induced effects of one extra dimension in the processes like $Zb\bar{b}$ and some rare top decays ($t \to c\gamma$ and $t \to ch$). We would like to investigate how one of the precisely known electroweak variable R_b could constrain the nmUED parameter space. We will preface this by a brief description of required Lagrangian and overlap integrals. That will be followed by a discussion on processes with necessary Feynman diagrams. In the subsequent sections we elaborate on the results and the bounds obtained in the cases of mUED and nmUED. This chapter is mainly based on Refs. [169, 172].

4.1 Lagrangian and Overlap Integrals

This section includes a short description of required Lagrangian and overlap integrals. In the analysis of loop induced processes by extra dimension, the five dimensional kinetic and Yukawa terms of the respective fields are needed at boundary points. Clearly, the five dimensional actions given in Eq. 2.69 and in Eqs. 2.78-2.80 in the Chapter 2 are required in this study.

First we should briefly discuss the mass matrices in quark sector. From Eq. 2.95 in Section. 2.5, we know that the strength of mixing is proportional to the quark mass and hence is significant for the top sector. In case of new physics effect on $Zb\bar{b}$ coupling all we need the third generation top quark mass and therefore all the related discussion on the physical eigenstates and mixing strength in quark sector are given in Sec. 2.5.1.2. However, in rare top decays, to incorporate the GIM mechanism, we consider the mixing in the down sector too. In that case, α_n is given by $\frac{1}{2}\tan^{-1}\left(\frac{m_b}{M_{Qn}}\right)$ where m_b denotes the SM bottom quark mass. In the nth KK-level, the mass term can be written as

$$\begin{pmatrix} \bar{Q}^{(m)}_{j_L} & \bar{D}^{(m)}_{L} \end{pmatrix} \begin{pmatrix} -M_{Qn}\delta^{mn} & m_j\alpha_1\mathcal{I}^{mn} \\ m_j\alpha_1 & M_{Qn}\delta^{mn} \end{pmatrix} \begin{pmatrix} Q^{(n)}_{j_R} \\ D^{(n)}_{R} \end{pmatrix} + \text{h.c.} \tag{4.1}$$

We can relate the gauge eigenstates $Q_j^{(n)}$ $(D^{(n)})$ and mass eigenstates $Q_j^{\prime(n)}$ $(D^{\prime(n)})$ in a similar way as (in this notation j refers to the down quark flavor),

$$Q^{(n)}_{j_{L/R}} = \mp \cos\alpha_n Q^{\prime(n)}_{j_{L/R}} + \sin\alpha_n D^{\prime(n)}_{L/R}, \tag{4.2a}$$

$$D^{(n)}_{L/R} = \pm \sin\alpha_n Q^{\prime(n)}_{j_{L/R}} + \cos\alpha_n D^{\prime(n)}_{L/R}. \tag{4.2b}$$

The mass eigenstates, in this case, also share the same mass eigenvalue,

$$m_{Q_b^{\prime(n)}} = m_{D^{\prime(n)}} = \sqrt{m_b^2 + M_{Qn}^2} \equiv M_{\text{bottom}}. \tag{4.3}$$

Now we mention about a few overlap integrals that appear in our calculations,

$$I_A^{lk} = \int_0^{\pi R} dy\,[1 + r_f\{\delta(y) + \delta(y-\pi R)\}]\, f^{(l)}_{Qt_L}(y)\; f^{(k)}_{\phi}(y)(f^{(k)}_{W_\mu}(y))\; f^{(0)}_{b_L}(y), \tag{4.4a}$$

$$= \int_0^{\pi R} dy\,[1 + r_f\{\delta(y) + \delta(y-\pi R)\}]\, f^{(l)}_{Qb_L}(y)\; f^{(k)}_{\phi}(y)(f^{(k)}_{W_\mu}(y))\; f^{(0)}_{t_R}(y), \tag{4.4b}$$

$$I_B^{lk} = \int_0^{\pi R} dy\; f^{(l)}_{Qt_R}(y)\; f^{(k)}_{W_5}(y)\; f^{(0)}_{b_L}(y), \tag{4.4c}$$

$$= \int_0^{\pi R} dy\; f^{(l)}_{Qb_R}(y)\; f^{(k)}_{W_5}(y)\; f^{(0)}_{t_L}(y), \tag{4.4d}$$

$$I_C^{k} = \int_0^{\pi R} dy\,[1 + r_f\{\delta(y) + \delta(y-\pi R)\}]\, f^{(0)}_{Qt_R}(y)\; f^{(k)}_{\phi}(y)(f^{(k)}_{W_\mu}(y))\; f^{(0)}_{b_L}(y), \tag{4.4e}$$

$$= \int_0^{\pi R} dy\,[1 + r_f\{\delta(y) + \delta(y-\pi R)\}]\, f^{(0)}_{Qt_L}(y)\; f^{(k)}_{\phi}(y)(f^{(k)}_{W_\mu}(y))\; f^{(0)}_{b_R}(y). \tag{4.4f}$$

The overlap integrals given in Eqs. 4.4a, 4.4c and in Eq. 4.4e arise in the analysis of $Zb\bar{b}$ whereas the same overlap integrals given in Eqs. 4.4b, 4.4d and in Eq. 4.4f appear in the study of flavor-changing rare top decays. These are the overlap integrals that modify the respective couplings. These overlap integrals can also be written as

$$I_A^{lk} = \frac{1}{\sqrt{r_f + \pi R}} I_a^{lk}, \tag{4.5a}$$

$$I_B^{lk} = \frac{1}{\sqrt{r_f + \pi R}} I_b^{lk}, \tag{4.5b}$$

$$I_C^{k} = \frac{1}{\sqrt{r_f + \pi R}} I_c^{k}, \tag{4.5c}$$

where the integral parts of Eqs. 4.4 have been embedded in the new overlap integrals, *viz.* $I_a^{lk}, I_b^{lk}, I_c^k$; apart from the integral part I_c^k includes another parameter-dependent multiplicative factor $1/\sqrt{r_f + \pi R}$. Fig. 4.1 shows characteristic behavior of the overlap integrals with respect to various BLT parameters. It should be kept in mind that even though for some choice of

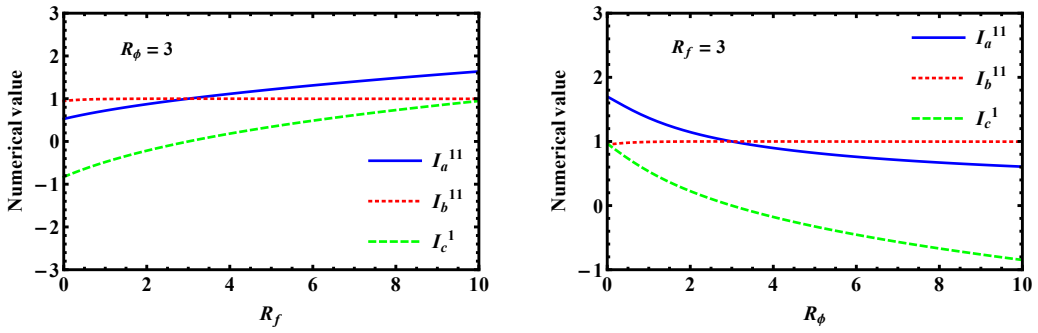

FIGURE 4.1: Characteristic dependence of overlap integrals on the BLT parameters. Here $R_{\phi,f} = r_{\phi,f}/R$ and we take only first KK-modes into account, *i.e.* we take $j, k = 1$ in Eqs. 4.4.

BLT parameters the numerical value of the overlap integrals can be greater than unity, the final values of the relevant couplings remain within the perturbativity limit.

Besides, in cases of the overlap integrals I_a^{lk} and I_b^{lk} when l differs from k (in the case of even $l + k$) values of the integrals diminish generally by an order of magnitude than the $l = k$ case. For example, when $R_f = 1$ and $R_\phi = 2$: $I_a^{11} = 0.82$, $I_a^{22} = 0.88$, $I_a^{33} = 0.92$, $I_a^{44} = 0.94$, $I_a^{55} = 0.96$, $I_a^{31} = 0.01$, $I_a^{51} = 0.004$, $I_a^{53} = 0.03$, $I_a^{42} = 0.03$; $I_b^{11} \sim I_b^{22} \sim I_b^{33} \sim I_b^{44} \sim I_b^{55} = 0.99$ and $I_b^{31} = 0.07$, $I_b^{51} = 0.02$, $I_b^{42} = 0.08$. In case of $Zb\bar{b}$ analysis we will be only considering the interactions with $l = k$ neglecting the other sub-dominant contributions coming from interactions in which $l \neq k$. This kind of approximation is not used in the analysis of rare decays. The expressions for the integrals (after integrating over y) are given in Appendix H along with the necessary Feynman rules given in Appendices F and G.

4.2 A Brief Description of Loop-induced Processes

This section starts with the analysis of the radiative calculation of $Zb\bar{b}$ vertex. The subsequent parts will describe the rare top decays ($t \to c\gamma$ and $t \to ch$).

4.2.1 Calculation of Radiative Correction to the $Zb\bar{b}$ Coupling

We are now going to lay down the details of the calculation leading to the correction of the $Zb\bar{b}$ vertex in the framework of nmUED. We will first briefly discuss the meaning of R_b and its correlation to $Zb\bar{b}$ coupling in the SM as a preamble. The tree level $Zb\bar{b}$ coupling, in the SM, can be given as

$$\frac{g}{\cos\theta_W}\bar{b}^{(0)}\gamma^\mu(g_L^0 P_L + g_R^0 P_R)b^{(0)}Z_\mu^{(0)}, \tag{4.6}$$

where $Z_\mu^{(0)}$ and $b^{(0)}$'s are the SM fields; $P_{R,L} = (1 \pm \gamma_5)/2$ are the right- and left-chirality projectors respectively and

$$g_L^0 = -\frac{1}{2} + \frac{1}{3}\sin^2\theta_W, \tag{4.7a}$$

$$g_R^0 = \frac{1}{3}\sin^2\theta_W. \tag{4.7b}$$

Any higher order quantum corrections, whether being from SM or from new physics (NP) can be incorporated uniformly as the modification to this tree level couplings defined as

$$g_L = g_L^0 + \delta g_L^{\rm SM} + \delta g_L^{\rm NP}, \tag{4.8a}$$

$$g_R = g_R^0 + \delta g_R^{\rm SM} + \delta g_R^{\rm NP}. \tag{4.8b}$$

Here $\delta g_{L/R}^{\rm SM}$ corresponds to the radiative corrections from SM and $\delta g_{L/R}^{\rm NP}$ denotes the contributions from new physics (NP) [215]. These corrections in turn can modify the Z decay width to b quarks normalized to the total hadronic decay width of Z defined by a dimensionless variable

$$R_b \equiv \frac{\Gamma(Z \to b\bar{b})}{\Gamma(Z \to \text{hadrons})}. \tag{4.9}$$

Generally, at one loop order (in SM & also in NPs), g_L gets correction proportional to m_t^2 whereas g_R receives correction proportional to m_b^2 (due to the difference in couplings between two chiralities); here m_t (m_b) is the zero mode top (bottom) quark mass. We have neglected the b mass in our calculation and thus a shift in $\delta g_L^{\rm NP}$ translates into a shift in R_b as

$$\delta R_b = 2R_b(1-R_b)\frac{\hat{g}_L}{\hat{g}_L^2 + \hat{g}_R^2}\delta g_L^{\rm NP}, \tag{4.10}$$

with $\hat{g}_L$ and $\hat{g}_R$ given by

$$\hat{g}_L^b = \sqrt{\rho_b}\,(-\frac{1}{2} + \kappa_b\,\frac{1}{3}\,\sin^2\theta_W), \tag{4.11a}$$

$$\hat{g}_R^b = \frac{1}{3}\sqrt{\rho_b}\,\kappa_b\,\sin^2\theta_W, \tag{4.11b}$$

after incorporating the SM electroweak corrections only [127]. Here, $\rho_b = 0.9869$ and $\kappa_b = 1.0067$ [127].

Besides, the $g_L^{\rm NP}$ is calculable in a given framework while R_b is an experimentally measurable quantity. Thus Eq. 4.10 can be used to constrain the parameters of the model. We will perform the same exercise in the framework of nmUED. Required Feynman rules have been listed in Appendix F.

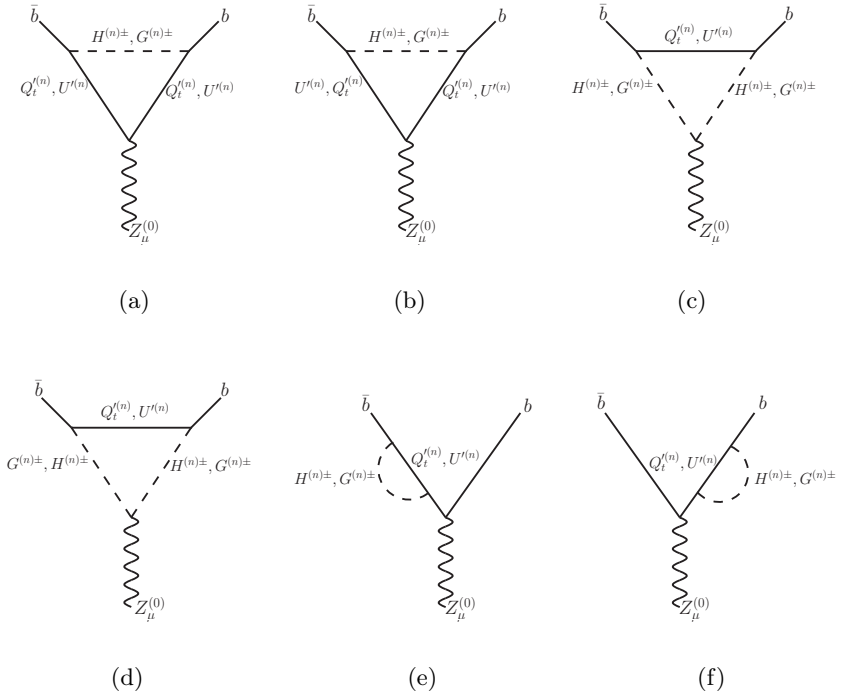

FIGURE 4.2: Loop involving KK-mode of scalar and fermion propagators of $Zb\bar{b}$ in the 't Hooft–Feynman gauge (excluding (0)-(0)-(n)).

Since we have neglected the interactions involving KK-states with unequal KK-numbers in an interaction vertex, the number of diagrams contributing to radiative corrections of the $Zb\bar{b}$ coupling in nmUED are same as that of (m)UED. Fig. 4.2 shows the Feynman diagrams involving KK excitations of top quarks and the charged Higgs/Goldstone bosons in the loop. The contributions coming from the diagrams of Fig. 4.2 have the dominant effect for the presence of Yukawa coupling which is proportional to m_t. In our calculations, we have considered momentum of the external $Z_\mu^{(0)}$ to be zero and have also neglected the b quark mass.

The amplitude of each diagram, for nth KK-mode, can be expressed in terms of a single function, $f^{(n)}(r_n, r'_n, M')$, defined as,

$$i\mathcal{M}^{(n)} = i\frac{g}{\cos\theta_W}\overline{u}(p_1,s_1)f^{(n)}(r_n,r'_n,M')\gamma^\mu P_L v(p_2,s_2)\epsilon_\mu(q)\ , \tag{4.12}$$

where $r_n \equiv m_t^2/M_{Qn}^2$, $r'_n \equiv M_W^2/M_{Qn}^2$ and $M' \equiv M_{\Phi n}^2/M_{Qn}^2$.

Amplitudes of different diagrams of Fig. 4.2 (evaluated in 't-Hooft-Feynman gauge) are given by

$$\begin{aligned} f_{1(a)}^{(n)}(r_n,r'_n,M') \;=\; & \frac{\beta}{(4\pi)^2}\frac{g^2}{8}\{-\frac{4}{3}\sin^2\theta_W\left(I_b^2+I_a^2\frac{m_t^2}{M_W^2}\right)+I_b^2\left(\cos^4\alpha_n+\sin^4\alpha_n\right) \\ & +2I_a^2\frac{m_t^2}{M_W^2}\sin^2\alpha_n\cos^2\alpha_n\}\Big[\delta_n-1+\{5(r_n+1)^2+3(r'_n+M')^2 \\ & -8(r_n+1)(r'_n+M')-2(1+r_n)^2\ln(1+r_n) \end{aligned}$$

$$
\begin{aligned}
& -2(M'+r'_n)^2\ln(M'+r'_n)+4(1+r_n)(M'+r'_n)\ln(M'+r'_n)\} \\
& /2\{(r_n+1)-(M'+r'_n)\}^2\Big], \qquad (4.13)
\end{aligned}
$$

$$
\begin{aligned}
f^{(n)}_{1(b)}(r_n,r'_n,M') &= \frac{\beta}{(4\pi)^2}\frac{g^2}{8}\{2I_b^2\sin^2\alpha_n\cos^2\alpha_n-2I_a^2\frac{m_t^2}{M_W^2}\sin^2\alpha_n\cos^2\alpha_n\} \\
& \Big[\delta_n-1+\{-3(r_n+1)^2+3(r'_n+M')^2 \\
& -2(1+r_n)^2\ln(1+r_n)-2(M'+r'_n)^2\ln(M'+r'_n) \\
& +8(1+r_n)(M'+r'_n)\ln(1+r_n)-4(1+r_n)(M'+r'_n)\ln(M'+r'_n)\} \\
& /2\{(r_n+1)-(M'+r'_n)\}^2\Big], \qquad (4.14)
\end{aligned}
$$

$$
\begin{aligned}
f^{(n)}_{1(c+d)}(r_n,r'_n,M') &= \frac{\beta}{(4\pi)^2}\frac{g^2}{8}\{(-1+2\sin^2\theta_W)\left(I_b^2+I_a^2\frac{m_t^2}{M_W^2}\right)-I_b^2\} \\
& \Big[\delta_n+\{3(r_n+1)^2+(r'_n+M')^2 \\
& -4(r_n+1)(r'_n+M')-2(1+r_n)^2\ln(1+r_n) \\
& -2(M'+r'_n)^2\ln(M'+r'_n)+4(1+r_n)(M'+r'_n)\ln(M'+r'_n)\} \\
& /2\{(r_n+1)-(M'+r'_n)\}^2\Big], \qquad (4.15)
\end{aligned}
$$

$$
\begin{aligned}
f^{(n)}_{1(e+f)}(r_n,r'_n,M') &= \frac{\beta}{(4\pi)^2}\frac{g^2}{8}\left(1-\frac{2}{3}\sin^2\theta_W\right)\left(I_b^2+I_a^2\frac{m_t^2}{M_W^2}\right) \\
& \Big[\delta_n+\{3(r_n+1)^2+(r'_n+M')^2 \\
& -4(r_n+1)(r'_n+M')-2(1+r_n)^2\ln(1+r_n) \\
& -2(M'+r'_n)^2\ln(M'+r'_n)+4(1+r_n)(M'+r'_n)\ln(M'+r'_n)\} \\
& /2\{(r_n+1)-(M'+r'_n)\}^2\Big]. \qquad (4.16)
\end{aligned}
$$

Here $\delta_n \equiv 2/\epsilon-\gamma+\log(4\pi)+\log(\mu^2/M_{Qn}^2)$ and μ is the 't-Hooft mass scale; $\beta \equiv \frac{\pi R+r_\phi}{\pi R+r_f}$. The symbols I_a and I_b stand for the overlap integrals given in Eq. 4.5a and in Eq. 4.5b respectively for $n=m$. Amplitudes of the diagrams 4.2(e) and 4.2(f) are multiplied by a factor of 1/2 which comes from the usual convention of contributing one-half of this correction into self-energy and the other half in the wave function renormalization. Total amplitude ($i\mathcal{M}_1^{(n)}$) of diagrams in Fig. 4.2 is obtained by adding the individual amplitudes for each diagram and is given by the following expression:

$$
\begin{aligned}
i\mathcal{M}_1^{(n)} = & \frac{i}{(4\pi)^2}\frac{g^3}{4\cos\theta_W}\overline{u}\,(p_1,s_1)\,\frac{r_n\beta}{\{(r_n+1)-(M'+r'_n)\}^2}\left(-I_b^2+I_a^2\frac{m_t^2}{M_W^2}\right) \\
& \times\Big[(1+r_n)-(M'+r'_n)+(M'+r'_n)\ln\left(\frac{M'+r'_n}{1+r_n}\right)\Big]\gamma^\mu P_L v\,(p_2,s_2)\,\epsilon_\mu(q). \qquad (4.17)
\end{aligned}
$$

From the above equation, it is evident that terms proportional to δ_n as well as to $\sin^2\theta_W$ cancel among themselves. In passing we would like to comment that any correction proportional to $\sin^2\theta_W$ in the $Zb\bar{b}$ vertex must be reflected in the renormalization of charge (of b quark). This

implies that any finite renormalization to the $\gamma b\bar{b}$ vertex must be the same (in amplitude) to any correction proportional to $\sin^2\theta_W$ in the $Zb\bar{b}$ coupling. We have explicitly checked that both of these corrections coming from diagrams of the same topology depicted in Fig. 4.2 identically vanishes.

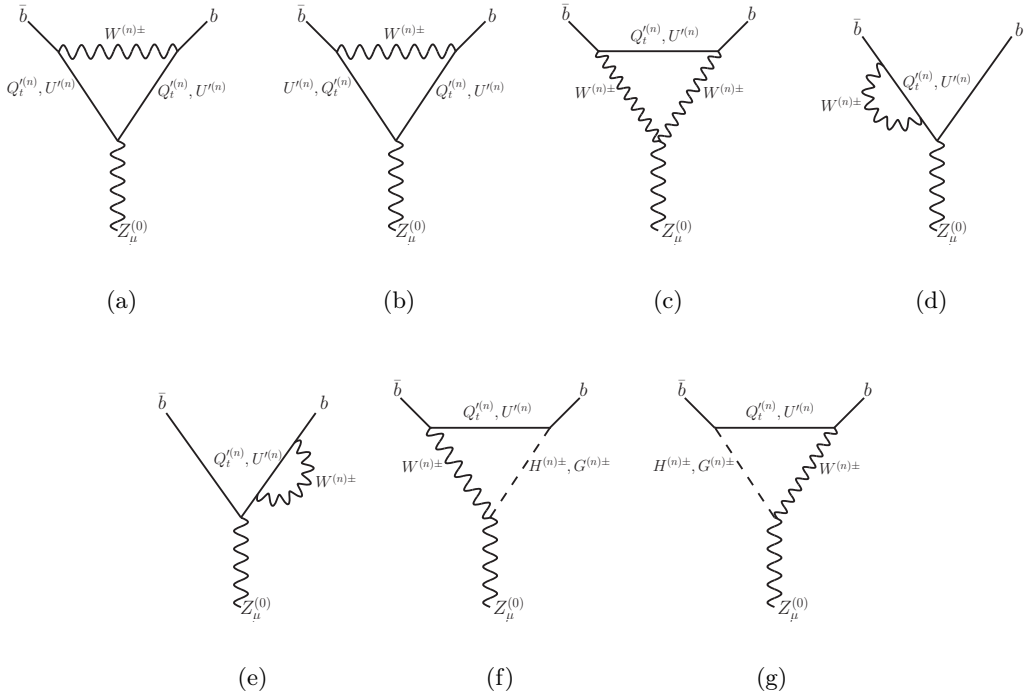

FIGURE 4.3: Loop involving KK-mode of W and Goldstone propagators of $Zb\bar{b}$ in the 't Hooft–Feynman gauge (excluding (0)-(0)-(n)).

There is a second set of diagrams contributing to the effective $Zb\bar{b}$ interaction arising from the KK excitations of W bosons and quarks. These have sub-dominant contributions with respect to the contributions coming from Fig. 4.2.

In the following we present the amplitudes of all diagrams given in Fig. 4.3 :

$$
\begin{aligned}
f^{(n)}_{2(a)}(r_n, r'_n, M') &= \frac{I_a^2\beta}{(4\pi)^2}\frac{g^2}{4}\{-\frac{4}{3}\sin^2\theta_W + \cos^4\alpha_n + \sin^4\alpha_n\}\Big[\delta_n - 2 \\
&\quad +\{5(r_n+1)^2 + 3(r'_n+M')^2 \\
&\quad -8(r_n+1)(r'_n+M') - 2(1+r_n)^2\ln(1+r_n) \\
&\quad -2(M'+r'_n)^2\ln(M'+r'_n) + 4(1+r_n)(M'+r'_n)\ln(M'+r'_n)\} \\
&\quad /2\{(r_n+1) - (M'+r'_n)\}^2\Big], \qquad (4.18)\\
f^{(n)}_{2(b)}(r_n, r'_n, M') &= \frac{I_a^2\beta}{(4\pi)^2}\frac{g^2}{4}\{2\sin^2\alpha_n\cos^2\alpha_n\}\Big[\delta_n - 2 + \{-3(r_n+1)^2 \\
&\quad +3(r'_n+M')^2 - 2(1+r_n)^2\ln(1+r_n) - 2(M'+r'_n)^2\ln(M'+r'_n) \\
&\quad +8(1+r_n)(M'+r'_n)\ln(1+r_n) - 4(1+r_n)(M'+r'_n)\ln(M'+r'_n)\}
\end{aligned}
$$

$$/2\{(r_n+1)-\left(M'+r'_n\right)\}^2\Big], \tag{4.19}$$

$$\begin{aligned} f^{(n)}_{2(c)}(r_n,r'_n,M') &= -\frac{I_a^2\beta}{(4\pi)^2}\frac{g^2}{4}\left(6\cos^2\theta_W\right)\Big[\delta_n-\frac{2}{3}+\{3(r_n+1)^2+(r'_n+M')^2 \\ &\quad -4(r_n+1)(r'_n+M')-2(1+r_n)^2\ln(1+r_n) \\ &\quad -2(M'+r'_n)^2\ln(M'+r'_n)+4(1+r_n)(M'+r'_n)\ln(M'+r'_n)\} \\ &\quad /2\{(r_n+1)-\left(M'+r'_n\right)\}^2\Big], \end{aligned} \tag{4.20}$$

$$\begin{aligned} f^{(n)}_{2(d+e)}(r_n,r'_n,M') &= \frac{I_a^2\beta}{(4\pi)^2}\frac{g^2}{4}\left(1-\frac{2}{3}\sin^2\theta_W\right)\Big[\delta_n-1+\{3(r_n+1)^2+(r'_n+M')^2 \\ &\quad -4(r_n+1)(r'_n+M')-2(1+r_n)^2\ln(1+r_n) \\ &\quad -2(M'+r'_n)^2\ln(M'+r'_n)+4(1+r_n)(M'+r'_n)\ln(M'+r'_n)\} \\ &\quad /2\{(r_n+1)-\left(M'+r'_n\right)\}^2\Big], \end{aligned} \tag{4.21}$$

$$\begin{aligned} f^{(n)}_{2(f+g)}(r_n,r'_n,M') &= \frac{I_a^2\beta}{(4\pi)^2}g^2\{(r_n+1)\sin^2\theta_W-1\} \\ &\quad \{-(1+r_n)+(M'+r'_n)+(1+r_n)\ln\left(\frac{1+r_n}{M'+r'_n}\right)\} \\ &\quad /\{(r_n+1)-\left(M'+r'_n\right)\}^2. \end{aligned} \tag{4.22}$$

In the diagrams of Fig. 4.3, the divergences along with the terms proportional to $\sin^2\theta_W$ do not cancel among themselves. The divergent terms are r_n independent. Following the prescription given in Ref. [216], we can write the renormalized amplitude as:

$$i\mathcal{M}^{(n)}_{2R}(r_n,r'_n,M')=i\mathcal{M}^{(n)}_{2}(r_n,r'_n,M')-i\mathcal{M}^{(n)}_{2}(r_n=0,r'_n,M'). \tag{4.23}$$

Finally summing up the contributions coming from all diagrams we have,

$$\begin{aligned} &i\mathcal{M}^{(n)}_{\rm total}=i\mathcal{M}^{(n)}_{1}+i\mathcal{M}^{(n)}_{2R}=\frac{i}{(4\pi)^2}\frac{g^3}{4\cos\theta_W}\overline{u}\left(p_1,s_1\right)\frac{r_n\beta}{\{(r_n+1)-(M'+r'_n)\}^2} \\ &\Bigg[\left\{-I_b^2+I_a^2\left(-2+\frac{m_t^2}{M_W^2}\right)\right\}\left\{(1+r_n)-(r'_n+M')+(r'_n+M')\ln\left(\frac{r'_n+M'}{1+r_n}\right)\right\} \\ &+4I_a^2\left\{-(1+r_n)+(r'_n+M')+(1+r_n)\ln\left(\frac{1+r_n}{r'_n+M'}\right)\right\}\Bigg] \\ &\gamma^\mu P_L v\left(p_2,s_2\right)\epsilon_\mu(q). \end{aligned} \tag{4.24}$$

Therefore, for each mode, the correction in g_L:

$$\delta g_L^{(n)\rm NP}=\sum_i f_i^n(r_n,r'_n,M')=\frac{\sqrt{2}G_F m_t^2}{16\pi^2}F^{(n)}_{\rm nmUED}(r_n,r'_n,M'), \tag{4.25}$$

where

$$\mathrm{F}^{(n)}_{\mathrm{nmUED}}(r_n, r'_n, M') = \frac{r_n\beta}{[(1+r_n)-(r'_n+M')]^2}\Bigg[\left\{I_a^2\left(1-\frac{2M_W^2}{m_t^2}\right)-I_b^2\frac{M_W^2}{m_t^2}\right\} \times\left\{(1+r_n)-(r'_n+M')+(r'_n+M')\ln\left(\frac{r'_n+m'}{1+r_n}\right)\right\} + \frac{4M_W^2}{m_t^2}I_a^2\left\{-(1+r_n)+(r'_n+M')+(1+r_n)\ln\left(\frac{1+r_n}{r'_n+M'}\right)\right\}\Bigg]. \tag{4.26}$$

The total new physics contribution δg_L^{NP} and similarly $\mathrm{F}_{\mathrm{nmUED}}$, can be obtained by summing $\delta g_L^{(n)\mathrm{NP}}$ over KK-modes (n). It can be verified that the new physics contribution δg_L^{NP} and hence $\mathrm{F}_{\mathrm{nmUED}}$ goes to zero when $R^{-1}\to\infty$, as expected in a decoupling theory.

4.2.1.1 Additional Diagrams

Here we mention the additional contributions to $Zb\bar{b}$ coupling arising only in nmUED scenario. Though these diagrams have negligible contributions, we still include a brief discussion for the completion of the analysis. Their contributions will be discussed explicitly in the next section (Sec. 4.3.1.2).

In nmUED, we can have the contributions from $\mathrm{F}^{(n,m)}_{\mathrm{nmUED}}$ (*i.e.* from $m=n$ and $m\neq n$ contributions) instead of $\mathrm{F}^{(n)}_{\mathrm{nmUED}}$ (only $m=n$ contributions), though the differences coming from these two are almost negligible. Moreover, there exists additional contributions coming from $\mathrm{F}^{(00n)}_{\mathrm{nmUED}}$. In case of m,n contributions the number of diagrams shown in Figs. 4.2, 4.3 remain the same, with all nth mode contributions from scalars and gauge fields replaced by its mth mode. Besides the M' in Eq. 4.24 will now be $M^2_{\Phi m}/M^2_{Qn}$. The diagrams of (0)-(0)-(n) type are shown in Fig 4.4. Here n is only even.

The diagrams in Fig. 4.4 follow the same analysis as that of Figs. 4.2 and 4.3. As we are dealing with KK-parity conserving scenario, only those diagrams are allowed which include vertices allowed by KK-parity. The contribution from (0)-(0)-(n) type diagrams is given by

$$F^{(00n)}_{\mathrm{nmUED}}(a_n, a'_n) = \frac{a_n\beta I_c^2}{[a_n-a'_n-1]^2}\Bigg[\{a_n-a'_n-1\}\left(1-\frac{6M_W^2}{m_t^2}\right)-(1+a'_n)\ln\left(\frac{a_n}{1+a'_n}\right) + \frac{2M_W^2}{m_t^2}(2a_n+a'_n+1)\ln\left(\frac{a_n}{1+a'_n}\right)\Bigg], \tag{4.27}$$

with $a_n\equiv m_t^2/M^2_{\Phi n}$, $a'_n\equiv M_W^2/M^2_{\Phi n}$. So if we consider all KK-number violating as well as KK-number conserving contributions, the $\mathrm{F}_{\mathrm{nmUED}}$ can be given by

$$F_{\mathrm{nmUED}} = \sum_{n,m}^{\infty} F^{(n,m)}_{\mathrm{nmUED}} + \sum_{n=\mathrm{even}}^{\infty}\mathrm{F}^{(00n)}_{\mathrm{nmUED}}. \tag{4.28}$$

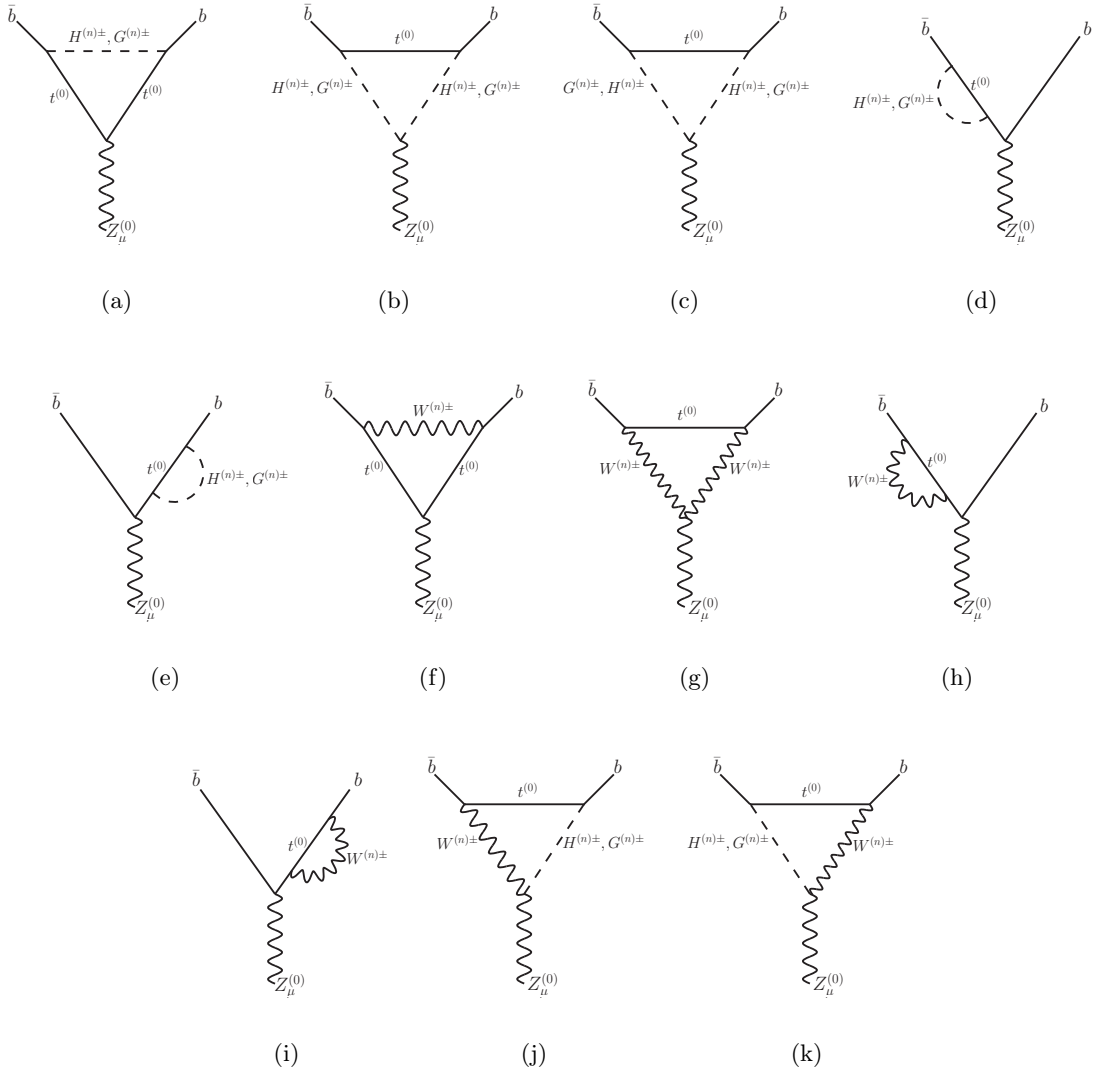

FIGURE 4.4: Loop involving (0)-(0)-(n) contributions of $Zb\bar{b}$ in the 't Hooft–Feynman gauge.

With $R^{-1} \to \infty$, the new physics contributions will go to zero.

4.2.2 Rare Top Decays

This section deals with some of the rare decays of the top quark in the nmUED model. In the SM, the flavor changing rare decays of top quarks occur at loop level. On top of this loop suppression, there exist CKM and GIM suppression [190, 191, 206]. Here we consider the decays, $t \to c\gamma$ and $t \to ch$. Evidently in the present model, the higher KK-mode particles contribute in these loop-driven processes. In the following first we will describe the general Lorentz structure for each decay amplitude with the corresponding Feynman diagrams. Here also, we use 't Hooft–Feynman gauge in our calculation as the divergences are more manageable in this gauge but at

the cost of having extra diagrams with unphysical scalars. We present the important Feynman rules in the Appendix G.

4.2.2.1 $t \to c\gamma$

We are now going to discuss the details of the calculation of the decay width of $t \to c\gamma$ in this model. The most general form of the amplitude of the decay $t(p) \to c(k_2)\gamma(k_1)$ for on-shell quarks and real photons can be given by [190, 214]

$$\mathcal{M}(t \to c\gamma) = \frac{i}{m_t + m_c}\bar{u}(k_2)[\sigma^{\mu\nu}k_{1\nu}\left(A_L P_L + B_R P_R\right)]u(p)\epsilon^*_\mu(k_1), \tag{4.29}$$

where u, $\bar{u}$ and ϵ_μ correspond to the incoming, outgoing spinors and photon polarization respectively; $P_{R,L} = (1 \pm \gamma_5)/2$ are the usual projection operators. The coefficients A_L and B_R yield the information about couplings, CKM matrix elements and the loop momenta integration. We have not included the effect of KK particle contribution on the CKM elements; for details see Ref. [137]. Note that when writing the full amplitude for the process $t \to c\gamma$ following all the Feynman rules (in the SM or in (n)mUED) one may come across terms proportional to $\gamma_\mu P_{R,L}$ in the amplitudes[1] of Feynman diagrams. But after summing over all the amplitudes of all the diagrams and then incorporating the GIM mechanism[2], the terms proportional to $\gamma_\mu P_{L,R}$ cancel. In the process all the divergences that appear in the individual diagrams also get cancelled. These remarks hold true irrespective of whether m_c is taken to be zero or not. However it is worth mentioning that in the limit $m_c \to 0$, which is a reasonable approximation, the coefficient A_L vanishes. In the case where $m_c \neq 0$, both A_L and B_R contribute. In these loop-driven processes, the apparent divergences get cancelled among the triangle and self-energy-type diagrams. In the general non-vanishing m_c case the decay width is given by

$$\Gamma_{t\to c\gamma} = \frac{1}{16\pi}\frac{(m_t^2 - m_c^2)^3}{m_t^3(m_c + m_t)^2}\left(|A_L|^2 + |B_R|^2\right). \tag{4.30}$$

The Feynman diagrams for this process are presented in Fig. 4.5 and in Fig. 4.6. In these diagrams, the superscripts (n) or (m) represents the nth (or mth) KK-mode of the corresponding particle. Since in mUED KK-number is conserved in any specific vertex we always have $m = n$; but in the case of nmUED, m and n can be different, obviously satisfying the conservation of the KK-parity. Clearly the quantities A_L and B_R contain the sum over the KK-modes. In our analysis we took the KK sum up to level five (as we have checked that the results of the KK sum up to level ten is almost same as that of the sum up to level five) as the contribution for

[1] To be precise, for the $m_c \neq 0$ case both $\gamma_\mu P_{L,R}$ are present, but in the $m_c = 0$ case, only $\gamma_\mu P_L$ appears.

[2] Basically the GIM mechanism implies the utilization of the relation, $V^*_{tj}V_{cj}[i\mathcal{M}(m_j)] = V^*_{tb}V_{cb}[i\mathcal{M}(m_b) - i\mathcal{M}(m_s)]$, where $\mathcal{M}$ represents the sum of the amplitudes of all the Feynman diagrams and m_s is the strange quark mass that we take to be zero.

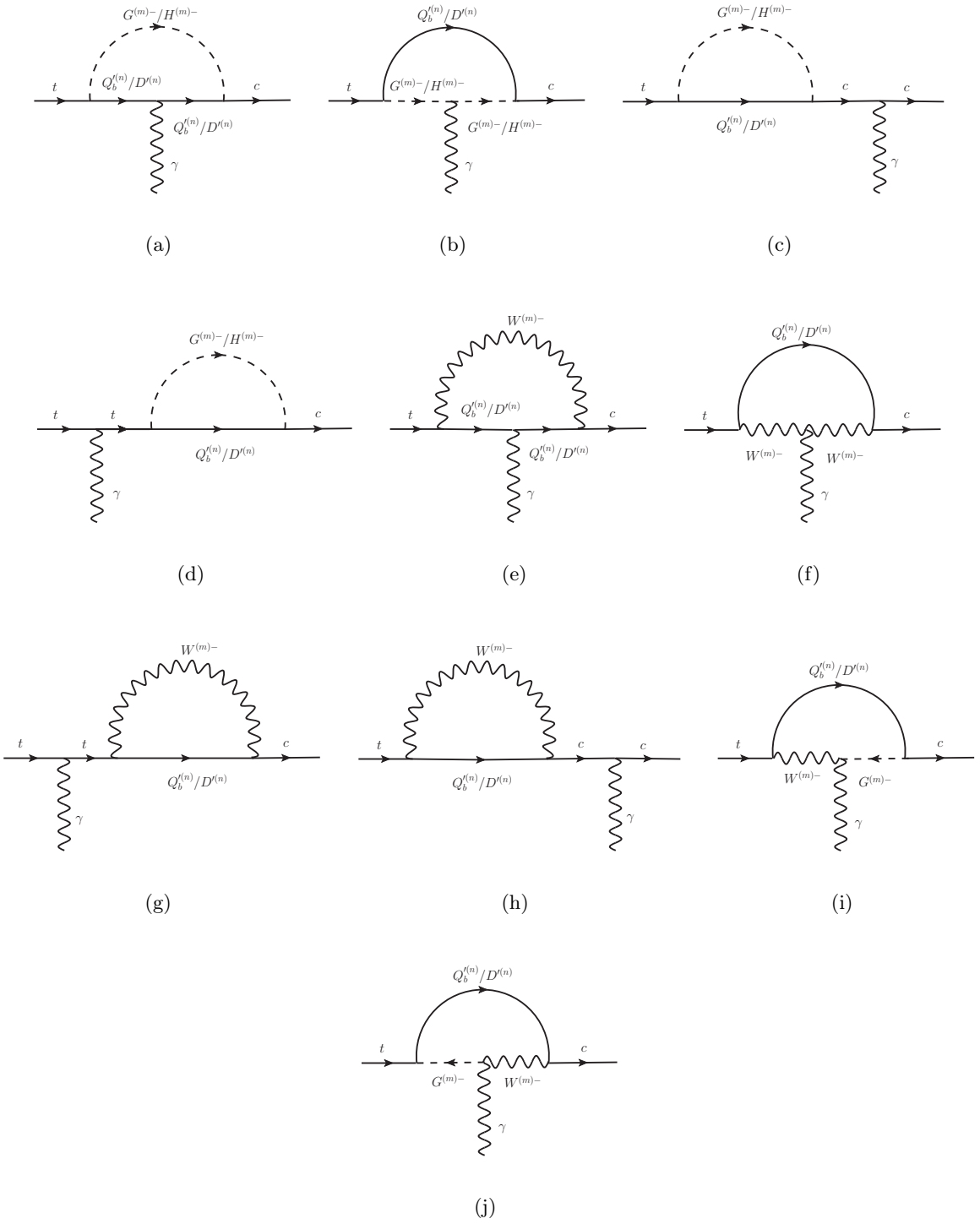

FIGURE 4.5: Necessary Feynman diagrams for the process $t \to c\gamma$ in the 't Hooft–Feynman gauge in nmUED. The particles in the legs contain no KK-indices as they represent the SM particles and their KK-indices are assumed to be zero (excluding (0)-(0)-(n)).

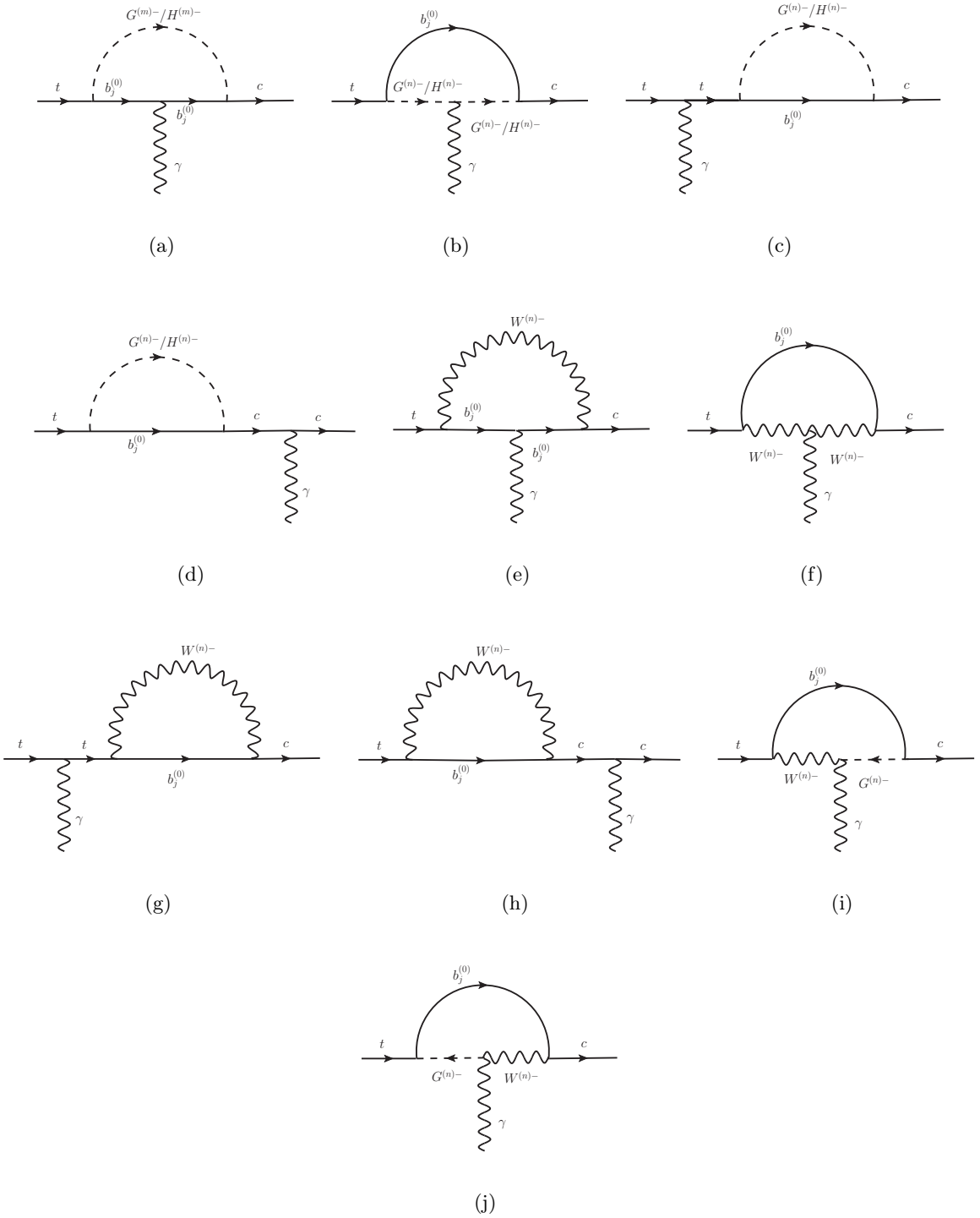

FIGURE 4.6: Necessary (0)-(0)-(n) type Feynman diagrams for the process $t \to c\gamma$ in the 't Hooft–Feynman gauge in nmUED.

higher modes decouples. Also Fig. 4.12 shows that the mass of m_c plays an insignificant role in the total decay width. Unless otherwise stated we consider a vanishing m_c in our numerical analysis.

4.2.2.2 $t \to ch$

One of the other important rare decays of the top quark is its flavor violating decay to the charm quark (c) and Higgs boson (h). The most general form of the amplitude of the decay $t(p) \to c(k_2)h(k_1)$ is given as

$$\mathcal{M}(t \to ch) = \bar{u}(k_2)\left[F_S + i\gamma_5 F_P\right] u(p), \tag{4.31}$$

where the F_S and F_P correspond to the scalar and pseudo-scalar form factors, respectively. The assertions we made in the case of $t \to c\gamma$ regarding the divergence cancellation etc. are true here also. Besides, we keep the information of couplings, CKM elements, and loop momenta embedded in these form factors.

It is straightforward to calculate the decay width of the process $t \to ch$ from the amplitude mentioned above. The decay width is

$$\begin{aligned}\Gamma_{t\to ch} = \frac{1}{16\pi m_t^3}\sqrt{\left(m_t^2-(m_c+m_h)^2\right)\left(m_t^2-(m_c-m_h)^2\right)} \\ \times\left(\{(m_c+m_t)^2-m_h^2\}|F_S|^2+\{(m_c-m_t)^2-m_h^2\}|F_P'|^2\right),\end{aligned} \tag{4.32}$$

with $F_P' = iF_P$ and in the last piece, *i.e.* in the form factor squared quantities, the KK sum is taken. Also, for $m_c = 0$ the two form factors are equal, *i.e.* $F_S = F_P'$. The relevant Feynman diagrams for this process are given in Fig. 4.7. The KK-indices m and n obey the same set of assertions mentioned in the previous Sec. 4.2.2.1.

4.3 Results

4.3.1 Bounds Obtained from $Zb\bar{b}$

We first begin our discussion with the present status of experimental and theoretical estimation of the $Zb\bar{b}$ coupling. Following Gfitter Collaboration [183] and an improved estimation of R_b after incorporating higher order effects in the framework of SM [184], the experimental and the theoretical (SM) values are

$$R_b^{\rm exp} = 0.21629 \pm 0.00066 \quad \text{and} \quad R_b^{\rm SM} = 0.21550 \pm 0.00003.$$

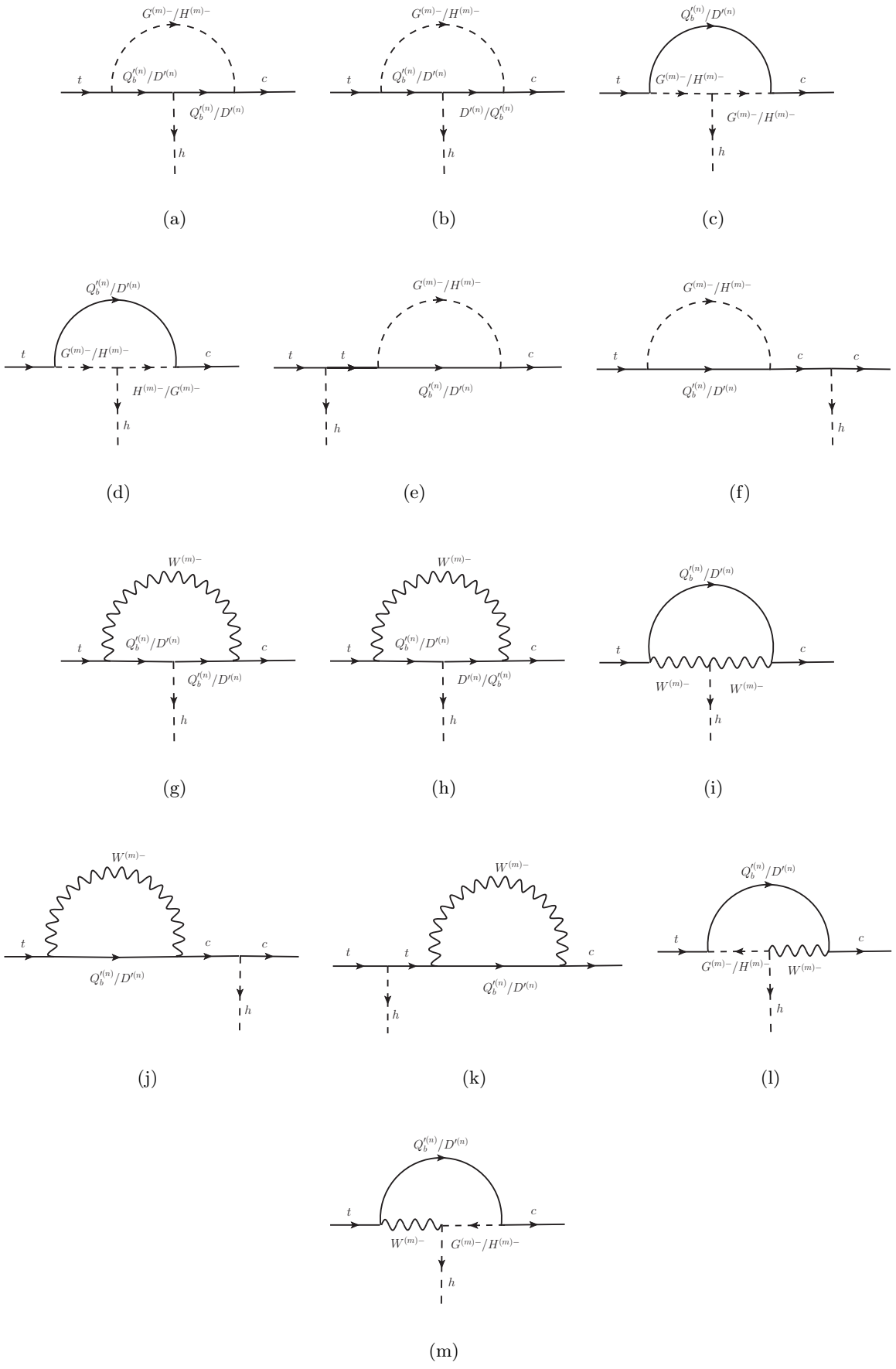

FIGURE 4.7: Feynman diagrams for the process $t \to ch$ in the 't Hooft–Feynman gauge in nmUED (excluding (0)-(0)-(n)).

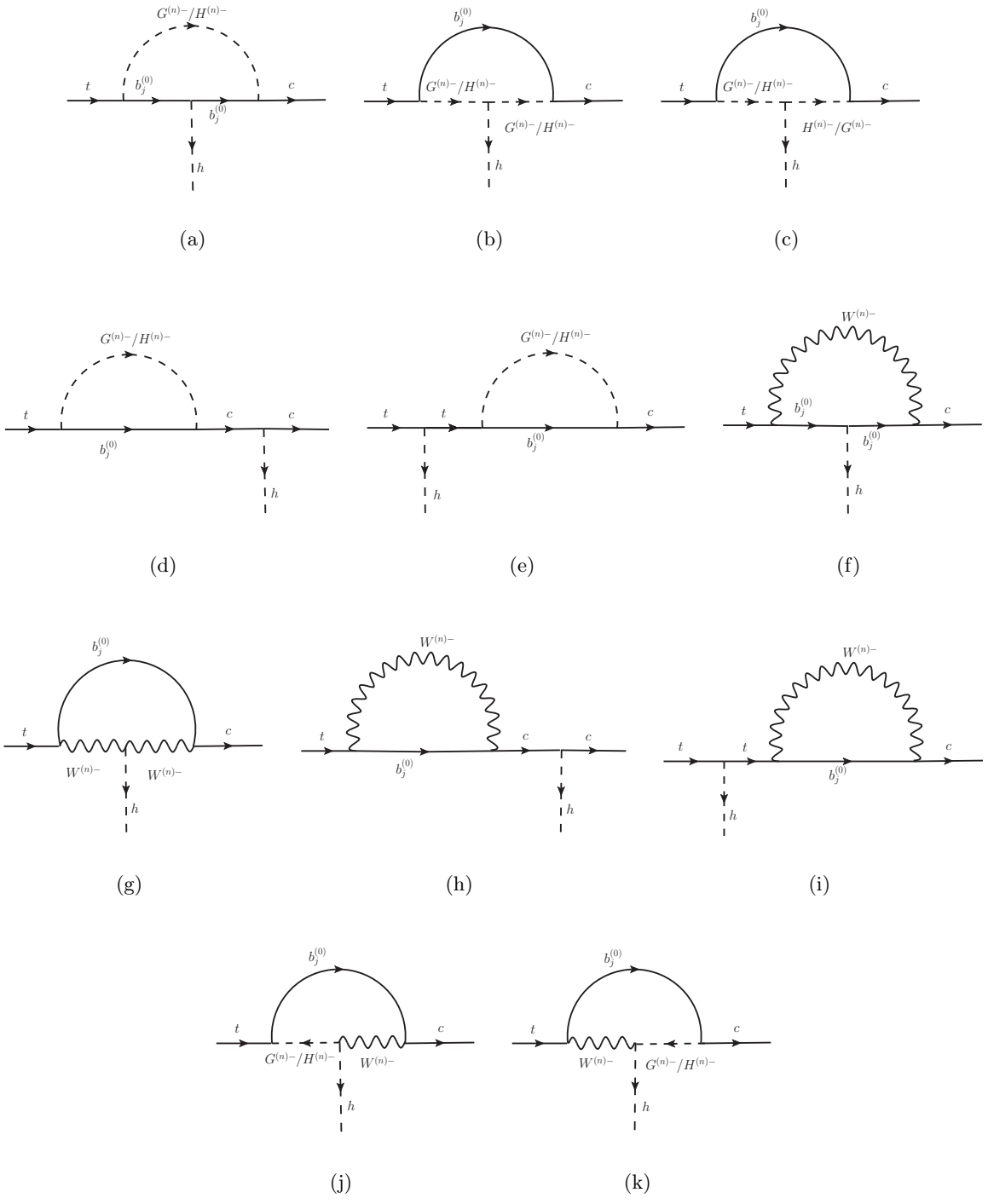

FIGURE 4.8: Feynman diagrams for the process $t \to ch$ in the 't Hooft–Feynman gauge in nmUED (excluding (0)-(0)-(n)).

Above results indicate an 1.2 *standard deviation* discrepancy between the experimental value of R_b and its SM estimate. Thus Eqs. 4.25 and 4.26 along with Eq. 4.10 can be used to translate this 1.2σ discrepancy on R_b to an allowed range for $\mathrm{F_{nmUED}}$: -0.3165 ± 0.2647. Clearly one can easily use this to constrain the model parameters of nmUED.

Since all the amplitudes listed in Fig. 4.2 contain terms proportional to gy_t^2, dominant contributions to $\mathrm{F_{nmUED}}$ come from the Feynman graphs listed in Fig. 4.2. The contributions from diagrams shown in Fig 4.3 are proportional only to g^3 with an exception to the diagrams 4.3(f) and 4.3(g); which has terms proportional to $g^2 y_t$ (here, y_t is the top quark Yukawa coupling). Total contribution of diagrams in Fig. 4.2 is nearly 1.5 times to that of the diagrams given in Fig 4.3.

4.3.1.1 Relook at the bound on R^{-1} in mUED from R_b

Before presenting the bounds obtained in the framework of nmUED, we would like to investigate the limit on the R^{-1} in case of UED keeping in mind the new estimate of SM radiative corrections to the $Zb\bar{b}$ vertex at two loop level [184]. Evidently one can retrieve the UED contributions to δg_L^{NP} by simply setting BLKT parameters to zero. In this limit, overlap integrals (I_1 and I_2) used in the couplings become unity and M_{Qn}, M_{gn} and $M_{\Phi n}$ all become equal to n/R in the nth KK-level; the ratios β, M' in Eq. 4.24 will be unity and our expression in UED completely agrees with the expression given in Ref. [137]. One can define a function $\mathrm{F_{UED}^{(n)}}$ in the same spirit following Eq. 4.26:

$$\begin{aligned}\mathrm{F_{UED}^{(n)}}(r_{1n}, r'_{1n}) = \quad & \frac{r_{1n}}{(r_{1n}-r'_{1n})^2}\Bigg[\left(1-3\frac{M_W^2}{m_t^2}\right)\{(r_{1n}-r'_{1n})+(1+r'_{1n})\ln\left(\frac{1+r'_{1n}}{1+r_{1n}}\right)\} \\ & +\frac{4M_W^2}{m_t^2}\{r'_{1n}-r_{1n}+(1+r_{1n})\ln\left(\frac{1+r_{1n}}{1+r'_{1n}}\right)\}\Bigg], \end{aligned} \tag{4.33}$$

with $r_{1n} \equiv m_t^2/m_n^2$, $r'_{1n} \equiv M_W^2/m_n^2$ and $m_n = n/R$.

In Fig. 4.9, we plot $\mathrm{F_{UED}}$ as function of R^{-1}, the only free parameter in the model after summing contributions ($\mathrm{F_{UED}^{(n)}}$) coming from KK-levels $n = 1-5$. This has been done in the view of recently discovered Higgs mass and its implication on the cut-off scale of UED[3]. Masses of the KK excitations increase with R^{-1} which in turn results in a decrement in the magnitude of $\mathrm{F_{UED}}$ due to the higher values of the masses of the propagators in the loop. One can easily check from Eq. 4.33, that in the limit $r'_{1n}, r_{1n} \to \infty$, $\mathrm{F_{UED}}$ is also vanishing which is the decoupling nature of the theory. The horizontal line in Fig. 4.9 represents the 95% C.L. upper limit on the value of $\mathrm{F_{UED}}$ calculated from difference between the experimental value of R_b and its theoretical (SM) estimate ($\mathrm{F_{UED}}$: -0.3165 ± 0.2647). Clearly the intersection of the horizontal line with the line

[3]See Sec. 2.4.1 of the Chapter 2.

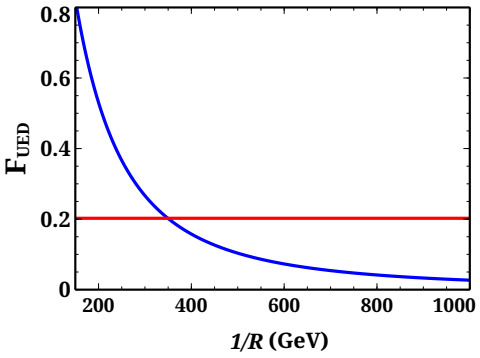

FIGURE 4.9: Variation of F_{UED} with R^{-1} in UED model. The horizontal line represents the 95 % C.L. upper limit on the value of F_{UED} calculated from the difference between the experimental value of R_b and its theoretical (SM) estimate.

showing the variation of F_{UED} would lead us to the present lower bound on R^{-1} from R_b. It clearly points that at 95% C.L. R^{-1} must be greater than 350 GeV, which shows a nominal improvement over the earlier limit which was 300 GeV [215]. If we overlook the correlation between the Higgs mass and the cut-off scale of UED, then one could sum up to 20-40 KK-levels. This would slightly push up the magnitude of F_{UED}[4] which in turn results into a higher value of the lower limit of R^{-1} (370 GeV). However, this limit is still not competitive to the bound derived from experimental data on SM Higgs production and its subsequent decay to WW [151][5]. For a detailed information on the bound on R^{-1} in case of UED, see the Sec. 2.4.

4.3.1.2 Possible bounds on nmUED from R_b

In this section we are going to lay down the analysis of the bounds obtained on the parameters in nmUED by using R_b. Contributions coming from each KK-level $F^{(n)}_{nmUED}$ have been already listed in Sec. 4.2.1. One has to sum over all the KK-levels to get the total contribution F_{nmUED}. We have taken into consideration the first 5 levels into the summation. Besides, we have explicitly checked that taking 20 levels into the summation would not change the results[6]. Like the previous chapter, here also we consider scaled BLTs, *i.e.* $R_{\phi,f}(\equiv r_{f,\phi}R^{-1})$. If we take scaled BLT parameters $< (-\pi)$, the zero modes become ghost-like with its norm being imaginary. Apart from this, we have observed that from unitarity analysis R_ϕ can be as high as 19, if we consider up to 5th KK-level. Negative values of $R_{f,\phi}$ below $(-\pi)$ would be physically unacceptable. Apart from this, all other values of $R_{f,\phi}$ are theoretically acceptable. It has been already mentioned in Sec. 4.1 that though for some choice of BLT parameters the numerical value of the overlap

[4]For $R^{-1} = 1$ TeV, values of F_{UED} after summing up to 5 levels and 20 levels are 0.0267 and 0.0292 respectively.

[5]This is due to the fact that experimental data from LHC on Higgs boson production and subsequent decay to WW is more consistent to the SM than R_b in which there is 1.2σ new physics window.

[6]For $R^{-1} = 1$ TeV and $r_\phi = 1.5$, $r_f = 1$, values of F_{nmUED} after summing upto 5 levels and 20 levels are 0.0439 and 0.0472 respectively.

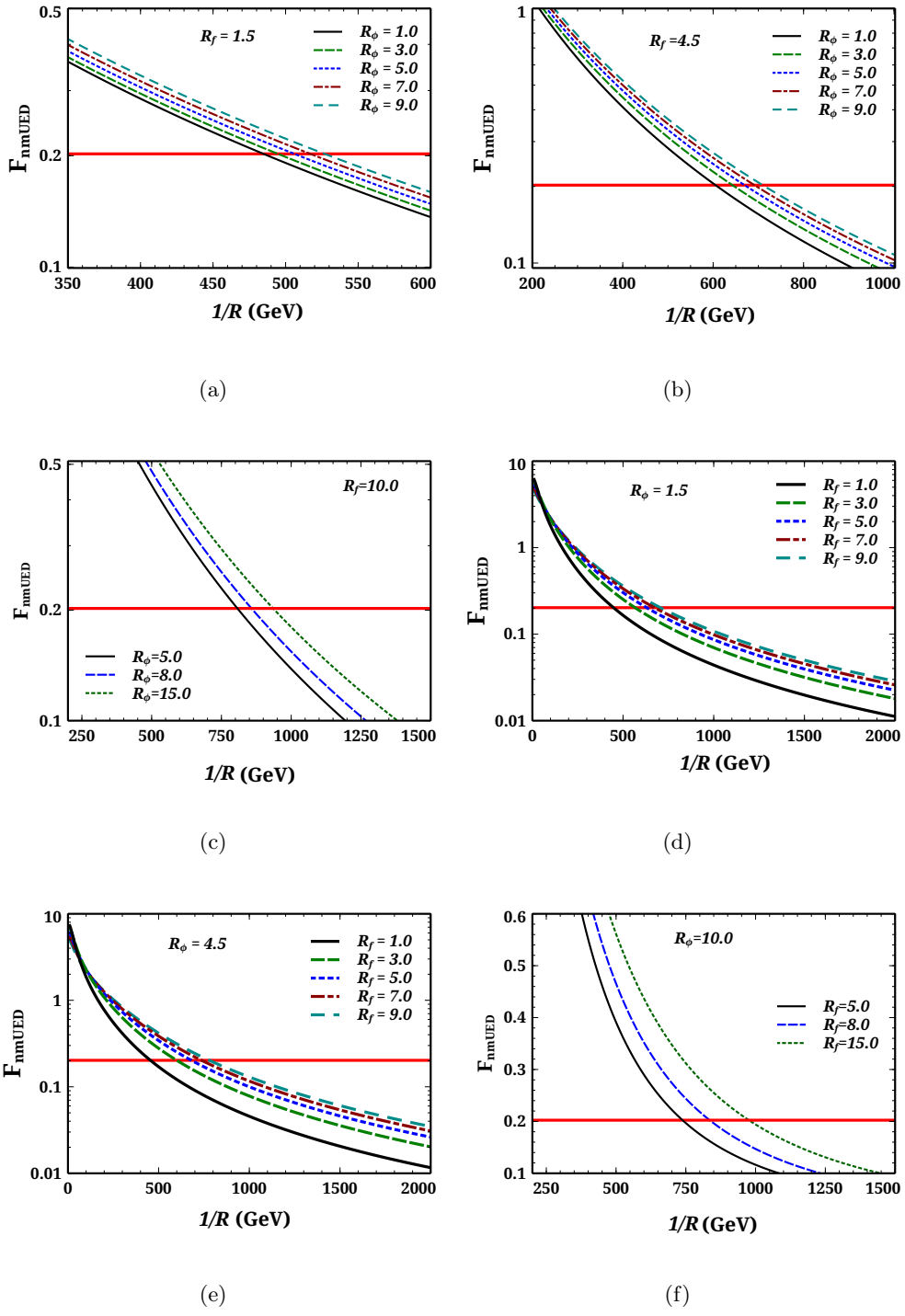

FIGURE 4.10: Variation of F_{nmUED} as function of R^{-1} for different values of BLKT parameters. The horizontal line represents the 95 % C.L. upper limit of the value of F_{nmUED} calculated from difference between the experimental value of R_b and its theoretical (SM) estimate.

integrals can be greater than unity, the final values of the relevant couplings will always remain within the perturbativity limit.

In Fig. 4.10, we have presented the variation of $F_{\rm nmUED}$ with R^{-1} for some representative values of the *scaled* BLKT parameters R_ϕ and R_f. One common feature that comes out from all of the plots is the monotonic decrement of $F_{\rm nmUED}$ with increasing R^{-1} which shows the decoupling nature of the new physics under our consideration that has been pointed out earlier in the case of UED. Panels (a,b and c) show the dependence of $F_{\rm nmUED}$ on R_ϕ keeping the value of R_f fixed to 1.5, 4.5 and 10.0 respectively. While in the lower panels of Fig. 4.10, we have presented how $F_{\rm nmUED}$ changes with varying R_f with two fixed values of R_ϕ namely 1.5 (d), 4.5 (e) and 10.0 (f) respectively.

From these figures 4.10 it is clear that R_ϕ and R_f have more or less same effects on $F_{\rm nmUED}$ and hence on $\delta g_L^{\rm NP}$. While the effect of R_ϕ is somewhat modest, $F_{\rm nmUED}$ is being more sensitive to any change in R_f. Therefore by increasing the BLT parameters one could enhance the radiative effects on the effective $Zb\bar{b}$ coupling. Evidently in nmUED, one could have a significant shift in the lower bound on R^{-1} from its UED value. For example, $R_\phi = 10.0$ and $R_f = 15.0$, the 95 % C.L. lower bound on R^{-1} is around 1 TeV. This limit comes down to 448 GeV for $R_f = 1$ and $R_\phi = 1.5$.

The role of R^{-1} in the framework of nmUED is quite similar as in the case of UED and has been explained above. We would also like to examine the role of R_f and R_ϕ. However we will do so a little later.

Finally in Fig. 4.11, we present the allowed parameter space in $R_\phi - R_f$ plane for several values of R^{-1}. We exhibit the contours of constant $F_{\rm nmUED}$ which corresponds to the 95 % C.L. upper limit. The region right to a particular line of R^{-1} is being ruled out from the consideration of R_b according to our analysis. Near vertical nature of the contours at lower values of R_f points out to the modest dependence of $F_{\rm nmUED}$ on R_ϕ that has been already shown in figure 4.10(a), (b) and (c). It has been exhibited from Fig. 4.10 that with higher values of BLKT parameters R_f and R_ϕ, $F_{\rm nmUED}$ is being increased in magnitude. Clearly as we go towards the right with increasing R_f and fixed R_ϕ for a particular value of R^{-1}, $F_{\rm nmUED}$ would increase. Furthermore the higher value of R^{-1} decreases $F_{\rm nmUED}$ showing the decoupling nature of new physics. Thus the increment of $F_{\rm nmUED}$ (with R_f) has been nullified by higher values of R^{-1} corresponding to different lines. Thus to compensate one must tune R^{-1} to a comparatively higher values. Besides, we have marked axes of Fig. 4.11 with scaled masses m_{Q1} ($\equiv M_{Q1}R$) and $m_{\Phi 1}$ ($\equiv M_{\Phi 1}R$), in the left panel; whereas, in the right one, we have marked the axes with scaled masses m_{Q2} and $m_{\Phi 2}$. This would facilitate one to get the bounds on masses of the $n = 1, 2$ KK excitations directly from this plot. For example, the line corresponding to $R^{-1} = 700$ GeV intersects the m_{Q1} axis at around 0.5 and m_{Q2} axis at around 1.24 which implies that for this particular value of R^{-1}, masses of $n = 1$ and $n = 2$ KK excitations of top quarks respectively below 350 GeV

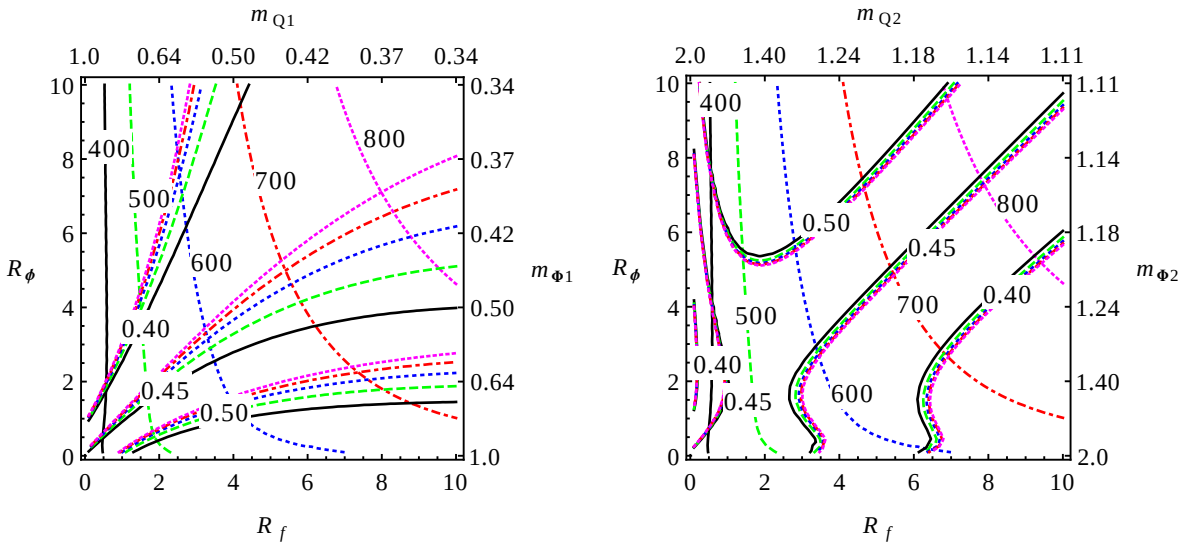

FIGURE 4.11: Contours of constant F_{nmUED} corresponding to 95% C.L. upper limit in $R_\phi - R_f$ plane. Different lines (marked with 400, 500, 600, 700 and 800) represent different values of R^{-1} (in GeV). Region right to a particular contour is being ruled out at 95% C.L. from the consideration of R_b for a given value of R^{-1}(in GeV) on each contour. We also present contours of the $W^{\pm(1)}t^{(1)}b^{(0)}$ coupling corresponding to three different values (0.4, 0.45 and 0.5) on the same plot for a same set of values of R^{-1} (left one) and that of $W^{\pm(2)}t^{(2)}b^{(0)}$ coupling for same values (in the right). In the left one, numbers along the top axis and right hand axis correspond to dimensionless quantities $M_{Q1}R$ and $M_{\Phi 1}R$ respectively whereas numbers along the top axis and right hand axis represent the respective dimensionless quantities $M_{Q2}R$ and $M_{\Phi 2}R$ in the right panel.

and 870 GeV are not allowed by the data. While the corresponding lower bound for $W^{(1)}$ mass for $R^{-1} = 700$ GeV is close to 540 GeV and lower bound for $W^{(2)}$ mass for same R^{-1} will be around 1 TeV which can be eventually obtained from the intersection of the same line with the $m_{\Phi 1}$ and $m_{\Phi 2}$ axes respectively.

The Fig 4.11 also represent the contours for constant (for three different) values of $W^{\pm(1)}f^{(1)}f^{(0)}$ and $W^{\pm(2)}f^{(2)}f^{(0)}$ couplings respectively. One can obtain several significant messages from these contours. Primarily the above coupling has a minimal dependence on R^{-1}. Secondly, the BLT parameters R_f and R_ϕ have opposite effects on the above interactions. While this couplings increase with R_ϕ, increasing values of R_f would try to decrease the strength of this interaction. For $n = 1$ the effect of R_f is more prominent. Similar conclusion can be drawn to $H^{\pm(1)/(2)}f^{(1)/(2)}f^{(0)}$ and $G^{\pm(1)/(2)}f^{(1)/(2)}f^{(0)}$ interactions. BLT parameters also have another bearing on F_{nmUED} through the masses of KK excitations. Heavier KK-masses would tend to decrease the magnitude of F_{nmUED} which is nothing but the evident upshot of the decoupling nature of the theory. It has been pointed out in Fig. 2.4 in Chapter 2 that KK-masses are decreasing function of respective BLT parameters. Thus BLT parameters have dual role to play

in the dynamics of F_{nmUED}. Let us state them one by one. An increasing R_ϕ would increase F_{nmUED} by increasing the relevant couplings and at the same time by decreasing the relevant KK-masses. On the other hand an increasing R_f would decrease the masses but it also decreases the couplings. These two effects play in opposite direction in determining the value of F_{nmUED}. However, rate at which F_{nmUED} increases with decreasing KK-mass, overcome the decrement of F_{nmUED} due to decreasing coupling with increasing R_f.

In passing we would like to make some comments on the terms which we have neglected by only considering interactions of SM particles with two KK-excitations having same KK-number. Evidently our calculation and results presented above do not take into account a number of Feynman graphs in which propagators in the loop correspond to KK excitations of different KK-numbers. To advocate our assumption, we present the values of F_{nmUED} for several values of R^{-1} for fixed R_ϕ and R_f in Table. 4.1. While presenting these numbers we have summed up to 5 KK-levels as before. In the second column of Table. 4.1, we have shown the values of F_{nmUED} when only KK-number conserving interactions are taken into account. While in the third column, the values of F_{nmUED} additionally includes contributions from all possible Feynman graphs involving KK-number violating interactions (excluding n or $m = 0$). Fourth column presents only (0)-(0)-(n) type interactions; furthermore this kind of interactions fall rapidly from $R^{-1} = 500$ GeV onwards. It is very clear from the numerical values of F_{nmUED} that our assumption was realistic and the corrections coming from Feynman graphs involving the KK-number non-conserving interactions are minuscule.

R^{-1} (GeV)	F_{nmUED} ($n = m$ terms only)	F_{nmUED} ($n = m$ and $n \neq m$ terms)	F_{nmUED} ((0)-(0)-(n) type only)
250	0.5442	0.5481	0.02278
350	0.3127	0.3148	0.01577
450	0.2003	0.2016	0.01163
550	0.1384	0.1393	0.00898
650	0.1009	0.1016	0.00717
750	0.0767	0.0773	0.00588
850	0.0602	0.0606	0.00492

TABLE 4.1: Values of F_{nmUED} for the contributions coming, only from the KK-number conserving interactions (second column), from all possible interactions (excluding (0)-(0)-(n)) (third column) and from only (0)-(0)-(n) type interactions to calculate the effective $Zb\bar{b}$ vertex at one loop. Numbers are presented for several values of R^{-1} (first column) and for R_f=1 and R_ϕ=1.5.

4.3.2 $t \to c\gamma$

Before we present the mUED and nmUED results of the $t \to c\gamma$ decay in the presence of single UED, it is important to relook at the SM results. The dominant decay mode of the top quark

is to a bottom quark and a W boson and its decay width is given by

$$\Gamma_{t\to bW} = \frac{g^2}{64\pi}|V_{tb}|^2 \left[1 - 3\left(\frac{m_W}{m_t}\right)^4 + 2\left(\frac{m_W}{m_t}\right)^6\right]. \tag{4.34}$$

For $M_W = 80.39$ GeV, $m_t = 174.98$ GeV [217], $\Gamma_{t\to bW}$ is approximately 1.5 GeV. This being the most prominent decay mode of the top quark any branching ratio can be given as

$$\mathrm{BR}(t \to XY) = \frac{\Gamma_{t\to XY}}{\Gamma_{t\to bW}}. \tag{4.35}$$

The SM prediction for the branching of $t \to c\gamma$ is

$$\mathrm{BR}(t \to c\gamma) = \left(4.6^{+1.2}_{-1.0} \pm 0.4^{+1.6}_{-0.5}\right) \times 10^{-14}, \tag{4.36}$$

where the first uncertainty corresponds to the uncertainty in bottom mass, the second due to the CKM mixing angle uncertainties, and the third from the variation of the renormalization scale between M_Z (+ve sign) and $1.5m_t$ (-ve sign) [190]. Taking the pole mass of the b quark to be 4.18 GeV [218] our SM prediction for the $t \to c\gamma$ branching ratio is 2.4×10^{-13} and for the running mass $\bar{m}_b(m_t) = 2.74$ GeV the branching ratio becomes 5.18×10^{-14}. Clearly the exact value of this decay width, as well as the other flavor violating decays of the top quark, is highly sensitive to the bottom quark mass, as has been pointed out in Ref. [191]. For the numerical evaluations we have used `Package-X` [219] and `LoopTools` [220].

From these numbers it is evident that the branching ratios for flavor changing top quark decays in the SM are exorbitantly suppressed, making the prospect of its detection at the LHC or even higher energetic FCC quite bleak. We discuss the present LHC reaches in our summary Sec. 4.5. On the other hand, as a positive side if any signature of these types of decays is found with a measurable amount of enhancement that must arise from some new physics beyond the SM.

4.3.2.1 mUED Results

In the mUED scenario the loop-induced decay of the top quark to charm quark and photon gets additional contribution from the higher mode KK particles running in the loop. The representative Feynman diagrams are shown in Fig. 4.5. Since in mUED, KK-number is a conserved quantity the KK-indices m and n in each vertex of the diagrams respect this symmetry; to be more precise, in all the diagrams, for mUED at least, m and n should be equal.

As has been mentioned in the model description, see Sec. 2.2, the only relevant parameter for the mUED set-up is the inverse of the compactification radius $1/R$ and the masses of all the KK particles are dependent on this quantity. The important difference from the SM in mUED

is basically the presence of KK counterparts of SM particles in the loop as well as the presence of charged KK scalars. Moreover, the mixing in the KK fermion sector plays an important role.

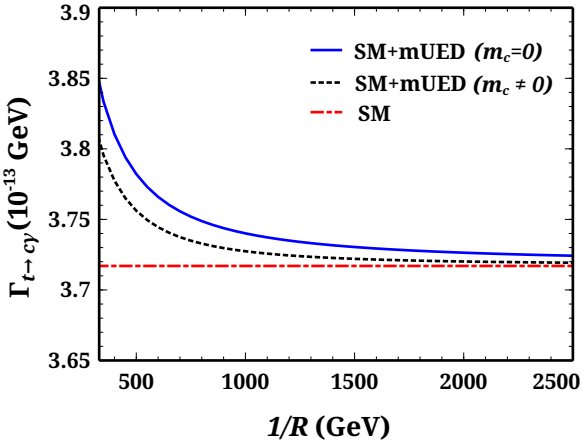

FIGURE 4.12: The decay width of the process $t \to c\gamma$ as a function of the inverse compactification radius $1/R$ in the case of mUED. For the $m_c \neq 0$ case, the charm quark mass is taken to be 1.275 GeV.

Fig. 4.12 summarizes the $t \to c\gamma$ decay width in mUED. We have calculated the decay width by taking the SM as well as the new physics, *i.e.* the mUED into account. Clearly for a higher value of the inverse compactification radius $1/R$ the masses of the KK-modes become too heavy and they decouple, effectively making a negligible contribution. The red (dash-dotted) line shows the SM only value that we obtained using the pole mass of the b-quark. At the higher values of $1/R$ the convergence of the blue (solid), for $m_c = 0$, and black (dotted), for $m_c \neq 0$, line with SM line only reflects the decoupling of the KK-modes. We take $m_c = 1.275$ GeV [218] for the $m_c \neq 0$ case.

The lower values (less than 1 TeV) of $1/R$ are disfavored from the LHC data [69]. Moreover from Fig. 4.12 we see that even for the lower values of $1/R$ the order of magnitude of the decay width does not change much. Thus, one can conclude that the mUED set-up can not enhance the branching ratio of $t \to c\gamma$ to any significant level from that of the SM value while remaining in the allowed ranges, obtained from the LHC, of the inverse compactification radius. However, the situation is different in the case of nmUED, as we see shortly.

4.3.2.2 nmUED Results

The presence of BLKT parameters makes the situation quite different from the minimal scenario. It has already been mentioned that the BLKT parameters control the mass spectrum via the transcendental equation [see Eq. 2.77], as well as the couplings via the appropriate overlap integrals. Like the mUED scenario, here also the loop-induced $t \to c\gamma$ process gets contributions from the higher KK excitations in the loop. But in this case the BLT parameters play a significant

role in determining the masses of those particles running in the loops as well as the relevant couplings. One other important distinction from the mUED scenario is that in nmUED, KK-number is no longer a conserved quantity, but still the conservation of KK-parity holds due to the presence of the same BLKT parameters at the two orbifold fixed points, $y = 0$ and πR. Consequently, unlike mUED, the couplings of particles with KK-numbers (0)-(0)-(n), where n is even, are present at tree-level. Thus, there are extra Feynman diagrams contributing in the process, *e.g.* in Fig. 4.5 the appropriate diagrams with n being zero will also contribute (Fig. 4.6).

We now discuss the results in the nmUED scenario. Note that we have two BLT parameters R_ϕ and R_f at our disposal (as in the case of radiative correction of $Zb\bar{b}$). Thus we consider two cases, one being the universal BLT case, *i.e.* $R_\phi = R_f$ making the same BLT for all types of fields and another being the case of $R_\phi \neq R_f$. First, take the case of universal BLT, *i.e.* $R_\phi = R_f \equiv r/R$.

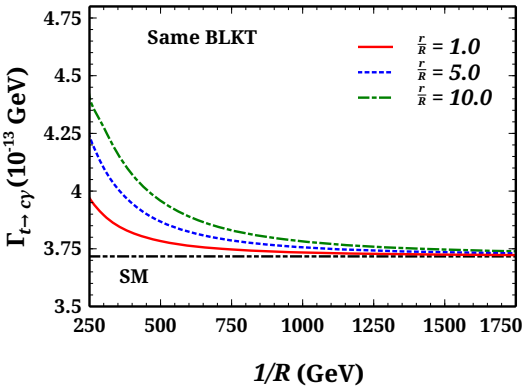

FIGURE 4.13: The decay width of the process $t \to c\gamma$ as a function of the inverse compactification radius $1/R$ in the case of nmUED for different values of BLT parameters. In this case we consider a universal BLT parameter r.

In in this scenario too, all the overlap integrals that modify the couplings become unity by virtue of the orthonormalization conditions, see Eqs. 2.84 and 4.4. Therefore, the effect of the common BLT parameter r/R is only to determine the masses of the KK particles running in the loop. Clearly this situation is almost like the mUED but with the freedom that the KK-masses can now be tuned with the BLT parameter r/R. In Fig. 4.13 we present the results for the same BLT case for different values of the parameter. The black (dash-dot-dot) line represents our SM value for the $t \to c\gamma$ decay width; the red (solid), blue (dotted), and green (dash-dotted) curves are for BLT parameter $r/R = 1.0$, 5.0, and 10.0 respectively.

We see that the contributions from the KK particles decouple at lower values (compared to the mUED case) of the compactification radius for lower values of r/R. This is expected as the higher values of r/R imply a lower (compared to the mUED case) KK-mass for a specific value of the inverse compactification radius $1/R$. Clearly for a specific value of $1/R$, a higher value of the BLT parameter would lead to a lower KK-mass than in the mUED thus making the propagator suppression less effective. Consequently it is evident that the higher value BLKT parameters

will result in a decoupling for higher values of $1/R$. However, like in mUED, in the universal BLT case also the value of the decay width does not change its order of magnitude from its SM value even for lower $1/R$. But unlike mUED a lower value of $1/R$ is not much constrained from LHC data in the nmUED scenario. To the best of our knowledge the only collider studies made in nmUED, to date are Refs. [164,165]. A detailed study of nmUED in the light of LHC data is underway.

Now we take up the case of different BLTs, *i.e.* $R_\phi \neq R_f$. Clearly in this case the KK excitations of fermions and the KK scalar/gauge bosons have different masses depending on their respective BLT parameters. Moreover, the couplings in this case get modified by the appropriate overlap integrals, mentioned in Eqs. 4.4. The variation of the $t \to c\gamma$ decay width for various choices of BLT parameters is shown in Fig. 4.14. Different choices of BLT parameters give rise to distinct features in the $1/R$ dependence of the decay width. Unlike the mUED or universal BLT scenario, here the total decay width (SM plus nmUED) can be smaller than the SM value for some choice of parameters. Moreover, the higher values of the BLT parameters (see the figure in the lower right panel of Fig. 4.14) can enhance the decay width by several orders of magnitude from the SM value, in the lower $1/R$ region. For example, for $R_f = 8$ and $R_\phi = 15$ and $1/R = 500$ GeV the decay rate can be $\sim 4.1 \times 10^{-12}$ GeV. But, for these sets of parameter values the masses of first KK-level particles are less than 200 GeV, to be precise $\sim$ 190 GeV for first KK-level fermions and $\sim$ 140 GeV for first KK-level bosons; and the second levels are of $\sim$ 570 GeV (fermions) and $\sim$ 540 GeV (bosons). We elaborate on the implications of this in Sec. 4.4. At this point it is worth mentioning that we find that the specific nature of the curves is mostly determined from the contribution from the Feynman diagrams that involve the KK excitations of the scalars. Moreover, as far as the nature of the curves are concerned, a naïve interpolation to the same BLT scenario from the different BLT scenario is not possible. In the different BLT case there are overlap integrals that modify the appropriate couplings. These overlap integrals depend on the KK-masses and, in some cases, on the difference of the KK-masses between two different types of particles (*e.g.*, in our case some overlap integrals depend on the the difference between $M_{\Phi n}$ and M_{Qn}). Also, in the amplitude of the diagrams the differences in the physical masses (physical masses, $m_X = M_X/R$) play a significant role. Thus depending on the choice of different BLT parameters the difference between m_{Qn} and $m_{\Phi n}$ can be positive or negative which, at the amplitude level, can positively or negatively contribute to the SM amplitude. So in the different BLT case, it is possible for some parameter region that the overall decay width be less than that of the SM prediction, leading to the specific nature of Fig. 4.14. The reverse is also possible, *e.g.* we have checked that for $1/R = 600$ GeV, $R_\phi = 6.0$, the KK contribution is always positive if $R_f < 0.58$ and in that case one can get the nature of Fig. 4.14 similar to that of Fig. 4.13, *i.e.* the curves show a monotonic increase as $1/R$ decreases. Clearly, if in future experiments the $t \to c\gamma$ decay width comes out to be a larger value than the SM calculations

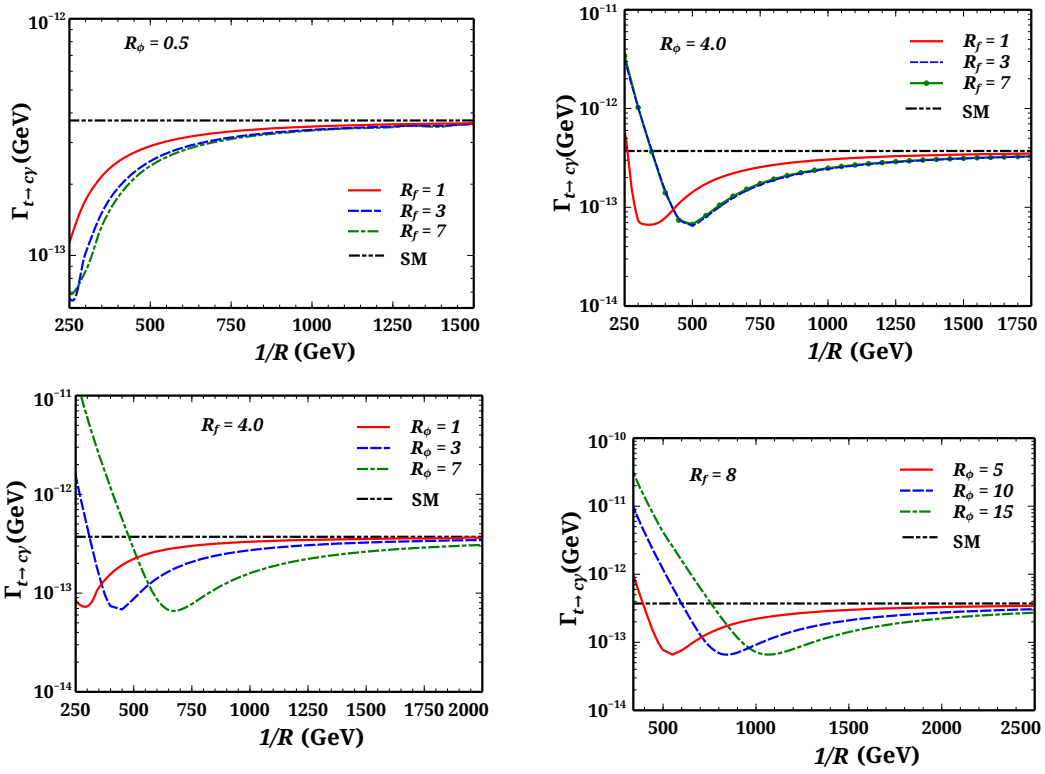

FIGURE 4.14: The decay width of the process $t \to c\gamma$ as a function of the inverse compactification radius $1/R$ in the case of nmUED for different values BLT parameters R_f $(= r_f/R)$ and R_ϕ $(= r_\phi/R)$.

then the higher BLT scenario will be favored provided the constraints on the $1/R$ from other observations are met.

We end the discussion on the $t \to c\gamma$ decay width in nmUED with the caveat that in our study we take a common BLT parameter for fermions R_f and for gauge/scalar fields a common R_ϕ and thus the situation can be generalized by considering different types of BLT parameters for different fields and that eventually results in richer details of this decay width.

4.3.3 $t \to ch$

The loop-induced flavor changing top quark decay to charm quark and Higgs boson was first calculated in Ref. [206]. For $m_t \simeq 175$ GeV and $m_h \in [40\text{ GeV}, 2M_W]$, according to Ref. [206], $\text{BR}(t \to ch) \simeq 10^{-7} - 10^{-8}$. However, this result was erroneous, which was subsequently pointed out and corrected in Ref. [188]. According to this, for $m_t = 175$ GeV, $m_c = 0$, $m_b = 5$ GeV, and $m_h = 120$ GeV,

$$\text{Br}(t \to ch) = 4.605 \times 10^{-14}. \tag{4.37}$$

The SM prediction for the same process has recently been calculated in Refs. [191, 205, 210] and according to these references,[7] the branching ratio is $\sim 10^{-15}$. Again, the root of all these differences in the exact value of the branching ratio is that the choice of values of various SM parameters, most crucially the value of m_b, differs in each studies. For $m_h = 125$ GeV and taking the pole mass of the b-quark to be 4.18 GeV our SM prediction for the $t \to ch$ branching ratio is 1.99×10^{-14} and for the running mass $\bar{m}_b(m_t) = 2.74$ GeV the branching ratio becomes 3.63×10^{-15}. We again emphasize that the exact estimation of the decay width is highly sensitive to the b-quark mass, m_b. After this discussion we present our results in mUED and nmUED.

4.3.3.1 mUED Results

The relevant Feynman diagrams for the process $t \to ch$ in the case of mUED can be found in Fig. 4.7. Again, the KK-indices m and n have to be taken appropriately maintaining the conservation of KK-number. Also, the other details, inherent to the model itself, remain the same as discussed in the case of $t \to c\gamma$; see Sec. 4.3.2.1.

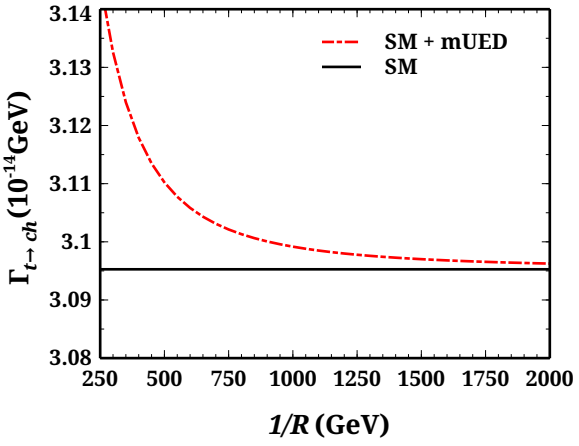

FIGURE 4.15: The decay width of the process $t \to ch$ as a function of the inverse compactification radius $1/R$ in the case of mUED.

In Fig. 4.15 we present our results for the decay width of $t \to ch$ in mUED. Like the $t \to c\gamma$ case, here also we take the pole mass of the b-quark. In this figure, the black (solid) line represents our SM value of the decay width and the red (dash-dotted) curve is for the decay width in the case of SM combined with the mUED spectrum. In this case also we find no order of magnitude enhancement of the branching ratio for any reasonable values of $1/R$. The situation is almost similar in the nmUED scenario also, as we discuss in the next subsection.

[7] The branching ratio is 3×10^{-15} in [191], $(3.00 \pm 0.17) \times 10^{-15}$ in [210], 5.8×10^{-15} in [205] etc.

4.3.3.2 nmUED Results

In Fig. 4.16 we present the results for the universal BLT scenario, *i.e.* $R_\phi = R_f \equiv r/R$. For this case also we find that the value of decay width is of the same order as that of the SM for all choices of r/R.

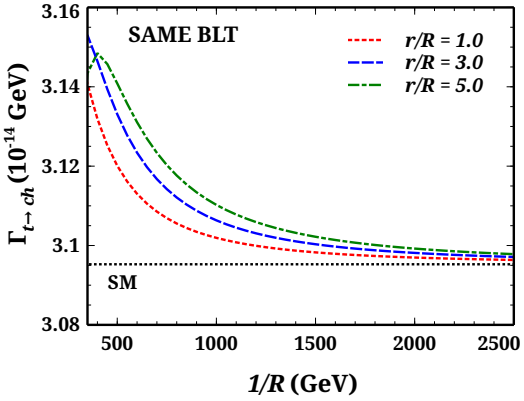

FIGURE 4.16: The decay width of the process $t \to ch$ as a function of the inverse compactification radius $1/R$ in the case of nmUED for different BLT parameters. In this case we consider a universal BLT parameter r.

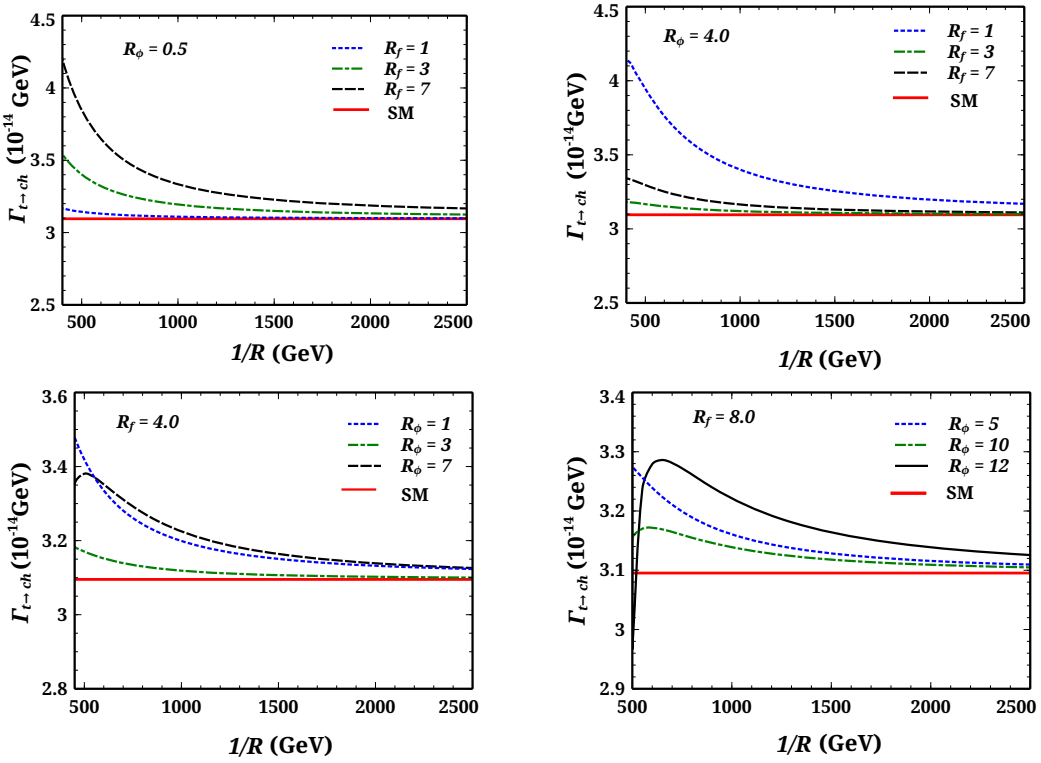

FIGURE 4.17: The decay width of the process $t \to ch$ as a function of the inverse compactification radius $1/R$ in the case of nmUED for different values of BLT parameters R_f $(= r_f/R)$ and R_ϕ $(= r_\phi/R)$.

The same thing happens in the distinct BLT ($R_\phi \neq R_f$) case also, as can be seen from Fig. 4.17, where we plotted the $t \to ch$ decay width for various choices of BLT parameters. In this case also a very high value of BLT parameters can significantly enhance the decay rate.

4.4 S, T, Uarameters, FCNC and Other Issues

The Peskin-Takeuchi parameters, *i.e.* S, T and U parameters, encode the oblique corrections to the electroweak gauge boson propagators [50]. These parameters put stringent constraints on many BSM physics scenarios. In nmUED these electroweak precision constraints are discussed in [81, 165, 171, 177]. Clearly in these cases the underlying action and some assumptions are different from our setup. For completeness we spell out these constraints in our case.

The effects on electroweak precision observables arise due to modifications to the Fermi constant G_F at tree-level. Actually in nmUED second level KK gauge bosons have tree-level couplings with SM fermions, and this modifies the effective four Fermi interactions and thus the G_F. Note that this is in contrast with the mUED scenario where there is no (2)-(0)-(0) coupling at the tree-level. The corrected Fermi constant in the case of nmUED can be given as

$$G_F = G_F^0 + \delta G_F, \tag{4.38}$$

where G_F^0 (δG_F) comes from the s-channel SM (even KK) $W^\pm$-boson exchange. More precisely they can be written as [171]

$$G_F^0 = \frac{g_2^2}{4\sqrt{2}M_W^2} \quad \text{and} \quad \delta G_F = \sum_{\substack{k\geq 2 \\ \text{even}}} \frac{g_2^2}{4\sqrt{2}M_{W^{(k)}}^2} (\sqrt{r_\phi + \pi R}\ I_3^k)^2, \tag{4.39}$$

where I_3^k is given in Eq. 4.4f. Now, in terms of these quantities the electroweak precision observables can be written as [165, 171]

$$S_{nmUED} = 0, \quad T_{nmUED} = -\frac{1}{\alpha}\frac{\delta G_F}{G_F}, \quad U_{nmUED} = \frac{4\sin\theta_W^2}{\alpha}\frac{\delta G_F}{G_F}. \tag{4.40}$$

Now, the most recent fit to the electroweak precision data gives [221]

$$S = 0.05 \pm 0.11, \qquad T = 0.09 \pm 0.13, \qquad U = 0.01 \pm 0.11, \tag{4.41}$$

from which we write

$$\begin{aligned} \hat{S} &= 0.05, \quad \sigma_S = 0.11, \\ \hat{T} &= 0.09, \quad \sigma_T = 0.13, \\ \hat{U} &= 0.01, \quad \sigma_U = 0.11\ . \end{aligned}$$

The S, T and U parameters are not independent parameters but are correlated. The correlation coefficients are given by [221]

$$\rho_{ST} = 0.90, \quad \rho_{SU} = -0.59, \quad \rho_{TU} = -0.83. \tag{4.42}$$

Now, constraints from S, T, U parameters can be imposed by evaluating the χ^2, given by

$$\chi^2 = \mathcal{A}^T \mathcal{C}^{-1} \mathcal{A}, \tag{4.43}$$

where $\mathcal{A}^T = (S_{nmUED} - \hat{S}, T_{nmUED} - \hat{T}, U_{nmUED} - \hat{U})$ and the covariance matrix $\mathcal{C}$ is given by

$$\mathcal{C} = \begin{pmatrix} \sigma_S^2 & \sigma_S \sigma_T \rho_{ST} & \sigma_S \sigma_U \rho_{SU} \\ \sigma_S \sigma_T \rho_{ST} & \sigma_T^2 & \sigma_T \sigma_U \rho_{TU} \\ \sigma_U \sigma_S \rho_{SU} & \sigma_U \sigma_T \rho_{TU} & \sigma_U^2 \end{pmatrix}. \tag{4.44}$$

For a maximal 2σ (3σ) deviation, given the two degrees of freedom, we need $\chi^2 \leq 6.18$ (9.21) [218]. In Fig. 4.18 we show the allowed region of parameter in the $R_\phi - R_f$ plane consistent with electroweak precision data at 2σ (and 3σ) deviation for inverse compactification radius, $1/R = 500$ and 1000 GeV. Note that the larger values of BLT parameters $R_{\phi,f}$ lead to a larger allowed parameter space that is in agreement with the result shown in Fig. 4.18 of Ref. [165]. We mention that the dominant effect on the electoweak precision observables comes from the modification of the Fermi constant. From the one-loop contribution of KK particles another set of subdominant modification in the precision observables results. However, a detailed one-loop contribution from the KK particles in the case of nmUED is subject to further study.

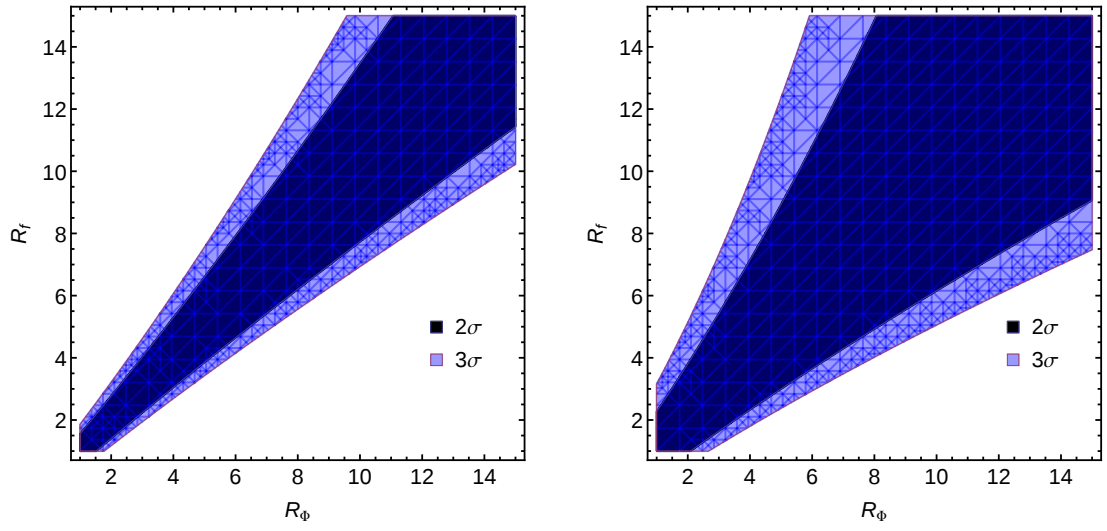

FIGURE 4.18: The shaded region, in the $R_\phi - R_f$ plane, represents the 2σ (dark blue) and 3σ (light blue) deviation region satisfying the electroweak precision constraints for $1/R$ =500 GeV (left) and 1000 GeV (right).

Normally BSM models suffer from the presence of tree-level FCNCs and appropriate symmetry etc. are imposed to get rid of them. In the most general setup of nmUED every field present in the model can have different BLT parameters. If there are different BLT parameters for fermions of different flavors then that leads to tree-level FCNCs. However, it has been shown in Ref. [177] that there exist no FCNCs if the fermion BLT parameters are flavor-blind, *i.e.* the BLT matrices are proportional to the unit matrix in flavor space. In our case we have used a universal BLT parameter for all fermions; clearly there is no tree-level FCNC in our present setup, no matter what the values of BLT parameters are.

In case of rare top decays, we have seen, at least in the case of $t \to c\gamma$, that somewhat large values of BLT parameters can result in an order of magnitude increment to the decay rate as compared to the SM. As it stands larger BLT parameters lead to smaller KK-masses. In this regard a few points are in order. Presently the bounds on new physics particles are quite high as can be seen from the exotic particle searches of ATLAS and CMS [222, 223]. In the case of mUED, LHC dilepton searches put constraints on second KK-level particles to be $m_{KK^{(2)}} \geq 1.4$ TeV [153]. Now, for the BLT parameters and R^{-1} that lead to a larger $\Gamma_{t\to c\gamma}$ compared to the SM the second level KK particles become much lighter. Clearly, a qualitative comparison with Ref. [153] shows that a lighter KK particle implies significant propagator enhancement leading the dilepton cross section to a degree that is ruled out by LHC dilepton data. We have checked that even the modification in couplings via the overlap integrals is not enough to evade these bounds. Thus the parameter space leading to an apparent enhancement in $\Gamma_{t\to c\gamma}$ is already ruled out from LHC dilepton searches. Also from Fig. 4.11, we can see that this parameter space is ruled out by the R_b value obtained by LEP collaboration.

In passing we mention that the collider signatures of nmUED can mimic supersymmetry (SUSY). However, one must remember that $n = 1$ KK-masses in nmUED are more closely spaced than the masses of SUSY partners in any conventional SUSY models. This hinders one from directly translating available bounds on conventional SUSY models to nmUED models.

4.5 Conclusions

We have performed a complete one-loop contribution to the $Zb\bar{b}$ vertex and also to flavor-changing top quark decays ($t \to c\gamma$ and $t \to ch$) in the context of minimal and non-minimal UED. In case of nmUED, kinetic and Yukawa terms are added to the fixed points of the extra space like dimension. These boundary-localized terms, with their coefficients as free parameters, parametrize the quantum corrections to the masses of the KK excitations and their mutual interactions. We have calculated the interactions necessary for our calculation. Some of these interactions are very similar to those in UED. However, some of the interactions are modified in

comparison to their UED counterparts by some overlap integrals involving the extra dimensional profiles of the fields present in an interaction vertex.

The effects of BLKTs on the masses of KK-modes and their interactions can be summarized as the following. For a given R^{-1}, increasing BLKT parameter would drive the respective masses to lower values. Strength of an interaction does not have such a simple dependence on the BLKT parameters. We have derived all the necessary interactions involving the KK excitations of top quarks, W bosons, charged Higgs and Goldstone bosons in the framework of nmUED with the assumption of equal gauge and Higgs BLKT parameters along with equal fermion and Yukawa BLT parameters. Gauge and Higgs BLKT parameters have been chosen to be equal to avoid the nontrivial scenario created by the presence of r_ϕ in equation of motion of the gauge fields, while unequal fermion BLKT parameter and Yukawa BLT parameter would lead to the KK-mode mixing in the definition of physical states of KK excitations of top quarks. So for the sake of a relatively simpler calculation we stick to the choice of equal fermion BLKT and Yukawa BLT parameters.

We have constrained the parameter space of these models from new physics contributions of $Zb\bar{b}$ coupling. In general, coupling of a b quark to the Z boson involves both the left- and right-chiral projectors. However, quantum corrections which go into the coefficient of the left-chiral projector are proportional to m_t^2 while the m_b^2 proportional terms go into the coefficient of the right-chiral projector. We have done the calculation in the limit where $m_b \to 0$. There are two main classes of Feynman diagrams contributing to $\delta g_L^{\rm NP}$ (the contribution to $Zb\bar{b}$ vertex in nmUED framework), in 't-Hooft Feynman gauge. First set of diagrams listed in Fig. 4.2, captures the dominant contribution (because of Yukawa coupling which is proportional to m_t) coming from the participation of KK excitations of top quarks and charged Higgs boson/Goldstones in the loops. The remaining set consists of contributions mainly coming from the KK excitations of W bosons and top quarks inside the loops. These diagrams are listed in Fig. 4.3.

The explicit expressions for the contributions coming from each of the diagrams are listed in the Section 4.2.1. Sum of the contributions to $\delta g_L^{\rm NP}$ from the diagrams in Fig. 4.2 is finite and independent of $\sin^2\theta_W$. While the second set of diagrams needs to be regularized, after summing up, it is still ultraviolet divergent and also contains a term which grows with R^{-1}[8]. We have used a regularization scheme following Ref. [137,216], upon which the total contribution becomes finite and also becomes independent of $\sin^2\theta_W$.

A recent theoretical estimation of the $Zb\bar{b}$ vertex in the framework of SM at two loop level has squeezed the window for new physics that might be operating at TeV scale. The experimentally measured value of R_b differs from the SM prediction at 1.2 σ level. We have used the experimental data and the recent results from the SM on R_b, to constrain the parameter space of non-minimal

[8]This term arises from the diagrams Fig. 4.3 (f) and (g), due to a direct proportionality on R^{-1} of the vertex $W-G-Z$.

Universal Extra Dimensional Model. We have relooked into the UED by setting the BLKT parameters to zero in our calculation. The resulting expressions can be used to put bound on R^{-1} in UED model using the same experimental data and the SM estimations of R_b. It has been found that R^{-1} in UED model should be greater than 350 GeV at 95 % C.L.

Next we focus into our main result. Comparing the numerical estimation of $\mathrm{F_{nmUED}}$ with the difference between experimental data and SM estimation we have constrained the parameters in nmUED. First we look into the limits on R^{-1}. Both the BLKT parameters have positive effects on $\mathrm{F_{nmUED}}$. This function is very sensitive to any change in R_f while the effect of R_ϕ is very mild. The bottom line is that both the BLKT parameters can push the allowed value of R^{-1} to higher values. Depending on magnitude of BLKT parameters R_ϕ and R_f (which we have chosen to be positive), lower limit on R^{-1} could be close to 1 TeV. Finally, we show contours of constant $\mathrm{F_{nmUED}}$ having the 95 % C.L. upper limit value for different values of R^{-1} in $R_\phi - R_f$ plane. As for a fixed value of R^{-1}, *i.e.* for a fixed curve the value of the function $\mathrm{F_{nmUED}}$ increases with increase of R_f the left side of that curve represents the allowed region of this function for respective R^{-1}.

Furthermore we have also verified, in the SM, the results of branching ratios of flavor-changing decays with the existing literature. As far as the experimental searches are concerned, both ATLAS and CMS collaborations have performed some searches of FCNC top decays. For example, using the 19.6 fb^{-1} data at $\sqrt{s} = 8$ TeV the CMS collaboration puts an upper bound on the rare decay to $c\gamma$ as $\mathrm{Br}(t \to c\gamma) < 0.182\%$ [224]. On the other hand for the $t \to ch$ channel, the ATLAS collaboration puts a bound of $\mathrm{Br}(t \to ch) < 0.51\%$ using 4.7 fb^{-1} data at $\sqrt{s} = 7$ TeV and 20.3 fb^{-1} at $\sqrt{s} = 8$ TeV [225]; whereas according to the CMS collaboration $\mathrm{Br}(t \to ch) < 0.56\%$ by using 19.5 fb^{-1} data at $\sqrt{s} = 8$ TeV [226]. Also see Ref. [227] for the projected limits for higher energies on top FCNCs at the LHC and ILC. From these numbers it is evident that even in the higher energetic Run-II of the LHC the sensitivity will not reach the limit to judge the small branching ratios as obtained from the theoretical calculations in the SM. However, there are many BSM scenarios in which these branching ratios are quite high and at the level that can be probed in the Run-II of LHC. The aim of this chapter is also to look into this issue of rare decays in one of the interesting BSM scenario, *i.e.* mUED and nmUED.

We show that both the decay widths of $t \to c\gamma$ and $t \to ch$ do not change much from the SM value in mUED for any reasonable choice of the inverse compactification radius $1/R$. This result is somewhat contrary to what has been obtained in Ref. [212] by using various simplifying assumptions. In passing we note that a similar picture arises for the rare B- and K-decays in the case of mUED [137]. On the other hand in the non-minimal case, *i.e.* in the presence of BLT parameters, if $R_{f,\phi} \geq 10$ and $R_f \neq R_\phi$ the $t \to c\gamma$ decay width can, in principle, enhance up to four orders of magnitude from its SM value while respecting the electroweak precision data. But the required R^{-1} along with such higher values of BLT parameters are not viable

from the LHC data. For the case $R_f = R_\phi$ we found no such enhancement. However in the case of $t \to ch$, irrespective of whether R_f and R_ϕ are equal or not the decay width does not get any enhancement compared to its SM result. Actually the GIM suppression is still at work, even though the KK particles are contributing to the processes, and the decay widths remain, in most of the cases, almost at the same level as that of SM.

5

Summary and Conclusions

The discovery of Higgs boson at LHC has profoundly vindicated the physics of electroweak symmetry breaking in the Standard Model. Still, there are some evidences which surely make an obvious need for going beyond the SM. Among all the variants of new physics, the existence of extra spatial dimensions have many conceptual and phenomenological implications. In this thesis, we consider a particular incarnation of extra dimensions which is termed as the Universal Extra Dimensional (UED) model. We have considered the model in its basic and also in its non-minimal version.

The basic category of the model (UED) is nothing but the higher dimensional version of the SM where all the particles can propagate in the extra dimension (the bulk). Their Kaluza-Klein excitations have simple mass fomulae and the couplings have close resemblance to that of the SM fields. In the non-minimal version some boundary localized terms are incorporated which eventually include the localized-kinetic and Yukawa terms as well as the mass and potential terms of various fields. This thesis mainly includes the procedure and results for obtaining the constraints on the model parameters from Unitarity (in scalar sector) and from some radiative corrections.

Chapter 1 starts with a brief description of the SM. The latter part of this chapter shows the experimental and the theoretical motivations to go beyond the SM. The second Chapter 2

elaborately describes the Universal Extra Dimensional model (UED) along with its minimal and non-minimal version. Chapter 2 also includes the bounds obtained on the extra dimensional parameter in case of UED and mUED. After delving into the detailed description of UED and its some specific phenomenological consequences, Chapters 3 and 4 contain some new work which constitutes the main part of this thesis.

In Chapter 3, we have constrained the parameters of the nmUED model in the scalar as well as in the gauge sectors from a study of Unitarity. In nmUED, the boundary terms are generated due to radiative corrections. So those terms are loop suppressed. The coefficients of boundary terms are the free parameters of the theory which we call the BLT parameters. Though the terms are loop suppressed and should be small, but we do not know the effective range of BLT parameters, or how do they behave in the four-dimensional effective theory. Unitarity analysis in gauge and scalar sectors will give the range of BLT parameters which maintains perturbativity of the model. We have performed this analysis in gauge and scalar sectors exploiting the equivalence theorem to get the upper bound on gauge and scalar BLT parameters (which are same in our analysis). Initially we have done partial wave analysis for some single channel processes and after that we have done coupled channel analysis to further constrain the respective parameters. We have estimated the bounds on the boundary localized parameters for specific KK-modes and also shown that the upper bounds on scalar BLT parameters get more constraint with increasing KK-modes. If we consider KK-modes up to 4-5, the scalar (*scaled*) BLT parameter can be taken as high as 19 which falls down to nearly unity if KK-number is taken up to 25.

Chapter 4 deals with some loop induced processes in the presence of one spatial extra dimension. This chapter is basically comprised of two parts; one is to constrain the nmUED parameter space using the experimental data and the SM estimations of R_b with R_b being the ratio of Z boson decay width to a pair of b quarks normalized to total hadronic decay width obtained by LEP collaboration. For specific choice of BLT parameters the lower bound on the inverse of compactification radius (R^{-1}) can be around 1 TeV. Another part deals with some flavor changing rare decays, $t \to c\gamma$ and $t \to ch$. For some choice of BLT parameters the respective decay widths have some considerable enhancement with respect to the SM value, but the corresponding parameter space is ruled out from LHC and also from LEP data (from R_b value).

It is also worth-noting that in the KK-parity conserving nmUED scenario the lightest KK particle is stable and can play the role of dark matter. But in this regard it is to be kept in mind that for some choice of BLT parameters it may so happen that some specific KK fermion becomes the LKP. Now, a KK fermion LKP is not preferable as it can have electric charge or if it is a KK neutrino it is excluded, as a viable dark matter candidate, by direct detection observations. KK-parity can be broken if there are asymmetric BLTs. Thus taking asymmetric BLT parameters in a way that guarantees enough KK-parity breaking to make the LKP unstable and sufficiently short-lived, the dark matter constraints can be relaxed.

Finally we add a few comments about the possible extensions in the ambit of this model. First, the effect of KK contribution on the CKM matrix elements (important in case of rare decays) can be systematically taken into account in the calculation of various loop induced decays. Secondly, in nmUED by utilizing the freedom of taking different BLT parameters for different types of fields one can, in principle, get a richer model set-up to look into the loop induced decays. Thirdly, and perhaps most importantly, by taking different BLT parameters at two orbifold fixed points for the same kind of field one can break KK-parity. The violation of KK-parity would lead to a host of new KK-parity violating vertices that can significantly modify the decay widths. It is imperative that these effects, which can lead to some interesting observations, be examined in detail.

A

Feynman Rules Relevant for Unitarity Analysis

In the following Feynman rules, 'n' or 'q' stands for KK-mode and '0' for SM.

A.1 (0)-(n)-(n) Coupling (n : even or odd)

$$h^{(0)}h^{(n)}h^{(n)} : -3i\left(\frac{m_h^2}{v}\right),$$
$$h^{(0)}A^{(n)}A^{(n)} : -\frac{i}{v}\left(\frac{m_h^2 M_{\Phi n}^2 + 2M_Z^2 M_{Zn}^2}{M_{Zn}^2}\right),$$
$$h^{(0)}G_Z^{(n)}G_Z^{(n)} : -\frac{i}{v}\left(\frac{m_h^2 M_Z^2}{M_{Zn}^2}\right),$$
$$h^{(0)}A^{(n)}G_Z^{(n)} : -i\frac{M_Z M_{\Phi n}}{v}\left(\frac{m_h^2 - M_{Zn}^2}{M_{Zn}^2}\right),$$
$$\chi^{(0)}h^{(n)}A^{(n)} : -\frac{i}{v}M_{\Phi n}\left(\frac{m_h^2 - M_Z^2}{M_{Zn}}\right),$$
$$\chi^{(0)}h^{(n)}G_Z^{(n)} : -i\frac{M_Z}{v}\left(\frac{m_{hn}^2}{M_{Zn}}\right),$$
$$h^{(0)}H^{(n)+}H^{(n)-} : -\frac{i}{v}\left(\frac{m_h^2 M_{\Phi n}^2 + 2M_W^2 M_{Wn}^2}{M_{Wn}^2}\right),$$

$$h^{(0)}G^{(n)+}G^{(n)-} : -i\frac{m_h^2}{v}\left(\frac{M_W^2}{M_{Wn}^2}\right),$$
$$h^{(0)}G^{(n)\pm}H^{(n)\mp} : \pm\frac{M_{\Phi n}M_W}{v}\left(\frac{m_h^2-M_{Wn}^2}{M_{Wn}^2}\right),$$
$$\phi^{(0)\mp}h^{(n)}G^{(n)\pm} : \pm\frac{M_W}{v}\left(\frac{m_{hn}^2}{M_{Wn}}\right),$$
$$\phi^{(0)\mp}h^{(n)}H^{(n)\pm} : -i\frac{M_{\Phi n}}{v}\left(\frac{m_h^2-M_W^2}{M_{Wn}}\right),$$
$$\phi^{(0)\mp}G_Z^{(n)}H^{(n)\pm} : \mp\frac{M_{\Phi n}M_Z}{v}\cos 2\theta_W\left(\frac{M_{Wn}}{M_{Zn}}\right),$$
$$\phi^{(0)\mp}A^{(n)}G^{(n)\pm} : i\frac{M_{\Phi n}M_W}{v}\left(\frac{M_{Zn}}{M_{Wn}}\right),$$
$$\phi^{(0)\pm}A^{(n)}H^{(n)\mp} : \pm\frac{\left(M_{\Phi n}^2+2M_W^2\right)\left(M_Z^2-M_W^2\right)}{vM_{Zn}M_{Wn}},$$
$$\chi^{(0)}H^{(n)\mp}G^{(n)\pm} : -i\frac{M_{\Phi n}M_W}{v}.$$

A.2 (n)-(n)-(q) Coupling; n : even or odd, q : even

$$h^{(n)}h^{(n)}h^{(q)} : -3i\left(\frac{m_h^2}{v}\right)I^{nnq},$$
$$A^{(n)}A^{(n)}h^{(q)} : -\frac{i}{vM_{Zn}^2}c1_{nnq},$$
$$H^{(n)+}H^{(n)-}h^{(q)} : -\frac{i}{vM_{Wn}^2}c2_{nnq},$$
$$h^{(n)}A^{(n)}G_Z^{(q)} : \frac{iM_Z}{vM_{Zn}M_{Zq}}c3_{nnq},$$
$$h^{(n)}A^{(n)}A^{(q)} : -\frac{i}{vM_{Zn}M_{Zq}}c4_{nnq},$$
$$G_Z^{(n)}G_Z^{(n)}h^{(q)} : -\frac{iM_Z^2}{vM_{Zn}^2}\left(m_h^2I^{nnq}+2M_{\Phi n}M_{\Phi q}I'^{qnn}\right),$$
$$G_Z^{(n)}h^{(n)}G_Z^{(q)} : -\frac{iM_Z^2}{vM_{Zn}M_{Zq}}c5_{nnq},$$
$$h^{(n)}G_Z^{(n)}A^{(q)} : \frac{iM_Z}{vM_{Zn}M_{Zq}}c6_{nnq},$$
$$A^{(n)}G_Z^{(n)}h^{(q)} : -i\frac{M_Z}{vM_{Zn}^2}c7_{nnq},$$
$$H^{(n)\pm}H^{(q)\mp}h^{(n)} : -\frac{i}{vM_{Wn}M_{Wq}}c8_{nnq},$$
$$G^{(n)+}G^{(n)-}h^{(q)} : -i\frac{M_W^2}{vM_{Wn}^2}\left(m_h^2I^{nnq}+2M_{\Phi n}M_{\Phi q}I'^{qnn}\right),$$

$$G^{(n)\mp}G^{(q)\pm}h^{(n)} : -i\frac{M_W^2}{vM_{Wn}M_{Wq}}c5_{nnq},$$
$$H^{(n)\pm}G^{(n)\mp}A^{(q)} : \frac{iM_W}{vM_{Zq}}c9_{nnq},$$
$$H^{(n)\pm}G^{(n)\mp}G_Z^{(q)} : \frac{iM_ZM_W}{vM_{Zq}}c10_{nnq},$$
$$H^{(n)\mp}H^{(q)\pm}G_Z^{(n)} : \mp\frac{M_Z}{vM_{Zn}M_{Wn}M_{Wq}}c11_{nnq},$$
$$G^{(n)\mp}H^{(q)\pm}h^{(n)} : \pm\frac{M_W}{vM_{Wn}M_{Wq}}c12_{nnq},$$
$$H^{(n)\pm}G^{(q)\mp}h^{(n)} : \pm\frac{M_W}{vM_{Wn}M_{Wq}}c13_{nnq},$$
$$H^{(n)\pm}G^{(q)\mp}G_Z^{(n)} : -i\frac{M_WM_ZM_{Wn}}{vM_{Zn}M_{Wq}}c14_{nnq},$$
$$H^{(n)\pm}H^{(q)\mp}A^{(n)} : \pm\frac{1}{vM_{Zn}M_{Wn}M_{Wq}}c15_{nnq},$$
$$H^{(n)\pm}G^{(q)\mp}A^{(n)} : i\frac{M_W}{vM_{Zn}M_{Wn}M_{Wq}}c16_{nnq},$$
$$G^{(n)\pm}H^{(q)\mp}A^{(n)} : i\frac{M_W}{vM_{Zn}M_{Wn}M_{Wq}}c17_{nnq},$$
$$G^{(n)\pm}G^{(q)\mp}A^{(n)} : \pm\frac{M_W^2M_{Zn}}{vM_{Wn}M_{Wq}}c18_{nnq},$$
$$G^{(n)\pm}H^{(n)\mp}h^{(q)} : \pm\frac{M_W}{vM_{Wn}^2}c19_{nnq},$$
$$G^{(n)\pm}H^{(q)\mp}G_Z^{(n)} : -i\frac{(1-\cos 2\theta_W)\,M_WM_ZM_{\Phi n}M_{Wq}}{vM_{Wn}M_{Zn}}I'^{qnn}.$$

A.3 (n)-(n)-(n) Coupling; n : even

$$h^{(n)}h^{(n)}h^{(n)} : -3i\left(\frac{m_h^2}{v}\right)I^{3n},$$
$$A^{(n)}A^{(n)}h^{(n)} : -\frac{i}{vM_{Zn}^2}c1_{3n},$$
$$H^{(n)+}H^{(n)-}h^{(n)} : -\frac{i}{vM_{Wn}^2}c2_{3n},$$
$$h^{(n)}A^{(n)}G_Z^{(n)} : \frac{iM_ZM_{\Phi n}}{vM_{Zn}^2}c3_{3n},$$
$$G_Z^{(n)}G_Z^{(n)}h^{(n)} : -\frac{iM_Z^2}{vM_{Zn}^2}c4_{3n},$$
$$G^{(n)+}G^{(n)-}h^{(n)} : -i\frac{M_W^2}{vM_{Wn}^2}c4_{3n},$$

$$G^{(n)\pm}H^{(n)\mp}A^{(n)} : i\frac{M_W}{vM_{Zn}}c5_{3n},$$
$$G^{(n)\pm}H^{(n)\mp}G_Z^{(n)} : -i\frac{M_W M_Z}{vM_{Zn}}c6_{3n},$$
$$G^{(n)\pm}H^{(n)\mp}h^{(n)} : \mp\frac{M_W M_{\Phi n}}{vM_{Wn}^2}c7_{3n}.$$

The overlap integrals $I^{3n}$and $I^{'3n}$ can be calculated from Eqs. 3.10 and 3.12 or 3.13 respectively.

A.4 Quartic Coupling (n)-(n)-(n)-(n); n : even or odd

$$h^{(n)}h^{(n)}h^{(n)}h^{(n)} : -3i\left(\frac{m_h^2}{v^2}\right)I^n,$$
$$h^{(n)}h^{(n)}A^{(n)}A^{(n)} : -\frac{i}{v^2M_{Zn}^2}\left(m_h^2M_{\Phi n}^2I^n + 2M_Z^4I'^n\right),$$
$$A^{(n)}A^{(n)}A^{(n)}A^{(n)} : -\frac{3i}{v^2M_{Zn}^4}\left(m_h^2M_{\Phi n}^4I^n + 4M_Z^4M_{\Phi n}^2I'^n\right),$$
$$h^{(n)}h^{(n)}G_Z^{(n)}G_Z^{(n)} : -\frac{iM_Z^2}{v^2M_{Zn}^2}\left(m_h^2I^n + 2M_{\Phi n}^2I'^n\right),$$
$$A^{(n)}A^{(n)}G_Z^{(n)}G_Z^{(n)} : -\frac{iM_Z^2}{v^2M_{Zn}^4}q1_n,$$
$$H^{(n)+}H^{(n)-}H^{(n)+}H^{(n)-} : -\frac{2i}{v^2M_{Wn}^4}\left(m_h^2M_{\Phi n}^4I^n + 4M_W^4M_{\Phi n}^2I'^n\right),$$
$$h^{(n)}G_Z^{(n)}H^{(n)\pm}G^{(n)\mp} : -i\frac{M_W M_Z M_{\Phi n}}{v^2M_{Zn}}\left(1-\cos 2\theta_W\right)I'^n,$$
$$h^{(n)}h^{(n)}H^{(n)+}H^{(n)-} : -\frac{i}{v^2M_{Wn}^2}\left(m_h^2M_{\Phi n}^2I^n + 2M_W^4I'^n\right),$$
$$h^{(n)}h^{(n)}G^{(n)+}G^{(n)-} : -\frac{iM_W^2}{v^2M_{Wn}^2}\left(m_h^2I^n + 2M_{\Phi n}^2I'^n\right),$$
$$G_Z^{(n)}G_Z^{(n)}H^{(n)+}H^{(n)-} : -\frac{iM_Z^2}{v^2M_{Wn}^2M_{Zn}^2}q2_n,$$
$$A^{(n)}A^{(n)}H^{(n)+}H^{(n)-} : -\frac{iM_{\Phi n}^2}{v^2M_{Wn}^2M_{Zn}^2}q3_n,$$
$$A^{(n)}A^{(n)}G^{(n)+}G^{(n)-} : -\frac{iM_W^2}{v^2M_{Wn}^2M_{Zn}^2}q4_n,$$
$$A^{(n)}G_Z^{(n)}G^{(n)\pm}H^{(n)\mp} : \pm\frac{M_W M_Z}{v^2M_{Wn}^2M_{Zn}^2}q5_n.$$

In the above expressions all the symbols ci_{nnq}s and qj_ns where $i : 1 \to 19$ and $j : 1 \to 5$, are given explicitly in APPENDIX B. The overlap intergrals $I^{nnq}, I^n, I'^{nnq}, I'^{qnn}, I'^n$ are obtained using the Eqs. 3.10-3.14. The explicit expression of I^n has been given in Eq. 3.27.

B

Explicit Expression of Abbreviations Used in Appendix A

$$c1_{nnq} : m_h^2 M_{\Phi n}^2 I^{nnq} + 2M_Z^2 M_{Zn}^2 I'^{nnq} - 2M_Z^2 M_{\Phi n} M_{\Phi q} I'^{qnn},$$

$$c2_{nnq} : m_h^2 M_{\Phi n}^2 I^{nnq} + 2M_W^2 M_{Wn}^2 I'^{nnq} - 2M_W^2 M_{\Phi n} M_{\Phi q} I'^{qnn},$$

$$c3_{nnq} : -m_h^2 M_{\Phi n} I^{nnq} + M_Z^2 M_{\Phi q} I'^{qnn} + M_Z^2 M_{\Phi n} I'^{nnq},$$

$$c4_{nnq} : m_h^2 M_{\Phi n} M_{\Phi q} I^{nnq} + M_Z^2 (2M_Z^2 + M_{\Phi q}^2) I'^{qnn} - M_Z^2 M_{\Phi n} M_{\Phi q} I'^{nnq},$$

$$c5_{nnq} : m_h^2 I^{nnq} + M_{\Phi n}^2 I'^{nnq} + M_{\Phi n} M_{\Phi q} I'^{qnn},$$

$$c6_{nnq} : -m_h^2 M_{\Phi q} I^{nnq} + M_{\Phi n} (I'^{qnn} (2M_Z^2 + M_{\Phi q}^2) - M_{\Phi n} M_{\Phi q} I'^{nnq}),$$

$$c7_{nnq} : m_h^2 M_{\Phi n} I^{nnq} - M_{Zn}^2 M_{\Phi n} I'^{nnq} - (M_Z^2 - M_{\Phi n}^2) M_{\Phi q} I'^{qnn},$$

$$c8_{nnq} : M_{\Phi n} M_{\Phi q} \left(m_h^2 I^{nnq} - M_W^2 I'^{nnq} \right) + M_W^2 \left(2M_W^2 + M_{\Phi q}^2 \right) I'^{qnn},$$

$$c9_{nnq} : M_{Zq}^2 I'^{qnn} - \left(M_{\Phi n} M_{\Phi q} I'^{nnq} + \cos 2\theta_W M_Z^2 I'^{qnn} \right),$$

$$c10_{nnq} : -M_{\Phi n} I'^{nnq} + \cos 2\theta_W M_{\Phi q} I'^{qnn},$$

$$c11_{nnq} : M_W^2 (M_{\Phi q}^2 - M_{\Phi n}^2) I'^{qnn} + M_{\Phi n} \cos 2\theta_W (I'^{qnn} M_{Wq}^2 M_{\Phi n} - I'^{nnq} M_{Wn}^2 M_{\Phi q}),$$

$$c12_{nnq} : -m_h^2 M_{\Phi q} I^{nnq} + M_{\Phi n} M_{Wq}^2 I'^{qnn} + M_{\Phi n} \left(M_W^2 I'^{qnn} - M_{\Phi n} M_{\Phi q} I'^{nnq} \right),$$

$$c13_{nnq} : -m_h^2 M_{\Phi n} I^{nnq} + M_{\Phi n} (M_W^2 I'^{nnq} - M_{\Phi q} M_{\Phi n} I'^{qnn}) + M_{\Phi q} M_{Wn}^2 I'^{qnn},$$

$$c14_{nnq} : M_{\Phi q} I'^{qnn} - \cos 2\theta_W M_{\Phi n} I'^{nnq},$$

$$c15_{nnq} : M_W^2 M_{Zn}^2 \left(M_{\Phi n} I'^{qnn} - M_{\Phi q} I'^{nnq}\right) + I'^{qnn} M_{\Phi n} M_W^2 \left(M_{\Phi q}^2 - M_{\Phi n}^2\right) - \cos 2\theta_W M_Z^2 \left(I'^{qnn} M_{Wq}^2 M_{\Phi n} - I'^{nnq} M_{Wn}^2 M_{\Phi q}\right),$$

$$c16_{nnq} : M_{\Phi n} M_{\Phi q} (M_Z^2 - M_W^2) I'^{qnn} - M_Z^2 M_{Wn}^2 \cos 2\theta_W I'^{nnq} + M_{Zn}^2 M_W^2 I'^{nnq},$$

$$c17_{nnq} : M_{Zn}^2 \left(M_{\Phi n} M_{\Phi q} I'^{nnq} + M_W^2 I'^{qnn}\right) - M_{Wq}^2 I'^{qnn} \left(M_{\Phi n}^2 + M_Z^2 \cos 2\theta_W\right),$$

$$c18_{nnq} : M_{\Phi n} I'^{nnq} - M_{\Phi q} I'^{qnn},$$

$$c19_{nnq} : m_h^2 M_{\Phi n} I^{nnq} - M_{Wn}^2 M_{\Phi n} I'^{nnq} + (M_{\Phi n}^2 - M_W^2) M_{\Phi q} I'^{qnn},$$

$$c1_{3n} : m_h^2 M_{\Phi n}^2 I^{3n} + 2 M_Z^4 I'^{3n},$$

$$c2_{3n} : m_h^2 M_{\Phi n}^2 I^{3n} + 2 M_W^4 I'^{3n},$$

$$c3_{3n} : -m_h^2 I^{3n} + 2 M_Z^2 I'^{3n},$$

$$c4_{3n} : m_h^2 I^{3n} + 2 M_{\Phi n}^2 I'^{3n},$$

$$c5_{3n} : M_Z^2 I'^{3n} \left(1 - \cos 2\theta_W\right),$$

$$c6_{3n} : M_{\Phi n} I'^{3n} \left(1 - \cos 2\theta_W\right),$$

$$c7_{3n} : -m_h^2 I^{3n} + 2 M_W^2 I'^{3n},$$

$$q1_n : 3 m_h^2 M_{\Phi n}^2 I^n + 2 (M_Z^4 - 4 M_Z^2 M_{\Phi n}^2 + M_{\Phi n}^4) I'^n,$$

$$q2_n : m_h^2 M_{\Phi n}^2 I^n + \left(2 M_W^4 - 4 M_W^2 M_{\Phi n}^2 (1 - \cos 2\theta_W) + M_{\Phi n}^4 (1 + \cos 4\theta_W)\right) I'^n,$$

$$q3_n : m_h^2 M_{\Phi n}^2 I^n + \left(2 M_W^4 + 4 M_W^2 M_Z^2 (1 - \cos 2\theta_W) + M_Z^4 (1 + \cos 4\theta_W)\right) I'^n,$$

$$q4_n : m_h^2 M_{\Phi n}^2 I^n + \left(M_Z^4 (1 + \cos 4\theta_W) - 4 M_Z^2 M_{\Phi n}^2 (1 - \cos 2\theta_W) + 2 M_{\Phi n}^4\right) I'^n,$$

$$q5_n : m_h^2 M_{\Phi n}^2 I^n + \left((1 - \cos 2\theta_W) \left(M_W^2 (M_Z^2 - M_{\Phi n}^2) + M_{\Phi n}^4\right) - M_Z^2 M_{\Phi n}^2 (3 + \cos 4\theta_W)\right) I'^n.$$

C

Expressions for a_0 of Relevant $(n),(n) \to (n),(n)$ Processes in Unitarity Analysis

$$a_0(h^{(n)}h^{(n)} \to h^{(n)}h^{(n)}) = -\frac{3}{16\pi}\frac{m_h^2}{v^2}\left[I^n + 3m_h^2\left\{\frac{1}{s-m_h^2} - \frac{2}{s-4m_{hn}^2}\ln\left(\frac{s-3m_h^2-4M_{\Phi n}^2}{m_h^2}\right)\right\}\right.$$
$$\left. + 3m_h^2\sum_{q=\text{even}}^{\infty} I^{nnq2}\left\{\frac{1}{s-m_{hq}^2} - \frac{2}{s-4m_{hn}^2}\ln\left(\frac{s-3m_h^2-4M_{\Phi n}^2+M_{\Phi q}^2}{m_{hq}^2}\right)\right\}\right], \quad \text{(C.1)}$$

$$a_0(A^{(n)}A^{(n)} \to A^{(n)}A^{(n)}) = -\frac{1}{16\pi}\frac{1}{v^2M_{Zn}^4}\left[3(m_h^2M_{\Phi n}^4I^n + 4M_Z^4M_{\Phi n}^2I'^n) + (m_h^2M_{\Phi n}^2 + 2M_Z^2M_{Zn}^2)^2\right.$$
$$\times\left\{\frac{1}{s-m_h^2} - \frac{2}{s-4M_{Zn}^2}\ln\left(\frac{s-4M_{Zn}^2+m_h^2}{m_h^2}\right)\right\} + \sum_{q=\text{even}}^{\infty} c1_{nnq}^2\left\{\frac{1}{s-m_{hq}^2}\right.$$
$$\left.\left. -\frac{2}{s-4M_{Zn}^2}\ln\left(\frac{s-4M_{Zn}^2+m_{hq}^2}{m_{hq}^2}\right)\right\}\right], \quad \text{(C.2)}$$

$$a_0(H^{(n)+}H^{(n)-} \to H^{(n)+}H^{(n)-}) = -\frac{1}{16\pi}\frac{1}{v^2M_{Wn}^4}\left[2(m_h^2M_{\Phi n}^4I^n + 4M_W^4M_{\Phi n}^2I'^n)\right.$$
$$+ (m_h^2M_{\Phi n}^2 + 2M_W^2M_{Wn}^2)^2\left\{\frac{1}{s-m_h^2} - \frac{2}{s-4M_{Wn}^2}\ln\left(\frac{s-4M_{Wn}^2+m_h^2}{m_h^2}\right)\right\}$$
$$\left. + \sum_{q=\text{even}}^{\infty} c2_{nnq}^2\left\{\frac{1}{s-m_{hq}^2} - \frac{2}{s-4M_{Wn}^2}\ln\left(\frac{s-4M_{Wn}^2+m_{hq}^2}{m_{hq}^2}\right)\right\}\right], \quad \text{(C.3)}$$

$$a_0(G_Z^{(n)}A^{(n)} \to G_Z^{(n)}A^{(n)}) = -\frac{1}{16\pi}\frac{M_Z^2}{v^2M_{Zn}^4}\left[q1_n + M_{\Phi n}^2\left(m_h^2 - M_{Zn}^2\right)^2\left\{\frac{1}{s-m_h^2}\right.\right.$$

$$-\frac{1}{\left(s-4M_{Zn}^2\right)}\ln\left(\frac{s-4M_{Zn}^2+m_h^2}{m_h^2}\right)\Bigg\}-\frac{m_h^2(m_h^2M_{\Phi n}^2+2M_Z^2M_{Zn}^2)}{\left(s-4M_{Zn}^2\right)}$$
$$\times\ln\left(\frac{s-4M_{Zn}^2+m_h^2}{m_h^2}\right)+\sum_{q=\text{even}}^{\infty}c7_{nnq}^2\left\{\frac{1}{s-m_{hq}^2}-\frac{1}{\left(s-4M_{Zn}^2\right)}\right.$$
$$\left.\times\ln\left(\frac{s-4M_{Zn}^2+m_{hq}^2}{m_{hq}^2}\right)\right\}-\sum_{q=\text{even}}^{\infty}\left(m_h^2I^{nnq}+2M_{\Phi n}M_{\Phi q}I'^{qnn}\right)$$
$$\times\frac{c1_{nnq}}{\left(s-4M_{Zn}^2\right)}\ln\left(\frac{s-4M_{Zn}^2+m_{hq}^2}{m_{hq}^2}\right)\Bigg], \tag{C.4}$$

$$a_0(h^{(n)}A^{(n)}\to h^{(n)}A^{(n)})=-\frac{1}{16\pi}\frac{1}{v^2M_{Zn}^2}\Big[\left(m_h^2M_{\Phi n}^2I^n+2M_Z^4I'^n\right)+M_{\Phi n}^2\left(m_h^2-M_Z^2\right)^2$$
$$\times\left\{\frac{1}{s-M_Z^2}-\frac{s}{(s-m_{hn}^2-M_{Zn}^2)^2}\ln X2_n\right\}-3m_h^2s\frac{\left(m_h^2M_{\Phi n}^2+2M_Z^2M_{Zn}^2\right)}{(s-m_{hn}^2-M_{Zn}^2)^2}\ln X3n$$
$$+\sum_{q=\text{even}}^{\infty}\frac{1}{M_{Zq}^2}\{M_Z^2c3_{nnq}^2+c4_{nnq}^2\}\left\{\frac{1}{s-M_{Zq}^2}-\frac{s}{(s-m_{hn}^2-M_{Zn}^2)^2}\ln Y2_{nq}\right\}$$
$$-\sum_{q=\text{even}}^{\infty}\frac{3m_h^2I^{nnq}c1_{nnq}s}{(s-m_{hn}^2-M_{Zn}^2)^2}\ln Y3nq\Big], \tag{C.5}$$

$$a_0(h^{(n)}G_Z^{(n)}\to h^{(n)}G_Z^{(n)})=-\frac{1}{16\pi}\frac{M_Z^2}{v^2M_{Zn}^2}\Big[\left(m_h^2I^n+2M_{\Phi n}^2I'^n\right)+m_{hn}^4\left\{\frac{1}{s-M_Z^2}\right.$$
$$\left.-\frac{s}{(s-m_{hn}^2-M_{Zn}^2)^2}\ln X2_n\right\}-\frac{3m_h^4s}{(s-m_{hn}^2-M_{Zn}^2)^2}\ln X3_n$$
$$+\sum_{q=\text{even}}^{\infty}\frac{1}{M_{Zq}^2}\{M_Z^2c5_{nnq}^2+c6_{nnq}^2\}\left\{\frac{1}{s-M_{Zq}^2}-\frac{s}{(s-m_{hn}^2-M_{Zn}^2)^2}\ln Y2_{nq}\right\}$$
$$-\sum_{q=\text{even}}^{\infty}\left(m_h^2I^{nnq}+2M_{\Phi n}M_{\Phi q}I'^{qnn}\right)\frac{3m_h^2I^{nnq}s}{(s-m_{hn}^2-M_{Zn}^2)^2}\ln Y3_{nq}\Big], \tag{C.6}$$

$$a_0(h^{(n)}G_Z^{(n)}\to H^{(n)\pm}G^{(n)\mp})=-\frac{1}{16\pi}\frac{M_ZM_W}{v^2M_{Zn}}\Big[M_{\Phi n}(1-\cos2\theta_W)I'^n+\frac{M_{\Phi n}m_h^2}{(s-M_Z^2)}$$
$$-\frac{2M_{\Phi n}m_{hn}^2\cos2\theta_W\sqrt{s}}{\sqrt{s-4M_{Wn}^2}(s-m_{hn}^2-M_{Zn}^2)}\ln X4_n+\sum_{q=\text{even}}^{\infty}\frac{(-M_Z^2c10_{nnq}c5_{nnq}+c9_{nnq}c6_{nnq})}{M_{Zq}^2(s-M_{Zq}^2)}$$
$$+\sum_{q=\text{even}}^{\infty}\frac{2\sqrt{s}}{\sqrt{s-4M_{Wn}^2}(s-m_{hn}^2-M_{Zn}^2)}$$
$$\times\left\{\frac{M_{\Phi n}M_{\Phi q}}{M_{Wn}^2M_{Wq}}I'^{qnn}c8_{nnq}-\frac{c11_{nnq}c12_{nnq}}{M_{Wn}^2M_{Wq}^2}-\frac{M_W^2}{M_{Wq}^2}c5_{nnq}c10_{nnq}\right\}\ln Y4_{nq}\Big], \tag{C.7}$$

$$a_0(H^{(n)\pm}h^{(n)}\to H^{(n)\pm}h^{(n)})=-\frac{1}{16\pi}\frac{1}{v^2M_{Wn}^2}\Big[\left(m_h^2M_{\Phi n}^2I^n+2M_W^4I'^n\right)+M_{\Phi n}^2\left(m_h^2-M_W^2\right)^2$$
$$\times\left\{\frac{1}{s-M_W^2}-\frac{s}{(s-m_{hn}^2-M_{Wn}^2)^2}\ln X7_n\right\}-3m_h^2\frac{\left(m_h^2M_{\Phi n}^2+2M_W^2M_{Wn}^2\right)s}{(s-m_{hn}^2-M_{Wn}^2)^2}\ln X8_n$$
$$+\sum_{q=\text{even}}^{\infty}\frac{\left(M_W^2c13_{nnq}^2+c8_{nnq}^2\right)}{M_{Wq}^2}\left\{\frac{1}{s-M_{Wq}^2}-\frac{s}{(s-m_{hn}^2-M_{Wn}^2)^2}\ln Y7_{nq}\right\}$$

$$- \sum_{q=\text{even}}^{\infty} 3m_h^2 I^{nnq} \frac{c2_{nnq} s}{(s - m_{hn}^2 - M_{Wn}^2)^2} \ln Y8_{nq} \Bigg], \tag{C.8}$$

$$a_0(G^{(n)\pm} h^{(n)} \to G^{(n)\pm} h^{(n)}) = -\frac{1}{16\pi} \frac{M_W^2}{v^2 M_{Wn}^2} \Big[\left(m_h^2 I^n + 2M_{\Phi n}^2 I'^n\right) + M_{\Phi n}^2 \left(m_h^2 - M_W^2\right)^2$$
$$\times \left\{ \frac{1}{s - M_W^2} - \frac{s}{(s - m_{hn}^2 - M_{Wn}^2)^2} \ln X7_n \right\} - 3m_h^4 \frac{s}{(s - m_{hn}^2 - M_{Wn}^2)^2} \ln X8_n$$
$$+ \sum_{q=\text{even}}^{\infty} \frac{\left(M_W^2 c5_{nnq}^2 + c12_{nnq}^2\right)}{M_{Wq}^2} \left\{ \frac{1}{s - M_{Wq}^2} - \frac{s}{(s - m_{hn}^2 - M_{Wn}^2)^2} \ln Y7_{nq} \right\}$$
$$- \sum_{q=\text{even}}^{\infty} \left(m_h^2 I^{nnq} + 2M_{\Phi n} M_{\Phi q} I'^{qnn}\right) \frac{3m_h^2 I^{nnq} s}{(s - m_{hn}^2 - M_{Wn}^2)^2} \ln Y8_{nq} \Bigg], \tag{C.9}$$

$$a_0(H^{(n)\pm} G_Z^{(n)} \to H^{(n)\pm} G_Z^{(n)}) = -\frac{1}{16\pi} \frac{M_Z^2}{v^2 M_{Zn}^2 M_{Wn}^2} \Big[q2_n + (M_{\Phi n}^2 M_{Wn}^4 \cos^2 2\theta_W) \left\{ \frac{1}{s - M_W^2} \right.$$
$$\left. - \frac{s}{(s - M_{Zn}^2 - M_{Wn}^2)^2} \ln X9_n \right\} - m_h^2 \left(m_h^2 M_{\Phi n}^2 + 2M_W^2 M_{Wn}^2\right)$$
$$\times \frac{s}{(s - M_{Zn}^2 - M_{Wn}^2)^2} \ln X10_n + \sum_{q=\text{even}}^{\infty} \frac{1}{M_{Wq}^2} \left(M_W^2 M_{Wn}^4 c14_{nnq}^2 + c11_{nnq}^2\right)$$
$$\times \left\{ \frac{1}{s - M_{Wq}^2} - \frac{s}{(s - M_{Zn}^2 - M_{Wn}^2)^2} \ln Y9_{nq} \right\}$$
$$- \sum_{q=\text{even}}^{\infty} \left(m_h^2 I^{nnq} + 2M_{\Phi n} M_{\Phi q} I'^{qnn}\right) \frac{s\ c2_{nnq}}{(s - M_{Zn}^2 - M_{Wn}^2)^2} \ln Y10_{nq} \Bigg], \tag{C.10}$$

$$a_0(H^{(n)\pm} A^{(n)} \to H^{(n)\pm} A^{(n)}) = -\frac{1}{16\pi} \frac{M_Z^2}{v^2 M_{Zn}^2 M_{Wn}^2} \left[M_{\Phi n}^2 q3_n + (M_{\Phi n}^2 + 2M_W^2)(M_Z^2 - M_W^2)^2 \right.$$
$$\times \left\{ \frac{1}{s - M_W^2} - \frac{s}{(s - M_{Zn}^2 - M_{Wn}^2)^2} \ln X9_n \right\}$$
$$- \left(m_h^2 M_{\Phi n}^2 + 2M_Z^2 M_{Zn}^2\right) \left(m_h^2 M_{\Phi n}^2 + 2M_W^2 M_{Wn}^2\right) \frac{s}{(s - M_{Zn}^2 - M_{Wn}^2)^2} \ln X10_n$$
$$+ \sum_{q=\text{even}}^{\infty} \frac{1}{M_{Wq}^2} \left(M_W^2 c16_{nnq}^2 + c15_{nnq}^2\right) \left\{ \frac{1}{s - M_{Wq}^2} - \frac{s}{(s - M_{Zn}^2 - M_{Wn}^2)^2} \ln Y9_{nq} \right\}$$
$$\left. - \sum_{q=\text{even}}^{\infty} c1_{nnq} c2_{nnq} \frac{s}{(s - M_{Zn}^2 - M_{Wn}^2)^2} \ln Y10_{nq} \right], \tag{C.11}$$

$$a_0(G^{(n)\pm} A^{(n)} \to G^{(n)\pm} A^{(n)}) = -\frac{1}{16\pi} \frac{M_W^2}{v^2 M_{Zn}^2 M_{Wn}^2} \left[q4_n + (M_{\Phi n}^2 M_{Zn}^4) \left\{ \frac{1}{s - M_W^2} \right. \right.$$
$$\left. - \frac{s\ \ln X9_n}{(s - M_{Zn}^2 - M_{Wn}^2)^2} \right\} - m_h^2 \left(m_h^2 M_{\Phi n}^2 + 2M_Z^2 M_{Zn}^2\right) \frac{s\ \ln X10_n}{(s - M_{Zn}^2 - M_{Wn}^2)^2}$$
$$+ \sum_{q=\text{even}}^{\infty} \frac{1}{M_{Wq}^2} \left(M_W^2 M_{Zn}^4 c18_{nnq}^2 + c17_{nnq}^2\right) \left\{ \frac{1}{s - M_{Wq}^2} - \frac{s\ \ln Y9_{nq}}{(s - M_{Zn}^2 - M_{Wn}^2)^2} \right\}$$
$$\left. - \sum_{q=\text{even}}^{\infty} \left(m_h^2 I^{nnq} + 2M_{\Phi n} M_{\Phi q} I'^{qnn}\right) c1_{nnq} \frac{s}{(s - M_{Zn}^2 - M_{Wn}^2)^2} \ln Y10_{nq} \right], \tag{C.12}$$

$$a_0(A^{(n)} G_Z^{(n)} \to G^{(n)\pm} H^{(n)\mp}) = -\frac{1}{16\pi} \frac{M_W M_Z}{v^2 M_{Zn}^2 M_{Wn}^2} \left[q5 + (m_h^2 - M_{Zn}^2)(m_h^2 - M_{Wn}) \frac{M_{\Phi n}^2}{s - m_h^2} \right.$$

$$
\begin{aligned}
&- \frac{2M_{\Phi n}^2 \cos 2\theta_W M_{Zn}^2 M_{Wn}^2}{\sqrt{\left(s-4M_{Zn}^2\right)\left(s-4M_{Wn}^2\right)}} \ln X6_n + \sum_{q=\text{even}}^{\infty} \frac{c7_{nnq} c19_{nnq}}{s-m_{hq}^2} \\
&+ \sum_{q=\text{even}}^{\infty} \left(M_W^2 M_{Wn}^2 M_{Zn}^2 c14_{nnq} c18_{nnq} + c17_{nnq} c11_{nnq} - M_{Wq}^2 (1-\cos 2\theta_W) \right. \\
&\left. \times M_{\Phi n} I'^{qnn} c15_{nnq} \right) \frac{2}{M_{Wq}^2 \sqrt{\left(s-4M_{Zn}^2\right)\left(s-4M_{Wn}^2\right)}} \ln Y6_{nq} \Bigg] . \qquad \text{(C.13)}
\end{aligned}
$$

The explicit expressions of the symbols of Xk_ns and Yk_{nq}s having $k : 1 \to 10$ are given in APPENDIX D.

D

Explicit Expression of Abbreviations Used in Appendix C

$$X1_n : \frac{s - 2m_h^2 - 4M_{\Phi n}^2 - \sqrt{\left(s - 4m_{hn}^2\right)\left(s - 4M_{Zn}^2\right)}}{2\sqrt{m_h^4 + M_Z^2\left(s - 4m_{hn}^2\right)}},$$

$$Y1_{nq} : \frac{s - 2m_h^2 - 4M_{\Phi n}^2 + 2M_{\Phi q}^2 - \sqrt{\left(s - 4m_{hn}^2\right)\left(s - 4M_{Zn}^2\right)}}{2\sqrt{\left(m_h^2 - M_{\Phi q}^2\right)^2 + M_{\Phi q}^2\left(s - 4M_{\Phi n}^2\right) + M_Z^2\left(s - 4m_{hn}^2\right)}},$$

$$X2_n : \frac{s\{2(m_{hn}^2 + M_{Zn}^2) - s\} - 2(sM_Z^2 + m_{hn}^2 M_{Zn}^2)}{m_{hn}^4 + M_{Zn}^4 - sM_Z^2},$$

$$Y2_{nq} : \frac{s\{2(m_{hn}^2 + M_{Zn}^2) - s\} - 2(sM_{Zq}^2 + m_{hn}^2 M_{Zn}^2)}{m_{hn}^4 + M_{Zn}^4 - sM_{Zq}^2},$$

$$X3_n : 1 + \frac{(s - m_{hn}^2 - M_{Zn}^2)^2}{sm_h^2},$$

$$Y3_{nq} : 1 + \frac{(s - m_{hn}^2 - M_{Zn}^2)^2}{sm_{hq}^2},$$

$$X4_n : \frac{\sqrt{s}\left(s - 2M_{\Phi n}^2 - m_{hn}^2 - M_{Zn}^2\right) - \sqrt{s - 4M_{Wn}^2}(s - m_{hn}^2 - M_{Zn}^2)}{2\sqrt{(s - m_{hn}^2 - M_{Zn}^2)\{sM_W^2 - M_{Wn}^2(m_{hn}^2 + M_{Zn}^2)\} + sM_{\Phi n}^4}},$$

$$Y4_{nq}: \frac{\sqrt{s}\left(s+2M_{\Phi q}^2-2M_{\Phi n}^2-m_{hn}^2-M_{Zn}^2\right)-\sqrt{s-4M_{Wn}^2}(s-m_{hn}^2-M_{Zn}^2)}{2\sqrt{(s-m_{hn}^2-M_{Zn}^2)\{sM_{Wq}^2-M_{Wn}^2(m_{hn}^2+M_{Zn}^2)\}+s(M_{\Phi q}^2-M_{\Phi n}^2)^2}},$$

$$X5_n: \frac{s-2m_h^2-4M_{\Phi n}^2-\sqrt{\left(s-4m_{hn}^2\right)\left(s-4M_{Wn}^2\right)}}{2\sqrt{m_h^4+M_W^2\left(s-4m_{hn}^2\right)}},$$

$$Y5_{nq}: \frac{s-2m_h^2-4M_{\Phi n}^2+2M_{\Phi q}^2-\sqrt{\left(s-4m_{hn}^2\right)\left(s-4M_{Wn}^2\right)}}{2\sqrt{\left(m_h^2-M_{\Phi q}^2\right)^2+M_{\Phi q}^2\left(s-4M_{\Phi n}^2\right)+M_W^2\left(s-4m_{hn}^2\right)}},$$

$$X6_n: \frac{s-2M_Z^2-4M_{\Phi n}^2-\sqrt{\left(s-4M_{Zn}^2\right)\left(s-4M_{Wn}^2\right)}}{2\sqrt{M_Z^4+M_W^2\left(s-4M_{Zn}^2\right)}},$$

$$Y6_{nq}: \frac{s-2M_Z^2-4M_{\Phi n}^2+2M_{\Phi q}^2-\sqrt{\left(s-4M_{Zn}^2\right)\left(s-4M_{Wn}^2\right)}}{2\sqrt{\left(M_Z^2-M_{\Phi q}^2\right)^2+M_{\Phi q}^2\left(s-4M_{\Phi n}^2\right)+M_W^2\left(s-4M_{Zn}^2\right)}},$$

$$X7_n: \frac{s\{2(m_{hn}^2+M_{Wn}^2)-s\}-2(sM_W^2+m_{hn}^2M_{Wn}^2)}{m_{hn}^4+M_{Wn}^4-sM_W^2},$$

$$Y7_{nq}: \frac{s\{2(m_{hn}^2+M_{Wn}^2)-s\}-2(sM_{Wq}^2+m_{hn}^2M_{Wn}^2)}{m_{hn}^4+M_{Wn}^4-sM_{Wq}^2},$$

$$X8_n: 1+\frac{(s-m_{hn}^2-M_{Wn}^2)^2}{sm_h^2},$$

$$Y8_{nq}: 1+\frac{(s-m_{hn}^2-M_{Wn}^2)^2}{sm_{hq}^2},$$

$$X9_n: \frac{s\{2(M_{Zn}^2+M_{Wn}^2)-s\}-2(sM_W^2+M_{Zn}^2M_{Wn}^2)}{M_{Zn}^4+M_{Wn}^4-sM_W^2},$$

$$Y9_{nq}: \frac{s\{2(M_{Zn}^2+M_{Wn}^2)-s\}-2(sM_{Wq}^2+M_{Zn}^2M_{Wn}^2)}{M_{Zn}^4+M_{Wn}^4-sM_{Wq}^2},$$

$$X10_n: 1+\frac{(s-M_{Zn}^2-M_{Wn}^2)^2}{sm_h^2},$$

$$Y10_{nq}: 1+\frac{(s-M_{Zn}^2-M_{Wn}^2)^2}{sm_{hq}^2}.$$

E

General Form of Matrix Elements in Coupled Channel Analysis

Here, we give the general form of the matrix elements explicitly where, the sum over KK-modes, the symmetry factors as well as the factor $1/\sqrt{2}$ due to the presence of dibosonic states have been taken into account. While writing the elements, the ordering of neutral fields are important; *e.g.* the combinations $h^{(n)}h^{(n)}A^{(n)}A^{(n)}$ will differ from $h^{(n)}A^{(n)}h^{(n)}A^{(n)}$ by a factor of $1/2$ as $h^{(n)}h^{(n)}$ or $A^{(n)}A^{(n)}$ altogether implies the presence of dibosonic state. Another noteworthy point is that the sum of the KK-numbers should be even, otherwise the elements will be zero ensuring the conservation of KK-parity.

E.1 Elements of matrix $\mathcal{A}_{15\times15}$

$$h^{(0)}h^{(0)}h^{(0)}h^{(0)} : -\frac{3}{2}\left(\frac{m_h^2}{v^2}\right),$$
$$h^{(0)}h^{(0)}h^{(n)}h^{(n)} : -\frac{3}{2}\left(\frac{m_h^2}{v^2}\right),$$
$$h^{(0)}h^{(n)}h^{(0)}h^{(n)} : -3\left(\frac{m_h^2}{v^2}\right),$$

$$h^{(n)}h^{(n)}h^{(0)}h^{(m)} : -\frac{3}{\sqrt{2}}\left(\frac{m_h^2}{v^2}\right) I^{nnm},$$
$$h^{(n)}h^{(0)}h^{(n)}h^{(m)} : -3\left(\frac{m_h^2}{v^2}\right) I^{nnm},$$
$$h^{(0)}h^{(n)}h^{(m)}h^{(p)} : -3\left(\frac{m_h^2}{v^2}\right) I^{nmp},$$
$$h^{(0)}h^{(n)}h^{(n)}h^{(n)} : -\frac{3}{\sqrt{2}}\left(\frac{m_h^2}{v^2}\right) I^{3n},$$
$$h^{(n)}h^{(n)}h^{(n)}h^{(n)} : -\frac{3}{2}\left(\frac{m_h^2}{v^2}\right) I^{n},$$
$$h^{(n)}h^{(n)}h^{(m)}h^{(m)} : -\frac{3}{2}\left(\frac{m_h^2}{v^2}\right) I^{nnmm},$$
$$h^{(n)}h^{(m)}h^{(n)}h^{(m)} : -3\left(\frac{m_h^2}{v^2}\right) I^{nnmm},$$
$$h^{(n)}h^{(n)}h^{(n)}h^{(m)} : -\frac{3}{\sqrt{2}}\left(\frac{m_h^2}{v^2}\right) I^{nnnm},$$
$$h^{(n)}h^{(n)}h^{(m)}h^{(p)} : -\frac{3}{\sqrt{2}}\left(\frac{m_h^2}{v^2}\right) I^{nnmp},$$
$$h^{(n)}h^{(m)}h^{(n)}h^{(p)} : -3\left(\frac{m_h^2}{v^2}\right) I^{nnmp},$$
$$h^{(n)}h^{(m)}h^{(p)}h^{(q)} : -3\left(\frac{m_h^2}{v^2}\right) I^{nmpq}.$$

E.2 Elements of matrix $\mathcal{D}_{10\times 10}$

$$A^{(n)}A^{(n)}A^{(n)}A^{(n)} : -\frac{3}{2v^2M_{Zn}^4}\left(m_h^2M_{\Phi n}^4I^n + 4M_Z^4M_{\Phi n}^2I'^n\right),$$
$$A^{(n)}A^{(n)}A^{(m)}A^{(m)} : -\frac{1}{2v^2M_{Zn}^2M_{Zm}^2}\left\{3m_h^2M_{\Phi n}^2M_{\Phi m}^2I^{nnmm} + 2M_Z^4\left(M_{\Phi m}^2I_1^{nnmm} + M_{\Phi n}^2I_1^{mmnn} + 4M_{\Phi n}M_{\Phi m}I_1^{nmnm}\right)\right\},$$
$$A^{(n)}A^{(m)}A^{(n)}A^{(m)} : -\frac{1}{v^2M_{Zn}^2M_{Zm}^2}\left\{3m_h^2M_{\Phi n}^2M_{\Phi m}^2I^{nnmm} + 2M_Z^4\left(M_{\Phi m}^2I_1^{nnmm} + M_{\Phi n}^2I_1^{mmnn} + 4M_{\Phi n}M_{\Phi m}I_1^{nmnm}\right)\right\},$$
$$A^{(n)}A^{(n)}A^{(n)}A^{(m)} : -\frac{3\left\{m_h^2M_{\Phi n}^3M_{\Phi m}I^{nnnm} + 2M_Z^4\left(M_{\Phi n}M_{\Phi m}I_1^{nnnm} + M_{\Phi n}^2I_1^{mnnn}\right)\right\}}{\sqrt{2}v^2M_{Zn}^3M_{Zm}},$$
$$A^{(n)}A^{(n)}A^{(m)}A^{(p)} : -\frac{1}{\sqrt{2}v^2M_{Zn}^2M_{Zm}M_{Zp}}\left\{3m_h^2M_{\Phi n}^2M_{\Phi m}M_{\Phi p}I^{nnmp} + 2M_Z^4\left(M_{\Phi n}^2I_1^{mpnn} + M_{\Phi m}M_{\Phi p}I_1^{nnmp} + 2M_{\Phi n}\left(M_{\Phi m}I_1^{npmn} + M_{\Phi p}I_1^{mnnp}\right)\right)\right\},$$
$$A^{(n)}A^{(m)}A^{(n)}A^{(p)} : -\frac{1}{v^2M_{Zn}^2M_{Zm}M_{Zp}}\left\{3m_h^2M_{\Phi n}^2M_{\Phi m}M_{\Phi p}I^{nnmp} + 2M_Z^4\left(M_{\Phi n}^2I_1^{mpnn} + M_{\Phi m}M_{\Phi p}I_1^{nnmp} + 2M_{\Phi n}\left(M_{\Phi m}I_1^{npmn} + M_{\Phi p}I_1^{mnnp}\right)\right)\right\},$$

$$A^{(n)}A^{(m)}A^{(p)}A^{(q)} : -\frac{1}{v^2 M_{Zn}M_{Zm}M_{Zp}M_{Zq}}\left[3m_h^2 M_{\Phi n}M_{\Phi m}M_{\Phi p}M_{\Phi q}I^{nmpq}\right.$$
$$+2M_Z^4\left\{M_{\Phi q}\left(M_{\Phi p}I_1^{nmpq}+M_{\Phi m}I_1^{npmq}\right)+M_{\Phi n}\left(M_{\Phi p}I_1^{mqnp}+M_{\Phi q}I_1^{mpnq}\right)\right.$$
$$\left.\left.+M_{\Phi m}\left(M_{\Phi p}I_1^{nqmp}+M_{\Phi n}I_1^{pqnm}\right)\right\}\right].$$

E.3 Elements of matrix $\mathcal{F}_{25\times 25}$

$$\phi^{(0)+}\phi^{(0)-}\phi^{(0)+}\phi^{(0)-} : -2\frac{m_h^2}{v^2},$$
$$\phi^{(0)+}H^{(n)-}\phi^{(0)+}H^{(n)-}/\phi^{(0)-}H^{(n)+}\phi^{(0)-}H^{(n)+} : -2\frac{m_h^2 M_{\Phi n}^2}{v^2 M_{Wn}^2},$$
$$\phi^{(0)+}\phi^{(0)-}H^{(n)+}H^{(n)-} : -\frac{2}{v^2 M_{Wn}^2}\left(m_h^2 M_{\Phi n}^2+M_W^4\right),$$
$$\begin{cases}\phi^{(0)+}H^{(n)+}H^{(n)-}H^{(m)-}\\ \phi^{(0)-}H^{(n)+}H^{(n)-}H^{(m)+}\end{cases} : -\frac{2\left\{m_h^2 M_{\Phi n}^2 M_{\Phi m}I^{nnm}+M_W^4\left(M_{\Phi m}I_1^{nnm}+M_{\Phi n}I_1^{mnn}\right)\right\}}{v^2 M_{Wn}^2 M_{Wm}},$$
$$\begin{cases}\phi^{(0)+}H^{(n)+}H^{(n)-}H^{(n)-}\\ \phi^{(0)-}H^{(n)+}H^{(n)-}H^{(n)+}\end{cases} : -\frac{2}{v^2 M_{Wn}^3}\left(m_h^2 M_{\Phi n}^3 I^{3n}+2M_W^4 M_{\Phi n}I'^{3n}\right),$$
$$\begin{cases}\phi^{(0)+}H^{(n)-}H^{(n)-}H^{(m)+}\\ \phi^{(0)-}H^{(n)+}H^{(n)+}H^{(m)-}\end{cases} : -\frac{2\left(m_h^2 M_{\Phi n}^2 M_{\Phi m}I^{nnm}+2M_W^4 M_{\Phi n}I_1^{mnn}\right)}{v^2 M_{Wn}^2 M_{Wm}},$$
$$\begin{cases}\phi^{(0)+}H^{(n)-}H^{(p)+}H^{(q)-}\\ \phi^{(0)-}H^{(n)+}H^{(p)-}H^{(q)+}\end{cases} : -\frac{2\left\{m_h^2 M_{\Phi n}M_{\Phi m}M_{\Phi p}I^{nmp}+M_W^4\left(M_{\Phi n}I_1^{mpn}+M_{\Phi p}I_1^{nmp}\right)\right\}}{v^2 M_{Wn}M_{Wm}M_{Wp}},$$
$$H^{(n)+}H^{(n)-}H^{(n)+}H^{(n)-} : -\frac{2}{v^2 M_{Wn}^4}\left(m_h^2 M_{\Phi n}^4 I^n+4M_W^4 M_{\Phi n}^2 I'^n\right),$$
$$H^{(n)+}H^{(n)-}H^{(m)+}H^{(m)-} : -\frac{2}{v^2 M_{Wn}^2 M_{Wm}^2}$$
$$\times\left\{m_h^2 M_{\Phi n}^2 M_{\Phi m}^2 I^{nnmm}+M_W^4\left(M_{\Phi m}^2 I_1^{nnmm}+M_{\Phi n}^2 I_1^{mmnn}+2M_{\Phi n}M_{\Phi m}I_1^{nmnm}\right)\right\},$$
$$H^{(n)+}H^{(m)-}H^{(n)+}H^{(m)-} : -\frac{2}{v^2 M_{Wn}^2 M_{Wm}^2}\left(m_h^2 M_{\Phi n}^2 M_{\Phi m}^2 I^{nnmm}+4M_W^4 M_{\Phi n}M_{\Phi m}I_1^{nmnm}\right),$$
$$\begin{cases}H^{(n)+}H^{(m)-}H^{(n)+}H^{(p)-}\\ H^{(n)-}H^{(m)+}H^{(n)-}H^{(p)+}\end{cases} : -\frac{2\left\{m_h^2 M_{\Phi n}^2 M_{\Phi m}M_{\Phi p}I^{nnmp}+2M_W^4 M_{\Phi n}\left(M_{\Phi m}I_1^{npnm}+M_{\Phi p}I_1^{nmnp}\right)\right\}}{v^2 M_{Wn}^2 M_{Wm}M_{Wp}},$$
$$\begin{cases}H^{(n)+}H^{(n)-}H^{(n)+}H^{(m)-}\\ H^{(n)-}H^{(n)+}H^{(n)-}H^{(m)+}\end{cases} : -\frac{2\left\{m_h^2 M_{\Phi n}^3 M_{\Phi m}I^{nnnm}+2M_W^4 M_{\Phi n}\left(M_{\Phi m}I_1^{nnnm}+M_{\Phi n}I_1^{mnnn}\right)\right\}}{v^2 M_{Wn}^3 M_{Wm}},$$
$$\begin{cases}H^{(n)+}H^{(n)-}H^{(m)+}H^{(p)-}\\ H^{(n)+}H^{(n)-}H^{(m)-}H^{(p)+}\end{cases} : -\frac{2}{v^2 M_{Wn}^2 M_{Wm}M_{Wp}}\left[m_h^2 M_{\Phi n}^2 M_{\Phi m}M_{\Phi p}I^{nnmp}\right.$$
$$\left.+M_W^4\left\{M_{\Phi n}\left(M_{\Phi m}I_1^{npnm}+M_{\Phi p}I_1^{nmnp}\right)+M_{\Phi n}^2 I_1^{mpnn}+M_{\Phi m}M_{\Phi p}I_1^{nnmp}\right\}\right],$$

$$H^{(n)+}H^{(m)-}H^{(p)+}H^{(q)-} : -\frac{2}{v^2 M_{Wn}M_{Wm}M_{Wp}M_{Wq}}\left[m_h^2 M_{\Phi n}M_{\Phi m}M_{\Phi p}M_{\Phi q}I^{nmpq}\right.$$
$$\left. + M_W^4\left\{M_{\Phi n}\left(M_{\Phi m}I_1^{pqnm} + M_{\Phi q}I_1^{mpnq}\right) + M_{\Phi p}\left(M_{\Phi m}I_1^{nqmp} + M_{\Phi q}I_1^{nmpq}\right)\right\}\right].$$

E.4 Elements of matrix $\mathcal{B}_{15\times 10}$

$$h^{(0)}h^{(0)}A^{(n)}A^{(n)} : -\frac{1}{2}\frac{\left(m_h^2 M_{\Phi n}^2 + 2M_Z^4\right)}{v^2 M_{Zn}^2},$$
$$h^{(0)}h^{(n)}A^{(m)}A^{(m)} : -\frac{1}{\sqrt{2}}\frac{\left(m_h^2 M_{\Phi m}^2 I^{nmm} + 2M_Z^4 I_1^{mmn}\right)}{v^2 M_{Zm}^2},$$
$$h^{(0)}h^{(n)}A^{(m)}A^{(p)} : -\frac{\left(m_h^2 M_{\Phi m}M_{\Phi p}I^{nmp} + 2M_Z^4 I_1^{mpn}\right)}{v^2 M_{Zm}M_{Zp}},$$
$$h^{(n)}h^{(n)}A^{(n)}A^{(n)} : -\frac{1}{2}\frac{\left(m_h^2 M_{\Phi n}^2 I^{n} + 2M_Z^4 I'^{n}\right)}{v^2 M_{Zn}^2},$$
$$h^{(n)}h^{(n)}A^{(m)}A^{(m)} : -\frac{1}{2}\frac{\left(m_h^2 M_{\Phi m}^2 I^{nnmm} + 2M_Z^4 I_1^{mmnn}\right)}{v^2 M_{Zm}^2},$$
$$h^{(n)}h^{(n)}A^{(m)}A^{(p)} : -\frac{1}{\sqrt{2}}\frac{\left(m_h^2 M_{\Phi m}M_{\Phi p}I^{nnmp} + 2M_Z^4 I_1^{mpnn}\right)}{v^2 M_{Zm}M_{Zp}},$$
$$A^{(n)}A^{(n)}h^{(m)}h^{(p)} : -\frac{1}{\sqrt{2}}\frac{\left(m_h^2 M_{\Phi n}^2 I^{mpnn} + 2M_Z^4 I_1^{nnmp}\right)}{v^2 M_{Zn}^2},$$
$$h^{(n)}h^{(m)}A^{(n)}A^{(m)} : -\frac{1}{\sqrt{2}}\frac{\left(m_h^2 M_{\Phi n}M_{\Phi m}I^{nmnm} + 2M_Z^4 I_1^{nmnm}\right)}{v^2 M_{Zn}M_{Zm}},$$
$$h^{(n)}h^{(m)}A^{(p)}A^{(q)} : -\frac{\left(m_h^2 M_{\Phi p}M_{\Phi q}I^{nmpq} + 2M_Z^4 I_1^{pqnm}\right)}{v^2 M_{Zp}M_{Zq}}.$$

E.5 Elements of matrix $\mathcal{E}_{10\times 25}$

$$\phi^{(0)+}\phi^{(0)-}A^{(n)}A^{(n)} : -\frac{1}{\sqrt{2}}\frac{\left(m_h^2 M_{\Phi n}^2 + 2M_Z^4\cos^2\theta_W\right)}{v^2 M_{Zn}^2},$$
$$\phi^{(0)\pm}H^{(m)\mp}A^{(n)}A^{(n)} : -\frac{1}{\sqrt{2}v^2 M_{Zn}^2 M_{Wm}}\left[m_h^2 M_{\Phi n}^2 M_{\Phi m}I^{nnm}\right.$$
$$\left. + 2M_Z^2\left\{\cos^2\theta_W M_{\Phi m}M_Z^2 I_1^{nnm} + M_{\Phi n}M_W^2 I_1^{mnn}\left(1-\cos 2\theta_W\right)\right\}\right],$$
$$\phi^{(0)\pm}H^{(n)\mp}A^{(n)}A^{(n)} : -\frac{1}{\sqrt{2}v^2 M_{Zn}^2 M_{Wn}}\left[m_h^2 M_{\Phi n}^3 I^{3n}\right.$$
$$\left. + 2M_Z^2 M_{\Phi n}I'^{3n}\left\{\cos^2 2\theta_W M_Z^2 + M_W^2\left(1-\cos 2\theta_W\right)\right\}\right],$$

$$\phi^{(0)\pm}H^{(n)\mp}A^{(n)}A^{(m)} : -\frac{1}{v^2 M_{Zn}M_{Zm}M_{Wn}}\left[m_h^2 M_{\Phi n}^2 M_{\Phi m} I^{nnm} + 2M_Z^4\cos^2 2\theta_W M_{\Phi n} I_1^{mnn}\right.$$
$$\left. + M_W^2 M_Z^2\left(1-\cos 2\theta_W\right)\left(M_{\Phi m}I_1^{nnm} + M_{\Phi n}I_1^{mnn}\right)\right],$$
$$\phi^{(0)\pm}H^{(p)\mp}A^{(n)}A^{(m)} : -\frac{1}{v^2 M_{Zn}M_{Zm}M_{Wp}}\left[m_h^2 M_{\Phi n} M_{\Phi m} M_{\Phi p} I^{nmp} + 2M_Z^4\cos^2 2\theta_W M_{\Phi p} I_1^{nmp}\right.$$
$$\left. + M_W^2 M_Z^2\left(1-\cos 2\theta_W\right)\left(M_{\Phi m}I_1^{pnm} + M_{\Phi n}I_1^{pmn}\right)\right],$$
$$A^{(n)}A^{(n)}H^{(n)+}H^{(n)-} : -\frac{M_{\Phi n}^2}{\sqrt{2}v^2 M_{Wn}^2 M_{Zn}^2}q3_n,$$
$$A^{(n)}A^{(n)}H^{(m)+}H^{(m)-} : -\frac{1}{\sqrt{2}v^2 M_{Zn}^2 M_{Wm}^2}\left[m_h^2 M_{\Phi n}^2 M_{\Phi m}^2 I^{nnmm} + 2M_Z^4\cos^2 2\theta_W M_{\Phi m}^2 I_1^{nnmm}\right.$$
$$\left. + 4M_W^2 M_Z^2 M_{\Phi n}M_{\Phi m}\left(1-\cos 2\theta_W\right)I_1^{nmnm} + 2M_W^4 M_{\Phi n}^2 I_1^{mmnn}\right],$$
$$A^{(n)}A^{(m)}H^{(p)+}H^{(p)-} : -\frac{1}{v^2 M_{Zn}M_{Zm}M_{Wp}^2}\left[m_h^2 M_{\Phi n}M_{\Phi m}M_{\Phi p}^2 I^{nmpp} + 2M_Z^4\cos^2 2\theta_W M_{\Phi p}^2 I_1^{nmpp}\right.$$
$$+ 2M_W^2 M_Z^2 M_{\Phi p}\left(1-\cos 2\theta_W\right)\left(M_{\Phi n}I_1^{pmnp} + M_{\Phi m}I_1^{nppm}\right)$$
$$\left. + 2M_W^4 M_{\Phi n}M_{\Phi m}I_1^{ppnm}\right],$$
$$A^{(n)}A^{(m)}H^{(n)+}H^{(n)-} : -\frac{1}{v^2 M_{Zn}M_{Zm}M_{Wn}^2}\left[m_h^2 M_{\Phi n}^3 M_{\Phi m} I^{nnnm}\right.$$
$$+ 2M_Z^4\cos^2 2\theta_W M_{\Phi n}^2 I_1^{mnnn} + 2M_W^4 M_{\Phi n}M_{\Phi m}I_1^{nnnm}$$
$$\left. + 2M_W^2 M_Z^2 M_{\Phi n}\left(1-\cos 2\theta_W\right)\left(M_{\Phi n}I_1^{mnnn} + M_{\Phi m}I_1^{nnnm}\right)\right],$$
$$A^{(n)}A^{(n)}H^{(m)\pm}H^{(p)\mp} : -\frac{1}{\sqrt{2}v^2 M_{Zn}^2 M_{Wm}M_{Wp}}\left[m_h^2 M_{\Phi n}^2 M_{\Phi m}M_{\Phi p} I^{nnmp}\right.$$
$$+ 2M_Z^4\cos^2 2\theta_W M_{\Phi m}M_{\Phi p}I_1^{nnmp} + 2M_W^4 M_{\Phi n}^2 I_1^{mpnn}$$
$$\left. + 2M_W^2 M_Z^2 M_{\Phi n}\left(1-\cos 2\theta_W\right)\left(M_{\Phi m}I_1^{npmn} + M_{\Phi p}I_1^{mnnp}\right)\right],$$
$$A^{(n)}A^{(n)}H^{(m)\pm}H^{(n)\mp} : -\frac{1}{\sqrt{2}v^2 M_{Zn}^2 M_{Wm}M_{Wn}}\left[m_h^2 M_{\Phi n}^3 M_{\Phi m} I^{nnnm}\right.$$
$$+ 2M_Z^4\cos^2 2\theta_W M_{\Phi n}M_{\Phi m}I_1^{nnnm} + 2M_W^4 M_{\Phi n}^2 I_1^{mnnn}$$
$$\left. + 2M_W^2 M_Z^2 M_{\Phi n}\left(1-\cos 2\theta_W\right)\left(M_{\Phi n}I_1^{mnnn} + M_{\Phi m}I_1^{nnnm}\right)\right],$$
$$A^{(n)}A^{(m)}H^{(p)\pm}H^{(q)\mp} : -\frac{1}{v^2 M_{Zn}M_{Zm}M_{Wp}M_{Wq}}\left[m_h^2 M_{\Phi n}M_{\Phi m}M_{\Phi p}M_{\Phi q} I^{nmpq}\right.$$
$$+ 2M_Z^4\cos^2 2\theta_W M_{\Phi p}M_{\Phi q}I_1^{nmpq} + 2M_W^4 M_{\Phi n}M_{\Phi m}I_1^{pqnm}$$
$$+ M_W^2 M_Z^2\left(1-\cos 2\theta_W\right)\left\{M_{\Phi p}\left(M_{\Phi n}I_1^{mqnp} + M_{\Phi m}I_1^{nqmp}\right)\right.$$
$$\left.\left. + M_{\Phi q}\left(M_{\Phi n}I_1^{mpnp} + M_{\Phi m}I_1^{npmq}\right)\right\}\right],$$
$$A^{(n)}A^{(m)}H^{(n)\pm}H^{(m)\mp} : -\frac{1}{v^2 M_{Zn}M_{Zm}M_{Wn}M_{Wm}}\left[m_h^2 M_{\Phi n}^2 M_{\Phi m}^2 I^{nmnm}\right.$$
$$+ 2M_Z^4\cos^2 2\theta_W M_{\Phi n}M_{\Phi m}I_1^{nmnm} + 2M_W^4 M_{\Phi n}M_{\Phi m}I_1^{mnnm} + M_W^2 M_Z^2\left(1-\cos 2\theta_W\right)$$
$$\left.\times\left\{M_{\Phi n}\left(M_{\Phi n}I_1^{mmnn} + M_{\Phi m}I_1^{nnmm}\right) + M_{\Phi m}\left(M_{\Phi n}I_1^{mnnm} + M_{\Phi m}I_1^{nnmm}\right)\right\}\right],$$
$$A^{(n)}A^{(m)}H^{(n)\pm}H^{(p)\mp} : -\frac{1}{v^2 M_{Zn}M_{Zm}M_{Wn}M_{Wp}}\left[m_h^2 M_{\Phi n}^2 M_{\Phi m}M_{\Phi p} I^{nmnp}\right.$$
$$+ 2M_Z^4\cos^2 2\theta_W M_{\Phi n}M_{\Phi p}I_1^{nmnp} + 2M_W^4 M_{\Phi n}M_{\Phi m}I_1^{npnm} + M_W^2 M_Z^2\left(1-\cos 2\theta_W\right)$$

$$\times \left\{ M_{\Phi n} \left(M_{\Phi n} I_1^{mpnn} + M_{\Phi m} I_1^{npmn} \right) + M_{\Phi p} \left(M_{\Phi n} I_1^{mnnp} + M_{\Phi m} I_1^{nnmp} \right) \right\} \Big] .$$

E.6 Elements of matrix $\mathcal{C}_{15\times 25}$

$$h^{(0)}h^{(0)}H^{(n)+}H^{(n)-} : -\frac{1}{\sqrt{2}v^2 M_{Wn}^2} \left(m_h^2 M_{\Phi n}^2 + 2M_W^4 \right) ,$$

$$h^{(0)}h^{(n)}H^{(n)\pm}\phi^{(0)\mp} : -\frac{m_h^2}{v^2}\frac{M_{\Phi n}}{M_{Wn}},$$

$$h^{(n)}h^{(n)}H^{(m)\pm}\phi^{(0)\mp} : -\frac{m_h^2}{\sqrt{2}v^2}\frac{M_{\Phi m}}{M_{Wm}} I^{nnm},$$

$$h^{(n)}h^{(n)}H^{(n)\pm}\phi^{(0)\mp} : -\frac{m_h^2}{\sqrt{2}v^2}\frac{M_{\Phi n}}{M_{Wn}} I^{3n},$$

$$h^{(n)}h^{(m)}H^{(p)\pm}\phi^{(0)\mp} : -\frac{m_h^2}{v^2}\frac{M_{\Phi p}}{M_{Wp}} I^{nmp},$$

$$h^{(n)}h^{(m)}H^{(n)\pm}\phi^{(0)\mp} : -\frac{m_h^2}{v^2}\frac{M_{\Phi n}}{M_{Wn}} I^{nnm},$$

$$h^{(0)}h^{(n)}H^{(n)+}H^{(n)-} : -\frac{1}{v^2 M_{Wn}^2} \left(m_h^2 M_{\Phi n}^2 I^{3n} + 2M_W^4 I'^{3n} \right) ,$$

$$h^{(0)}h^{(n)}H^{(m)+}H^{(m)-} : -\frac{1}{v^2 M_{Wm}^2} \left(m_h^2 M_{\Phi m}^2 I^{nmm} + 2M_W^4 I_1^{mmn} \right) ,$$

$$h^{(0)}h^{(n)}H^{(m)\pm}H^{(p)\mp} : -\frac{1}{v^2 M_{Wm} M_{Wp}} \left(m_h^2 M_{\Phi m} M_{\Phi p} I^{nmp} + 2M_W^4 I_1^{mpn} \right) ,$$

$$h^{(0)}h^{(n)}H^{(n)\pm}H^{(m)\mp} : -\frac{1}{v^2 M_{Wn} M_{Wm}} \left(m_h^2 M_{\Phi n} M_{\Phi m} I^{nnm} + 2M_W^4 I_1^{mnn} \right) ,$$

$$h^{(n)}h^{(n)}H^{(n)+}H^{(n)-} : -\frac{1}{\sqrt{2}v^2 M_{Wn}^2} \left(m_h^2 M_{\Phi n}^2 I^{n} + 2M_W^4 I'^{n} \right) ,$$

$$h^{(n)}h^{(n)}H^{(m)+}H^{(m)-} : -\frac{1}{\sqrt{2}v^2 M_{Wm}^2} \left(m_h^2 M_{\Phi m}^2 I^{nnmm} + 2M_W^4 I_1^{mmnn} \right) ,$$

$$h^{(n)}h^{(m)}H^{(p)+}H^{(p)-} : -\frac{1}{v^2 M_{Wp}^2} \left(m_h^2 M_{\Phi p}^2 I^{nmpp} + 2M_W^4 I_1^{ppnm} \right) ,$$

$$h^{(n)}h^{(m)}H^{(n)+}H^{(n)-} : -\frac{1}{v^2 M_{Wn}^2} \left(m_h^2 M_{\Phi n}^2 I^{nmnn} + 2M_W^4 I_1^{nnnm} \right) ,$$

$$h^{(n)}h^{(n)}H^{(m)\pm}H^{(p)\mp} : -\frac{1}{\sqrt{2}v^2 M_{Wm} M_{Wp}} \left(m_h^2 M_{\Phi m} M_{\Phi p} I^{nnmp} + 2M_W^4 I_1^{mpnn} \right) ,$$

$$h^{(n)}h^{(n)}H^{(n)\pm}H^{(m)\mp} : -\frac{1}{\sqrt{2}v^2 M_{Wn} M_{Wm}} \left(m_h^2 M_{\Phi n} M_{\Phi m} I^{nnnm} + 2M_W^4 I_1^{mnnn} \right) ,$$

$$h^{(n)}h^{(m)}H^{(p)\pm}H^{(q)\mp} : -\frac{1}{v^2 M_{Wp} M_{Wq}} \left(m_h^2 M_{\Phi p} M_{\Phi q} I^{nmpq} + 2M_W^4 I_1^{pqnm} \right) .$$

E.7 Matrix elemnts of $\mathcal{M}^{(2)}_{NC,20\times20}$

$$
\begin{aligned}
h^{(0)}A^{(n)}h^{(0)}A^{(n)} &: -\frac{\left(m_h^2 M_{\Phi n}^2 + 2M_Z^4\right)}{v^2 M_{Zn}^2},\\
h^{(0)}A^{(m)}h^{(n)}A^{(m)} &: -\frac{\left(m_h^2 M_{\Phi m}^2 I^{nmm} + 2M_Z^4 I_1^{mmn}\right)}{v^2 M_{Zm}^2},\\
h^{(0)}A^{(m)}h^{(n)}A^{(p)} &: -\frac{\left(m_h^2 M_{\Phi m} M_{\Phi p} I^{nmp} + 2M_Z^4 I_1^{mpn}\right)}{v^2 M_{Zm} M_{Zp}},\\
h^{(n)}A^{(n)}h^{(n)}A^{(n)} &: -\frac{\left(m_h^2 M_{\Phi n}^2 I^{n} + 2M_Z^4 I'^{n}\right)}{v^2 M_{Zn}^2},\\
h^{(n)}A^{(m)}h^{(n)}A^{(m)} &: -\frac{\left(m_h^2 M_{\Phi m}^2 I^{nnmm} + 2M_Z^4 I_1^{mmnn}\right)}{v^2 M_{Zm}^2},\\
h^{(n)}A^{(m)}h^{(n)}A^{(p)} &: -\frac{\left(m_h^2 M_{\Phi m} M_{\Phi p} I^{nnmp} + 2M_Z^4 I_1^{mpnn}\right)}{v^2 M_{Zm} M_{Zp}},\\
A^{(n)}h^{(m)}A^{(n)}h^{(p)} &: -\frac{\left(m_h^2 M_{\Phi n}^2 I^{mpnn} + 2M_Z^4 I_1^{nnmp}\right)}{v^2 M_{Zn}^2},\\
h^{(n)}A^{(n)}h^{(m)}A^{(m)} &: -\frac{\left(m_h^2 M_{\Phi n} M_{\Phi m} I^{nmnm} + 2M_Z^4 I_1^{nmnm}\right)}{v^2 M_{Zn} M_{Zm}},\\
h^{(n)}A^{(p)}h^{(m)}A^{(q)} &: -\frac{\left(m_h^2 M_{\Phi p} M_{\Phi q} I^{nmpq} + 2M_Z^4 I_1^{pqnm}\right)}{v^2 M_{Zp} M_{Zq}}.
\end{aligned}
$$

E.8 Matrix elemnts of $\mathcal{G}_{CC,20\times20}$

$$
\begin{aligned}
&\phi^{(0)+}A^{(n)}\phi^{(0)+}A^{(n)} : \sqrt{2}\ \phi^{(0)+}\phi^{(0)-}A^{(n)}A^{(n)},\\
&\phi^{(0)+}A^{(n)}H^{(m)+}A^{(n)} : \sqrt{2}\ \phi^{(0)\pm}H^{(m)\mp}A^{(n)}A^{(n)},\\
&\phi^{(0)+}A^{(n)}H^{(n)+}A^{(n)} : \sqrt{2}\ \phi^{(0)\pm}H^{(n)\mp}A^{(n)}A^{(n)},\\
&\phi^{(0)+}A^{(n)}H^{(n)+}A^{(m)} : \phi^{(0)\pm}H^{(n)\mp}A^{(n)}A^{(m)},\\
&\phi^{(0)+}A^{(n)}H^{(p)+}A^{(m)} : \phi^{(0)\pm}H^{(p)\mp}A^{(n)}A^{(m)},\\
&A^{(n)}H^{(n)+}A^{(n)}H^{(n)+} : \sqrt{2}\ A^{(n)}A^{(n)}H^{(n)+}H^{(n)-},\\
&A^{(n)}H^{(m)+}A^{(n)}H^{(m)+} : \sqrt{2}\ A^{(n)}A^{(n)}H^{(m)+}H^{(m)-},\\
&A^{(n)}H^{(p)+}A^{(m)}H^{(p)+} : A^{(n)}A^{(m)}H^{(p)+}H^{(p)-},\\
&A^{(n)}H^{(n)+}A^{(m)}H^{(n)+} : A^{(n)}A^{(m)}H^{(n)+}H^{(n)-},\\
&A^{(n)}H^{(m)+}A^{(n)}H^{(p)+} : \sqrt{2}\ A^{(n)}A^{(n)}H^{(m)\pm}H^{(p)\mp},\\
&A^{(n)}H^{(m)+}A^{(n)}H^{(n)+} : \sqrt{2}\ A^{(n)}A^{(n)}H^{(m)\pm}H^{(n)\mp},\\
&A^{(n)}H^{(p)+}A^{(m)}H^{(q)+} : A^{(n)}A^{(m)}H^{(p)\pm}H^{(q)\mp},
\end{aligned}
$$

$A^{(n)}H^{(n)+}A^{(m)}H^{(m)+} : A^{(n)}A^{(m)}H^{(n)\pm}H^{(m)\mp}$,
$A^{(n)}H^{(n)+}A^{(m)}H^{(p)+} : A^{(n)}A^{(m)}H^{(n)\pm}H^{(p)\mp}$.

E.9 Matrix elemnts of $\mathcal{H}_{CC,25\times25}$

$h^{(0)}H^{(n)+}h^{(0)}H^{(n)+} : \sqrt{2}\ h^{(0)}h^{(0)}H^{(n)+}H^{(n)-}$,
$\phi^{(0)+}h^{(0)}H^{(n)+}h^{(n)} : h^{(0)}h^{(n)}H^{(n)\pm}\phi^{(0)\mp}$,
$\phi^{(0)+}h^{(n)}H^{(m)+}h^{(n)} : \sqrt{2}\ h^{(n)}h^{(n)}H^{(m)\pm}\phi^{(0)\mp}$,
$\phi^{(0)+}h^{(n)}H^{(n)+}h^{(n)} : \sqrt{2}\ h^{(n)}h^{(n)}H^{(n)\pm}\phi^{(0)\mp}$,
$\phi^{(0)+}h^{(n)}H^{(p)+}h^{(m)} : h^{(n)}h^{(m)}H^{(p)\pm}\phi^{(0)\mp}$,
$\phi^{(0)+}h^{(n)}H^{(n)+}h^{(m)} : h^{(n)}h^{(m)}H^{(n)\pm}\phi^{(0)\mp}$,
$h^{(0)}H^{(n)+}h^{(n)}H^{(n)+} : h^{(0)}h^{(n)}H^{(n)+}H^{(n)-}$,
$h^{(0)}H^{(m)+}h^{(n)}H^{(m)+} : h^{(0)}h^{(n)}H^{(m)+}H^{(m)-}$,
$h^{(0)}H^{(m)+}h^{(n)}H^{(p)+} : h^{(0)}h^{(n)}H^{(m)\pm}H^{(p)\mp}$,
$h^{(0)}H^{(n)+}h^{(n)}H^{(m)+} : h^{(0)}h^{(n)}H^{(n)\pm}H^{(m)\mp}$,
$h^{(n)}H^{(n)+}h^{(n)}H^{(n)+} : \sqrt{2}\ h^{(n)}h^{(n)}H^{(n)+}H^{(n)-}$,
$h^{(n)}H^{(p)+}h^{(m)}H^{(p)+} : h^{(n)}h^{(m)}H^{(p)+}H^{(p)-}$,
$h^{(n)}H^{(m)+}h^{(n)}H^{(m)+} : \sqrt{2}\ h^{(n)}h^{(n)}H^{(m)+}H^{(m)-}$,
$h^{(n)}H^{(n)+}h^{(m)}H^{(n)+} : h^{(n)}h^{(m)}H^{(n)+}H^{(n)-}$,
$h^{(n)}H^{(m)+}h^{(n)}H^{(p)+} : h^{(n)}h^{(n)}H^{(m)\pm}H^{(p)\mp}$,
$h^{(n)}H^{(n)+}h^{(n)}H^{(m)+} : \sqrt{2}\ h^{(n)}h^{(n)}H^{(n)\pm}H^{(m)\mp}$,
$h^{(n)}H^{(p)+}h^{(m)}H^{(q)+} : h^{(n)}h^{(m)}H^{(p)\pm}H^{(q)\mp}$.

F

Feynman Rules Relevant for $Zb\bar{b}$ Analysis

In the following Feynman rules, all momenta and fields are assumed to flow into the vertices. Obviously in UED the BLT parameters are vanishing and so the overlap integrals and β will be unity and $\alpha_n = \frac{1}{2}\tan^{-1}\left(\frac{m_t}{n/R}\right)$ and $M_{\Phi k} = k/R$. Moreover for UED, the conservation of KK-number will ensure that there will be no (0)-(0)-(n) type coupling. To avoid cluttering we suppress the indices in the overlap integrals. Basically by I_c we mean I_c^m and by $I_{a,b}$ we imply $I_{a,b}^{nn}$.

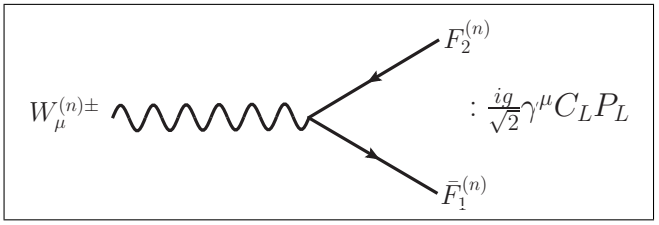

$W^{(n)+}\bar{Q}_t'^{(n)}b_L^{(0)}: C_L = -I_a\sqrt{\beta}\cos\alpha_n,$

$W^{(n)+}\bar{U}'^{(n)}b_L^{(0)}: C_L = I_a\sqrt{\beta}\sin\alpha_n,$

$W^{(n)+}\bar{t}^{(0)}b^{(0)}: C_L = I_c\sqrt{\beta},$

$W^{(n)-}\bar{b}_L^{(0)}Q_t'^{(n)}: C_L = -I_a\sqrt{\beta}\cos\alpha_n,$

$W^{(n)-}\bar{b}_L^{(0)}U'^{(n)}: C_L = I_a\sqrt{\beta}\sin\alpha_n,$

$W^{(n)-}\bar{b}^{(0)}t^{(0)}: C_L = I_c\sqrt{\beta}.$

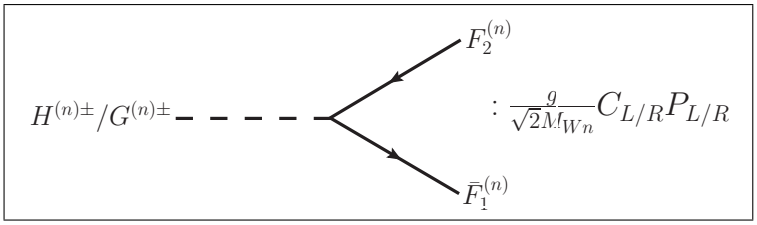

$$H^{(n)+}\bar{Q}_t'^{(n)}b_L^{(0)}: C_L = -i\sqrt{\beta}\left(I_a\frac{m_t M_{\Phi n}}{M_W}\sin\alpha_n - I_b M_W\cos\alpha_n\right),$$
$$H^{(n)-}\bar{b}_L^{(0)}Q_t'^{(n)}: C_R = -i\sqrt{\beta}\left(I_a\frac{m_t M_{\Phi n}}{M_W}\sin\alpha_n - I_b M_W\cos\alpha_n\right),$$
$$G^{(n)+}\bar{Q}_t'^{(n)}b_L^{(0)}: C_L = \sqrt{\beta}\left(I_a m_t\sin\alpha_n + I_b M_{\Phi n}\cos\alpha_n\right),$$
$$G^{(n)-}\bar{b}_L^{(0)}Q_t'^{(n)}: C_R = -\sqrt{\beta}\left(I_a m_t\sin\alpha_n + I_b M_{\Phi n}\cos\alpha_n\right),$$
$$H^{(n)+}\bar{U}'^{(n)}b_L^{(0)}: C_L = i\sqrt{\beta}\left(I_a\frac{m_t M_{\Phi n}}{M_W}\cos\alpha_n + I_b M_W\sin\alpha_n\right),$$
$$H^{(n)-}\bar{b}_L^{(0)}U'^{(n)}: C_R = i\sqrt{\beta}\left(I_a\frac{m_t M_{\Phi n}}{M_W}\cos\alpha_n + I_b M_W\sin\alpha_n\right),$$
$$G^{(n)+}\bar{U}'^{(n)}b_L^{(0)}: C_L = -\sqrt{\beta}\left(I_a m_t\cos\alpha_n - I_b M_{\Phi n}\sin\alpha_n\right),$$
$$G^{(n)-}\bar{b}_L^{(0)}U'^{(n)}: C_R = \sqrt{\beta}\left(I_a m_t\cos\alpha_n - I_b M_{\Phi n}\sin\alpha_n\right),$$
$$\bar{t}^{(0)}H^{(n)+}b^{(0)}: C_L = i\sqrt{\beta}\,I_c\,\frac{M_{\Phi n}}{M_W}\,m_t, \qquad \bar{b}^{(0)}H^{(n)-}t^{(0)}: C_R = i\sqrt{\beta}\,I_c\,\frac{M_{\Phi n}}{M_W}\,m_t,$$
$$\bar{t}^{(0)}G^{(n)+}b^{(0)}: C_L = -\sqrt{\beta}\,I_c\,m_t, \qquad \bar{b}^{(0)}G^{(n)-}t^{(0)}: C_R = \sqrt{\beta}\,I_c\,m_t.$$

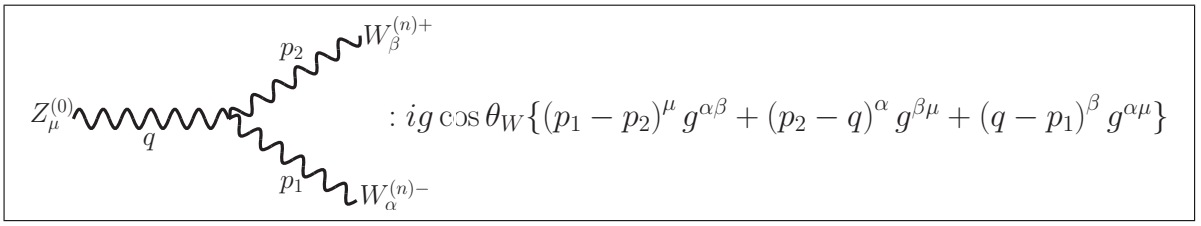

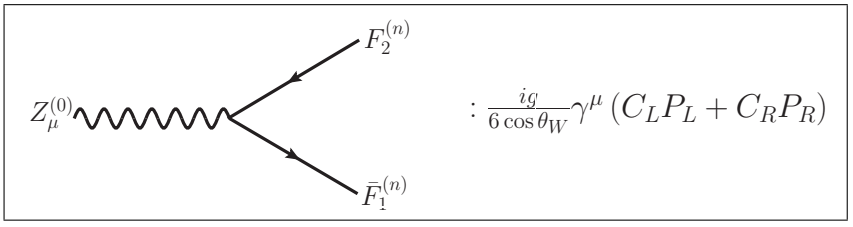

$$Z^{(0)}\bar{Q}_t'^{(n)}Q_t'^{(n)}: \begin{cases} C_L = -4\sin^2\theta_W + 3\cos^2\alpha_n \\ C_R = -4\sin^2\theta_W + 3\cos^2\alpha_n \end{cases}, \quad Z^{(0)}\bar{U}'^{(n)}U'^{(n)}: \begin{cases} C_L = -4\sin^2\theta_W + 3\sin^2\alpha_n \\ C_R = -4\sin^2\theta_W + 3\sin^2\alpha_n \end{cases},$$
$$Z^{(0)}\bar{Q}_t'^{(n)}U'^{(n)}: \begin{cases} C_L = -3\sin\alpha_n\cos\alpha_n \\ C_R = -3\sin\alpha_n\cos\alpha_n \end{cases}, \qquad Z^{(0)}\bar{U}'^{(n)}Q_t'^{(n)}: \begin{cases} C_L = -3\sin\alpha_n\cos\alpha_n \\ C_R = -3\sin\alpha_n\cos\alpha_n \end{cases}.$$

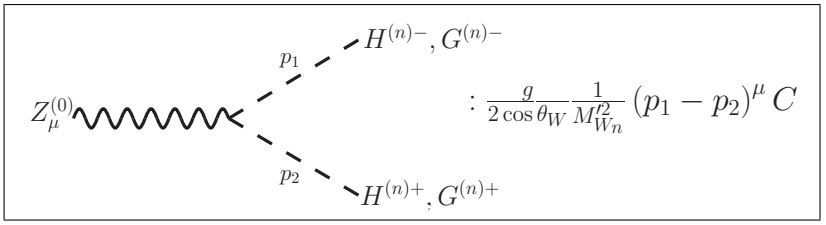

$Z^{(0)}H^{(n)+}H^{(n)-}: C = i\{(-1+2\sin^2\theta_W)M_{\Phi n}^2 - 2\cos^2\theta_W M_W^2\},$
$Z^{(0)}G^{(n)+}G^{(n)-}: C = i\{(-1+2\sin^2\theta_W)M_W^2 - 2\cos^2\theta_W M_{\Phi n}^2\},$
$Z^{(0)}H^{(n)-}G^{(n)+}: C = -M_{\Phi n}M_W,$
$Z^{(0)}G^{(n)-}H^{(n)+}: C = M_{\Phi n}M_W.$

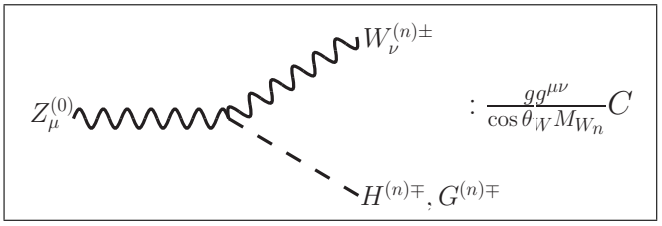

$Z^{(0)}W^{(n)+}G^{(n)-}: C = \left(-M_W^2\sin^2\theta_W + M_{\Phi n}^2\cos^2\theta_W\right),$
$Z^{(0)}W^{(n)-}G^{(n)+}: C = \left(M_W^2\sin^2\theta_W - M_{\Phi n}^2\cos^2\theta_W\right),$
$Z^{(0)}W^{(n)+}H^{(n)-}: C = -iM_{\Phi n}M_W,$
$Z^{(0)}W^{(n)-}H^{(n)+}: C = -iM_{\Phi n}M_W.$

G

Feynman Rules Relevant for Rare Top Decays

All the momenta and fields are assumed to be incoming. Like in Appendix F, here also, to avoid cluttering, we write I_c^m by I_c and $I_{a,b}^{nm}$ by $I_{a,b}$. Also $\beta = \left(\frac{\pi+R_\phi}{\pi+R_f}\right)$. Obviously in UED the BLT parameters are vanishing and so the overlap integrals and β will be unity and $\alpha_n = \frac{1}{2}\tan^{-1}\left(\frac{m_j}{n/R}\right)$ and $M_{\Phi k} = k/R$. As said before, for UED, the conservation of KK-number will ensure that there will be no (0)-(0)-(n) type coupling.

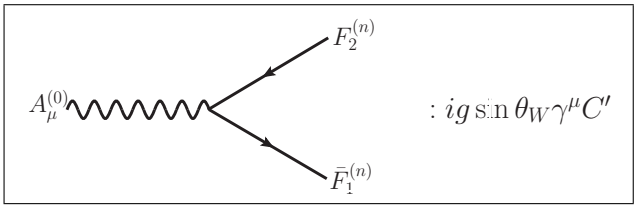

$A_\mu^{(0)}\bar{Q}_j'^{(n)}Q_j'^{(n)}$: $C' = -\frac{1}{3}$,

$A_\mu^{(0)}\bar{Q}_j'^{(n)}D'^{(n)}$: $C' = 0$,

$A_\mu^{(0)}\bar{b}_j^{(0)}b_j^{(0)}$: $C' = -\frac{1}{3}$,

$A_\mu^{(0)}\bar{D}'^{(n)}D'^{(n)}$: $C' = -\frac{1}{3}$,

$A_\mu^{(0)}\bar{D}'^{(n)}Q_j'^{(n)}$: $C' = 0$,

$A_\mu^{(0)}\bar{t}_i^{(0)}t_i^{(0)}$: $C' = \frac{2}{3}$.

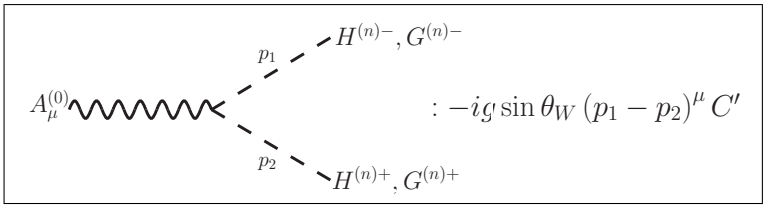

$A_\mu^{(0)} H^{(n)+} H^{(n)-}$: $C' = 1$, $A_\mu^{(0)} G^{(n)+} G^{(n)-}$: $C' = 1$, $A_\mu^{(0)} H^{(n)\pm} G^{(n)\mp}$: $C' = 0$.

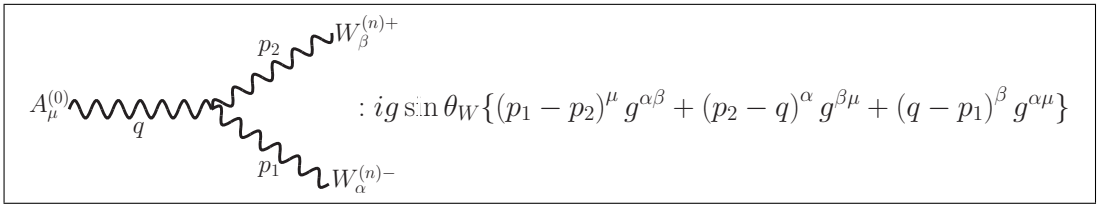

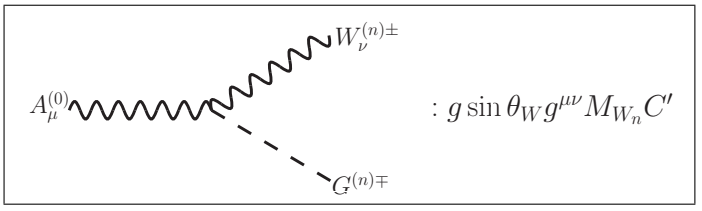

$A_\mu^{(0)} G^{(n)-} W_\nu^{(n)+}$: $C' = 1$, $A_\mu^{(0)} G^{(n)+} W_\nu^{(n)-}$: $C' = -1$.

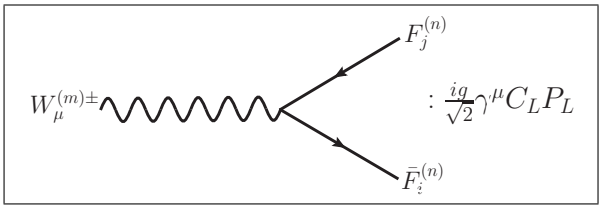

$W^{(m)+} \bar{t}_i^{(0)} Q_j'^{(n)}$: $C_L = -I_a \sqrt{\beta} \cos\alpha_n V_{ij}$, $W^{(m)-} \bar{Q}_j'^{(n)} t_i^{(0)}$: $C_L = -I_a \sqrt{\beta} \cos\alpha_n V_{ij}^*$,
$W^{(m)+} \bar{t}_i^{(0)} D_j'^{(n)}$: $C_L = I_a \sqrt{\beta} \sin\alpha_n V_{ij}$, $W^{(m)-} \bar{D}_j'^{(n)} t_i^{(0)}$: $C_L = I_a \sqrt{\beta} \sin\alpha_n V_{ij}^*$,
$W^{(m)+} \bar{t}_i^{(0)} b_j^{(0)}$: $C_L = I_c \sqrt{\beta} V_{ij}$, $W^{(m)-} \bar{b}_j^{(0)} t_i^{(0)}$: $C_L = I_c \sqrt{\beta} V_{ij}^*$.

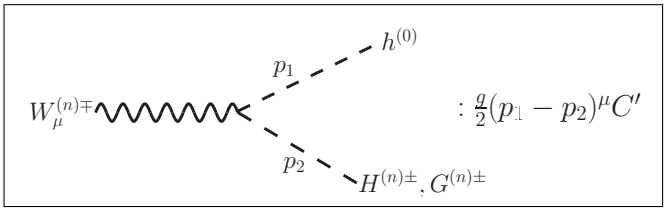

$h^{(0)} H^{(n)\pm} W^{(n)\mp}$: $C' = \mp i \dfrac{M_{\Phi n}}{M_{Wn}}$, $h^{(0)} G^{(n)\pm} W^{(n)\mp}$: $C' = \dfrac{M_W}{M_{Wn}}$.

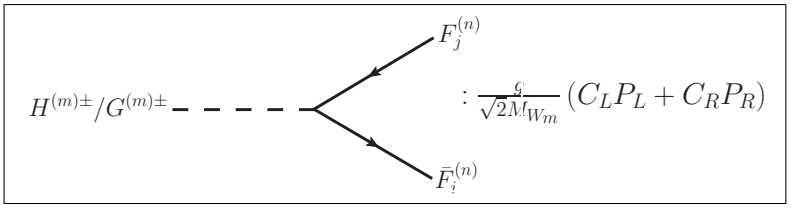

$$\bar{t}_i^{(0)} G^{(m)+} Q_j'^{(n)}: \begin{cases} C_L = \sqrt{\beta} I_a m_i \cos\alpha_n V_{ij} \\ C_R = -\sqrt{\beta}\left(I_a m_j \sin\alpha_n + I_b M_{\Phi m}\cos\alpha_n\right) V_{ij} \end{cases},$$

$$\bar{Q}_j'^{(n)} G^{(m)-} t_i^{(0)}: \begin{cases} C_L = \sqrt{\beta}\left(I_a m_j \sin\alpha_n + I_b M_{\Phi m}\cos\alpha_n\right) V_{ij}^* \\ C_R = -\sqrt{\beta} I_a m_i \cos\alpha_n V_{ij}^* \end{cases},$$

$$\bar{t}_i^{(0)} G^{(m)+} D_j'^{(n)}: \begin{cases} C_L = -\sqrt{\beta} I_a m_i \sin\alpha_n V_{ij} \\ C_R = \sqrt{\beta}\left(I_a m_j \cos\alpha_n - I_b M_{\Phi m}\sin\alpha_n\right) V_{ij} \end{cases},$$

$$\bar{D}_j'^{(n)} G^{(m)-} t_i^{(0)}: \begin{cases} C_L = -\sqrt{\beta}\left(I_a m_j \cos\alpha_n - I_b M_{\Phi m}\sin\alpha_n\right) V_{ij}^* \\ C_R = \sqrt{\beta} I_a m_i \sin\alpha_n V_{ij}^* \end{cases},$$

$$\bar{t}_i^{(0)} H^{(m)+} Q_j'^{(n)}: \begin{cases} C_L = -i\sqrt{\beta} I_a \dfrac{m_i M_{\Phi m}}{M_W}\cos\alpha_n V_{ij} \\ C_R = i\sqrt{\beta}\left(I_a \dfrac{m_j M_{\Phi m}}{M_W}\sin\alpha_n - I_b M_W \cos\alpha_n\right) V_{ij} \end{cases},$$

$$\bar{Q}_j'^{(n)} H^{(m)-} t_i^{(0)}: \begin{cases} C_L = i\sqrt{\beta}\left(I_a \dfrac{m_j M_{\Phi m}}{M_W}\sin\alpha_n - I_b M_W \cos\alpha_n\right) V_{ij}^* \\ C_R = -i\sqrt{\beta} I_a \dfrac{m_i M_{\Phi m}}{M_W}\cos\alpha_n V_{ij}^* \end{cases},$$

$$\bar{t}_i^{(0)} H^{(m)+} D_j'^{(n)}: \begin{cases} C_L = i\sqrt{\beta} I_a \dfrac{m_i M_{\Phi m}}{M_W}\sin\alpha_n V_{ij} \\ C_R = -i\sqrt{\beta}\left(I_a \dfrac{m_j M_{\Phi m}}{M_W}\cos\alpha_n + I_b M_W \sin\alpha_n\right) V_{ij} \end{cases},$$

$$\bar{D}_j'^{(n)} G^{(m)-} t_i^{(0)}: \begin{cases} C_L = -i\sqrt{\beta}\left(I_a \dfrac{m_j M_{\Phi m}}{M_W}\cos\alpha_n + I_b M_W \sin\alpha_n\right) V_{ij}^* \\ C_R = i\sqrt{\beta} I_a \dfrac{m_i M_{\Phi m}}{M_W}\sin\alpha_n V_{ij}^* \end{cases},$$

$$\bar{t}_i^{(0)} G^{(m)+} b_j^{(0)}: \begin{cases} C_L = -\sqrt{\beta} I_c m_i V_{ij} \\ C_R = \sqrt{\beta} I_c m_j V_{ij} \end{cases}, \qquad \bar{b}_j^{(0)} G^{(m)-} t_i^{(0)}: \begin{cases} C_L = -\sqrt{\beta} I_c m_j V_{ij}^* \\ C_R = \sqrt{\beta} I_c m_i V_{ij}^* \end{cases},$$

$$\bar{t}_i^{(0)} H^{(m)+} b_j^{(0)}: \begin{cases} C_L = i\sqrt{\beta} I_c \dfrac{M_{\Phi m}}{M_W} m_i V_{ij} \\ C_R = -i\sqrt{\beta} I_c \dfrac{M_{\Phi m}}{M_W} m_j V_{ij} \end{cases}, \quad \bar{b}_j^{(0)} H^{(m)-} t_i^{(0)}: \begin{cases} C_L = -i\sqrt{\beta} I_c \dfrac{M_{\Phi m}}{M_W} m_j V_{ij}^* \\ C_R = i\sqrt{\beta} I_c \dfrac{M_{\Phi m}}{M_W} m_i V_{ij}^* \end{cases}.$$

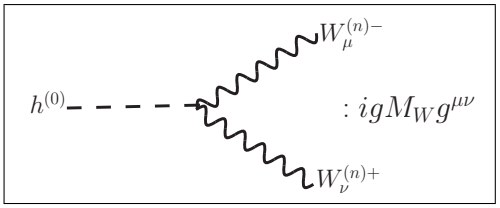

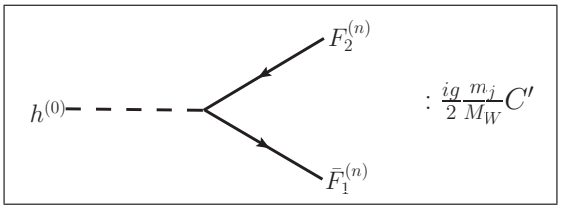

$h^{(0)}\bar{Q}_j'^{(n)}Q_j'^{(n)}: C' = -\sin 2\alpha_n,$ $h^{(0)}\bar{D}'^{(n)}D'^{(n)}: C' = -\sin 2\alpha_n,$

$h^{(0)}\bar{Q}_j'^{(n)}D'^{(n)}: C' = \cos 2\alpha_n\gamma_5,$ $h^{(0)}\bar{D}'^{(n)}Q_j'^{(n)}: C' = -\cos 2\alpha_n\gamma_5,$

$h^{(0)}\bar{b}_j^{(0)}b_j^{(0)}: C' = -1,$ $h^{(0)}\bar{t}_i^{(0)}t_i^{(0)}: C' = -\dfrac{m_i}{m_j}.$

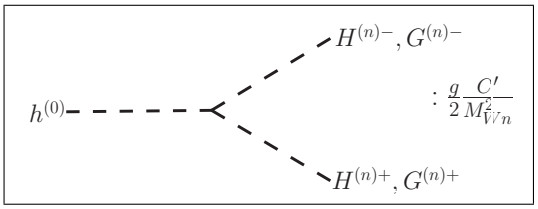

$h^{(0)}H^{(n)+}H^{(n)-}: C' = -im_h^2 M_W,$ $h^{(0)}G^{(n)+}G^{(n)-}: C' = -i\dfrac{m_h^2 M_{\Phi n}^2 + 2M_W^2 M_{Wn}^2}{M_W},$

$h^{(0)}H^{(n)+}G^{(n)-}: C' = -M_{\Phi n}(m_h^2 - M_{Wn}^2),$ $h^{(0)}H^{(n)-}G^{(n)+}: C' = M_{\Phi n}(m_h^2 - M_{Wn}^2).$

H

Explicit Expression of Overlap Integrals Used in Appendix F and in Appendix G

I_a, I_b and I_c have the following form:

$$
\begin{aligned}
I_a &= \frac{2}{\pi R}\left[\frac{1}{\sqrt{1+\frac{r_f^2 M_{Qn}^2}{4}+\frac{r_f}{\pi R}}}\right]\left[\frac{1}{\sqrt{1+\frac{r_\phi^2 M_{\Phi n}^2}{4}+\frac{r_\phi}{\pi R}}}\right]\frac{M_{\Phi n}^2\left(-r_f+r_\phi\right)}{\left(M_{Qn}^2-M_{\Phi n}^2\right)},\\
I_b &= \frac{2}{\pi R}\left[\frac{1}{\sqrt{1+\frac{r_f^2 M_{Qn}^2}{4}+\frac{r_f}{\pi R}}}\right]\left[\frac{1}{\sqrt{1+\frac{r_\phi^2 M_{\Phi n}^2}{4}+\frac{r_\phi}{\pi R}}}\right]\frac{M_{\Phi n}M_{Qn}\left(-r_f+r_\phi\right)}{\left(M_{Qn}^2-M_{\Phi n}^2\right)},\\
I_c &= \sqrt{\frac{2}{\pi R}}\left[\frac{1}{\sqrt{1+\frac{r_\phi^2 M_{\Phi n}^2}{4}+\frac{r_\phi}{\pi R}}}\right]\frac{\left(r_f-r_\phi\right)}{\left(\sqrt{\pi\, R+r_f}\right)}.
\end{aligned}
$$

Bibliography

[1] S. L. Glashow, *Partial Symmetries of Weak Interactions*, *Nucl. Phys.* **22** (1961) 579–588.

[2] A. Salam and J. C. Ward, *Electromagnetic and weak interactions*, *Phys. Lett.* **13** (1964) 168–171.

[3] S. Weinberg, *A Model of Leptons*, *Phys. Rev. Lett.* **19** (1967) 1264–1266.

[4] A. Salam, *Weak and electromagnetic interactions*, in *Elementary particle theory* (N. Svartholm, ed.), pp. 367–377, Almquist & Wiksell.

[5] **Particle Data Group** Collaboration, C. Patrignani et al., *Review of Particle Physics*, *Chin. Phys.* **C40** (2016), no. 10 100001.

[6] S. L. Glashow, J. Iliopoulos, and L. Maiani, *Weak Interactions with Lepton-Hadron Symmetry*, *Phys. Rev.* **D2** (1970) 1285–1292.

[7] N. Cabibbo, *Unitary Symmetry and Leptonic Decays*, *Phys. Rev. Lett.* **10** (1963) 531–533. [,648(1963)].

[8] M. Kobayashi and T. Maskawa, *CP Violation in the Renormalizable Theory of Weak Interaction*, *Prog. Theor. Phys.* **49** (1973) 652–657.

[9] R. Aleksan, B. Kayser, and D. London, *Determining the quark mixing matrix from CP violating asymmetries*, *Phys. Rev. Lett.* **73** (1994) 18–20, [hep-ph/9403341].

[10] I. I. Y. Bigi and A. I. Sanda, *On the other five KM triangles*, hep-ph/9909479.

[11] C. Jarlskog, *Commutator of the Quark Mass Matrices in the Standard Electroweak Model and a Measure of Maximal CP Violation*, *Phys. Rev. Lett.* **55** (1985) 1039.

[12] C. Jarlskog, *A Basis Independent Formulation of the Connection Between Quark Mass Matrices, CP Violation and Experiment*, *Z. Phys.* **C29** (1985) 491–497.

[13] C. Jarlskog and R. Stora, *Unitarity Polygons and CP Violation Areas and Phases in the Standard Electroweak Model*, *Phys. Lett.* **B208** (1988) 268–274.

[14] C. Bouchiat, J. Iliopoulos, and P. Meyer, *An Anomaly Free Version of Weinberg's Model*, *Phys. Lett.* **B38** (1972) 519–523.

[15] Y. Nambu and G. Jona-Lasinio, *Dynamical Model of Elementary Particles Based on an Analogy with Superconductivity. 1.*, *Phys. Rev.* **122** (1961) 345–358.

[16] Y. Nambu and G. Jona-Lasinio, *DYNAMICAL MODEL OF ELEMENTARY PARTICLES BASED ON AN ANALOGY WITH SUPERCONDUCTIVITY. II*, *Phys. Rev.* **124** (1961) 246–254.

[17] J. Goldstone, *Field Theories with Superconductor Solutions*, *Nuovo Cim.* **19** (1961) 154–164.

[18] J. Goldstone, A. Salam, and S. Weinberg, *Broken Symmetries*, *Phys. Rev.* **127** (1962) 965–970.

[19] F. Englert and R. Brout, *Broken Symmetry and the Mass of Gauge Vector Mesons*, *Phys. Rev. Lett.* **13** (1964) 321–323.

[20] P. W. Higgs, *Broken symmetries, massless particles and gauge fields*, *Phys. Lett.* **12** (1964) 132–133.

[21] P. W. Higgs, *Broken Symmetries and the Masses of Gauge Bosons*, *Phys. Rev. Lett.* **13** (1964) 508–509.

[22] G. S. Guralnik, C. R. Hagen, and T. W. B. Kibble, *Global Conservation Laws and Massless Particles*, *Phys. Rev. Lett.* **13** (1964) 585–587.

[23] V. L. Ginzburg and L. D. Landau, *On the Theory of superconductivity*, *Zh. Eksp. Teor. Fiz.* **20** (1950) 1064–1082.

[24] D. J. Gross, *The discovery of asymptotic freedom and the emergence of qcd*, *Proc. Nat. Acad. Sci.* **102** (2005) 9099–9108.

[25] S. Bethke, *Experimental tests of asymptotic freedom*, *Prog. Part. Nucl. Phys.* **58** (2007) 351–386, [hep-ex/0606035].

[26] C. Amsler and A. Masoni, *The $\eta(1405)$, $\eta(1475)$, $f_1(1420)$, and $f_1(1510)$*, .

[27] D. J. Gross and F. Wilczek, *Ultraviolet Behavior of Nonabelian Gauge Theories*, *Phys. Rev. Lett.* **30** (1973) 1343–1346.

[28] H. D. Politzer, *Reliable Perturbative Results for Strong Interactions?*, *Phys. Rev. Lett.* **30** (1973) 1346–1349.

[29] H. Fritzsch, M. Gell-Mann, and H. Leutwyler, *Advantages of the Color Octet Gluon Picture*, *Phys. Lett.* **B47** (1973) 365–368.

[30] G. 't Hooft, *Renormalization of Massless Yang-Mills Fields*, *Nucl. Phys.* **B33** (1971) 173–199.

[31] G. 't Hooft, *Renormalizable Lagrangians for Massive Yang-Mills Fields*, *Nucl. Phys.* **B35** (1971) 167–188.

[32] T. W. B. Kibble, *Symmetry breaking in nonAbelian gauge theories*, *Phys. Rev.* **155** (1967) 1554–1561.

[33] Y. Nambu, *Axial vector current conservation in weak interactions*, *Phys. Rev. Lett.* **4** (1960) 380–382.

[34] **ATLAS** Collaboration, G. Aad et al., *Observation of a new particle in the search for the Standard Model Higgs boson with the ATLAS detector at the LHC*, *Phys. Lett.* **B716** (2012) 1–29, [arXiv:1207.7214].

[35] **CMS** Collaboration, S. Chatrchyan et al., *Observation of a new boson at a mass of 125 GeV with the CMS experiment at the LHC*, *Phys. Lett.* **B716** (2012) 30–61, [arXiv:1207.7235].

[36] https://atlas.web.cern.ch/Atlas/GROUPS/PHYSICS/CombinedSummaryPlots/HIGGS/.

[37] **CMS** Collaboration, V. Khachatryan et al., *Precise determination of the mass of the Higgs boson and tests of compatibility of its couplings with the standard model predictions using proton collisions at 7 and 8 TeV*, *Eur. Phys. J.* **C75** (2015), no. 5 212, [arXiv:1412.8662].

[38] *Projections for measurements of Higgs boson signal strengths and coupling parameters with the ATLAS detector at a HL-LHC*, Tech. Rep. ATL-PHYS-PUB-2014-016, CERN, Geneva, Oct, 2014.

[39] T. D. Lee and C. S. Wu, *WEAK INTERACTIONS*, *Ann. Rev. Nucl. Part. Sci.* **15** (1965) 381–476.

[40] **Gargamelle Neutrino** Collaboration, F. J. Hasert et al., *Observation of Neutrino Like Interactions Without Muon Or Electron in the Gargamelle Neutrino Experiment*, *Phys. Lett.* **46B** (1973) 138–140.

[41] F. J. Hasert et al., *Search for Elastic ν_μ Electron Scattering*, *Phys. Lett.* **46B** (1973) 121–124.

[42] **Gargamelle Neutrino** Collaboration, F. J. Hasert et al., *Observation of Neutrino Like Interactions without Muon or Electron in the Gargamelle Neutrino Experiment*, *Nucl. Phys.* **B73** (1974) 1–22.

[43] A. Benvenuti et al., *Observation of Muonless Neutrino Induced Inelastic Interactions*, *Phys. Rev. Lett.* **32** (1974) 800–803.

[44] **UA1** Collaboration, G. Arnison et al., *Recent Results on Intermediate Vector Boson Properties at the CERN Super Proton Synchrotron Collider*, *Phys. Lett.* **B166** (1986) 484–490.

[45] **UA2** Collaboration, R. Ansari et al., *Measurement of the Standard Model Parameters from a Study of W and Z Bosons*, *Phys. Lett.* **B186** (1987) 440–451.

[46] **Particle Data Group** Collaboration, D. E. Groom et al., *Review of particle physics. Particle Data Group*, *Eur. Phys. J.* **C15** (2000) 1–878.

[47] **SLD Electroweak Group, DELPHI, ALEPH, SLD, SLD Heavy Flavour Group, OPAL, LEP Electroweak Working Group, L3** Collaboration, S. Schael et al., *Precision electroweak measurements on the Z resonance*, *Phys. Rept.* **427** (2006) 257–454, [hep-ex/0509008].

[48] H. Park, *A Measurement of the left-right cross-section asymmetry in Z0 production with polarized e+ e- collisions*. PhD thesis, Oregon U., 1993.

[49] G. Bhattacharyya, *A Pedagogical Review of Electroweak Symmetry Breaking Scenarios*, *Rept. Prog. Phys.* **74** (2011) 026201, [arXiv:0910.5095].

[50] M. E. Peskin and T. Takeuchi, *Estimation of oblique electroweak corrections*, *Phys. Rev.* **D46** (1992) 381–409.

[51] E. Otten and C. Weinheimer, *Neutrino mass limit from tritium beta decay*, *Rept.Prog.Phys.* **71** (2008) 086201, [arXiv:0909.2104].

[52] C. S. Wu, E. Ambler, R. W. Hayward, D. D. Hoppes, and R. P. Hudson, *Experimental Test of Parity Conservation in Beta Decay*, *Phys. Rev.* **105** (1957) 1413–1414.

[53] T. D. Lee and C.-N. Yang, *Question of Parity Conservation in Weak Interactions*, *Phys. Rev.* **104** (1956) 254–258.

[54] D. Griffiths, *Introduction to Elementary Particles*. Wiley-VCH, 2008.

[55] J. H. Christenson, J. W. Cronin, V. L. Fitch, and R. Turlay, *Evidence for the 2 pi Decay of the k(2)0 Meson*, *Phys. Rev. Lett.* **13** (1964) 138–140.

[56] **BaBar** Collaboration, B. Aubert et al., *Measurement of CP violating asymmetries in B^0 decays to CP eigenstates*, *Phys. Rev. Lett.* **86** (2001) 2515–2522, [hep-ex/0102030].

[57] **Belle** Collaboration, A. Abashian et al., *Measurement of the CP violation parameter $\sin 2\phi_1$ in B^0_d meson decays*, *Phys. Rev. Lett.* **86** (2001) 2509–2514, [hep-ex/0102018].

[58] A. B. Carter and A. I. Sanda, *CP Violation in B Meson Decays*, *Phys. Rev.* **D23** (1981) 1567.

[59] R. D. Peccei, *The Strong CP Problem*, *Adv. Ser. Direct. High Energy Phys.* **3** (1989) 503–551.

[60] R. D. Peccei and H. R. Quinn, *CP Conservation in the Presence of Instantons*, *Phys. Rev. Lett.* **38** (1977) 1440–1443.

[61] **Planck** Collaboration, P. A. R. Ade et al., *Planck 2013 results. XVI. Cosmological parameters*, *Astron. Astrophys.* **571** (2014) A16, [arXiv:1303.5076].

[62] F. Zwicky, *Die Rotverschiebung von extragalaktischen Nebeln*, *Helv. Phys. Acta* **6** (1933) 110–127. [Gen. Rel. Grav.41,207(2009)].

[63] M. Aaronson, J. Huchra, and J. Mould, *The infrared luminosity/H I velocity-width relation and its application to the distance scale*, *ApJ* **229** (Apr., 1979) 1–13.

[64] J. A. Tyson, G. P. Kochanski, and I. P. Dell'Antonio, *Detailed mass map of CL0024+1654 from strong lensing*, *Astrophys.J.* **498** (1998) L107, [astro-ph/9801193].

[65] R. Massey, J. Rhodes, R. Ellis, N. Scoville, A. Leauthaud, et al., *Dark matter maps reveal cosmic scaffolding*, *Nature* **445** (2007) 286, [astro-ph/0701594].

[66] D. Clowe, M. Bradac, A. H. Gonzalez, M. Markevitch, S. W. Randall, et al., *A direct empirical proof of the existence of dark matter*, *Astrophys.J.* **648** (2006) L109–L113, [astro-ph/0608407].

[67] G. Hinshaw, D. Larson, E. Komatsu, D. N. Spergel, C. L. Bennett, J. Dunkley, M. R. Nolta, M. Halpern, R. S. Hill, N. Odegard, L. Page, K. M. Smith, J. L. Weiland, B. Gold, N. Jarosik, A. Kogut, M. Limon, S. S. Meyer, G. S. Tucker, E. Wollack, and E. L. Wright, *Nine-year Wilkinson Microwave Anisotropy Probe (WMAP) Observations: Cosmological Parameter Results*, *ApJS* **208** (Oct., 2013) 19, [arXiv:1212.5226].

[68] S. Arrenberg, L. Baudis, K. Kong, K. T. Matchev, and J. Yoo, *Kaluza-Klein Dark Matter: Direct Detection vis-a-vis LHC*, *Phys.Rev.* **D78** (2008) 056002, [arXiv:0805.4210].

[69] G. Servant, *Status Report on Universal Extra Dimensions After LHC8*, arXiv:1401.4176.

[70] G. Servant and T. M. Tait, *Elastic scattering and direct detection of Kaluza-Klein dark matter*, *New J.Phys.* **4** (2002) 99, [hep-ph/0209262].

[71] G. Servant and T. M. Tait, *Is the lightest Kaluza-Klein particle a viable dark matter candidate?*, *Nucl.Phys.* **B650** (2003) 391–419, [hep-ph/0206071].

[72] K. Kong and K. T. Matchev, *Precise calculation of the relic density of Kaluza-Klein dark matter in universal extra dimensions*, *JHEP* **0601** (2006) 038, [hep-ph/0509119].

[73] T. Flacke and D. W. Maybury, *Constraints on UED KK-neutrino dark matter from magnetic dipole moments*, *Int.J.Mod.Phys.* **D16** (2007) 1593–1600, [hep-ph/0601161].

[74] F. Burnell and G. D. Kribs, *The Abundance of Kaluza-Klein dark matter with coannihilation*, *Phys.Rev.* **D73** (2006) 015001, [hep-ph/0509118].

[75] G. Belanger, M. Kakizaki, and A. Pukhov, *Dark matter in UED: The Role of the second KK level*, *JCAP* **1102** (2011) 009, [arXiv:1012.2577].

[76] T. Flacke, D. Hooper, and J. March-Russell, *Improved bounds on universal extra dimensions and consequences for LKP dark matter*, *Phys.Rev.* **D73** (2006) 095002, [hep-ph/0509352].

[77] S. Arrenberg, L. Baudis, K. Kong, K. T. Matchev, and J. Yoo, *Kaluza-Klein Dark Matter: Direct Detection vis-a-vis LHC (2013 update)*, arXiv:1307.6581.

[78] M. Kakizaki, S. Matsumoto, Y. Sato, and M. Senami, *Relic abundance of LKP dark matter in UED model including effects of second KK resonances*, *Nucl.Phys.* **B735** (2006) 84–95, [hep-ph/0508283].

[79] M. Kakizaki, S. Matsumoto, Y. Sato, and M. Senami, *Significant effects of second KK particles on LKP dark matter physics*, *Phys.Rev.* **D71** (2005) 123522, [hep-ph/0502059].

[80] M. Kakizaki, S. Matsumoto, and M. Senami, *Relic abundance of dark matter in the minimal universal extra dimension model*, *Phys.Rev.* **D74** (2006) 023504, [hep-ph/0605280].

[81] T. Flacke, A. Menon, and D. J. Phalen, *Non-minimal universal extra dimensions*, *Phys.Rev.* **D79** (2009) 056009, [arXiv:0811.1598].

[82] T. Flacke, *Phenomenology of dark matter in non-minimal UED*, *AIP Conf.Proc.* **1200** (2010) 583–586.

[83] P. Ehrenfest, *In that way does it become manifest in the fundamental laws of physics that space has three dimensions?*, *Proceedings of the Amsterdam Academy* **20** (1917) 200–209.

[84] S. Raychaudhuri and K. Sridhar, *Particle Physics of Brane Worlds and Extra Dimensions*. Cambridge University Press.

[85] M. Tegmark, *On the dimensionality of space-time*, *Class. Quant. Grav.* **14** (1997) L69–L75.

[86] G. Nordstrom, *On the possibility of unifying the electromagnetic and the gravitational fields*, *Phys.Z.* **15** (1914) 504–506, [physics/0702221].

[87] T. Kaluza, *On the Problem of Unity in Physics*, *Sitzungsber.Preuss.Akad.Wiss.Berlin (Math.Phys.)* **1921** (1921) 966–972.

[88] P. Jordan, *Formation of the Stars and Development of the Universe*, *Nature* **164** (1949) 637–640.

[89] O. Klein, *Quantum Theory and Five-Dimensional Theory of Relativity. (In German and English)*, *Z.Phys.* **37** (1926) 895–906.

[90] E. Witten, *Search for a Realistic Kaluza-Klein Theory*, *Nucl. Phys.* **B186** (1981) 412.

[91] G. Veneziano, *Construction of a crossing - symmetric, Regge behaved amplitude for linearly rising trajectories*, *Nuovo Cim.* **A57** (1968) 190–197.

[92] C. Lovelace, *Veneziano theory*, *Proc. Roy. Soc. Lond.* **A318** (1970) 321–354.

[93] J. Scherk and J. H. Schwarz, *Dual Models for Nonhadrons*, *Nucl. Phys.* **B81** (1974) 118–144.

[94] I. Antoniadis, *A Possible new dimension at a few TeV*, *Phys.Lett.* **B246** (1990) 377–384.

[95] P. Horava and E. Witten, *Heterotic and type I string dynamics from eleven-dimensions*, *Nucl. Phys.* **B460** (1996) 506–524, [hep-th/9510209].

[96] P. Horava and E. Witten, *Eleven-dimensional supergravity on a manifold with boundary*, *Nucl. Phys.* **B475** (1996) 94–114, [hep-th/9603142].

[97] J. Polchinski, *Dirichlet Branes and Ramond-Ramond charges*, *Phys. Rev. Lett.* **75** (1995) 4724–4727, [hep-th/9510017].

[98] N. Arkani-Hamed, S. Dimopoulos, and G. R. Dvali, *The Hierarchy problem and new dimensions at a millimeter*, *Phys. Lett.* **B429** (1998) 263–272, [hep-ph/9803315].

[99] L. Randall and R. Sundrum, *A Large mass hierarchy from a small extra dimension*, *Phys. Rev. Lett.* **83** (1999) 3370–3373, [hep-ph/9905221].

[100] L. Randall and R. Sundrum, *An Alternative to compactification*, *Phys. Rev. Lett.* **83** (1999) 4690–4693, [hep-th/9906064].

[101] J. M. Maldacena, *The Large N limit of superconformal field theories and supergravity*, *Int. J. Theor. Phys.* **38** (1999) 1113–1133, [hep-th/9711200]. [Adv. Theor. Math. Phys.2,231(1998)].

[102] T. Appelquist, H.-C. Cheng, and B. A. Dobrescu, *Bounds on universal extra dimensions*, *Phys. Rev.* **D64** (2001) 035002, [hep-ph/0012100].

[103] V. Rubakov and M. Shaposhnikov, *Do We Live Inside a Domain Wall?*, *Phys.Lett.* **B125** (1983) 136–138.

[104] V. Rubakov and M. Shaposhnikov, *Extra Space-Time Dimensions: Towards a Solution to the Cosmological Constant Problem*, *Phys.Lett.* **B125** (1983) 139.

[105] C. Csaki, *TASI lectures on extra dimensions and branes*, in *From fields to strings: Circumnavigating theoretical physics. Ian Kogan memorial collection (3 volume set)*, pp. 605–698, 2004. hep-ph/0404096. [,967(2004)].

[106] R. Sundrum, *Tasi 2004 lectures: To the fifth dimension and back*, hep-th/0508134.

[107] T. Gherghetta, *TASI Lectures on a Holographic View of Beyond the Standard Model Physics*, arXiv:1008.2570.

[108] https://atlas.web.cern.ch/Atlas/GROUPS/PHYSICS/CombinedSummaryPlots/EXOTICS/ATLAS_Exotics_Summary/history.html.

[109] https://twiki.cern.ch/twiki/bin/view/CMSPublic/PhysicsResultsEXO#CMS_EXO_Summary_of_Mass_Limits.

[110] R. N. Mohapatra and A. Perez-Lorenzana, *Neutrino mass, proton decay and dark matter in TeV scale universal extra dimension models*, *Phys. Rev.* **D67** (2003) 075015, [hep-ph/0212254].

[111] K. R. Dienes, E. Dudas, and T. Gherghetta, *Extra space-time dimensions and unification*, *Phys. Lett.* **B436** (1998) 55–65, [hep-ph/9803466].

[112] N. Arkani-Hamed and S. Dimopoulos, *New origin for approximate symmetries from distant breaking in extra dimensions*, *Phys. Rev.* **D65** (2002) 052003, [hep-ph/9811353].

[113] B. A. Dobrescu and E. Poppitz, *Number of fermion generations derived from anomaly cancellation*, *Phys. Rev. Lett.* **87** (2001) 031801, [hep-ph/0102010].

[114] H.-C. Cheng, B. A. Dobrescu, and C. T. Hill, *Electroweak symmetry breaking and extra dimensions*, *Nucl. Phys.* **B589** (2000) 249–268, [hep-ph/9912343].

[115] K. R. Dienes, E. Dudas, and T. Gherghetta, *Grand unification at intermediate mass scales through extra dimensions*, *Nucl.Phys.* **B537** (1999) 47–108, [hep-ph/9806292].

[116] A. Perez-Lorenzana and R. Mohapatra, *Effect of extra dimensions on gauge coupling unification*, *Nucl.Phys.* **B559** (1999) 255, [hep-ph/9904504].

[117] G. Altarelli and F. Feruglio, *SU(5) grand unification in extra dimensions and proton decay*, *Phys.Lett.* **B511** (2001) 257–264, [hep-ph/0102301].

[118] T. Appelquist, B. A. Dobrescu, E. Ponton, and H.-U. Yee, *Proton stability in six-dimensions*, *Phys.Rev.Lett.* **87** (2001) 181802, [hep-ph/0107056].

[119] D. Hooper and S. Profumo, *Dark matter and collider phenomenology of universal extra dimensions*, *Phys.Rept.* **453** (2007) 29–115, [hep-ph/0701197].

[120] L. O'Raifeartaigh and N. Straumann, *Early history of gauge theories and Kaluza-Klein theories*, hep-ph/9810524.

[121] H.-C. Cheng, *Introduction to Extra Dimensions*, in *Physics of the large and the small, TASI 09, proceedings of the Theoretical Advanced Study Institute in Elementary Particle Physics, Boulder, Colorado, USA, 1-26 June 2009*, pp. 125–162, 2011. arXiv:1003.1162.

[122] H.-C. Cheng, K. T. Matchev, and M. Schmaltz, *Radiative corrections to Kaluza-Klein masses*, *Phys.Rev.* **D66** (2002) 036005, [hep-ph/0204342].

[123] G. D. Kribs, *TASI 2004 lectures on the phenomenology of extra dimensions*, in *Physics in D >= 4. Proceedings, Theoretical Advanced Study Institute in elementary particle physics, TASI 2004, Boulder, USA, June 6-July 2, 2004*, pp. 633–699, 2006. hep-ph/0605325.

[124] F. J. Petriello, *Kaluza-Klein effects on Higgs physics in universal extra dimensions*, *JHEP* **05** (2002) 003, [hep-ph/0204067].

[125] H. Georgi, A. K. Grant, and G. Hailu, *Brane couplings from bulk loops*, *Phys.Lett.* **B506** (2001) 207–214, [hep-ph/0012379].

[126] **CMS** Collaboration, S. Chatrchyan et al., *Observation of a new boson at a mass of 125 GeV with the CMS experiment at the LHC*, *Phys.Lett.* **B716** (2012) 30–61, [arXiv:1207.7235].

[127] **Particle Data Group** Collaboration, J. Beringer et al., *Review of Particle Physics (RPP)*, *Phys.Rev.* **D86** (2012) 010001.

[128] A. Datta, U. K. Dey, A. Raychaudhuri, and A. Shaw, *Boundary Localized Terms in Universal Extra-Dimensional Models through a Dark Matter perspective*, *Phys. Rev.* **D88** (2013) 016011, [arXiv:1305.4507].

[129] T. Flacke, D. W. Kang, K. Kong, G. Mohlabeng, and S. C. Park, *Electroweak Kaluza-Klein Dark Matter*, arXiv:1702.02949.

[130] K. Agashe, N. G. Deshpande, and G. H. Wu, *Universal extra dimensions and $b \to s\gamma$*, *Phys. Lett.* **B514** (2001) 309–314, [hep-ph/0105084].

[131] A. J. Buras, A. Poschenrieder, M. Spranger, and A. Weiler, *The Impact of universal extra dimensions on B —> X(s) gamma, B —> X(s) gluon, B —> X(s) mu+ mu-, K(L) —> pi0 e+ e- and epsilon-prime / epsilon*, *Nucl. Phys.* **B678** (2004) 455–490, [hep-ph/0306158].

[132] **Indian Association for the Cultivation of Science** Collaboration, A. Datta and A. Shaw, *Effects of non-minimal Universal Extra Dimension on $B \to X_s\gamma$*, *Phys. Rev.* **D95** (2017), no. 1 015033, [arXiv:1610.09924].

[133] I. Gogoladze and C. Macesanu, *Precision electroweak constraints on Universal Extra Dimensions revisited*, *Phys. Rev.* **D74** (2006) 093012, [hep-ph/0605207].

[134] T. Kakuda, K. Nishiwaki, K.-y. Oda, and R. Watanabe, *Universal extra dimensions after Higgs discovery*, *Phys. Rev.* **D88** (2013) 035007, [arXiv:1305.1686].

[135] P. Nath and M. Yamaguchi, *Effects of Kaluza-Klein excitations on (g(mu)-2)*, *Phys. Rev.* **D60** (1999) 116006, [hep-ph/9903298].

[136] D. Chakraverty, K. Huitu, and A. Kundu, *Effects of universal extra dimensions on B0 - antiB0 mixing*, *Phys. Lett.* **B558** (2003) 173–181, [hep-ph/0212047].

[137] A. J. Buras, M. Spranger, and A. Weiler, *The Impact of universal extra dimensions on the unitarity triangle and rare K and B decays*, *Nucl. Phys.* **B660** (2003) 225–268, [hep-ph/0212143].

[138] T. Appelquist and H.-U. Yee, *Universal extra dimensions and the Higgs boson mass*, *Phys. Rev.* **D67** (2003) 055002, [hep-ph/0211023].

[139] T. G. Rizzo and J. D. Wells, *Electroweak precision measurements and collider probes of the standard model with large extra dimensions*, *Phys. Rev.* **D61** (2000) 016007, [hep-ph/9906234].

[140] A. Strumia, *Bounds on Kaluza-Klein excitations of the SM vector bosons from electroweak tests*, *Phys. Lett.* **B466** (1999) 107–114, [hep-ph/9906266].

[141] C. D. Carone, *Electroweak constraints on extended models with extra dimensions*, *Phys. Rev.* **D61** (2000) 015008, [hep-ph/9907362].

[142] A. Belyaev, M. Brown, J. Moreno, and C. Papineau, *Discovering Minimal Universal Extra Dimensions (MUED) at the LHC*, *JHEP* **06** (2013) 080, [arXiv:1212.4858].

[143] M. Battaglia, A. K. Datta, A. De Roeck, K. Kong, and K. T. Matchev, *Contrasting supersymmetry and universal extra dimensions at colliders*, *eConf* **C050318** (2005) 0302, [hep-ph/0507284].

[144] A. Datta, K. Kong, and K. T. Matchev, *Discrimination of supersymmetry and universal extra dimensions at hadron colliders*, *Phys. Rev.* **D72** (2005) 096006, [hep-ph/0509246]. [Erratum: Phys. Rev.D72,119901(2005)].

[145] B. Bhattacherjee and K. Ghosh, *Search for the minimal universal extra dimension model at the LHC with $\sqrt{s}$=7 TeV*, *Phys. Rev.* **D83** (2011) 034003, [arXiv:1006.3043].

[146] H. Murayama, M. M. Nojiri, and K. Tobioka, *Improved discovery of a nearly degenerate model: MUED using MT2 at the LHC*, *Phys. Rev.* **D84** (2011) 094015, [arXiv:1107.3369].

[147] A. Datta, A. Datta, and S. Poddar, *Enriching the exploration of the mUED model with event shape variables at the CERN LHC*, *Phys. Lett.* **B712** (2012) 219–225, [arXiv:1111.2912].

[148] G. Belanger, A. Belyaev, M. Brown, M. Kakizaki, and A. Pukhov, *Testing Minimal Universal Extra Dimensions Using Higgs Boson Searches at the LHC*, *Phys. Rev.* **D87** (2013), no. 1 016008, [arXiv:1207.0798].

[149] **ATLAS** Collaboration, G. Aad et al., *Measurements of Higgs boson production and couplings in diboson final states with the ATLAS detector at the LHC*, *Phys. Lett.* **B726** (2013) 88–119, [arXiv:1307.1427]. [Erratum: Phys. Lett.B734,406(2014)].

[150] **CMS Collaboration** Collaboration, *Combination of standard model Higgs boson searches and measurements of the properties of the new boson with a mass near 125 GeV*, Tech. Rep. CMS-PAS-HIG-13-005, CERN, Geneva, 2013.

[151] A. Datta, A. Patra, and S. Raychaudhuri, *Higgs Boson Decay Constraints on a Model with a Universal Extra Dimension*, *Phys. Rev.* **D89** (2014), no. 9 093008, [arXiv:1311.0926].

[152] **ATLAS Collaboration** Collaboration, *Search for Diphoton Events with Large Missing Transverse Momentum in 7 TeV pp Collision Data with the ATLAS Detector*, Tech. Rep. ATLAS-CONF-2012-072, CERN, Geneva, Jul, 2012.

[153] L. Edelhäuser, T. Flacke, and M. Krämer, *Constraints on models with universal extra dimensions from dilepton searches at the LHC*, *JHEP* **08** (2013) 091, [arXiv:1302.6076].

[154] J. M. Cornell, S. Profumo, and W. Shepherd, *Dark matter in minimal universal extra dimensions with a stable vacuum and the "right" Higgs boson*, *Phys. Rev.* **D89** (2014), no. 5 056005, [arXiv:1401.7050].

[155] M. Blennow, H. Melbeus, T. Ohlsson, and H. Zhang, *RG running in a minimal UED model in light of recent LHC Higgs mass bounds*, *Phys. Lett.* **B712** (2012) 419–424, [arXiv:1112.5339].

[156] A. Datta and S. Raychaudhuri, *Vacuum Stability Constraints and LHC Searches for a Model with a Universal Extra Dimension*, *Phys. Rev.* **D87** (2013), no. 3 035018, [arXiv:1207.0476].

[157] T. Flacke, K. Kong, and S. C. Park, *A Review on Non-Minimal Universal Extra Dimensions*, *Mod. Phys. Lett.* **A30** (2015), no. 05 1530003, [arXiv:1408.4024].

[158] G. R. Dvali, G. Gabadadze, M. Kolanovic, and F. Nitti, *The Power of brane induced gravity*, *Phys. Rev.* **D64** (2001) 084004, [hep-ph/0102216].

[159] M. Carena, T. M. P. Tait, and C. E. M. Wagner, *Branes and orbifolds are opaque*, *Acta Phys. Polon.* **B33** (2002) 2355, [hep-ph/0207056].

[160] F. del Aguila, M. Perez-Victoria, and J. Santiago, *Bulk fields with general brane kinetic terms*, *JHEP* **0302** (2003) 051, [hep-th/0302023].

[161] F. del Aguila, M. Perez-Victoria, and J. Santiago, *Bulk fields with brane terms*, *Eur.Phys.J.* **C33** (2004) S773–S775, [hep-ph/0310352].

[162] F. del Aguila, M. Perez-Victoria, and J. Santiago, *Physics of brane kinetic terms*, *Acta Phys.Polon.* **B34** (2003) 5511–5522, [hep-ph/0310353].

[163] F. del Aguila, M. Perez-Victoria, and J. Santiago, *Effective description of brane terms in extra dimensions*, *JHEP* **10** (2006) 056, [hep-ph/0601222].

[164] A. Datta, K. Nishiwaki, and S. Niyogi, *Non-minimal Universal Extra Dimensions: The Strongly Interacting Sector at the Large Hadron Collider*, *JHEP* **1211** (2012) 154, [arXiv:1206.3987].

[165] A. Datta, K. Nishiwaki, and S. Niyogi, *Non-minimal Universal Extra Dimensions with Brane Local Terms: The Top Quark Sector*, *JHEP* **1401** (2014) 104, [arXiv:1310.6994].

[166] A. Datta, U. K. Dey, A. Shaw, and A. Raychaudhuri, *Universal Extra-Dimensional Models with Boundary Localized Kinetic Terms: Probing at the LHC*, *Phys.Rev.* **D87** (2013) 076002, [arXiv:1205.4334].

[167] A. Datta, A. Raychaudhuri, and A. Shaw, *LHC limits on KK-parity non-conservation in the strong sector of universal extra-dimension models*, *Phys.Lett.* **B730** (2014) 42–49, [arXiv:1310.2021].

[168] U. K. Dey and T. S. Ray, *Constraining minimal and nonminimal universal extra dimension models with Higgs couplings*, *Phys.Rev.* **D88** (2013), no. 5 056016, [arXiv:1305.1016].

[169] T. Jha and A. Datta, $Z \to b\bar{b}$ *in non-minimal Universal Extra Dimensional Model*, *JHEP* **1503** (2015) 012, [arXiv:1410.5098].

[170] A. Shaw, *KK-parity non-conservation in UED confronts LHC data*, *Eur. Phys. J.* **C75** (2015), no. 1 33, [arXiv:1405.3139].

[171] A. Datta and A. Shaw, *Nonminimal universal extra dimensional model confronts $B_s \to \mu^+\mu^-$*, *Phys. Rev.* **D93** (2016), no. 5 055048, [arXiv:1506.08024].

[172] U. K. Dey and T. Jha, *Rare top decays in minimal and nonminimal universal extra dimension models*, *Phys. Rev.* **D94** (2016), no. 5 056011, [arXiv:1602.03286].

[173] T. Jha, *Unitarity Constraints on non-minimal Universal Extra Dimensional Model*, arXiv:1604.02481.

[174] F. del Aguila, M. Perez-Victoria, and J. Santiago, *Some consequences of brane kinetic terms for bulk fermions*, hep-ph/0305119.

[175] A. Datta and A. Shaw, *A note on gauge-fixing in the electroweak sector of UED with BLKTs*, arXiv:1408.0635.

[176] A. Muck, *The standard model in 5D: Theoretical consistency and experimental constraints*. PhD thesis, Wurzburg U., 2004.

[177] T. Flacke, K. Kong, and S. C. Park, *Phenomenology of Universal Extra Dimensions with Bulk-Masses and Brane-Localized Terms*, *JHEP* **05** (2013) 111, [arXiv:1303.0872].

[178] B. W. Lee, C. Quigg, and H. B. Thacker, *Weak Interactions at Very High-Energies: The Role of the Higgs Boson Mass*, *Phys. Rev.* **D16** (1977) 1519.

[179] R. S. Chivukula, D. A. Dicus, and H.-J. He, *Unitarity of compactified five-dimensional Yang-Mills theory*, *Phys. Lett.* **B525** (2002) 175–182, [hep-ph/0111016].

[180] S. De Curtis, D. Dominici, and J. R. Pelaez, *Strong tree level unitarity violations in the extra dimensional standard model with scalars in the bulk*, *Phys. Rev.* **D67** (2003) 076010, [hep-ph/0301059].

[181] A. Cordero-Cid, H. Novales-Sanchez, and J. J. Toscano, *The Standard Model with one universal extra dimension*, *Pramana* **80** (2013) 369–412, [arXiv:1108.2926].

[182] I. García-Jiménez, M. A. López-Osorio, E. Martínez-Pascual, G. I. Nápoles-Cañedo, H. Novales-Sánchez, and J. J. Toscano, *Standard Model with extra dimensions and its zeta function regularization*, arXiv:1603.03128.

[183] M. Baak, M. Goebel, J. Haller, A. Hoecker, D. Kennedy, R. Kogler, K. Moenig, M. Schott, and J. Stelzer, *The Electroweak Fit of the Standard Model after the Discovery of a New Boson at the LHC*, *Eur. Phys. J.* **C72** (2012) 2205, [arXiv:1209.2716].

[184] A. Freitas and Y.-C. Huang, *Electroweak two-loop corrections to $sin^2\theta^{b\bar{b}}_{eff}$ and R_b using numerical Mellin-Barnes integrals*, *JHEP* **08** (2012) 050, [arXiv:1205.0299]. [Erratum: JHEP10,044(2013)].

[185] N. G. Deshpande and G. Eilam, *FLAVOR CHANGING ELECTROMAGNETIC TRANSITIONS*, *Phys.Rev.* **D26** (1982) 2463.

[186] N. G. Deshpande and M. Nazerimonfared, *Flavor Changing Electromagnetic Vertex in a Nonlinear R_ξ Gauge*, *Nucl.Phys.* **B213** (1983) 390–408.

[187] J. Diaz-Cruz, R. Martinez, M. Perez, and A. Rosado, *Flavor Changing Radiative Decay of the t Quark*, *Phys.Rev.* **D41** (1990) 891–894.

[188] B. Mele, S. Petrarca, and A. Soddu, *A New evaluation of the $t \to cH$ decay width in the standard model*, *Phys.Lett.* **B435** (1998) 401–406, [hep-ph/9805498].

[189] B. Mele, S. Petrarca, and A. Soddu, *The $t \to cH$ decay width in the standard model*, hep-ph/9912235.

[190] J. Aguilar-Saavedra and B. Nobre, *Rare top decays $t \to c\gamma$, $t \to cg$ and CKM unitarity*, *Phys.Lett.* **B553** (2003) 251–260, [hep-ph/0210360].

[191] J. Aguilar-Saavedra, *Top flavor-changing neutral interactions: Theoretical expectations and experimental detection*, *Acta Phys.Polon.* **B35** (2004) 2695–2710, [hep-ph/0409342].

[192] K.-F. Chen, W.-S. Hou, C. Kao, and M. Kohda, *When the Higgs meets the Top: Search for $t \to ch^0$ at the LHC*, *Phys. Lett.* **B725** (2013) 378–381, [arXiv:1304.8037].

[193] H. Khanpour, S. Khatibi, M. K. Yanehsari, and M. M. Najafabadi, *Single top quark production as a probe of anomalous $tq\gamma$ and tqZ couplings at the FCC-ee*, arXiv:1408.2090.

[194] H. Hesari, H. Khanpour, M. K. Yanehsari, and M. M. Najafabadi, *Probing the Top Quark Flavour-Changing Neutral Current at a Future Electron-Positron Collider*, *Adv. High Energy Phys.* **2014** (2014) 476490, [arXiv:1412.8572].

[195] D. Kim and M. Park, *Enhancement of new physics signal sensitivity with mistagged charm quarks*, arXiv:1507.03990.

[196] H. Hesari, H. Khanpour, and M. M. Najafabadi, *Direct and Indirect Searches for Top-Higgs FCNC Couplings*, *Phys. Rev.* **D92** (2015), no. 11 113012, [arXiv:1508.07579].

[197] S. Khatibi and M. M. Najafabadi, *Top quark flavor changing via photon*, arXiv:1511.00220.

[198] J. Guasch and J. Sola, *FCNC top quark decays: A Door to SUSY physics in high luminosity colliders?*, *Nucl. Phys.* **B562** (1999) 3–28, [hep-ph/9906268].

[199] G. Eilam, A. Gemintern, T. Han, J. M. Yang, and X. Zhang, *Top quark rare decay $t \to ch$ in R-parity violating SUSY*, *Phys. Lett.* **B510** (2001) 227–235, [hep-ph/0102037].

[200] M. Frank and I. Turan, *$t \to cg$, $c\gamma$, cZ in the left-right supersymmetric model*, *Phys.Rev.* **D72** (2005) 035008, [hep-ph/0506197].

[201] J. J. Cao, G. Eilam, M. Frank, K. Hikasa, G. L. Liu, I. Turan, and J. M. Yang, *SUSY-induced FCNC top-quark processes at the large hadron collider*, *Phys. Rev.* **D75** (2007) 075021, [hep-ph/0702264].

[202] J. Cao, Z. Heng, L. Wu, and J. M. Yang, *R-parity violating effects in top quark FCNC productions at LHC*, *Phys. Rev.* **D79** (2009) 054003, [arXiv:0812.1698].

[203] J. Cao, C. Han, L. Wu, J. M. Yang, and M. Zhang, *SUSY induced top quark FCNC decay $t \to ch$ after Run I of LHC*, *Eur. Phys. J.* **C74** (2014), no. 9 3058, [arXiv:1404.1241].

[204] A. Dedes, M. Paraskevas, J. Rosiek, K. Suxho, and K. Tamvakis, *Rare Top-quark Decays to Higgs boson in MSSM*, *JHEP* **11** (2014) 137, [arXiv:1409.6546].

[205] D. Bardhan, G. Bhattacharyya, D. Ghosh, M. Patra, and S. Raychaudhuri, *A Detailed Analysis of Flavour-changing Decays of Top Quarks as a Probe of New Physics at the LHC*, arXiv:1601.04165.

[206] G. Eilam, J. Hewett, and A. Soni, *Rare decays of the top quark in the standard and two Higgs doublet models*, *Phys.Rev.* **D44** (1991) 1473–1484.

[207] E. O. Iltan, *$t \to cH^0$ decay in the general two Higgs doublet model*, *Phys. Rev.* **D65** (2002) 075017, [hep-ph/0111318].

[208] A. Arhrib, *Top and Higgs flavor changing neutral couplings in two Higgs doublets model*, *Phys. Rev.* **D72** (2005) 075016, [hep-ph/0510107].

[209] R. Gaitán, R. Martinez, and J. H. M. de Oca, *Rare top decay $t \to c\gamma$ with flavor changing neutral scalar interactions in THDM*, arXiv:1503.04391.

[210] G. Abbas, A. Celis, X.-Q. Li, J. Lu, and A. Pich, *Flavour-changing top decays in the aligned two-Higgs-doublet model*, *JHEP* **06** (2015) 005, [arXiv:1503.06423].

[211] T.-J. Gao, T.-F. Feng, and J.-B. Chen, *$t \to c\gamma$ and $t \to cg$ in warped extra dimensions*, *JHEP* **1302** (2013) 029, [arXiv:1303.0082].

[212] G. Gonzalez-Sprinberg, R. Martinez, and J. A. Rodriguez, *FCNC top quark decays in extra dimensions*, *Eur.Phys.J.* **C51** (2007) 919–926.

[213] A. Cordero-Cid, M. A. Perez, G. Tavares-Velasco, and J. J. Toscano, *Effective Lagrangian approach to Higgs-mediated FCNC top quark decays*, *Phys. Rev.* **D70** (2004) 074003, [hep-ph/0407127].

[214] A. Datta and M. Duraisamy, *Model Independent Predictions for Rare Top Decays with Weak Coupling*, *Phys.Rev.* **D81** (2010) 074008, [arXiv:0912.4785].

[215] J. F. Oliver, J. Papavassiliou, and A. Santamaria, *Universal extra dimensions and Z —> b anti-b*, *Phys. Rev.* **D67** (2003) 056002, [hep-ph/0212391].

[216] J. Bernabeu, A. Pich, and A. Santamaria, *Gamma (Z —> B anti-B): A Signature of Hard Mass Terms for a Heavy Top*, *Phys. Lett.* **B200** (1988) 569–574.

[217] **D0** Collaboration, V. M. Abazov et al., *Precision measurement of the top-quark mass in lepton+jets final states*, *Phys. Rev. Lett.* **113** (2014) 032002, [arXiv:1405.1756].

[218] **Particle Data Group** Collaboration, K. A. Olive et al., *Review of Particle Physics*, *Chin. Phys.* **C38** (2014) 090001.

[219] H. H. Patel, *Package-X: A Mathematica package for the analytic calculation of one-loop integrals*, *Comput. Phys. Commun.* **197** (2015) 276–290, [arXiv:1503.01469].

[220] T. Hahn and M. Perez-Victoria, *Automatized one loop calculations in four-dimensions and D-dimensions*, *Comput. Phys. Commun.* **118** (1999) 153–165, [hep-ph/9807565].

[221] **Gfitter Group** Collaboration, M. Baak, J. Cúth, J. Haller, A. Hoecker, R. Kogler, K. Mönig, M. Schott, and J. Stelzer, *The global electroweak fit at NNLO and prospects for the LHC and ILC*, *Eur. Phys. J.* **C74** (2014) 3046, [arXiv:1407.3792].

[222] https://atlas.web.cern.ch/Atlas/GROUPS/PHYSICS/CombinedSummaryPlots/EXOTICS/ATLAS_Exotics_Summary/ATLAS_Exotics_Summary.pdf.

[223] https://twiki.cern.ch/twiki/pub/CMSPublic/PhysicsResultsCombined/exo-limits_DecJamboree2015.pdf.

[224] **CMS** Collaboration, *Search for anomalous single top quark production in association with a photon*, Tech. Rep. CMS-PAS-TOP-14-003, CERN, Geneva, 2014.

[225] **ATLAS** Collaboration, G. Aad et al., *Search for top quark decays $t \to qH$ with $H \to \gamma\gamma$ using the ATLAS detector*, *JHEP* **1406** (2014) 008, [arXiv:1403.6293].

[226] **CMS** Collaboration, *Combined multilepton and diphoton limit on $t \to cH$*, Tech. Rep. CMS-PAS-HIG-13-034, CERN, Geneva, 2014.

[227] **Top Quark Working Group** Collaboration, K. Agashe et al., *Working Group Report: Top Quark*, arXiv:1311.2028.